DISSERTATION

System-Level Modeling and Optimization of MIMO HSDPA Networks

Conducted for the purpose of receiving the academic title
"Doktor der technischen Wissenschaften"

Dipl.-Ing. Martin Wrulich
Matrikelnummer: 9961105
Neubaugasse 47/19, 1070 Wien, Austria

October 27, 2009

Submitted at Vienna University of Technology
Faculty of Electrical Engineering and Information Technology

Vienna, September 2009

For those I love.

Supervisor

Univ.Prof. Dr.-Ing. Dipl.-Ing. Markus Rupp
Institut für Nachrichtentechnik und Hochfrequenztechnik
Technische Universität Wien, Österreich

Examiner

Prof. Dipl. El.-Ing. ETHZ, Dipl. Math. ETHZ, Dr. Sc. Techn. (ETHZ) Bernard Henri Fleury
Department of Electronic Systems
Aalborg Universitet, Denmark

Abstract

Interaction between the Medium Access Control (MAC)-layer and the physical-layer routines is one of the basic concepts of modern wireless networks. Physical-layer dependent resource allocation and scheduling guarantee efficient network utilization. Accordingly, classical link-level analyses, focusing only on the physical-layer are not sufficient anymore for optimum transceiver structure and algorithm development.

This thesis presents the development and application of a system-level description suitable for the downlink of Multiple-Input Multiple-Output (MIMO) enhanced High-Speed Downlink Packet Access (HSDPA), with particular focus on the Double Transmit Antenna Array (D-TxAA) transmission mode. The system-level model allows for investigating and evaluating transmission systems and algorithms in the context of cellular networks. Two separate models are proposed to obtain a complete system-level description: (i) a link-quality model, analytically describing the MIMO HSDPA link quality in a so-called equivalent fading parameter structure, and (ii) a link-performance model, capable of predicting the BLock Error Ratio (BLER) performance of the transmission.

Based on this novel system-level model, a flexible system-level simulator is developed. The simulator, implemented in MATLAB, is subsequently applied to a set of different optimizations. First, some general investigations of the system behavior of D-TxAA MIMO HSDPA in the cellular network context are conducted. This leads to recommendations and guidelines for network planning. Afterwards a Radio Link Control (RLC) based D-TxAA stream number decision algorithm with enhanced robustness against outdated User Equipment (UE) Channel Quality Indicator (CQI) feedback is developed. Similarly, a novel content-aware Medium Access Control for High-Speed Downlink Packet Access (MAC-hs) scheduler increasing the Quality of Experience (QoE) for video-streaming is proposed and its performance is assessed. Besides the research focusing on the High-Speed Downlink Shared CHannel (HS-DSCH) also the signaling channels—being very important for the operation of wireless networks—are investigated. In particular, an optimization of the Common Pilot CHannel (CPICH) power allocation for various network configurations is conducted. The findings are especially important for MIMO HSDPA trials, but can also be valuable for the optimization of already existing MIMO HSDPA cell clusters.

Finally, a multi-user interference-aware Minimum Mean Squared Error (MMSE) equalizer is developed. This novel receiver takes the structure of the Transmit Antenna Array (TxAA) interference in the cell into account. The underlying system-model represents an extension to the classical single-user analysis. The theoretical limits and the throughput are evaluated by means of physical-layer and system-level investigations under realistic channel conditions. The results show significant performance gains of the interference-aware equalizer for channels with large delay spread.

Kurzfassung

Die Einbindung der Medium Access Control (MAC)-schicht in Vorgänge der Bitübertragungs-schicht ist eines der grundlegenden Konzepte moderner Funknetzwerke. Die Allokation und das Scheduling passend zur Bitübertragungsschicht garantiert eine effiziente Ausnutzung der Netzwerk-Ressourcen. Das bedeutet jedoch auch, dass die klassische Betrachtung der Über-tragungsstrecke—mit Fokus auf die Bitübertragungsschicht—nicht mehr ausreicht um optimale Sende- und Empfangsstrukturen sowie Algorithmen zu entwickeln.

Diese Dissertation präsentiert die Entwicklung und einige Anwendungen eines system-level Modells, das geeignet ist, den Downlink von Mehrfachantennen (MIMO) High-Speed Downlink Packet Access (HSDPA) darzustellen. Besonderer Fokus wird dabei auf den Double Transmit Antenna Array (D-TxAA) Übertragungsmodus gelegt. Das vorgeschlagene Modell erlaubt die Untersuchung und das Testen von Übertragungssystemen und Algorithmen im Kontext von zel-lulären Netzwerken. Um eine vollständige Systembeschreibung zu erhalten, werden zwei getren-nte Modelle entwickelt: (i) ein link-quality Modell, welches die MIMO HSDPA Verbindungs-qualität analytisch in einer sogenannten äquivalenten Schwund-Parameter-Struktur darstellt, und (ii) ein link-performance Modell, welches eine Vorhersage der Blockfehlerrate (BLER) der Übertragung ermöglicht.

Basierend auf diesem neuen System-Modell wird außerdem ein neuartiger, flexibler system-level Simulator entwickelt. Der in MATLAB implementierte Simulator wird anschließend für eine Reihe von Optimierungen verwendet. Zuerst wird eine allgemeine Untersuchung der System-Leistung von D-TxAA MIMO HSDPA im Kontext zellulärer Netzwerke durchgeführt. Die gewonnen Erkenntnisse führen zu einigen Empfehlungen und Richtlinien für die Funknetzplanung. Danach wird ein Radio Link Control (RLC) basierender Algorithmus entwickelt und getestet, welcher für D-TxAA die geeignete Anzahl der parallelen Sendeströme ermittelt. Der Algorithmus ze-ichnet sich insbesondere durch eine erhöhte Robustheit gegen Fehler bei den Kanalqualitäts-Rückmeldungen der mobilen Endgeräte aus. Anschließend wird ein neuer Scheduler vorgestellt, welcher Informationen über den Inhalt der zu übertragenen Pakete verwendet um die Qualität von gestreamten Videos zu erhöhen. Neben der Forschung mit Fokus auf den HSDPA Datenkanal (HS-DSCH) werden auch die Signalisierungskanäle—welche sehr wichtig für das Betreiben von Funknetzwerken sind—untersucht. Insbesondere wird die optimale Leistungsverteilung des Pilot-Kanals (CPICH) für unterschiedliche Netzwerk-Konfigurationen bestimmt. Die gewonnen Erken-ntnisse sind sehr wichtig für MIMO HSDPA Testversuche, aber auch für die Optimierung von eventuell schon bestehenden MIMO HSDPA Zellgruppen.

Abschließend wird ein Minimum Mean Squared Error (MMSE) Entzerrer entwickelt, der die Interferenz-Struktur von Transmit Antenna Array (TxAA) Übertragungen berücksichtigt. Das zugrundeliegende System-Modell ist eine Erweiterung der klassischen Einfachnutzer Sichtweise. Durch Simulationen der Funkübertragungsstrecke und system-level Simulationen werden sowohl die theoretischen Limits als auch die Datendurchsatz-Leistungsfähigkeit unter realistischen Be-dingungen untersucht. Die Ergebnisse zeigen beachtliche Leistungsgewinne des vorgeschlagenen Entzerrers bei Funkkanälen mit großen Laufzeiten.

Acknowledgements

Contents

List of Figures

List of Tables

Chapter 1.

Introduction

> What seems impossible one minute becomes, through faith, possible the next.
>
> *(Norman Vincent Peale)*

WIRELESS radio communication represents one of the most persistently growing markets within the last 15 to 20 years. Research in this field is particularly exciting because of the technological and social impacts it already has and will enable. Improvements in signal processing algorithms and their implications nowadays affect our daily live that has become more and more dependent on modern communication services. Voice, and more recently data services, have driven an economic boost in many regions of the world, most recently in India and China.[1] Even in times of economical crisis, the telecommunications market has proven to be robust and may identify itself as a driving force in financial-crisis market recovery [2].

The scientific challenge in wireless communications and the macro-economic importance of the research in this field have driven numerous facilities and their faculties to participate in the ongoing advance of technology and services. It is this enthusiasm that also infected me, establishing the basis for my research.

1.1. Motivation for this Dissertation

Todays cellular networks deployed by mobile network operators are based on the Wideband Code-Division Multiple Access (WCDMA) transmission standard. The Universal Mobile Telecommunications System (UMTS) is the first generation WCDMA network successfully building the groundwork for fast data services in addition to voice traffic. As an advancement of UMTS, High-Speed Downlink Packet Access (HSDPA) has introduced a number of features aiming at increased data rates and lower latency [3]. It is the fastest system based on WCDMA available today.

Recent developments in the hardware of mobile phones and in the services provided led to a dramatically increased demand in peak data rate. Furthermore, the number of users taking advantage of data service driven applications has been growing extensively during the last years. Since bandwidth is a scarce resource nowadays, spectral efficiency has to be increased to satisfy the demand for these high data rates in cellular mobile communication systems. Multiple-Input Multiple-Output (MIMO) techniques promise such an increase in spectral efficiency without the need to increase transmit power or to utilize additional bandwidth [4]. Accordingly, the question of how to exploit MIMO gains has been in focus of research for almost 15 years. For

---

[1]There is already an increasing effort of building up wireless networks in Africa [1], but the total revenue generated is still small compared to the other regions.

commercial deployments, however, a large number of antennas at the mobile terminal is usually not desired due to limited space, battery capacity, and cost arguments. The latest step in mobile communications leads towards a completely new physical layer [5] that utilizes Orthogonal Frequency-Division Multiple Access (OFDMA) in combination with MIMO as the wireless radio access method for the downlink.

In Austria—among other European countries—the licensing of the 2100 MHz band for WCDMA occurred at the tail end of the technology bubble, thus the utilized spectrum was acquired with immense costs. Together with the necessary investments in base-station and core-network equipment the mobile network operators now have to amortize their tied up capital by exploiting the existing infrastructure as good as possible, focusing on return of investment. This has led to an increased interest in the possible enhancements of Single-Input Single-Output (SISO) HSDPA due to easy deployment in the existing networks. The 3rd Generation Partnership Project (3GPP) has considered numerous proposals for the MIMO upgrade of Frequency Division Duplex (FDD)[2] HSDPA [6]. In late 2006, 3GPP decided in favor of Double Transmit Antenna Array (D-TxAA) to be the next evolutionary step of the classical SISO HSDPA [7]. D-TxAA supports single-antenna and multi-antenna mobile devices, offering flexibility and a cost-efficient upgrade for mobile network operators as well as new business opportunities for equipment manufacturers.

Importance of System-Level Modeling

Starting with HSDPA, 3GPP networks also began to utilize the channel information more efficiently by means of the information offered by the Channel Quality Indicator (CQI) reports. Accordingly, the network-side can select the algorithms in an adaptive manner to exploit multi-user diversity or combat both intra-cell as well as inter-cell interference. This affects the statistics of the channel realizations a user equipment observes when receiving data from the network in the downlink.

To illustrate this argument, Figure 1.1 shows the empirical distribution of the magnitude of the channel coefficients observed by a user when different scheduling mechanisms are employed. For this simple example, both the NodeB and each User Equipment (UE) were equipped with one single antenna. In the terminology of this work, this is called a 1×1 or simply *SISO* system. For each individual user $u = 1, \ldots, U$, an independent channel coefficient $h_i^{(u)}$ with i denoting the discrete time index, was generated according to a single-tap Rayleigh block-fading channel [8]. All channel coefficients have an average power of one. There are $U = 25$ users active, each with the same average receive power.

Figure 1.1 compares the influence of various types of schedulers (Round Robin (RR), Proportional Fair (PF) and Maximum Carrier-to-Interference Ratio (max C/I)) in terms of the empirical probability density function (epdf) of the magnitude of the channel epdf($|h|$) as seen by the respectively scheduled user. It can be observed that the RR scheduler preserves the Rayleigh distribution of $|h|$. Note however that this conclusion only holds because the individual channels of the users are assumed to be statistically independent. In fact, when a more sophisticated scheduler that takes advantage of any available Channel State Information (CSI) is utilized, the situation changes dramatically. Both, the PF and the max C/I scheduler deform the epdf significantly, which clearly shows that the assumption of Rayleigh distributed fading

---

[2]UMTS specifications define FDD and Time Division Duplex (TDD) operation modes, whereas in Europe mostly FDD is used. Only in the Czech Republic TDD UMTS is deployed.
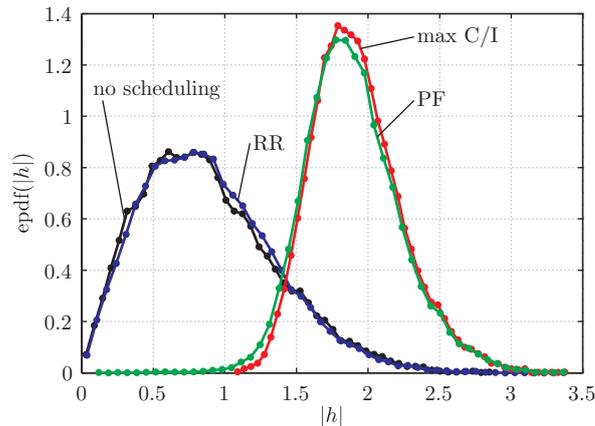
Figure 1.1.: Influence of the scheduler algorithm on the epdf of the channel coefficients magnitude $|h|$, as observed by the user. RR denotes the round robin scheduler, PF the proportional fair scheduler, and max C/I the maximum carrier-to-interference ratio scheduler.

coefficients—which is sometimes used to derive optimum receivers—is not valid anymore.[3]

Furthermore, already starting today, the step towards higher layers than the Medium Access Control (MAC) layer is investigated using cross-layer approaches which connect the core-network and the physical layer even more. This will also be an important part of future generation wireless networks, like for example 3GPP Long Term Evolution (LTE) [9] to boost the throughput and delay performance. Accordingly even more network investigations are required to determine potential performance gains or flaws are required. Besides this argument, network operators are mainly interested in the performance of transmission techniques when employed in a cellular network. The performance prediction of future transmission standards helps network planning, as well as the business and investment division to assess where upgrades to higher capacity equipment is beneficial, and to which extent.[4] Similarly, NodeB and core-network equipment manufacturers need simulations to develop and test their algorithms in a network-related context.

All these arguments show that the classical link-level investigations and simulations focusing purely on the physical-layer are not sufficient anymore. Thus, to conduct research in the context of cellular networks a mathematical abstraction of the physical-layer is needed. Such a *system-level description* is required to be accurate and computationally feasible for large-scale simulations, but should ideally also be utilizable for analytical investigations. The models avail-

---

[3]For this simple simulation, I chose the PF metric of each user u at the discrete time instant i to be

$$\mu_i^{(u)} \triangleq \frac{\tilde{R}_i^{(u)}}{\frac{1}{i}\sum_{k=1}^{i} R_k^{(u)}}, \quad \tilde{R}_i^{(u)} = B_{\mathrm{f}} \log_2\left(1 + \frac{|h_i^{(u)}|^2}{\sigma_{\mathrm{n}}^2}\right),$$

with $\tilde{R}_i^{(u)}$ describing the instantaneous realizable user data rate, which I approximated by the capacity of the link for a given bandwidth $B_{\mathrm{f}} = 5\,\mathrm{MHz}$ and a noise covariance of $\sigma_{\mathrm{n}}^2 = 1$. The realized user data rate, given by the rate achieved when a user was really scheduled, is denoted $R_k^{(u)}$ in the above metric. Similarly, the max C/I scheduler is following the user metric $\mu_i^{(u)} \triangleq |h_i^{(u)}|^2$. The scheduled user is then evaluated for both scheduler types as $u^{(\mathrm{s})} \triangleq \arg\max_{u=1,\dots,U} \mu_i^{(u)}$.

[4]At least in the technical sense, whereas system-level simulations can also be coupled with business related data, as for example done by Symena GmbH [10].

able in literature do not cover MIMO HSDPA so far. Besides, many of them lack sufficient accuracy, analytical applicability, or computational efficiency. The presented work is targeted to provide a system-level description that solves these issues in a comprehensive way.

Importance of System-Level Optimization

The opportunities offered by the interaction of the lower layers and the MIMO extension of HSDPA are very diverse. Unfortunately, most of the existing algorithms only exploit parts of these possibilities. Todays schedulers do not consider content-information, MIMO adaptation algorithms work independent of global interference-minimization goals, and receivers treat the downlink as single-user situation, to name a few.

Pressure on cost and the wish to exploit the full performance potential of the acquired hardware, however, requires close-to optimum network algorithms and transceiver structures. My thesis is thus also aiming at improvements to some network algorithms as well as to the classical Minimum Mean Squared Error (MMSE) equalizer structure.

1.2. Scope of Work and Contributions

As already outlined, the main objective of this thesis is the development and application of a suitable *system-level description*[5] for the downlink of MIMO enhanced HSDPA, with particular focus on the D-TxAA transmission mode. My proposed system-level model serves as a basis for the concept of a system-level simulator and its implementation in a MATLAB-environment. This simulator then builds a platform to investigate various parts of HSDPA networks.

Especially in packet-data-driven networks, like HSDPA, the system-level performance strongly depends on the algorithms in use. As a matter of fact, the increased adaptability of the physical layer can be utilized to fine-tune the network elements in order to realize potential gains or make it more robust. To some extent, these approaches may also be considered to be *cross-layer* like [11], where information from higher layers may be utilized. With the Radio Link Control (RLC) being of main interest, I put the focus of my thesis on the downlink of HSDPA. The conducted investigations result in the development and testing of improved network-based algorithms. These algorithms show substantial benefits compared to previously published methods.

Although this work addresses MIMO HSDPA, the basic methodology of the system-level modeling as well as the simulation concept may also be useful for future mobile communication systems. System-level analysis provides the necessary tools for the study and the development of such networks and their network-based—potentially cross-layer—algorithms.

In the following, the organization of this thesis in chapters and the novel contributions therein are explained. Furthermore, the relevant original publications (co)-authored are cited and commented.

Chapter 2: HSDPA and its MIMO Enhancements

At the beginning, I review the basic properties of HSDPA and its MIMO-enhanced successor, D-TxAA HSDPA. I put a special focus on the aspects of the standards that play an important role in the context of my related investigations. The description explains the basic algorithms of the core network and the wireless access scheme that define HSDPA compared to UMTS.

---

[5]An accurate definition of the term *system-level description* is provided in Chapter 3.

Also some of the most important aspects concerning the underlying MIMO principles on which D-TxAA is build upon are elaborated.

Chapter 3: System-Level Modeling for MIMO Enhanced HSDPA

In this chapter, the concept of the proposed system-level modeling approach is introduced first, explaining the motivation and the basic constraints behind it, as well as its application in network-based research. I also elaborate on the difference between *physical-layer*, also called *link-level*, investigations and *system-level* based network studies, and discuss the advantages and limits of both aspects. Some of these findings have already been published in [12–14].

First, a computationally efficient *link-quality* model is developed, which analytically describes the MIMO HSDPA link quality in the network context. The proposed model is very flexible in describing various transmission setups, including even higher order spatial multiplexing schemes than the standardized D-TxAA mode. Furthermore, the interference terms in the link-quality model are described by means of so-called *equivalent fading parameters*, which can be evaluated prior to the system-level simulation. This allows to dramatically reduce the computational complexity needed during the runtime of the system-level simulation. The link-quality model is then validated against link-level simulation results, showing an almost perfect approximation of the *true* Signal-to-Interference-and-Noise Ratio (SINR). By analytical analysis, I also identify a fundamental performance limit of the D-TxAA Spatial Division Multiple Access (SDMA) user-separation capabilities, when utilizing the standard 3GPP pre-coding codebook. To highlight the virtue of the proposed model, I elaborate on the modeling deficiencies of a pure statistical approach, and assess the computational complexity reduction in a semi-analytical framework. The core parts of the link-quality model were published in [12, 13, 15, 16].

Second, my concept for the *link-performance* model which describes the BLock Error Ratio (BLER) performance of the system is presented. In principle, the model is composed of a transmission parameter adaptive mapping/compression of the link-quality model parameters and a successive Additive White Gaussian Noise (AWGN) based BLER performance prediction. Consecutively, the training of the link performance model, meaning the tuning of the parameters within the utilized compression/mapping description, is conducted. The necessary link-level simulations also serve to validate the link-performance model [14, 17].

In short, the novel contributions to the area of system-level modeling research are:

- The proposed link-quality model provides an highly accurate description of the HSDPA link-quality in the network context that has not been available before [12, 15].

- The model uses equivalent fading parameters to render the effects of the channel, which can be calculated prior to the system-level simulation. This allows a huge reduction of the computational complexity during system-level simulation runtime [13, 14].

- The link-performance model utilizes an established conceptual approach, but introduces the idea of slot-based sampled compression/mapping in the Mutual Information (MI) domain [14, 17].

- In addition, the necessary training for the tuning parameters are conducted in the SINR domain, which provides a good fit over the whole BLER region of interest [14, 16].

Finally, let me point out that the developed link-quality model is currently used by Nokia Siemens Networks (NSN) in their packet-based system-level simulator Mobile Radio Simulation

Environment (MoRSE) where it serves as the core for the development and testing of base-station equipment and algorithms. The link-quality and the link-performance models have also been utilized within the C 10 and C 12 projects [12, 17] conducted at ftw. in collaboration with Infineon AG.

Chapter 4: System-Level Simulation Based Optimization of MIMO Enhanced HSDPA

The proposed system-level model serves as the core for the development of a system-level simulator. First, the concept of the system-level simulator including its advantages and limitations is explained. Then, network performance prediction results from a set of D-TxAA system-level simulations are presented and discussed. I relate the obtained statistics of the average user throughput to fairness measures and compare different network setups by means of their average and maximum sector throughputs. I also shortly discuss the consequences of the double-stream operation onto the fairness in the network. Some of these results have been published in [14].

Consecutively, a novel RLC-based stream number decision algorithm with enhanced robustness against signaling errors from the UE side is proposed [18]. The system-level simulator is also utilized to conduct performance evaluations of an optimized cross-layer scheduler. Also the achievable Quality of Experience (QoE) gains in an HSDPA network [19, 20] are investigated. Finally, by extending the proposed system-level model, Common Pilot CHannel (CPICH) power optimizations for various antenna configurations are performed [21]. The presented results give the optimum average CPICH power values maximizing the HSDPA link-quality.

The findings presented in this chapter can be summarized as follows:

- A flexible system-level simulator concept suitable for performance analysis and algorithm testing in the MAC layer is proposed [14].

- New MIMO HSDPA network performance results including guidelines for the network planing are derived [14].

- A robust RLC stream number decision algorithm, residing in the NodeB is developed. The algorithm is able to outperform UE based stream number determining in case of short channel coherence time [18].

- A novel cross-layer content-aware scheduler exploiting information about the physical-layer link-quality to increase the QoE for streamed videos in an HSDPA network is proposed [19, 20].

- Optimum CPICH power values for various antenna deployments, channel characteristics, and MIMO transmission modes are evaluated [21].

Chapter 5: Multi-User MMSE Equalization for MIMO Enhanced HSDPA

The previous chapters were based on the assumption of a classical single-user MMSE receiver. In Chapter 5, however, I investigate the structure of the intra-cell interference when multiple users are simultaneously active. In fact, the special form of the interference imposed by the multi-user Transmit Antenna Array (TxAA) transmission requires an enhanced system model to derive an interference-aware MMSE equalizer. The proposed equalizer takes the *pre-coding state* of the cell into account. By means of system-level analysis, I investigate the interference suppression capabilities and the theoretical performance limits of the developed receiver when perfect knowledge of the pre-coding state is available [17, 22, 23]. In a practical setup, however, only the pre-coding information of the desired user is known. The basic principle applied to

derive a suitable blind estimator is the Gaussian Maximum Likelihood (ML) approach. Some semi-analytical results on the complexity order of the interference-aware equalizer and the pre-coding state estimator also show that the overall complexity increase is only moderate [24].

Finally, physical-layer and system-level simulations are performed that show significant throughput performance gains of the interference-aware MMSE equalizer compared to the classical single-user MMSE equalizer [25].

In short, the main contributions of this chapter are:

- A system model representing the TxAA multi-user interference structure is presented, the corresponding MMSE equalizer is derived, and its theoretical limits are investigated [17, 22, 23].

- A training-based and a blind pre-coding state estimator are developed and their performances are compared [25].

- Physical-layer and system-level simulation results show the large throughput performance gain of the proposed interference-aware MMSE equalizer [24, 25].

Chapter 6: Conclusions

Chapter 6 concludes the main part of my thesis. The contributions and implications of my presented work are discussed. I also elaborate on the lessons learned and give an outlook on possible further research.

Appendix A: Additional Informative Material

The first appendix combines additional information and details on the explanations in the main chapters of the thesis. I give further information on some of the HSDPA concepts that are not necessarily needed for the expert in the context of the presented work, but still lead to a better understanding of the subject. Details on the assumptions, theorems, and algorithms referenced and utilized in the main part of the thesis are also discussed. Additional simulation results for some of the findings in the main part round off the information presented in this chapter.

Appendix B: Further System-Level Modeling, Simulations, Optimizations, and Validation

The main part of this thesis addresses MIMO HSDPA. However, currently SISO HSDPA is still the standard deployed in wireless networks. Thus, this appendix presents some system-level research for SISO HSDPA [26] that I have conducted as part of a cooperation with mobilkom austria AG.

Furthermore, some of the signaling channels of HSDPA are allowed to utilize Space-Time Transmit Diversity (STTD) schemes. Thus a link-quality model based on Alamouti encoded transmission is studied here [15]. These findings are not necessary for the work in the main part of the thesis. Nevertheless they might be useful for future extended system-level simulations.

Chapter 2.

HSDPA and its MIMO Enhancements

> However far modern science and techniques have fallen short of their inherent possibilities, they have taught mankind at least one lesson: Nothing is impossible.
>
> *(Lewis Mumford)*

RADIO access evolution attempts to enable the smooth usage of modern applications in wireless telecommunication networks. Since the introduction of the Global System for Mobile communications (GSM) in 1991, the ecosystem of equipment vendors, application providers and service enablers has grown significantly. Moreover, the development and availability of wireless broadband techniques now allows for an even tighter integration of web-based services on mobile devices. In the context of wireless networks, the key parameters defining the application performance include the data rate and the network latency. Some applications require only low bit rates of a few tens of kbit/s but demand very low delay, like Voice over IP (VoIP) and online games [27]. On the other hand, the download time of large files is only defined by the maximum data rate, and latency does not play a big role.

In terms of penetration, mobile wireless telephony has passed the fixed line volumes already in 2004, whereas the broadband coverage is still lacking behind [28]. However, the mobile broadband (data cards) penetration rate for example in Austria has now (2009) reached 11.4 % [29]. Current surveys forecast a maximum penetration of approximately 25 % for European markets [30].[1] HSDPA playes a big, if not the most important role in the success of mobile broadband services. The dramatic push of the typical data rates, as well as the achievable peak data rate compared to UMTS together with the lowered latency received a lot of attention from customers. In addition, the rapid decline in prices [31] and the low cost hardware to connect conveniently to HSDPA networks are very attractive for the end users. Nowadays, no or only little effort is required to adapt Internet applications to the mobile environment.

Essentially, HSDPA for the first time offers a broadband wireless access with seamless mobility and extensive coverage. Together with High-Speed Uplink Packet Access (HSUPA), HSDPA forms the so-called High-Speed Packet Access (HSPA), which can be deployed on top of the existing WCDMA UMTS networks, either on the same carrier,[2] or—for high capacity and high bit rate—on another carrier thus consequently denoting a pure HSDPA operation. The ever increasing demand for HSDPA broadband wireless access however drives mobile network operators to allocate their spectrum resources in a progressive way towards HSPA usage.

---

[1] In Indonesia actually, HSDPA broadband access passed the fixed broadband access in 2008!

[2] This requires the split of the spreading code resources in the cell.
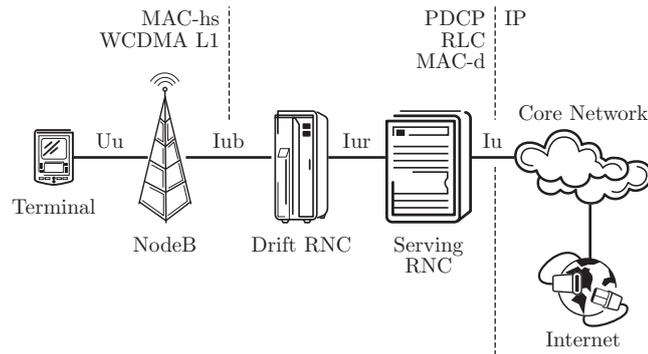
Figure 2.1.: Network architecture for HSDPA including the protocol gateways.

2.1. HSDPA Principles

The introduction of HSDPA in the 3GPP Release 5 implied a number of changes in the whole system architecture. As a matter of fact, not only the terminal but also the NodeB and the Radio Network Controller (RNC) were affected [32].

2.1.1. Network Architecture

The principal network architecture for the operation of HSDPA is still equal to the architecture for UMTS networks [3], see Figure 2.1. Basically, the network can be split in three parts, (i) the UE or terminal connected via the Uu interface, (ii) the Universal mobile telecommunications system Terrestrial Radio Access Network (UTRAN), including everything from the NodeB to the serving RNC, and (iii) the core network, connected via the Iu interface, that establishes the link to the internet. Within the UTRAN, several NodeBs—each of which can control multiple sectors[3]—are connected to the drift RNC via the Iub interface. This intermediate RNC is needed for the soft handover functionality in Release 99, and is also formally supported by HSDPA. However, for HSDPA, soft handover has been discarded, thus eliminating the need to run user data over multiple Iub and Iur interfaces to connect the NodeB with the drift RNCs and the serving RNC. This also implies that the HSDPA UE is only attached to one NodeB, and in case of mobility a hard-handover between different NodeBs is necessary. In conclusion, the typical HSDPA scenario could be represented by just one single RNC [33], allowing me to treat it as a single RNC in this work.

For the HSDPA operation, the NodeB has to handle downlink scheduling, dynamic resource allocation, Quality of Service (QoS) provisioning, load and overload control, fast Hybrid Automatic Repeat reQuest (HARQ) retransmission handling, as well as the physical layer processing itself. The drift RNC on the other hand performs the layer two processing and keeps control over the radio resource reservation for HSDPA, downlink code allocation and code tree handling, overall load and overload control, as well as admission control. Finally, the serving RNC is responsible for the QoS parameters mapping and handover control.

The buffer in the NodeB in cooperation with the scheduler enables having a higher peak data rate for the radio interface Uu than the average rate on the Iub. For 7.2 Mbit/s terminal devices,

---

[3]In this work, I use the following terminology: a *NodeB* (that means base-station, or site) contains multiple *cells* (that means sectors) in a sectored network.

Application Layer (Encoder)	Application side
RTP Real-Time Transport Protocol	
UDP User Datagram Protocol	Core-Network transport
IP Internet Protocol	
PDCP Paket Data Convergence Protocol	Gateway
RLC Radio Link Control	Physical layer coordination
MAC-d	
MAC-c/sh	
MAC-hs	Wireless transmission handling
PHY Physical Layer	
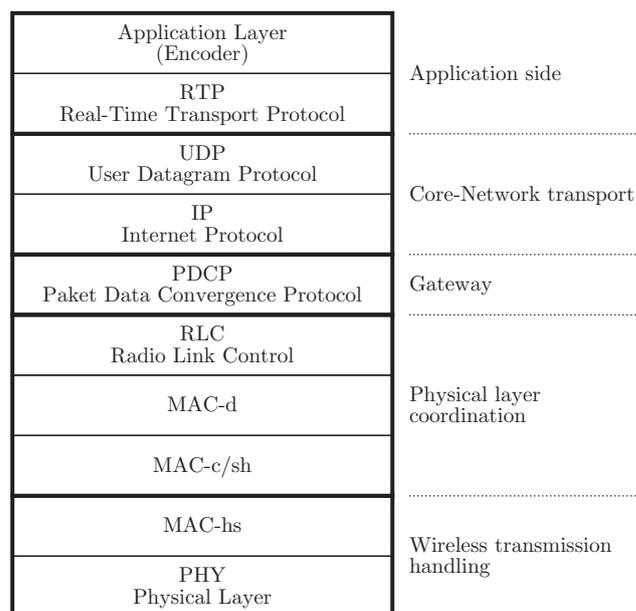
Figure 2.2.: Protocol design in UMTS from the application to the physical layer.

the Iub connection speed can somewhere be chosen around 1 Mbit/s [33]. With the transmission buffer in the NodeB, the flow control has to take care to avoid potential buffer overflows.

In the core network, the Internet Protocol (IP) plays the dominant role for packet-switched interworking. On the UTRAN side, the headers of the IP packets are compressed by the Packet Data Convergence Protocol (PDCP) protocol to improve the efficiency of small packet transmissions, for example VoIP. The RLC protocol handles the segmentation and retransmission for both user and control data. For HSDPA the RLC may be operated either (i) in unacknowledged mode, when no RLC layer retransmission will take place, or (ii) in acknowledged mode, so that data delivery is ensured. The MAC layer functionalities of UMTS have been broadened for HSDPA, in particular a new MAC protocol entity, the Medium Access Control for High-Speed Downlink Packet Access (MAC-hs) has been introduced in the NodeB. Now, the MAC layer functionalities of HSDPA can operate independently of UMTS, but take the overall resource limitations in the air into account. The RNC retains the Medium Access Control dedicated (MAC-d) protocol, but the only remaining functionality is the transport channel switching. All other functionalities, such as scheduling and priority handling, are moved to the MAC-hs. Figure 2.2 illustrates the stack of protocols in UMTS based networks including their purpose.

For the operation of HSDPA, new transport channels and new physical channels have been defined. Figure 2.3 shows the physical channels as employed between the NodeB and the UE, as well as their connection to the utilized transport channels and logical channels [34]. The physical channels correspond in this context to the *layer one* of the Open Systems Interconnection (OSI) model, with each of them being defined by a specific carrier frequency, scrambling code, spreading code,[4] as well as start and stop timing. For the communication to the MAC layer, the physical channels are combined into the so-called transport channels. In HSDPA operated networks, only two transport channels are needed, (i) the High-Speed Downlink Shared CHannel (HS-

---

[4]Also called *channelization code.*
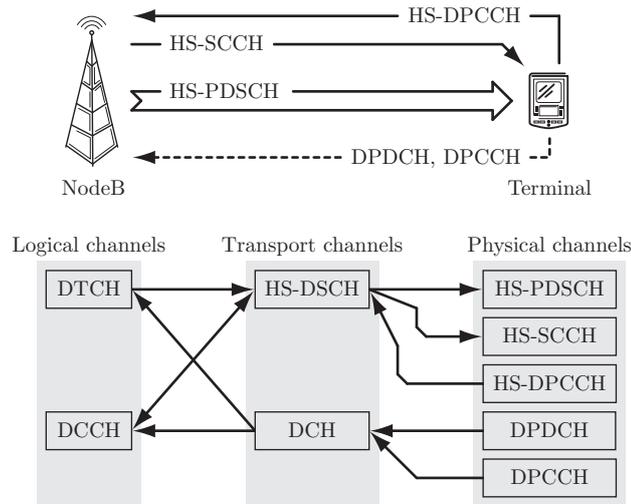
Figure 2.3.: Communication channel design of HSDPA. Downlink information is illustrated by arrows pointing towards the physical channels, and vice versa.

DSCH), responsible for carrying the downlink information (both data and control), and (ii) the Dedicated CHannel (DCH), responsible for carrying the uplink information (again, both uplink and control). Finally, the logical channels are formed in the MAC to convey the information to the higher layers, headed by the RLC layer. In particular, for the HSDPA operation, there are two logical channels, (i) the Dedicated Traffic CHannel (DTCH), carrying data, and (ii) the Dedicated Control CHannel (DCCH), carrying control information.

2.1.2. Physical Layer

HSDPA utilizes the same WCDMA based transmission scheme as UMTS with the basic idea of utilizing spreading codes to introduce individual physical channels [33]. Furthermore, scrambling codes are used to distinguish different NodeBs. However, for HSDPA many important innovations have been included in the WCDMA context. Let me start by first elaborating on the utilized physical channels as depicted in Figure 2.3 [34].

HS-PDSCH – The High-Speed Physical Downlink Shared CHannel is used to carry the data from the HS-DSCH. Each HS-PDSCH corresponds to exactly one spreading code with fixed spreading factor SF = 16 from the set of spreading codes reserved for HS-DSCH transmission. The HS-PDSCH does not carry any layer one control information.

HS-SCCH – The High-Speed Shared Control CHannel carries downlink signaling related to the HS-DSCH transmission. It also has a fixed spreading factor SF = 128 and carries a constant rate of 60 kbit/s.

HS-DPCCH – The High-Speed Dedicated Physical Control CHannel carries uplink feedback signaling related to the HS-DSCH transmission and to the HS-SCCH control information. The spreading factor of the HS-DPCCH is SF = 256, which corresponds to a fixed rate of 15 kbit/s.

DPDCH – The Dedicated Physical Data CHannel is used to carry the uplink data of the DCH transport channel. There may be more than one DPDCH on the uplink, with the spreading factor ranging from SF = 256 down to SF = 4.

DPCCH – The Dedicated Physical Control CHannel carries the layer one control information associated to the DPDCH. The layer one control information consists of known pilot bits to support channel estimation for coherent detection, Transmit Power-Control (TPC) commands, FeedBack Information (FBI), and an optional Transport-Format Combination Indicator (TFCI). The DPCCH utilizes a spreading factor of SF = 256, which corresponds to a fixed rate of 15 kbit/s.

In WCDMA, thus also in HSDPA, timing relations are denoted in terms of multiple of chips. In the 3GPP specifications, suitable multiples of the chips are: (i) a *radio frame* which is the processing duration of 38 400 chips,[5] corresponding to a duration of 10 ms, (ii) a *slot* consisting of 2 560 chips, thus defining a radio frame to comprise 15 slots, and (iii) a *sub-frame*, which corresponds to three slots or 7 560 chips, which is also called Transmission Time Interval (TTI), because it defines the basic timing interval for the HS-DSCH transmission of one *transport block*.

The general HSDPA operation principle brings a new paradigm in the dynamical adaptation to the channel as utilized in UMTS. Formerly relying on the fast power control [3], now the NodeB obtains information about the channel quality of each active HSDPA user on the basis of physical layer feedback, denoted CQI [7]. Link adaptation is then performed by means of Adaptive Modulation and Coding (AMC), which allows for an increased dynamic range compared to the possibilities of the fast power control. The transport format used by the AMC, that is modulation alphabet size and effective channel coding rate, is chosen to achieve a chosen target BLER.[6] Now one may ask why a system should be operated at an error rate that is bound above zero. Two main arguments for this basic ideology of link adaptation is that (i) in practical systems the UE has to inform the network about the correct or incorrect reception of a packet. Since this information is needed to guarantee a reliable data transmission, it makes no sense to push the error probability of the data channel lower than the error rate of the signaling channel. Furthermore, by fixing the BLER to a given value, (ii) the link adaptation has the possibility to remove outage events of the channel.

On top of the link adaptation in terms of the modulation alphabet size and the effective coding rate, HSDPA can take excessive use of the multi-code operation, up to the full spreading code resource allocation in a cell. The other new key technology is the physical-layer retransmission. Whereas in UMTS retransmissions are handled by the RNC, in HSDPA the NodeB buffers the incoming packets and in case of decoding failure, retransmission automatically takes place from the base station, without RNC involvement. Should the physical layer operation fail, then RNC based retransmission may still be applied on top. Finally, as already mentioned, the NodeB now is in charge of the scheduling and resource allocation. Table 2.1 summarizes the key differences between UMTS and HSDPA [33].

HSDPA User Data Transmission

Together with the various new features as listed in Table 2.1, Release 5 HSDPA also came along with the support of higher order modulation, in particular 16 QAM. This made it necessary that not only the phase has to be estimated correctly—as in the UMTS case—but also the amplitude

---

[5]In the 3GPP WCDMA systems, the chip rate is fixed at 3.84 Mchips/s, utilizing a bandwidth of 5 MHz.

[6]One block denotes one TTI in HSDPA.

Table 2.1.: Fundamental properties of UMTS and HSDPA [33].

Feature	UMTS	HSDPA
Variable spreading factor	No	No
Fast power control	Yes	No
Adaptive Modulation and Coding	No	Yes
Multi-code operation	Yes	Yes, extended
Physical-layer retransmissions	No	Yes
NodeB-based scheduling and resource allocation	No	Yes
Soft handover	Yes	No

needs to be evaluated. HSDPA utilizes for this purpose the CPICH which offers the phase information directly, and can be used to estimate the power offset to the HS-DSCH power level. This suggests that the NodeB should avoid power changes during the TTI period [33]. The user allocation due to the NodeB based scheduling happens every TTI, adapting the modulation and coding to the channel quality information as received from the UE.

The coding for the HS-DSCH is turbo-coding of rate $1/3$,[7] and there is only one transport channel active at a time, thus fewer steps in multiplexing/de-multiplexing are needed [35]. Each TTI, a Cyclic Redundancy Check (CRC) field is appended to the user data to allow for detection of decoding failure. To gain as much as possible from eventually necessary retransmissions, the UE stores the received data in a buffer. When the NodeB retransmits exactly the same chips, the UE can combine the individual received bits in a maximum ratio combining sense, called *soft combining*. However, in HSDPA, the HARQ stage is capable of changing the rate matching between retransmissions, thus tuning the redundancy information. The relative number of parity bits to systematic bits accordingly varies, which can be exploited by the receiver in the UE to achieve an additional *incremental redundancy* gain when decoding the packet [36–38].

HSDPA Control Information Transmission

Control information for the downlink of HSDPA is exchanged on the HS-SCCH and the HS-DPCCH. The HS-SCCH carries time-critical signaling information which allows the terminal to demodulate the assigned spreading codes. Its information can be split into two parts, with the first part comprising the information needed to identify the relevant spreading codes in the HS-DSCH. The second part contains less urgent information, such as which HARQ process is being transmitted, if the transmission contains new data, or if not, which redundancy version has been used for channel encoding as well as the transport block size. For every simultaneously active user in the cell there is one distinct HS-SCCH necessary, such that the individual terminals know their relevant decoding information as depicted in Figure 2.4. The individual HS-SCCHs are scrambled with user-specific sequences, which depends on the user identification number managed by the NodeB. To avoid errors due to wrong control information, the second part of the HS-SCCH is protected by a CRC.

For the link adaptation and the retransmission handling, HSDPA needs uplink physical layer feedback information. This uplink information is carried on the HS-DPCCH. It contains the HARQ information regarding the decoding of the last received packet, and the CQI information

---

[7]This is due to the fact that the turbo-encoder used is based on the 3GPP Release 99 turbo-encoder.
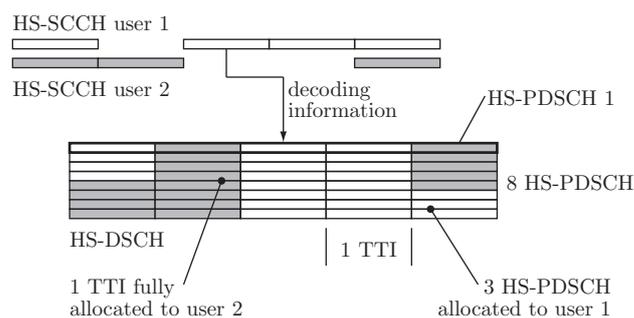
Figure 2.4.: Multi-user transmission on the HS-DSCH. Every user needs his own HS-SCCH to obtain the necessary decoding information.
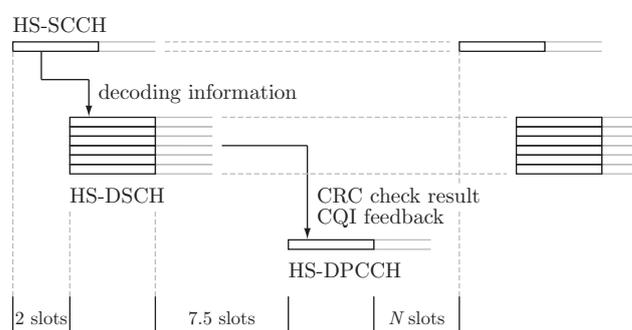
Figure 2.5.: HSDPA timing relations between the main physical channels.

of the current channel state. The CQI reporting frequency is controlled by a system parameter signaled by higher layers. The evaluation of the CQI report is defined in an abstract way in [7], which leaves the practical implementation open to the vendors.[8]

HSDPA Timing Relations

HSDPA is synchronous in terms of the terminal response for a packet transmitted in the downlink. The network side, on the other hand, is asynchronous in terms of when a packet or a retransmission for an earlier transmission is sent. This provides the NodeB scheduler the necessary freedom to act according to its decision metric, buffer levels, and other relevant information. The terminal operation times between the different events are specified accurately from the HS-SCCH reception on [7,34], especially the transmission of the HS-DPCCH is accurate within a 256 chip window, corresponding to any variations due to the need for symbol alignment. Figure 2.5 depicts the timing relations between the main downlink HSDPA channels.

Terminal Capabilities

The support of the HSDPA functionality is optional for the terminals. Furthermore, the requirements of the high-speed data transmission, in particular the higher order modulation, the code-multiplex of different spreading codes, the minimum interval time between two consecutive utilized TTIs for data transmission, and the dimensioning of the buffer storing the received

---

[8]A practical implementation possibility can for example be found in [39].

samples for retransmission combining put tough constraints on the equipment. Accordingly, the 3GPP defined twelve UE *capability classes* effectively specifying the maximum throughput that can be handled by the device [7, 40]. The highest capability is provided by category ten, which allows the theoretical maximum data rate of 14.4 Mbit/s. This rate is achievable with one-third rate turbo coding and significant puncturing,[9] resulting in a code rate close to one. For a list of terminal capability classes, see for example [33].

2.1.3. MAC Layer

The HSDPA MAC layer comprises three key functionalities: (i) the scheduling, (ii) the HARQ retransmission handling, and (iii) the link adaptation, respectively resource allocation [41]. Note that the 3GPP specifications do not contain any parameters for the scheduler operation, which is left open for individual implementation to the vendors. Similar arguments hold for the other two functionalities, with the exception that (ii) and (iii) have to obey more stringent restrictions due to the interworking with the UE side.

For the operation of the HARQ retransmissions, the MAC-hs layer has to consider some important points. To avoid wasting time between transmission of the data block and reception of the ACKnowledged (ACK)/Non-ACKnowledged (NACK) response, which would result in lowered throughput, multiple independent HARQ *processes* can be run in parallel within one HARQ entity. The algorithm in use for this behavior is an N Stop And Wait (N-SAW) algorithm [42]. However, the retransmission handling has to be aware of the UE minimum inter-TTI interval for receiving data, which depends on the UE capability class.

The terminal is signaled some MAC layer parameters, with the MAC-hs Packet Data Unit (PDU) consisting of the MAC-hs header and the MAC-hs payload. It is built by one or more MAC-hs Service Data Units (SDUs) and potential padding if they do not fit the size of the transport block available. As the packets are not arriving in sequence after the MAC HARQ operation, the terminal MAC layer has to cope with the packet reordering. The MAC header therefore includes a Transmission Sequence Number (TSN) and a Size Index Identifier (SID) that reveals the MAC-d PDU size and the number of MAC PDUs of the size indicated by the SID.

The MAC-d is capable of distinguishing between different services by means of MAC-d *flows*, each of which can have different QoS settings assigned. In the MAC-hs, every MAC-d flow obtains its own queue, to allow different reordering queues at the UE end. Note however that only one transport channel may exist in a single TTI and thus, in a single MAC-hs PDU. This means that flows from different services can only be scheduled in consecutive TTIs [33, 42].

2.1.4. Radio Resource Management

The Radio Resource Management (RRM) algorithms are responsible for transferring the physical layer enhancements of HSDPA to capacity gain while providing attractive end user performance and system stability. At the RNC, the HSDPA related algorithms include physical resource allocation, admission control and mobility management. On the NodeB side, RRM includes HS-DSCH link adaptation, the already explained packer scheduler and HS-SCCH power control.

In order for the NodeB to transmit data on the HS-DSCH, the controlling RNC needs to allocate channelization codes and power for the transmission. As a minimum, one HS-SCCH code and one HS-PDSCH code have to be assigned to the NodeB. The communication between the RNC and the NodeB follows the NodeB Application Part (NBAP) protocol [43]. In case

---

[9]Puncturing is performed in the rate-matching stage.
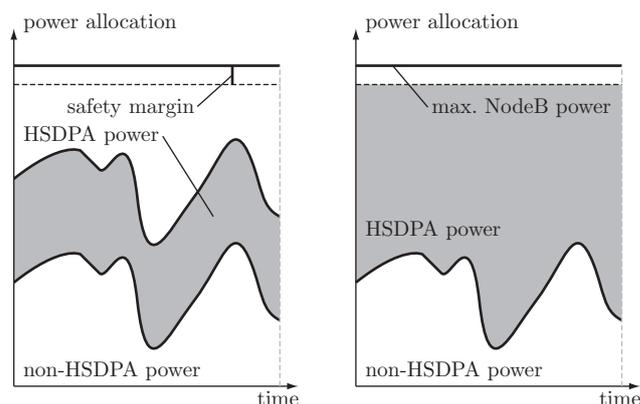
Figure 2.6.: HSDPA power allocation principles: the left figure depicts the explicit power allocation by means of NBAP messages (i), while the right figure is the fast NodeB based power allocation (ii).

that both HSDPA and UMTS traffic are operated on the same carrier, the RNC can assign and release spreading codes to HSDPA dynamically to prevent blocking of UMTS connections.

Another scarce downlink resource is the transmission power. The power budget for a cell consists of the power needed for common UMTS channels, like the CPICH, power for the UMTS transmissions, and power for the HSDPA transmission. In principle, there are two different possibilities of allocating the power of HSDPA in the base station downlink power budget [44]:

(i) The RNC can dynamically allocate HSDPA power by sending NBAP messages to the NodeB, which effectively keeps the HSDPA power at a fixed level, whereas the UMTS power varies according to the fast closed loop power control.

(ii) The other option is that no NBAP messages are sent and the base station is allowed to allocate all unused power for HSDPA.

The behavior is illustrated in Figure 2.6. Note that some safety margin has to be reserved in order to account for unpredictable variations of the non-HSDPA power, for example due to the fast power control of UMTS.

The HS-DSCH link adaptation at the NodeB is adjusted every TTI. In order for the UE to determine the current transmit power utilized by the HS-DSCH, the RNC sends a Radio Resource Control (RRC) message, which contains the power offset Γ in relation to the CPICH. A simple link adaptation algorithm would follow the CQI values reported by the UE directly. However, when a change in Γ occurs, the NodeB has to take that into account and remap the CQI value accordingly. The HS-SCCH is the exception to the AMC link adaptation of HSDPA. This channel is power controlled, where the 3GPP specifications do not explicitly specify any power control mechanism. Some ideas about the implementation of a power control for the HS-SCCH can be found in [33].

The last RRM algorithm is the packet scheduler, which determines how to share the available resources to the pool of users eligible to receive data. There are numerous scheduler ideas established, the most famous and well-known are

- the round robin scheduler, which assigns the physical resources equally amongst all active users in the cell,

- the maximum carrier-to-interference ratio scheduler, which assigns the physical resources to the user with the best carrier-to-interference ratio in order to maximize the cell throughput,[10] and

- the proportional fair scheduler trying to balance between throughput maximization and fairness.[11]

Besides these allocation strategies, the scheduler can schedule multiple users within one TTI. Up to 15 HS-PDSCH may be used by the NodeB, which gives the scheduler the freedom to maximize spectral efficiency when scheduling more than one user at once. On the other hand, the scheduler may require a multi-user policy, if there are many HSDPA users that require a low source data rate but strict upper bounds on the delay, like for example VoIP.

2.2. MIMO Enhancements of HSDPA

MIMO techniques are regarded as the crucial enhancement of todays wireless access technologies to allow for a significant increase in spectral efficiency. They have drawn attention since the discovery of potential capacity gains [4,48] which has motivated the scientific community to consider the potential of MIMO to increase user data rates, system throughput, coverage, and QoS with respect to delay and outage. Basically, MIMO as a technique offers two gain mechanisms: (i) *diversity*, including *array gain* [49], and (ii) *spatial multiplexing gain*.[12]

The spatial multiplexing gain can be observed by investigating the ergodic channel capacity of a MIMO link. Consider an i.i.d. Rayleigh block fading channel $\mathbf{H}$ between N_T transmit and N_R receive antennas with an receive antenna Signal-to-Noise Ratio (SNR) ϱ. The ergodic capacity of the MIMO channel when no CSI is available at the transmitter,

$$C_\mathrm{E} = \mathbb{E}\{C(\mathbf{H})\} = \mathbb{E}\left\{\log_2 \det\left(\mathbf{I} + \frac{\varrho}{N_\mathrm{T}}\mathbf{H}\mathbf{H}^\mathrm{H}\right)\right\} = \mathbb{E}\left\{\sum_{i=1}^{r}\log\left(1 + \frac{\varrho}{N_\mathrm{T}}\lambda_i\right)\right\}, \qquad (2.1)$$

can be interpreted to unravel multiple scalar spatial pipes, also called *modes*, between the transmitter and the receiver. The number of non-zero eigenvalues λ_i of $\mathbf{H}\mathbf{H}^\mathrm{H}$, defined by the rank r of the matrix $\mathbf{H}$, corresponds to the number of parallel independent data *streams* that can be transmitted simultaneously. This specifies the spatial multiplexing gain of the channel. In general, the capacity increase due to the utilization of MIMO can be approximated by [51]

$$C_\mathrm{E} \approx \min\{N_\mathrm{T}, N_\mathrm{R}\} \log_2\left(\frac{\varrho}{N_\mathrm{T}}\right), \qquad (2.2)$$

where $\min\{N_\mathrm{T}, N_\mathrm{R}\}$ defines the spatial multiplexing gain. Thus, every $3\,\mathrm{dB}$ increase in receive SNR results in $\min\{N_\mathrm{T}, N_\mathrm{R}\}$ additional bits of capacity at high SNR. This behavior is depicted in the left part of Figure 2.7. Clearly, the spatial multiplexing gain—thus the number of simultaneously transmitted data streams—in the $N_\mathrm{T} \times N_\mathrm{R} = 4 \times 2$ case is the same as in the 2×2 case.

---

[10]In fact, the maximum carrier-to-interference ratio scheduler tries to maximize the achievable sum-throughput for every TTI which for a single-user scheduler results in scheduling the user with the maximum carrier-to-interference ratio.

[11]A possible definition of *fairness*, in terms of allocation fairness and data-rate fairness can be found in [45–47], and is treated in greater detail in Section 4.2.

[12]More recently, the spatial multiplexing gain of MIMO systems is studied in the more general framework of the *degrees of freedom* [50], which also can be extended to whole networks.
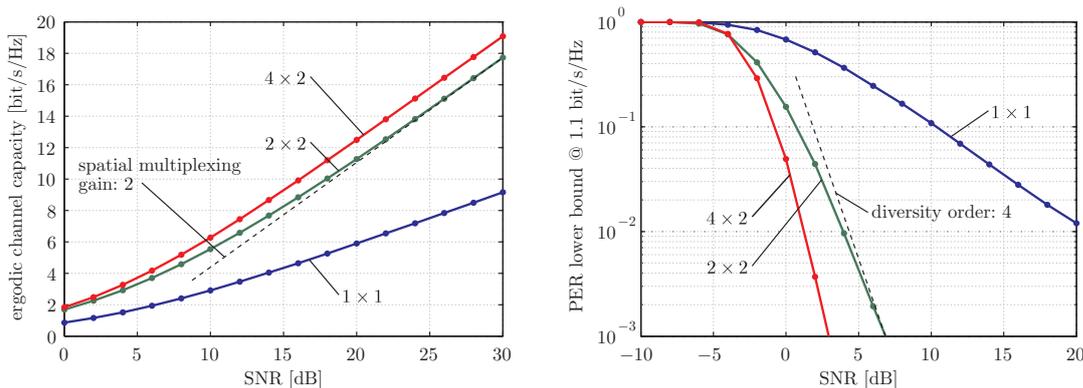
Figure 2.7.: Ergodic channel capacity and PER lower bound for i.i.d. Rayleigh block fading MIMO channels without CSI at the transmitter. The spatial multiplexing gain and the diversity orders can be observed by determining the slopes of the curves.

However, an additional array gain—noticeable by the shift to the left—can be observed. The array gain, however, diminishes quickly with the number of transmit antennas, thus effectively limiting the benefits of only adding spatial resources at the transmitter side.

Diversity, on the other hand, describes the error probability decrease as a function of the SNR. MIMO channels can offer significant improvement in terms of diversity. If perfect channel codes are considered and the transmitter has no CSI again, the Packet Error Ratio (PER) will equal the outage probability for that signaling rate. This also defines the *outage capacity* of MIMO channels. Thus, for a system with unity bandwidth transmitting packets with a bit rate R, the PER can be lower bounded by

$$\Pr\{\text{packet error}\} \geq \Pr\{C(\mathbf{H}) < R\}. \tag{2.3}$$

The magnitude of the slope of the PER curve then can be used to define the diversity order of the MIMO system. It has been shown that the achievable slope can be up to $N_\mathrm{T}N_\mathrm{R}$ for fixed rate transmissions [52], which directly implies that every antenna deployed can increase the diversity order. The right part of Figure 2.7 illustrates the diversity order, which can be read off the slope of the PER lower bound, that is, the orders of magnitude gained by an increase of $10\,\mathrm{dB}$ in the receive SNR [53]. I chose the rate at which the lower bound is evaluated to be $1.1\,\mathrm{bit/s/Hz}$, because this is the expected spectral efficiency of MIMO enhanced HSDPA. A rigorous definition of the terms spatial-multiplexing gain and diversity can be found in [54].

The spatial-multiplexing and the diversity gain are strongly influenced by antenna correlation at the transmitter and the receiver side, as well as path-coupling, also called *bottleneck scenario* [49]. Accordingly, receiver antenna deployment is not the main focus, since the average mobile terminal will only have limited space and battery capacity impeding complex signal processing algorithms. Furthermore, additional Radio Frequency (RF) frontends needed for multi-antenna operation would increase the terminal costs significantly. Thus, in mobile communications emphasis has been put on transmitter antenna processing techniques, in particular

- spatial multiplexing schemes, like for example Vertical Bell Laboratories Layered Space-Time (V-BLAST) techniques [4], trying to extract the gain in spectral efficiency of the MIMO channel, or

- diversity schemes, like for example Alamouti space-time coding [55], trying to extract the diversity gain offered by the MIMO channel.

Both classes of schemes can in principle be operated in *closed loop* mode—utilizing feedback information provided by the UE—or *open loop* mode, which does not rely on feedback.

Current insights [56] suggest that for variable rate link adapted systems with HARQ retransmission spatial multiplexing is the best choice, even for high UE speed scenarios. However, STTD techniques are considered to be very useful for signaling channels which operate at a fixed rate and without retransmissions, called *un-acknowledged* mode. Other Space-Time Block Codes (STBCs) are not considered for WCDMA MIMO extensions at the moment, but are discussed for future generation wireless networks. One example is the Golden-STBC, which achieves full-rate and full-diversity [57].

2.2.1. Physical Layer Changes

Focusing on the FDD mode of HSDPA, 3GPP has considered numerous proposals for the MIMO enhancement [6]. The most promising ones were (i) Per-Antenna Rate Control (PARC), (ii) Double Space-Time Transmit Diversity with Sub-Group Rate Control (DSTTD-SGRC), and (iii) D-TxAA. In late 2006, the 3GPP finally decided in favor of D-TxAA to be the next evolutionary step of the classical SISO HSDPA, which—among many other changes—established the 3GPP Release 7. D-TxAA offers the flexibility to exploit the MIMO gains, spatial multiplexing and diversity, respectively, and tries to benefit from channel quality adaptability by means of closed loop feedback.

This scheme focuses on two transmit and two receive antennas. An overview of the D-TxAA scheme is depicted in Figure 2.8. Channel coding, interleaving, as well as spreading and scrambling—the Transport CHannel (TrCH) processing—are implemented as in the non-MIMO mode, with a *primary transport block* being always present. However, now the physical layer supports the transport of a *secondary transport block* to a UE within one TTI. This simultaneous transmission of two code-words aims at the spatial multiplexing gain of the MIMO channel. The pre-coding on the other hand is designed to extract (at least some) of the diversity offered. The pre-coding weights for the TxAA operation of the transmitter are determined from a quantized set by the UE [7], and serve as *beamforming* to maximize the receive SINR. In case of a single-stream transmission, the primary pre-coding vector, determined by $[w_1, w_2]^{\mathrm{T}}$, is utilized for the transmission of the primary transport block. In a double stream transmission, the secondary pre-coding vector $[w_3, w_4]^{\mathrm{T}}$ is chosen orthogonal to the primary one. This has the benefit of increasing the separation of the two streams in the signal space [58], and also keeps the amount of feedback bits constant for single and double stream transmission modes. The two CPICHs are utilized for the channel estimation, receive power evaluation, and serving NodeB evaluation.

The evaluated feedback in form of the Precoding Control Information (PCI) is fed back to the NodeB within a composite CQI/PCI report on the HS-DPCCH which implies a change in the meaning of the feedback bits compared to Release 5 HSDPA [34].[13] In order for a particular UE receiver to adapt to the pre-coding utilized by the NodeB for this user at the time of the transmission, the currently employed pre-coding weights are signaled on the HS-SCCH.

Theoretically, D-TxAA allows for a doubled data rate compared to the actual possible SISO HSDPA data rates [59], which can be utilized in high SNR regions. In principle, the scheme

---

[13]I will use the terms *Release 5 HSDPA* and *SISO HSDPA* interchangeably.
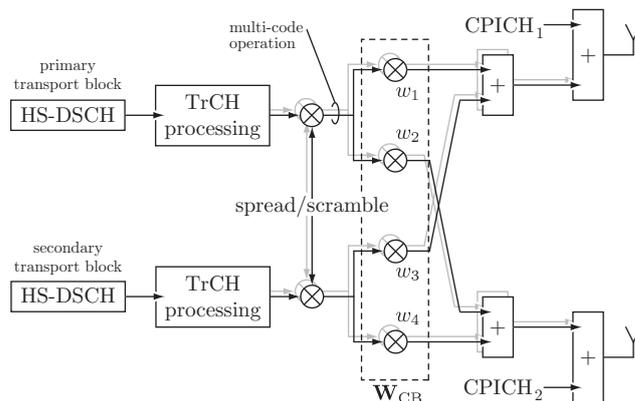
Figure 2.8.: Overview of the D-TxAA transmitter scheme for MIMO enhanced HSDPA.

can also be extended to systems with more than two transmit antennas on the transmit and/or the receiver side, and findings in this research area currently influence the standardization of the 3GPP LTE development.

With the introduction of a second simultaneously transmitted stream, 3GPP also had to update the CQI reporting to support individual reports for the individual streams. This ensures an independent link adaptation. Accordingly, the UE has to report two CQI values depending on the channel quality as seen by the corresponding stream. In practice, the signaling of the two CQI values is performed in a combined way, thus only one equivalent CQI value is fed back to the NodeB [7]. To evaluate the Transport Format Combination (TFC) for the consecutive transmission to this particular user, the network utilizes a mapping from the CQI value to the TFCI, which specifies the transmission parameters. These mappings, however, depend on the UE capabilities. The 3GPP thus introduced two new UE capability classes, namely 15 and 16, in Release 7. For both UE classes, the mapping tables for the single stream and the double stream transmission are defined in [7]. An excerpt of the CQI mapping Table I, which is used in the double stream transmission mode for UEs of capability class 16 is given in Table 2.2, which holds for the CQI of both streams, respectively. The Transport Block Size (TBS) specifies the number of bits transported within one TTI. It has to be noted that, in contrast to the Release 5 SISO HSDPA mapping tables where obviously only one stream is transmitted, a CQI value of zero does not denote an *out of range* report. As a matter of fact, in unfavorable channel conditions the network would be wise to switch to a single stream transmission long before the UE becomes out of range. Furthermore, the TFCs for CQI values zero and one appear to be equal. However, in case of a CQI zero report, the NodeB would increase its transmission power by 3 dB [7], which is not the case for the CQI one report. Finally, the last remark I want to make is that all TFCs request an utilization of 15 multiplexed spreading codes, which leaves no room for any other data-channels operated in parallel. Although the UE is assuming the transmission of data on all 15 spreading codes for the evaluation of the CQI report, the network does not have to stick to this restriction. Based on the RNC information, the NodeB may as well assign only a subset of the 15 available spreading codes for the D-TxAA operation, which then requires a remapping of the TFC for the UE CQI reports. In addition, multi-user scheduling could still be performed by allocating each stream to one user, respectively. This transmission mode is sometimes called Multi-User (MU) MIMO HSDPA [60, 61], but is currently not included in the 3GPP standard.

Table 2.2.: Excerpt of the CQI mapping Table I [7], utilized in double stream transmissions for MIMO capable UEs.

CQI	TBS [bits]	nr. codes	modulation
0	4 581	15	4 QAM
1	4 581	15	4 QAM
2	5 101	15	4 QAM
⋮	⋮	⋮	⋮
6	11 835	15	4 QAM
7	14 936	15	16 QAM
⋮	⋮	⋮	⋮
14	27 952	15	16 QAM

As elaborated in [62], the most interesting property of MIMO HSDPA for network operators is the fact that most of the 3GPP Release 7 enhancements are expected to be software upgrades to the network, excluding of course the need for multiple antennas at the NodeB.

2.2.2. MAC Layer Changes

The MAC layer of UMTS as well needed some enhancements to support the multi-stream operation of D-TxAA. In particular, the MAC-hs now has to deal with:

  (i) a more complicated scheduling that has to distinguish between single stream and double stream transmissions,

 (ii) a more complex resource allocation problem, because a decision regarding the number of utilized streams and the power allocation of those has to be solved, and

(iii) the HARQ process handling has to be conducted for both streams in case of a double stream transmission.

Most of the questions arising in this context are not covered by the standard [41], but are rather left open for vendor specific implementation, which also leaves much room for research in terms of the RRM opportunities offered by the MIMO enhancements.

2.2.3. Simplifications of the Core Network

As part of Release 7, 3GPP also tried to simplify the core-network architecture of HSDPA. In particular, 3GPP networks more and more will be used for IP-based packet services. In Release 5, the network elements in the user and the control plane are (i) NodeB, (ii) RNC, (iii) Serving-General packet radio service Support Node (SGSN) and Gateway-General packet radio service Support Node (GGSN), see also Figure 2.1. A flat network architecture, saving unnecessary network elements, however, is expected to reduce latency and thus improve the overall performance of IP-based services. Thus, in Release 7, the user plane can tunnel the SGSN effectively reducing the number of network elements that have to process the data. This reduced overhead in terms of hardware and delay is important for achieving low cost per bit and enabling competitive flat rate offerings [62].

Chapter 3.

System-Level Modeling of MIMO-Enhanced HSDPA

> While all models are unrealistic,
> some of them are actually useful.
>
> *(George Box)*

U‌SEFUL modeling in the context of wireless networks is in general a difficult task, which requires careful investigations of many different parameter settings and a design that avoids leading to potentially wrong conclusions. *System-level modeling* is particularly demanding in this sense, because in addition to the design requirements, the computational complexity plays a crucial role.

So what is system-level modeling all about? One thing that emerges when investigating the term system-level is that it is quite extensively[1] used in the literature. As a matter of fact, every comprehensive investigation of a technical system—not only in the context of a cellular system—may be denoted system-level analysis. Examples are electronic design methodology, virtualization for operating systems, hardware-software co-design for Very High Speed Integrated Circuits (VHSIC), or network synthesis. In the scope of this work however, the term *system-level model* describes:

> A model capable of representing the physical layer of a wireless transmission system in an abstract, yet accurate way that is less complex to evaluate than computing all the algorithms and reproducing all relevant effects involved in the physical layer in their full detail, and can be described by a low number of parameters.

Given this rather conceptional definition, what are system-level models needed for? Usually, physical-layer simulations are used to identify and evaluate promising transmission techniques. Whereas these investigations are suitable for the deployment of receiver algorithms, feedback strategies, coding design, and so on, they are not directly capable of reflecting network issues like cell planing, scheduling, and interference situations in the context of massive multi-user operation [14]. Therefore, to understand the network and user performance under typical operating conditions in various deployment scenarios, network simulations are crucial [63–65]. Such a wireless network defines the *system* to which the term system-level is referring. Accordingly, *system-level simulations* are built to comprise the full network, thus trying to cover at least

(i) network deployment issues including network performance [26, 66, 67],

(ii) multi-user and multi-NodeB (inter-cell) interference [68–70],

(iii) RLC and admission control algorithms [71, 72], as well as

---

[1]For example, a search for the term *system level* on Google returned approximately 3 160 000 hits.

(iv) scheduling [73, 74].

One of the major difficulties of system-level analyses, however, is the computational complexity involved in evaluating the performance of the radio links between all base-stations and mobile terminals. Performing such a large number of individual physical-layer—or also often called *link-level*—simulations is clearly prohibitive in terms of the computational complexity. Thus, a system-level model has to simplify the physical link in a sufficiently accurate way to capture the essential behavior [12, 75–78].

To summarize, an ideal system-level model has to be (i) sufficiently accurate, (ii) flexible in terms of the scenarios it is capable of representing, as well as applicable for analytic investigations, (iii) implementable with very low computational complexity, and (iv) describable by a reasonable number of parameters. However, even an ideal model can have some traps. Let me put some advisable mistrust in the words of [79].

- Don't believe in the 33rd order consequences of a 1st order model. Catch phrase: *Cum grano salis.*[2]

- Don't extrapolate beyond the region of fit. Catch phrase: *Don't go off the deep end.*

- Don't believe the model is reality. Catch phrase: *Don't eat the menu.*

- Don't fall in love with your model. Catch phrase: *Pygmalion.*[3]

3.1. Concept of System-Level Modeling

After having defined the scope of a system-level model, it remains to sketch the concept behind it. As already mentioned, the basic idea is to find a suitable mathematical abstraction of the physical layer. Generally speaking, such a model consists of two concatenated parts. To illustrate that, Figure 3.1 shows a very abstract view of the transmission in a wireless communication system. Here, the whole transmission chain is divided in a first part handling the *physical layer processing*, which includes in HSDPA

- spreading/de-spreading, scrambling/de-scrambling

- modulation,

- pre-coding, space-time coding,

- channel estimation, synchronization, and

- receiver processing,

and a second part handling the *channel encoding and decoding* including in HSDPA

- turbo coding/decoding,

- interleaving, rate-matching, HARQ, and

- demapping.

---

[2]The direct translation would be: *With a grain of salt*, however, the saying is nowadays used to advise the reader that the point made should not be taken literally in every aspect.

[3]According to Ovid, Pygmalion is a legendary figure of Cyprus. He is told to have been a sculptor who falls in love with a statue he has made.
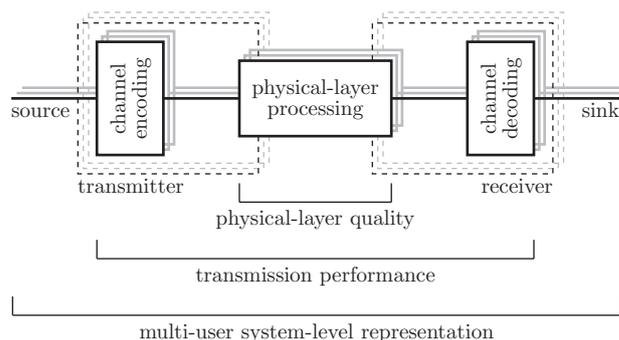
Figure 3.1.: Abstract illustration of the transmission chain in wireless communication systems.

Note that both parts incorporate the transmitter and the receiver, respectively. When introducing a split like that, the physical-layer processing can be modeled by a *link-quality model*,[4] which describes the physical-layer quality, and a *link-performance model*, describing the transmission performance with respect to the channel coding and decoding. For system-level purposes, the link-quality model has to incorporate the effects of

- the interference structure, that is intra-cell and inter-cell interference, incorporating possible multi-user interference (see again Figure 3.1),

- the influence of other channels than the evaluated one, for example the synchronization channel, or other DCH channels,

- the power allocation in the cell as well as in the whole network, and

- the channel effects, in particular the macro-scale pathloss, the antenna gain, the shadow-fading and the small-scale fading.

At this point it is important to note that the small-scale[5] fading has to be covered by the system-level model to allow for the accurate evaluation of NodeB-based schedulers, which operate on a 2 ms TTI basis in HSDPA. If those effects are covered, such a system-level model is often referred to as *actual value interface* [81, 83].

The link-performance model then has to—based on the evaluations of the link-quality model—represent the coding/decoding performance in terms of the BLER, given a link-adaptation strategy [84]. Considering the flexibility of the HSDPA physical layer, this model has to cover a wide range of conditions. Together, both models provide means to assess the figures of merit in a system-level context, and they are often commonly referred to as *system-level interface*.

Figure 3.2 depicts the relations of the two models in a system-level approach. On top of the already mentioned influencing factors, the figure also shows the connection to the algorithms and deployment issues that influence the system performance. In particular,

---

[4]This model is also often called *link-measurement model* [80]. However, in this work I will stick to the more descriptive term *link-quality model*.

[5]Sometimes in the system-level literature, for example [64, 81], the small-scale fading is denoted *fast fading*, in order to point out the difference to slowly changing channel effects like shadow-fading. However, the notation *fast* strongly depends on the relative speed of the transmitter, the receiver, and the channel, thus rendering this term rather inaccurate. Furthermore, the classical literature [82], defines fast fading to be fading which changes the channel condition within the duration of one symbol, which is usually not modeled in the system-level context. Accordingly, in the context of this work I will stick to the term *small-scale fading* for Rayleigh fading like effects.
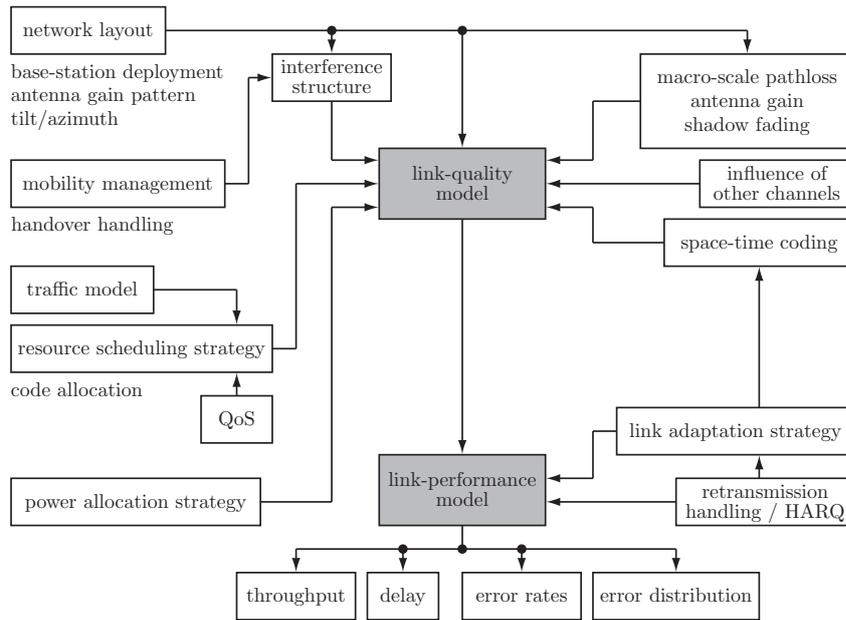
Figure 3.2.: System-level relations between the *link-quality model* and the *link-performance model* as well as other influencing parameters and algorithms.

- the network layout as well as the mobility management in the network affect the channel and interference structure,

- the power allocation strategy can adaptively enhance the physical-layer conditions in the cell, and

- the resource scheduling strategy—which depends on the traffic and the QoS settings—controls the performance in a direct way.

3.2. Applicability of other Published Work

In order to enable a comparison of a large variety of system realizations, it is desirable to have link-quality and link-performance models that are general enough to cover different multiple access strategies and receiver types. The existing system-level models for SISO WCDMA systems, for example [63, 85], cannot be used in a straightforward way for MIMO enhanced systems, and none of the published work accurately models the proposed D-TxAA scheme so far. Either the utilization of MMSE equalizers[6] is not supported [75, 86], multiple-stream operation is not covered [72], the mandatory pre-coding is missing [85], or no full analytical description is derived to be available for system-level evaluations [71, 72]. Furthermore, all of the cited work need to compute the full complex-valued MIMO channel matrix on system-level, which implies a large computational burden.

In this work, I propose a computationally efficient *system-level interface* which provides a complete analytical description of the post-equalization symbol-level SINR [13, 14]. My model

---

[6]These are recommended by 3GPP, as already mentioned in Chapter 2.

shows a structure that identifies the relevant interference terms which enables for example also receiver optimizations [22, 23]. Parts of the contents of this chapter have been published in [12–14, 16, 17, 26].

One of the crucial components of the model is that it allows for the generation of so-called *fading parameters*, prior to the system-level simulation itself. These fading parameters include nearly all link-related procedures, thus during the runtime of the system-level simulation only scalar real-valued multiplications are needed to compute the SINR. This *significantly* reduces the computational effort. In principle, this idea has already been touched in [78] for WCDMA UMTS, however in the context of MIMO it has to be generalized and fairly extended to be utilizable to derive a suitable description.

3.3. Computationally Efficient Link-Quality Model

To be able to derive an accurate and computationally efficient system-level model, an analytical model of the MIMO HSDPA link quality is needed. The basics of the physical layer transmission have already been defined in Chapter 2. In particular the D-TxAA mode [6] is depicted in Figure 2.8. To represent this transmission setting, I adapted the framework of [87] in order to reflect one individual link between a NodeB and a UE.

Figure 3.3 depicts the model where the transmitter and the receiver are equipped with N_{T} and N_{R} antennas, respectively. Note that this description allows for the modeling of more than two spatial multiplexed data streams, which is the maximum supported by Release 7 MIMO HSDPA. Accordingly, as illustrated in Figure 3.3, N_{S} parallel data streams $s^{(0)}, \ldots, s^{(N_{\text{S}}-1)}$ enter the system. Each data stream $s^{(n)}, n = 1, \ldots, N_{\text{S}}$ is individually encoded and modulated, like depicted in Figure 2.8, and is then being spread by a number of spreading sequences $\varphi_k^{(n)}$ with k specifying the individual spreading code. This represents multi-code usage on each stream. The set of individual spreading codes utilized for stream n is denoted Φ_n, thus $\varphi_k^{(n)} \in \Phi_n$. The streams are of course scrambled as well, but for sake of clarity, I did not depict the scrambling/descrambling. Let me, however, still denote the scrambling sequence utilized for this particular link by ψ.

Assumption 3.1. There is only one scrambling code active for each link.

Thus both streams are scrambled with the same scrambling sequence,[7] however the NodeB could still apply different scrambling codes for different users. Note that by this convention, the model does not allow individual streams to be separately scrambled. The inverse operations of the spreading and scrambling at the receiver side are consequently denoted $\bar{\varphi}_k^{(n)}$ and $\bar{\psi}$.

The spread and scrambled sequences $x^{(n)}, n = 1, \ldots, N_{\text{S}}$ are then mapped to the N_{T} transmit antennas using the pre-coding matrix $\mathbf{W}_{\text{CB}} \in \mathbb{C}^{N_{\text{T}} \times N_{\text{S}}}$, which contains the pre-coding weights $w_1, \ldots, w_{N_{\text{T}} N_{\text{S}}}$, similar to Figure 2.8, where $\mathbf{W}_{\text{CB}}$ is defined by $w_1, \ldots, w_4$. At the receiver, the signals are gathered with N_{R} antennas and chip spaced sampled before they enter the discrete-time receive filter. The MIMO channel $\mathbf{H} \in \mathbb{C}^{N_{\text{R}} \times N_{\text{T}} L_{\text{h}}}$ is modeled as time-discrete, frequency-selective channel,

$$\mathbf{H} = \begin{bmatrix} h_0^{(1,1)} & \cdots & h_0^{(1,N_{\text{T}})} & h_1^{(1,1)} & \cdots & h_1^{(1,N_{\text{T}})} & \cdots & h_{L_{\text{h}}-1}^{(1,N_{\text{T}})} & \cdots & h_{L_{\text{h}}-1}^{(1,N_{\text{T}})} \\ \vdots & & \vdots & \vdots & & \vdots & \ddots & \vdots & & \vdots \\ h_0^{(N_{\text{R}},1)} & \cdots & h_0^{(N_{\text{R}},N_{\text{T}})} & h_1^{(N_{\text{R}},1)} & \cdots & h_1^{(N_{\text{R}},N_{\text{T}})} & \cdots & h_{L_{\text{h}}-1}^{(N_{\text{R}},N_{\text{T}})} & \cdots & h_{L_{\text{h}}-1}^{(N_{\text{R}},N_{\text{T}})} \end{bmatrix}. \quad (3.1)$$

---

[7]The scrambling code is, as opposed to the spreading code, is not targeted for a spreading of the utilized bandwidth, but rather to separate cells in the downlink and users in the uplink. The scrambling codes are designed specifically to show good cross-correlation properties (Gold codes).
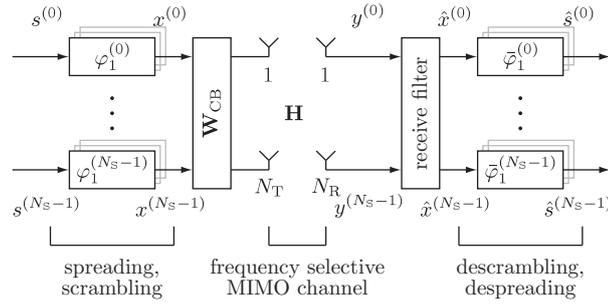
Figure 3.3.: System model for a WCDMA system, reflecting the parallel transmission of N_S streams over N_T transmit antennas and reception with N_R receive antennas utilizing a receive filter.

The entry $h_l^{(n_\mathrm{r},n_\mathrm{t})}, l = 0, \ldots, L_\mathrm{h}-1, n_\mathrm{r} = 1, \ldots, N_\mathrm{R}, n_\mathrm{t} = 1, \ldots, N_\mathrm{T}$ denotes the l-th sampled chip of the channel impulse response from transmit antenna n_t to receive antenna n_r, with a total channel length of L_h chip intervals. Note that pulse-shaping, transmit and receive band-filtering, as well as the sampling operation can be incorporated in the MIMO channel matrix. To account for the pre-coding, I define an equivalent time-discrete channel $\mathbf{H}_\mathrm{w} \in \mathbb{C}^{N_\mathrm{R} \times N_\mathrm{S} L_\mathrm{h}}$ that includes the pre-coding matrix $\mathbf{W}_\mathrm{CB}$ and the MIMO channel,

$$\mathbf{H}_\mathrm{w} \triangleq \mathbf{H}\left(\mathbf{I}_{L_\mathrm{h}} \otimes \mathbf{W}_\mathrm{CB}\right), \tag{3.2}$$

with $\mathbf{I}_{L_\mathrm{h}}$ denoting the identity matrix of size $L_\mathrm{h} \times L_\mathrm{h}$, and $\otimes$ being the Kronecker product. Furthermore, let me define the transmit and receive vectors as

$$\mathbf{y}_i \triangleq \begin{bmatrix} y_i^{(1)} & \cdots & y_i^{(N_\mathrm{R})} \end{bmatrix}^\mathrm{T}, \tag{3.3}$$

$$\mathbf{x}_i \triangleq \begin{bmatrix} x_i^{(0)} & \cdots & x_i^{(N_\mathrm{S}-1)} & x_{i-1}^{(0)} & \cdots & x_{i-1}^{(N_\mathrm{S}-1)} & \cdots & x_{i-L_\mathrm{h}+1}^{(0)} & \cdots & x_{i-L_\mathrm{h}+1}^{(N_\mathrm{S}-1)} \end{bmatrix}^\mathrm{T}, \tag{3.4}$$

and the noise vector as

$$\mathbf{n}_i \triangleq \begin{bmatrix} n_i^{(1)} & \cdots & n_i^{(N_\mathrm{R})} \end{bmatrix}^\mathrm{T}, \tag{3.5}$$

with $i \in \mathbb{N}$ denoting the discrete-time index, like in Chapter 2. Then the input-output relation for one link, formulated by means of the equivalent MIMO channel matrix, is given by

$$\mathbf{y}_i = \mathbf{H}_\mathrm{w} \mathbf{x}_i + \mathbf{n}_i. \tag{3.6}$$

The description in Equation (3.6) certainly allows for the description of the D-TxAA scheme which implies that $N_\mathrm{T} = N_\mathrm{R} = 2$ and $N_\mathrm{S} = 1, 2$. However, the input-output relation can be used for more than two independent data streams, thus supporting possible future extensions of the scheme, or other transmission schemes like [15].

3.3.1. Equalizer

To derive a suitable link-quality model also the receive filter has to be taken into account.

Assumption 3.2. Only linear equalizers at the receiver are considered.

This accordingly excludes Successive Interference Cancellation (SIC) receivers as well as ML based structures. Note that currently Release 5 HSDPA devices utilize a Rake-receiver [88], and Release 7 HSDPA devices are recommended to employ MMSE equalizers [89]. Thus, this restriction does not impose a dramatic problem for current networks, however, for further enhanced set-ups, the modeling would have to be refined at this point.

For the derivation of the receive filter, the input-ouput relation in Equation (3.6) has to be extended for L_f received chips at the N_R receive antennas, specifying the filter length. By defining the *stacked* versions of the parameters introduced so far,

$$\tilde{\mathbf{y}}_i \triangleq \begin{bmatrix} \mathbf{y}_i^\mathrm{T} & \cdots & \mathbf{y}_{i-L_\mathrm{f}+1}^\mathrm{T} \end{bmatrix}^\mathrm{T}, \tag{3.7}$$

$$\tilde{\mathbf{x}}_i \triangleq \begin{bmatrix} x_i^{(0)} & \cdots & x_i^{(N_\mathrm{S}-1)} & x_{i-1}^{(0)} & \cdots & x_{i-1}^{(N_\mathrm{S}-1)} & \cdots & x_{i-L_\mathrm{h}-L_\mathrm{f}+2}^{(0)} & \cdots & x_{i-L_\mathrm{h}-L_\mathrm{f}+2}^{(N_\mathrm{S}-1)} \end{bmatrix}^\mathrm{T}, \tag{3.8}$$

and

$$\tilde{\mathbf{n}}_i \triangleq \begin{bmatrix} \mathbf{n}_i^\mathrm{T} & \cdots & \mathbf{n}_{i-L_\mathrm{f}+1}^\mathrm{T} \end{bmatrix}^\mathrm{T}, \tag{3.9}$$

as well as the stacked equivalent MIMO channel matrix $\tilde{\mathbf{H}}_\mathrm{w} \in \mathbb{C}^{N_\mathrm{R}L_\mathrm{f} \times N_\mathrm{S}(L_\mathrm{h}+L_\mathrm{f}-1)}$,

$$\tilde{\mathbf{H}}_\mathrm{w} \triangleq \begin{bmatrix} \mathbf{H}_\mathrm{w} & \mathbf{0}_{N_\mathrm{R},N_\mathrm{S}} & \cdots & \mathbf{0}_{N_\mathrm{R},N_\mathrm{S}} \\ \mathbf{0}_{N_\mathrm{R},N_\mathrm{S}} & \mathbf{H}_\mathrm{w} & & \mathbf{0}_{N_\mathrm{R},N_\mathrm{S}} \\ \vdots & & \ddots & \\ \mathbf{0}_{N_\mathrm{R},N_\mathrm{S}} & \mathbf{0}_{N_\mathrm{R},N_\mathrm{S}} & \cdots & \mathbf{H}_\mathrm{w} \end{bmatrix}, \tag{3.10}$$

where $\mathbf{0}_{N_\mathrm{R},N_\mathrm{S}}$ denotes the all-zero matrix of dimension $N_\mathrm{R} \times N_\mathrm{S}$, the input-output relation becomes

$$\tilde{\mathbf{y}}_i = \tilde{\mathbf{H}}_\mathrm{w}\tilde{\mathbf{x}}_i + \tilde{\mathbf{n}}_i. \tag{3.11}$$

Note, however, that the stacked equivalent channel matrix $\tilde{\mathbf{H}}_\mathrm{w}$ cannot be represented by a Kronecker product, because the matrix does not have a block diagonal structure, as indicated by the size of the matrices $\mathbf{0}_{N_\mathrm{R},N_\mathrm{S}}$.

One particular example of a receive filter that—as already mentioned is recommended by the 3GPP for Release 7 HSDPA—is the MMSE equalizer. For the input output relation of Equation (3.11), the cost function of the MMSE receiver can be formulated as

$$J(\mathbf{F}) = \mathbb{E}\left\{ \left\| \mathbf{F}\tilde{\mathbf{y}}_i - \mathbf{x}_{i-\tau}^\mathrm{S} \right\|^2 \right\}, \tag{3.12}$$

where τ defines the delay of the MMSE filter, which has to fulfill $\tau \geq L_\mathrm{h}$ to include at least all observations affected by $\mathbf{x}_i$. The vector of transmit chips to be estimated is defined as

$$\mathbf{x}_{i-\tau}^\mathrm{S} \triangleq \begin{bmatrix} x_{i-\tau}^{(0)} & \cdots & x_{i-\tau}^{(N_\mathrm{S}-1)} \end{bmatrix}^\mathrm{T}, \tag{3.13}$$

thus representing the chips of all transmitted streams at time index $i - \tau$. A filter satisfying Equation (3.12) tries to restore the orthogonality of the individual spreading codes caused by the multi-path propagation. This problem has already been investigated, for example in [87, 90], and its solution turns out to be given by the suitable formulated Wiener-Hopf equation, leading to

$$\mathbf{F} = \mathbf{R}_{\mathbf{x}_{i-\tau}^\mathrm{S}\tilde{\mathbf{x}}_i}\tilde{\mathbf{H}}_\mathrm{w}^\mathrm{H} \left(\tilde{\mathbf{H}}_\mathrm{w}\mathbf{R}_{\tilde{\mathbf{x}}_i}\tilde{\mathbf{H}}_\mathrm{w}^\mathrm{H} + \mathbf{R}_{\tilde{\mathbf{n}}_i} \right)^{-1}. \tag{3.14}$$

Assuming white, i.i.d., uncorrelated transmit sequences, the covariance matrices can be evaluated to have the following structure,

$$\mathbf{R}_{\mathbf{x}_{i-\tau}^{\mathrm{S}} \tilde{\mathbf{x}}_i} = \begin{bmatrix} \mathbf{0}_{N_{\mathrm{S}} \times N_{\mathrm{S}} \tau} & \mathbf{P} & \mathbf{0}_{N_{\mathrm{S}} \times N_{\mathrm{S}}(L_{\mathrm{f}}+L_{\mathrm{h}}-\tau+2)} \end{bmatrix}, \tag{3.15}$$

$$\mathbf{R}_{\tilde{\mathbf{x}}_i} = \mathbf{I}_{L_{\mathrm{f}}+L_{\mathrm{h}}-1} \otimes \mathbf{P}, \tag{3.16}$$

with

$$\mathbf{P} \triangleq \mathrm{diag}\left\{ \begin{bmatrix} P_1 & \cdots & P_n & \cdots & P_{N_{\mathrm{S}}} \end{bmatrix} \right\} \tag{3.17}$$

specifying the powers utilized on each stream n, $P_n = \mathbb{E}\left\{ \left| x_i^{(n)} \right|^2 \right\} = \sigma_{x_i^{(n)}}^2$, respectively.

The equalizer length L_{f} and the detection delay τ are important parameters that influence the performance of the system, but an optimization of these is not within the scope of this work.

Assumption 3.3. The equalizer delay is set to $\tau = L_{\mathrm{f}}/2$, see for example [89].

Note that this choice does not affect the system-level modeling itself, but the simulation results presented in Section 3.3.4.

3.3.2. WCDMA MIMO in the Network Context

In a multi-cell, multi-user scenario, Equation (3.11) has to be extended to cover the signals from all sectors and all users, as well as all spreading codes that are active at that moment. To do so, let me define the transmit—and accordingly the receive sequence—in Equation (3.11) to correspond to a set of utilized spreading and scrambling sequences,

$$\tilde{\mathbf{x}}_i = \sum_{\varphi_k \in \Phi} \tilde{\mathbf{x}}_i^{(\varphi_k, \psi)}, \tag{3.18}$$

where $\varphi_k \in \Phi, \Phi \triangleq \Phi_0 \cup \cdots \cup \Phi_{N_{\mathrm{S}}-1}$. The entries of $\tilde{\mathbf{x}}_i^{(\varphi_k, \psi)}$ additionally have to fulfill

$$x_i^{(n),(\varphi_k,\psi)} \triangleq \begin{cases} x_i^{(n)} & : \varphi_k^{(n)} = \varphi_k, \\ 0 & : \varphi_k^{(n)} \neq \varphi_k, \end{cases} \tag{3.19}$$

which allows for representing cases in which different streams utilize only partly-, or even non-overlapping spreading code sets $\Phi_n, n = 0, \ldots, N_{\mathrm{S}} - 1$.

Furthermore, let me index the users of a sector by the pair (u, b) with $u = 1, \ldots, U(b)$, because the number of active users can be different for each sector b, and $b = 1, \ldots, B$. I used the term *sector* here, because potentially every sector of a NodeB can be independently controlled in terms of its radio resources, that is, the power and spreading code allocation. In principle, a link in a sectored network would be specified by the triple user, sector, base-station, (u, z, b), where $z = 1, \ldots, Z(b)$ and b denote the sector and base-station index, respectively. For sake of notational simplicity, however, I chose to index the sectors individually, for which I used b as the index. In most practical networks, the number of sectors per base-station is constant, thus not imposing the need to identify the links by the triple. For a single-sector network, the pair (u, b) is obviously sufficient as well. Thus, the transmit signal of one particular link utilizing a given spreading and scrambling code pair is denoted $\tilde{\mathbf{x}}_i^{(\varphi_k,\psi),(u,b)}$.

With the individual link being specified by (u, b), the set of utilized spreading codes on that link is denoted by $\Phi^{(u,b)}$. This, however, would require the pair of spreading and scrambling sequences to be indexed by (u, b), that is, $\varphi_k \to \varphi_k^{(u,b)}$ and $\psi \to \psi^{(u,b)}$ to be mathematically precise. Nevertheless I dropped these indices, again for sake of notational simplicity. By these definitions, the power of one stream n on link (u, b), is given by

$$P_n^{(u,b)} = \mathbb{E}\left\{ \left| \sum_{\varphi_k^{(n)} \in \Phi_n^{(u,b)}} x_i^{(n),(\varphi_k^{(n)},\psi),(u,b)} \right|^2 \right\} = \sum_{\varphi_k^{(n)} \in \Phi_n^{(u,b)}} \sigma^2_{x_i^{(n),(\varphi_k^{(n)},\psi),(u,b)}} = \sum_{\varphi_k^{(n)} \in \Phi_n^{(u,b)}} P_{n,\varphi_k^{(n)}}^{(u,b)},$$

(3.20)

with $P_{n,\varphi_k^{(n)}}^{(u,b)}$ denoting the power on stream n and spreading code $\varphi_k^{(n)}$ for the link (u, b).

Assumption 3.4. For Equation (3.20) to hold, the data sequences on the individual spreading codes are uncorrelated.

The interference on one particular user u_0, which I will call the *desired user*, is received over B frequency selective MIMO channels. This is the user for whom the physical-layer quality has to be evaluated. The base-station/sector to which this user is attached to with index b_0 will be called *target sector* in the following. However, due to the user specific pre-coding, the equivalent channel matrix $\tilde{\mathbf{H}}_\mathrm{w}$ will be different for different individual users. Accordingly, let me index the channel matrices involved in the network context as $\tilde{\mathbf{H}}_\mathrm{w}^{(u,b)}$. Using these definitions, the total received signal at the desired user can be evaluated by summation over all active sectors and users, as well as spreading codes, respectively,

$$\tilde{\mathbf{y}}_i^{(u_0)} = \sum_{b=1}^{B} \sum_{u=1}^{U(b)} \sum_{\varphi_k \in \Phi^{(u,b)}} \tilde{\mathbf{H}}_\mathrm{w}^{(u,b)} \tilde{\mathbf{x}}_i^{(\varphi_k,\psi),(u,b)} + \tilde{\mathbf{n}}_i.$$

(3.21)

The received signal is then passed through the receive filter, which leads to the useful post-equalization signal given by

$$\hat{\mathbf{x}}_i^{(u_0)} = \sum_{b=1}^{B} \sum_{u=1}^{U(b)} \sum_{\varphi_k \in \Phi^{(u,b)}} \mathbf{F} \tilde{\mathbf{H}}_\mathrm{w}^{(u,b)} \tilde{\mathbf{x}}_i^{(\varphi_k,\psi),(u,b)} + \mathbf{F} \tilde{\mathbf{n}}_i.$$

(3.22)

To analyze this relation and identify the different interference terms, it is necessary to decompose the receive filter into the according filters responsible for each stream,

$$\mathbf{F} = \begin{bmatrix} \mathbf{f}^{(0)} & \cdots & \mathbf{f}^{(n)} & \cdots & \mathbf{f}^{(N_\mathrm{S}-1)} \end{bmatrix}^\mathrm{T},$$

(3.23)

as well as the channel matrix into its columns,

$$\tilde{\mathbf{H}}_\mathrm{w}^{(u,b)} = \begin{bmatrix} \mathbf{h}_0^{(u,b)} & \cdots & \mathbf{h}_m^{(u,b)} & \cdots & \mathbf{h}_{N_\mathrm{S}(L_\mathrm{f}+L_\mathrm{h}-1)-1}^{(u,b)} \end{bmatrix},$$

(3.24)

where m is the index of the transmit chips for all streams entering the receive filter. Accordingly, the post-equalization signal of Equation (3.22) for stream n can be written as

$$\hat{x}_i^{(n),(u_0)} = \sum_{b=1}^{B} \sum_{u=1}^{U(b)} \sum_{\varphi_k \in \Phi^{(u,b)}} \sum_{m=0}^{N_\mathrm{S}(L_\mathrm{f}+L_\mathrm{h}-1)-1} \left(\mathbf{f}^{(n)} \right)^\mathrm{T} \mathbf{h}_m^{(u,b)} x_{i-\lfloor m/N_\mathrm{S} \rfloor}^{(\lfloor m/N_\mathrm{S} \rfloor),(\varphi_k,\psi),(u,b)} + \left(\mathbf{f}^{(n)} \right)^\mathrm{T} \tilde{\mathbf{n}}_i, \quad (3.25)$$

where $\lfloor m/N_S \rceil$ denotes the remainder of the integer division which represents the index of the substream, and $\lfloor m/N_S \rfloor$ denotes the largest integer smaller than m/N_S which corresponds to the delay of the transmit chip.

After the receive filtering $\hat{x}_i^{(n),(u_0)}$ is multiplied with the complex conjugated scrambling and spreading codes and integrated over the period of a symbol[8] to obtain the estimated transmit symbols $\hat{s}^{(n)}$ for stream n, respectively.

3.3.3. Description of the Equivalent Fading Parameters

Nearly all relevant performance metrics in wireless communications are evaluated with respect to SINR. Accordingly, I am deriving a suitable description of the SINR as observed in the network context to represent the physical-layer quality. The applicability of the SINR in order to predict the BLER performance of the overall transmission scheme also seems intuitive.

Assumption 3.5. In the following, the NodeB utilizes only one scrambling sequence for all of its links.

Also note that this reflects a typical WCDMA scenario as currently implemented for Release 5 HSDPA and simplifies the notation, thus in the following I will not use the index ψ anymore. For the derivation of the SINR, Equation (3.25) has to be decomposed into the different relevant interference and desired signal power terms. Note that all of the following power terms apply to the desired user u_0 and target sector b_0.

Desired Signal

The power of the desired signal on stream n and spreading code φ_k is given by the resulting power after the receive filter at delay τ,

$$P^{s}_{n,\varphi_k} \triangleq P^{s,(u_0,b_0)}_{n,\varphi_k} = \left| \left(\mathbf{f}^{(n)} \right)^{\mathrm{T}} \mathbf{h}^{(u_0,b_0)}_{\tau N_S + n} \right|^2 P^{(u_0,b_0)}_{n,\varphi_k^{(n)}}, \tag{3.26}$$

where I dropped the indication of the desired user and sector in the resulting power term for sake of notational simplicity. The idea now is to define the desired signal power as the multiplication of the power on stream n and spreading code $\varphi_k^{(n)}$—which is known in a system-level simulation—with a so-called *equivalent fading parameter*. Here, the equivalent fading parameter of the desired signal on stream n, G^s_n, also called *desired signal gain*, is defined as

$$\boxed{G^s_n \triangleq \left| \left(\mathbf{f}^{(n)} \right)^{\mathrm{T}} \mathbf{h}^{(u_0,b_0)}_{\tau N_S + n} \right|^2 \Rightarrow P^s_{n,\varphi_k} = G^s_n P^{(u_0,b_0)}_{n,\varphi_k^{(n)}}.} \tag{3.27}$$

This fading parameter contains the full information about the consequences of the physical-layer onto the desired signal.

Intra-cell Interference

The intra-cell interference is composed by a number of terms, in particular

---

[8]Which corresponds to SF chip periods T_c, with $T_c = 1/3840000\,\mathrm{s}$ in WCDMA systems.

- the remaining Inter-Symbol Interference (ISI) after equalization,

$$P_{n,\varphi_k}^{\mathrm{ISI}} \triangleq P_{n,\varphi_k}^{\mathrm{ISI},(u_0,b_0)} = \sum_{\substack{m=0 \\ m \notin [\tau N_{\mathrm{S}}, \tau N_{\mathrm{S}}+N_{\mathrm{S}}-1]}}^{N_{\mathrm{S}}(L_{\mathrm{f}}+L_{\mathrm{h}}-1)-1} \left| \left(\mathbf{f}^{(n)} \right)^{\mathrm{T}} \mathbf{h}_m^{(u_0,b_0)} \right|^2 P_{\lfloor m/N_{\mathrm{S}} \rfloor, \varphi_k^{(\lfloor m/N_{\mathrm{S}} \rfloor)}}^{(u_0,b_0)}, \qquad (3.28)$$

- the inter-code interference when the same scrambling but a different spreading code is used,

$$P_{n,\varphi_k}^{\mathrm{IC}} \triangleq P_{n,\varphi_k}^{\mathrm{IC},(u_0,b_0)} = \sum_{\substack{m=0 \\ m \notin [\tau N_{\mathrm{S}}, \tau N_{\mathrm{S}}+N_{\mathrm{S}}-1]}}^{N_{\mathrm{S}}(L_{\mathrm{f}}+L_{\mathrm{h}}-1)-1} \left| \left(\mathbf{f}^{(n)} \right)^{\mathrm{T}} \mathbf{h}_m^{(u_0,b_0)} \right|^2 \sum_{\substack{\tilde{\varphi}_k \in \Phi^{(u,b)} \\ \tilde{\varphi}_k \neq \varphi_k}} P_{\lfloor m/N_{\mathrm{S}} \rfloor, \tilde{\varphi}_k^{(\lfloor m/N_{\mathrm{S}} \rfloor)}}^{(u_0,b_0)}, \quad (3.29)$$

- the time-aligned intra-cell interference from users with the same spreading code as the desired user,

$$P_{n,\varphi_k}^{\mathrm{intra_1}} \triangleq P_{n,\varphi_k}^{\mathrm{intra_1},(u_0,b_0)} = \sum_{\substack{u=1 \\ u \neq u_0}}^{U(b_0)} \sum_{m=\tau N_{\mathrm{S}}}^{\tau N_{\mathrm{S}}+N_{\mathrm{S}}-1} \left| \left(\mathbf{f}^{(n)} \right)^{\mathrm{T}} \mathbf{h}_m^{(u,b_0)} \right|^2 P_{\lfloor m/N_{\mathrm{S}} \rfloor, \varphi_k^{(\lfloor m/N_{\mathrm{S}} \rfloor)}}^{(u,b_0)}, \qquad (3.30)$$

- the not time-aligned intra-cell interference from users with the same spreading code caused by multi-path propagation,

$$P_{n,\varphi_k}^{\mathrm{intra_2}} \triangleq P_{n,\varphi_k}^{\mathrm{intra_2},(u_0,b_0)} = \sum_{\substack{u=1 \\ u \neq u_0}}^{U(b_0)} \sum_{\substack{m=0 \\ m \notin [\tau N_{\mathrm{S}}, \tau N_{\mathrm{S}}+N_{\mathrm{S}}-1]}}^{N_{\mathrm{S}}(L_{\mathrm{f}}+L_{\mathrm{h}}-1)-1} \left| \left(\mathbf{f}^{(n)} \right)^{\mathrm{T}} \mathbf{h}_m^{(u,b_0)} \right|^2 P_{\lfloor m/N_{\mathrm{S}} \rfloor, \varphi_k^{(\lfloor m/N_{\mathrm{S}} \rfloor)}}^{(u,b_0)}, \quad (3.31)$$

- and the intra-cell interference from users with the same scrambling code, but different spreading code

$$\begin{aligned} P_{n,\varphi_k}^{\mathrm{intra_3}} &\triangleq P_{n,\varphi_k}^{\mathrm{intra_3},(u_0,b_0)} \\ &= \sum_{\substack{u=1 \\ u \neq u_0}}^{U(b_0)} \sum_{\substack{m=0 \\ m \notin [\tau N_{\mathrm{S}}, \tau N_{\mathrm{S}}+N_{\mathrm{S}}-1]}}^{N_{\mathrm{S}}(L_{\mathrm{f}}+L_{\mathrm{h}}-1)-1} \left| \left(\mathbf{f}^{(n)} \right)^{\mathrm{T}} \mathbf{h}_m^{(u,b_0)} \right|^2 \sum_{\substack{\tilde{\varphi}_k \in \Phi^{(u,b)} \\ \tilde{\varphi}_k \neq \varphi_k}} P_{\lfloor m/N_{\mathrm{S}} \rfloor, \tilde{\varphi}_k^{(\lfloor m/N_{\mathrm{S}} \rfloor)}}^{(u,b_0)}. \end{aligned} \qquad (3.32)$$

As already mentioned, due to the assumption that there is only one scrambling code per link, as well as the more restrictive assumption that the NodeB uses only one scrambling code overall, no interference term for inter-scrambling code interference appears in the context of the intra-cell interference. Furthermore, let me point out that in a practical system implementation of MIMO HSDPA, it is not very likely that other users will be scheduled in parallel to the desired user utilizing the same—or even overlapping—spreading code sets. In such a case, the users would only be separated by means of SDMA, and the resulting interference is increased by the spreading gain.

Assumption 3.6. Accordingly, no pure SDMA user separation is performed, which implies that

$$P_{n,\varphi_k}^{\mathrm{intra_1}} = 0. \qquad (3.33)$$

From the remaining terms $P_{n,\varphi_k}^{\text{ISI}}$ and $P_{n,\varphi_k}^{\text{IC}}$ represent the intra-cell interference generated by the desired user himself, which can be called *self interference*,

$$P_{n,\varphi_k}^{\text{self}} \triangleq P_{n,\varphi_k}^{\text{ISI}} + P_{n,\varphi_k}^{\text{IC}} = \sum_{\substack{m=0 \\ m \notin [\tau N_{\text{S}}, \tau N_{\text{S}} + N_{\text{S}} - 1]}}^{N_{\text{S}}(L_{\text{f}}+L_{\text{h}}-1)-1} \left| \left(\mathbf{f}^{(n)}\right)^{\text{T}} \mathbf{h}_m^{(u_0,b_0)} \right|^2 P_{\lfloor m/N_{\text{S}} \rfloor}^{(u_0,b_0)}. \tag{3.34}$$

Similarly, $P_{n,\varphi_k}^{\text{intra}_2}$ and $P_{n,\varphi_k}^{\text{intra}_3}$ specify the intra-cell interference generated by all other users in the sector, which may be called *other-user interference*,

$$P_{n,\varphi_k}^{\text{other}} \triangleq P_{n,\varphi_k}^{\text{intra}_2} + P_{n,\varphi_k}^{\text{intra}_3} = \sum_{\substack{u=1 \\ u \neq u_0}}^{U(b_0)} \sum_{\substack{m=0 \\ m \notin [\tau N_{\text{S}}, \tau N_{\text{S}} + N_{\text{S}} - 1]}}^{N_{\text{S}}(L_{\text{f}}+L_{\text{h}}-1)-1} \left| \left(\mathbf{f}^{(n)}\right)^{\text{T}} \mathbf{h}_m^{(u,b_0)} \right|^2 P_{\lfloor m/N_{\text{S}} \rfloor}^{(u,b_0)}. \tag{3.35}$$

Assumption 3.7. For the overall intra-cell interference, all streams $n = 0, \ldots, N_{\text{S}} - 1$ transmitted to a user u have the same power,

$$P_n^{(u,b)} \equiv \frac{1}{N_{\text{S}}} P^{(u,b)}, \tag{3.36}$$

with $P^{(u,b)}$ denoting the total power spent for user u by sector b.

Note that this limits the applicability of the model to cases where no dynamic power loading for the individual streams takes place. For more advanced power resource allocation, for example water-filling idea based algorithms, the model would have to be refined at this point.

Consequently, the total intra-cell interference, as seen by the desired user u_0 on stream n and spreading code φ_k, becomes

$$P_{n,\varphi_k}^{\text{intra}} = P_{n,\varphi_k}^{\text{self}} + P_{n,\varphi_k}^{\text{other}} = \underbrace{\frac{1}{N_{\text{S}}} P^{(u_0,b_0)} \sum_{\substack{m=0 \\ m \notin [\tau N_{\text{S}}, \tau N_{\text{S}} + N_{\text{S}} - 1]}}^{N_{\text{S}}(L_{\text{f}}+L_{\text{h}}-1)-1} \left| \left(\mathbf{f}^{(n)}\right)^{\text{T}} \mathbf{h}_m^{(u_0,b_0)} \right|^2}_{\text{self interference}}$$
$$+ \underbrace{\frac{1}{N_{\text{S}}} \sum_{\substack{u=1 \\ u \neq u_0}}^{U(b_0)} P^{(u,b_0)} \sum_{\substack{m=0 \\ m \notin [\tau N_{\text{S}}, \tau N_{\text{S}} + N_{\text{S}} - 1]}}^{N_{\text{S}}(L_{\text{f}}+L_{\text{h}}-1)-1} \left| \left(\mathbf{f}^{(n)}\right)^{\text{T}} \mathbf{h}_m^{(u,b_0)} \right|^2}_{\text{other-user interference}}. \tag{3.37}$$

So far, Equation (3.37) still does not allow for a decoupling into equivalent fading parameters and power terms, because $\mathbf{h}_m^{(u,b_0)}$ depends on the user index, and in particular on the choice of the users regarding their pre-coding. To obtain a model with low computational complexity, this mechanism however should be contained in the link-quality model itself, so that in a system-level simulation, no calculations of the pre-coding and the user specific equivalent MIMO channels has to be performed.

Assumption 3.8. For an equivalent fading parameter decomposition of the intra-cell interference, the actual intra-cell interference is approximated by its expected value with respect to the pre-coding choices of the other users,

$$\bar{P}_{n,\varphi_k}^{\text{intra}} = \mathbb{E}_w \left\{ P_{n,\varphi_k}^{\text{intra}} \right\}. \tag{3.38}$$

Accordingly, by defining the *intra-cell orthogonality* of stream n, o_n^{intra}, as well as the *beam-forming orthogonality gain* of stream n, o_n^{BF}, as

$$o_n^{\text{intra}} \triangleq \frac{1}{N_{\text{S}}} \frac{1}{G_n^{\text{s}}} \sum_{\substack{m=0 \\ m \notin [\tau N_{\text{S}}, \tau N_{\text{S}} + N_{\text{S}} - 1]}}^{N_{\text{S}}(L_{\text{f}} + L_{\text{h}} - 1) - 1} \left| \left(\mathbf{f}^{(n)} \right)^{\text{T}} \mathbf{h}_m^{(u_0, b_0)} \right|^2 = \frac{1}{N_{\text{S}}} \frac{1}{G_n^{\text{s}}} \gamma_{\text{s}}, \tag{3.39}$$

and

$$o_n^{\text{BF}} \triangleq \gamma_{\text{s}}^{-1} \mathbb{E}_w \left\{ \sum_{\substack{m=0 \\ m \notin [\tau N_{\text{S}}, \tau N_{\text{S}} + N_{\text{S}} - 1]}}^{N_{\text{S}}(L_{\text{f}} + L_{\text{h}} - 1) - 1} \left| \left(\mathbf{f}^{(n)} \right)^{\text{T}} \mathbf{h}_m^{(u, b_0)} \right|^2 \right\}, \tag{3.40}$$

the intra-cell interference power in Equation (3.37) does not depend on the user-individual choices of the pre-coding weights. By these definitions, it follows that

$$\bar{P}_{n, \varphi_k}^{\text{intra}} = \left[P^{(u_0, b_0)} + o_n^{\text{BF}} \sum_{\substack{u=1 \\ u \neq u_0}}^{U(b_0)} P^{(u, b_0)} \right] o_n^{\text{intra}} G_n^{\text{s}}. \tag{3.41}$$

The equivalent fading parameters again contain the full information about the physical-layer implications on the power distribution in the target sector.

In the practical implementation of the 3GPP Release 7 MIMO HSDPA standard, the pre-coding is strongly quantized to limit the amount of feedback needed. The current definition of the pre-coding codebook for Release 7 HSDPA is specified in [6]. If the codebook of the pre-coding utilized for a user u, $\mathbf{W}_{\text{CB}}^{(u)}$, is denoted as Ω, with its cardinality given by $|\Omega|$, the equivalent fading parameter o_n^{BF} can be evaluated as

$$o_n^{\text{BF}} \triangleq \gamma_{\text{s}}^{-1} \frac{1}{|\Omega|} \sum_{\mathbf{W}_{\text{CB}}^{(u)} \in \Omega} \sum_{\substack{m=0 \\ m \notin [\tau N_{\text{S}}, \tau N_{\text{S}} + N_{\text{S}} - 1]}}^{N_{\text{S}}(L_{\text{f}} + L_{\text{h}} - 1) - 1} \left| \left(\mathbf{f}^{(n)} \right)^{\text{T}} \mathbf{h}_m^{(u, b_0)} \right|^2. \tag{3.42}$$

Inter-Stream Interference

The interference generated by the parallel transmission of other spatially multiplexed streams is given by the term

$$P_{n, \varphi_k}^{\text{INT}} \triangleq P_{n, \varphi_k}^{\text{INT}, (u_0, b_0)} = \sum_{\substack{m=0 \\ m \neq n}}^{N_{\text{S}} - 1} \left| \left(\mathbf{f}^{(n)} \right)^{\text{T}} \mathbf{h}_{\tau N_{\text{S}} + m}^{(u_0, b_0)} \right|^2 P_{m, \varphi_k^{(m)}}^{(u_0, b_0)}, \tag{3.43}$$

from which the equivalent fading parameter for the *inter-stream interference orthogonality* can immediately be defined,

$$o_n^{\text{INT}} \triangleq \sum_{\substack{m=0 \\ m \neq n}}^{N_{\text{S}} - 1} \left| \left(\mathbf{f}^{(n)} \right)^{\text{T}} \mathbf{h}_{\tau N_{\text{S}} + m}^{(u_0, b_0)} \right|^2. \tag{3.44}$$

With this, the inter-stream interference can be calculated by

$$P_{n, \varphi_k}^{\text{INT}} = o_n^{\text{INT}} P_{m, \varphi_k^{(m)}}^{(u_0, b_0)}, \tag{3.45}$$

where the equivalent fading parameter o_n^{INT} now contains all the information about the physical-layer regarding the interference suppression between the individual streams being transmitted. Note that the inter-stream interference only occurs for those spreading codes that are used on both streams, and that this interference power will thus see a spreading gain at the receiver.

Inter-Cell Interference

The inter-cell interference is caused by all neighboring sectors in the network. Due to the scrambling code, the corresponding interference terms will not see a spreading factor gain. In general, the inter-cell interference power derived from Equation (3.25) is given by

$$P_{n,\varphi_k}^{\text{inter}} \triangleq P_{n,\varphi_k}^{\text{INT},(u_0,b)} = \sum_{\substack{b=1 \\ b \neq b_0}}^{B} \sum_{u=1}^{U(b)} \sum_{\varphi_k \in \Phi^{(u,b)}} \sum_{m=0}^{N_{\text{S}}(L_{\text{f}}+L_{\text{h}}-1)-1} \left| \left(\mathbf{f}^{(n)} \right)^{\text{T}} \mathbf{h}_m^{(u,b)} \right|^2 P_{\lfloor m/N_{\text{S}} \rceil, \varphi_k^{(\lfloor m/N_{\text{S}} \rceil)}}^{(u,b)}. \quad (3.46)$$

This description does not allow for a decomposition into power terms and equivalent fading parameters.

Assumption 3.9. The pre-coding applied by the neighboring cells is independent of the user-channel, thus

$$\mathbf{h}_m^{(u,b)} \to \mathbf{h}_m^{(b)}. \quad (3.47)$$

If this assumption, is taken into account, the inter-cell interference power can be rewritten as

$$P_{n,\varphi_k}^{\text{inter}} = \sum_{\substack{b=1 \\ b \neq b_0}}^{B} \sum_{m=0}^{N_{\text{S}}(L_{\text{f}}+L_{\text{h}}-1)-1} \left| \left(\mathbf{f}^{(n)} \right)^{\text{T}} \mathbf{h}_m^{(b)} \right|^2 \underbrace{\sum_{u=1}^{U(b)} \sum_{\varphi_k \in \Phi^{(u,b)}} P_{\lfloor m/N_{\text{S}} \rceil, \varphi_k^{(\lfloor m/N_{\text{S}} \rceil)}}^{(u,b)}}_{\text{total transmit power per stream}}, \quad (3.48)$$

where the total transmit power per stream—this is the power used for the transmission of the data channel HS-DSCH on one particular stream—of the sector can be expressed as

$$P_n^{(b)} \triangleq \sum_{u=1}^{U} P_n^{(u,b)}. \quad (3.49)$$

If furthermore Assumption 3.7 is used, the inter-cell interference power becomes

$$P_{n,\varphi_k}^{\text{inter}} = \sum_{\substack{b=1 \\ b \neq b_0}}^{B} \sum_{m=0}^{N_{\text{S}}(L_{\text{f}}+L_{\text{h}}-1)-1} \left| \left(\mathbf{f}^{(n)} \right)^{\text{T}} \mathbf{h}_m^{(b)} \right|^2 \frac{1}{N_{\text{S}}} P^{(b)}, \quad (3.50)$$

with $P^{(b)}$ being the total power spend by sector b for data transmission.

That being said, the equivalent fading parameter specifying the *inter-cell interference gain* is defined as

$$\boxed{G_{n,b}^{\text{inter}} \triangleq \frac{1}{N_{\text{S}}} \sum_{m=0}^{N_{\text{S}}(L_{\text{f}}+L_{\text{h}}-1)-1} \left| \left(\mathbf{f}^{(n)} \right)^{\text{T}} \mathbf{h}_m^{(b)} \right|^2,} \quad (3.51)$$

thus rendering the inter-cell interference to be evaluated by

$$P_{n,\varphi_k}^{\text{inter}} = \sum_{\substack{b=1 \\ b \neq b_0}}^{B} G_{n,b}^{\text{inter}} P^{(b)}. \quad (3.52)$$

The inter-cell interference gain equivalent fading parameter represents for every neighboring sector the influence of the according transmissions onto stream n of the desired user. Some details about the generation of the equivalent fading parameter $G_{n,b}^{\text{inter}}$ and the implications of Assumption 3.9 can be found in Appendix A.6.

Thermal Noise

The thermal noise is modeled as white and Gaussian random process, statistically independent and with identical average power on all receive antennas. Accordingly, the power of the noise can be calculated as

$$P^{\text{noise}} = \mathbb{E}\left\{ \left\| \left(\mathbf{f}^{(n)} \right)^{\text{T}} \tilde{\mathbf{n}}_i \right\|^2 \right\} = \sigma_{\text{n}}^2 \, \mathbb{E}\left\{ \left\| \mathbf{f}^{(n)} \right\|^2 \right\}. \tag{3.53}$$

3.3.4. Generation of the Equivalent Fading Parameters

The major benefit of the equivalent fading parameter description is that these factors can be evaluated prior to the system-level simulation and stored for multiple applications. To do so, a fading simulation has to be conducted that calculates the receive filter as well as the pre-coding of the desired user for the intra-cell channel $\tilde{\mathbf{H}}_{\text{w}}^{(u_0,b_0)}$, and evaluates the equivalent fading parameters G_n^{s}, o_n^{intra}, o_n^{BF}, o_n^{INT}, as well as the equivalent fading parameter for the inter-cell interference $G_{n,b}^{\text{inter}}$.

To assess the characteristics of the so obtained equivalent fading parameter representation, I performed a set of simulations for a number of channels and system set-ups. The MIMO channel coefficients were generated according to the improved Zheng model, see [8,91] and the MMSE equalizer weights and the pre-coding coefficients were determined assuming perfect channel knowledge at the receiver. Furthermore, no signalization errors on the signaling channel for the pre-coding index are assumed. Details on the pre-coding codebook as well as the pre-coding choice algorithm can be found in Appendix A.2. A realistic pre-coding delay was implemented such that the actual MMSE weights are slightly mismatched to the channel conditions, with the mismatch depending on the coherence time of the channel. Note that in the utilized Jakes fading model, the coherence time is a function of the Doppler spread, directly related to the speed of the UE.

Assumption 3.10. For the equivalent fading parameter generation

- all channel delay profiles equal, and
- all streams utilize the same set of spreading codes, $\Phi_n \equiv \Phi$, which is required for the 3GPP D-TxAA HSDPA operation.

Figure 3.4 shows the empirical cumulative distribution functions (ecdfs) in case of a 2×1 single-stream transmission, both for International Telecommunication Union (ITU) Pedestrian A (PedA) and Pedestrian B (PedB) channels, as well as for *closed loop* and *open loop* operation. The term closed loop denotes that the pre-coding is active, thus the NodeB reacts to the feedback information of the UE after a delay of eleven slots, see Chapter 2. The term open loop on the other hand denotes that the pre-coding is not active, thus no channel adaptive weighting of the transmission takes place. For the single stream transmission mode obviously the inter-stream interference is not present, thus no ecdf for the equivalent fading parameter o_1^{INT} is plotted. Similarly, for the open-loop scenarios, no pre-coding gain for multi-user scheduling can

(a) PedA open-loop 2×1 single-stream.

(b) PedB open-loop 2×1 single-stream.

(c) PedA closed-loop 2×1 single-stream.

(d) PedB closed-loop 2×1 single-stream.
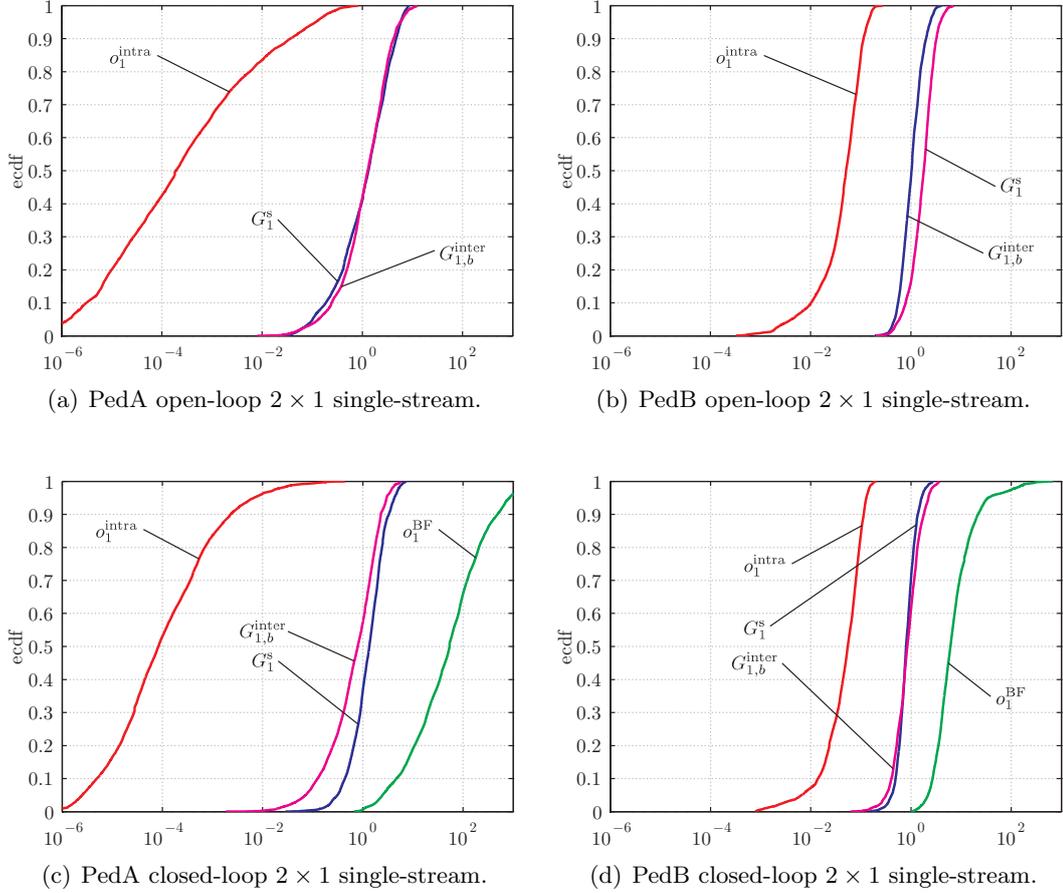
Figure 3.4.: The ecdf of the equivalent fading parameters in case of a single-stream transmission over a $N_\mathrm{T} \times N_\mathrm{R} = 2 \times 1$ MIMO channel.

be achieved, thus the equivalent fading parameter of the beamforming orthogonality o_1^BF is also not depicted.

When comparing Figure 3.4(a) with Figure 3.4(b), it can be observed that the ecdf of the intra-cell interference orthogonality o_1^intra shifts significantly to the right for the ITU PedB channel. This implies that the receive filter is less able to restore the orthogonality of the channel, thus the intra-cell interference power will be high. Furthermore, the range of the equivalent fading parameters G_1^s and $G_{1,b}^\mathrm{inter}$ shrinks under PedB channel conditions.

A similar behavior can be observed in Figures 3.4(c) and 3.4(d). Since this is a closed-loop scenario, also the equivalent fading parameter that describes the beamforming orthogonality gain o_1^BF is depicted. This fading parameter describes the relative importance of the interference caused by other users in relation to the interference caused by the desired user. Accordingly, higher values of o_1^BF denote that the interference caused by other users contributes more significantly to the total intra-cell interference power level. In the PedB case, the beamforming orthogonality gain is smaller than in the PedA case, which implies that the contribution of the other users is less significant, however, because of the dramatically increased intra-cell orthogonality o_1^intra the overall intra-cell interference is much higher than in the PedA scenario. It

(a) PedA open-loop 2×2 double-stream.

(b) PedB open-loop 2×2 double-stream.

(c) PedA closed-loop 2×2 double-stream.

(d) PedB closed-loop 2×2 double-stream.
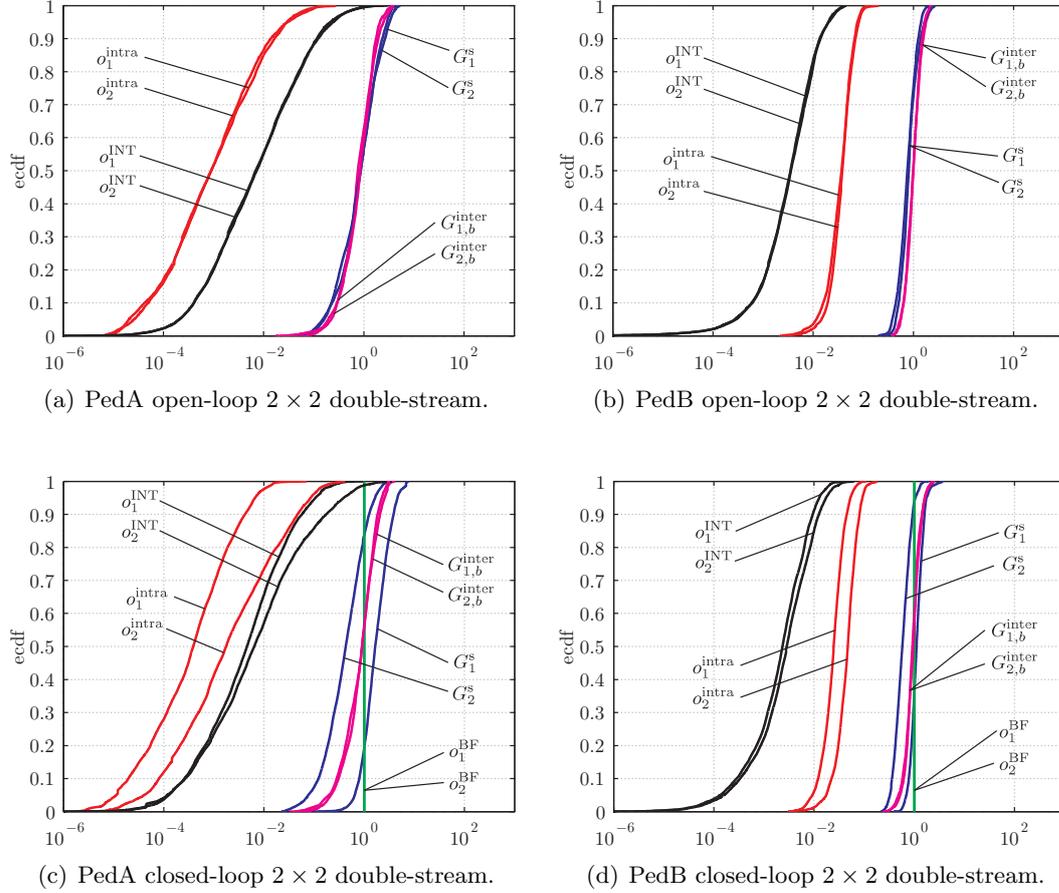
Figure 3.5.: The ecdfs of the equivalent fading parameters in case of a double-stream transmission over a $N_{\mathrm{T}} \times N_{\mathrm{R}} = 2 \times 2$ MIMO channel.

is important to know that both equivalent fading parameters, o_1^{intra} and o_1^{BF}, determine the intra-cell interference.

Figure 3.5 finally shows the ecdfs of the equivalent fading parameters for the 2×2 MIMO channel when utilizing a double stream transmission. In contrast to Figure 3.4, now also the ecdfs for the inter-stream interference orthogonality o_n^{INT} are included. In Figures 3.5(a) and 3.5(b), in addition to the behaviors identified so far, it can also be observed that the inter-stream interference orthogonality range is shrunk and shifted slightly to higher values in case of the longer delay spread PedB channel. This indicates that the receive filter cannot resolve the spatial separation of the streams equally well as in the PedA scenario. Furthermore, due to the open-loop operation, the equivalent fading parameters of both streams are equal, due to fact that no channel state information is exploited to adapt to by means of pre-coding.

The situation however changes when inspecting the ecdfs of the equivalent fading parameters for the closed-loop scenario. Figures 3.5(c) and 3.5(d) clearly show a favoring of stream one compared to stream two. For higher delay spread channels, the performance gap between the two streams becomes smaller, rendering the individual performance more equally. The reason for the performance gap between stream one and stream two lies in the pre-coding choice as

39

defined by 3GPP [6]. Due to the strong quantization of the utilizable pre-coding vectors, as well as the coupling between the pre-coding for stream one and stream two, always stream one will be favored. Details on this issue can be found in Appendix A.2.

Another interesting observation in Figures 3.5(c) and 3.5(d) is that the beamforming orthogonality gain o_n^{BF} is constant and equal to one in these simulation setups. A simple argument for this is that in a 2×2 MIMO channel, only two Degrees of Freedom (DoF) exist to separate users by the choice of the pre-coding vectors. In the double stream mode, however, both degrees of freedom are already used for the transmission of the two independent streams, such that the users cannot gain any further from a potential different choice of their corresponding pre-coding weights. Given this intuitive reasoning, let me put this into a more rigorous form.

Theorem 3.1. *Assume that $N_S = N_T = 2$ and the pre-coding matrix $\mathbf{W}_{CB}$ is unitary. Then the beamforming orthogonality gain is identical to one for all users and streams,*

$$o_n^{BF} \equiv 1. \tag{3.54}$$

Proof. The proof is given in Appendix A.4. □

Given the shape of the ecdfs in Figures 3.4 and 3.5, one might argue that the equivalent fading parameters could be described by normal-distributions with suitable mean and variance. The argument behind this is based on the central limit theorem, which states that the sum of a sufficiently large number of independent random variables, each with finite mean and variance, will be approximately normally distributed given a set of conditions. In particular, let the sum of M random variables be $S_M = X_1 + \cdots + X_M$. Then, defining the random variable $Z_M = (Z_M + M\mu)/(\sigma\sqrt{M})$, the distribution of Z_M converges towards the standard normal distribution $\mathcal{N}(0,1)$, with

$$\mathcal{N}(\mu,\sigma) \triangleq \frac{1}{\sigma\sqrt{2\pi}} \exp\left[\frac{(x-\mu)^2}{2\sigma^2}\right], \tag{3.55}$$

as the number of independent random variables tends to infinity, $M \to \infty$ [92].

To investigate this issue, I compared the distribution of the equivalent fading parameters G_n^{s}, o_n^{intra}, o_n^{INT}, and $G_{n,b}^{\text{inter}}$ of a closed loop D-TxAA double stream transmission for a 2×2 PedA MIMO channel. The results are given in Figure 3.6, showing a probability plot of the fading parameter compared to the reference line of the normal distribution.[9] It can clearly be observed that the equivalent fading parameters do not match the normal distribution.

There are at least two reasons that lead to a violation of the central limit theorem in this context: (i) the individual samples are not statistically independent, and (ii) the pre-coding—which is included in the equivalent fading parameters—is matched to the channel realizations. This however also implies that a coarse modeling of the equivalent fading parameters by random Gaussian processes—even if chosen to be correlated—would lead to substantial inaccuracy.

3.3.5. Influence of Non-Data Channels

So far, only the effects of the HS-DSCH have been considered, but in a network also synchronization and pilot channels, as well as other signaling channels are needed. In the context of the system-level modeling, the additional interference imposed by these channels can be split into

---

[9]A probability plot compares the distribution of a sample set to the normal distribution. The y-axis therefore is scaled such that the probability density function (pdf) of the normal distribution is stretched to a straight line. This allows a simple visual inspection of the difference between the normal distribution and the sample epdf.
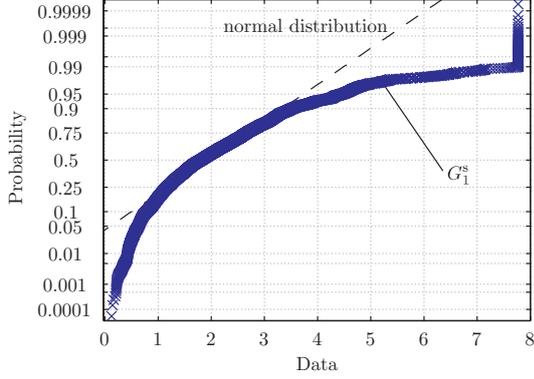
(a) Comparison of G_n^{s} of stream one against a normal distribution.
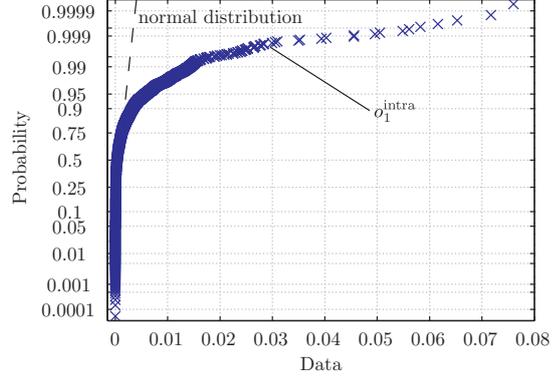
(b) Comparison of o_n^{intra} of stream one against a normal distribution.
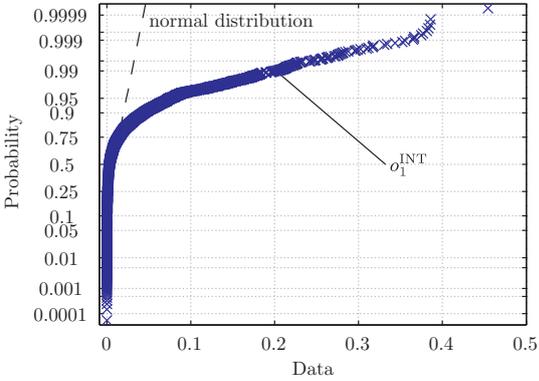
(c) Comparison of o_n^{INT} of stream one against a normal distribution.
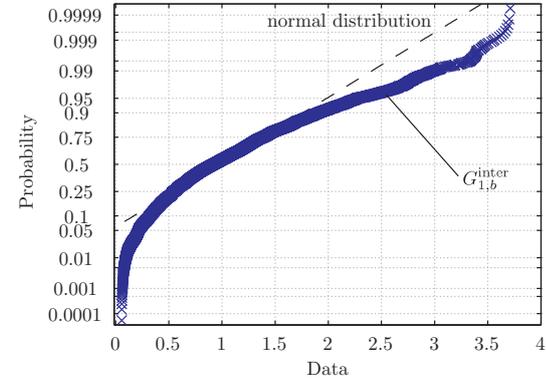
(d) Comparison of $G_{n,b}^{\mathrm{inter}}$ of stream one against a normal distribution.

Figure 3.6.: Comparison of the distributions of the equivalent fading parameters for a closed-loop 2×2 PedA double-stream transmission scenario against a normal distribution of equal variance.

two parts, (i) the channels without spreading, for example the synchronization channels, and (ii) the channels with spreading, for example the CPICH.

Assumption 3.11. No signaling channel cancelation at the receiver takes place.

If an enhanced interference cancellation receiver is utilized, the effect would have to be accounted for by a reduction of the interference power, thus requiring a more advanced modeling, see also Assumption 3.2.

In analogy to Section 3.3.3, the additionally imposed interference can be split into three separate parts. Considering the total transmit power of the non-spread channels in the target cell to be $P^{\mathrm{non\text{-}spread},(b_0)}$, the interference power directly affecting the desired stream n, can be approximated by

$$P_{n,\varphi_k}^{\mathrm{signaling_1}} \triangleq P_{n,\varphi_k}^{\mathrm{signaling_1},(b_0)} \approx G_n^{\mathrm{s}} P^{\mathrm{non\text{-}spread},(b_0)}, \tag{3.56}$$

which is only an approximation, because the signaling channels are not pre-coded. The interfer-

ence power added on top of all other streams, which are again interfering with the desired stream is

$$P_{n,\varphi_k}^{\text{signaling}_2} \triangleq P_{n,\varphi_k}^{\text{signaling}_2,(b_0)} \approx \sum_{\substack{m=0 \\ m\neq n}}^{N_{\text{S}}} o_n^{\text{INT}} P^{\text{non-spread},(b_0)}, \tag{3.57}$$

and the remaining inter-symbol and inter-code interference can be evaluated to be

$$P_{n,\varphi_k}^{\text{signaling}_3} \triangleq P_{n,\varphi_k}^{\text{signaling}_3,(b_0)} \approx o_n^{\text{intra}} G_n^{\text{s}} P^{\text{non-spread},(b_0)}. \tag{3.58}$$

Adding these individual parts, the total interference caused by the non-spread signaling channel is given by

$$\sum_{i=1}^{3} P_{n,\varphi_k}^{\text{signaling}_i} \approx P^{\text{non-spread},(b_0)} \left[G_n^{\text{s}} \left(1 + o_n^{\text{intra}} \right) + \sum_{\substack{m=0 \\ m\neq n}}^{N_{\text{S}}} o_n^{\text{INT}} \right]. \tag{3.59}$$

The interference caused by other spread channels can be treated similarly to the intra-cell interference, caused by loss of spreading code orthogonality. Assuming the total power of other spread channels in the cell to be $P^{\text{spread},(b_0)}$, the interference can be evaluated to be

$$P_{n,\varphi_k}^{\text{signaling}_4} \triangleq P_{n,\varphi_k}^{\text{signaling}_4,(b_0)} \approx o_n^{\text{intra}} G_n^{\text{s}} P^{\text{spread},(b_0)}, \tag{3.60}$$

and accordingly, the total signaling interference power becomes

$$P_{n,\varphi_k}^{\text{signaling}} = \sum_{i=1}^{4} P_{n,\varphi_k}^{\text{signaling}_i} = P^{\text{non-spread},(b_0)} \left[G_n^{\text{s}} \left(1 + o_n^{\text{intra}} \right) + \sum_{\substack{m=0 \\ m\neq n}}^{N_{\text{S}}} o_n^{\text{INT}} \right] + o_n^{\text{intra}} G_n^{\text{s}} P^{\text{spread},(b_0)}. \tag{3.61}$$

3.3.6. Resulting SINR Description

With these findings, the SINR on stream n and spreading code φ_k, as observed after equalization and despreading,[10] can be expressed as

$$\text{SINR}_{n,\varphi_k} = \frac{\text{SF} \cdot P_{n,\varphi_k}^{\text{s}} \frac{1}{L^{(b_0)}}}{\left(\text{SF} \cdot P_{n,\varphi_k}^{\text{INT}} + \bar{P}_{n,\varphi_k}^{\text{intra}} + P_{n,\varphi_k}^{\text{signaling}} \right) \frac{1}{L^{(b_0)}} + \sum_{\substack{b=1 \\ b\neq b_0}}^{B} G_{n,b}^{\text{inter}} P^{(b)} \frac{1}{L^{(b)}} + P^{\text{noise}}}, \tag{3.62}$$

where SF denotes the spreading factor of the HSDPA data channels. The term $\frac{1}{L^{(b)}}$ represents the macro-scale and shadow-fading path-loss components of the MIMO channel in the network context. Details about the composition and the modeling of this term will be given in Section 4.1. For D-TxAA HSDPA in particular, the inter-stream interference power $P_{n,\varphi_k}^{\text{INT}}$ in Equation (3.62) simplifies to

$$P_{n,\varphi_k}^{\text{INT}} = o_{\neg n}^{\text{INT}} P_{\neg n,\varphi_k^{(\neg n)}}^{(u_0,b_0)}, \tag{3.63}$$

where $\neg n$ denotes the opposite stream of stream n.

The description contains only equivalent fading parameters and power terms, which do not depend on each other. Accordingly, traces for the fading parameters may be generated prior

---

[10] Also often called symbol-level SINR.

to the system-level simulation, and thus only real-valued scalar multiplications will occur in Equation (3.62) when evaluated on system-level. It is also worth noticing that in principle only one trace for each equivalent fading parameter has to be generated, statistical independence between different realizations for different users can always be achieved by choosing independent starting indices, for example drawn uniformly over the length of the respective trace. However, if such an implementation is desired, the equivalent fading parameter traces have to be interpreted as a loop trace, which means that when the current index within the trace reaches its end, it will start from the beginning of the trace again. The index pointing to the current position in the trace thus has to be taken modulo the length of the trace. To avoid *edge*-effects when the trace index jumps from the end to the beginning, some sort of *smoothing* has to be performed, for example by linear interpolation.

Furthermore, although I only applied ITU channel profiles in this work, I want to point out that the proposed structure can be utilized for arbitrary channel models, like the Spatial Channel Model (SCM) or the Spatial Channel Model Extended (SCME) [93].

3.3.7. Validation

To show that the proposed link-quality model can accurately approximate the SINR for various operation modes of the physical layer, I conducted a set of link-level simulations. For this purpose, a physical-layer simulator was developed [21], to compare the *true* SINR with the SINR predicted by the model in Equation (3.62). The basic functionality of the physical-layer simulator is built on parts of the implementation of [94] with some necessary adaptions.

The utilized MIMO HSDPA physical-layer simulator emulates the transmission of the shared user-data channel HS-DSCH and the pilot channel(s) CPICH. The bit sequences in the simulator flow are encapsulated in TTIs of 2 ms each, as explained in Chapter 2. The channel model implemented is generating block-fading channel realizations on a TTI basis, using the Rayleigh fading generator of [8, 91]. For the validation simulations, however, some restrictions apply, in particular

- channel estimation is not taken into account, thus full CSI is assumed at the receiver,
- large-scale and shadow fading issues are not taken into account,[11] and
- inter-cell interference is not considered in the simulation.

Although these are restrictive assumptions, still the inter-stream and intra-cell interference modeling accuracy can be assessed very well.

Since Equation (3.62) predicts the SINR after equalization and de-spreading, the values obtained by the model with the *true* SINR have to be compared. By defining the de-spread symbol of the transmit chips for stream n utilizing spreading-code φ_k,

$$\hat{s}^{(n,\varphi_k)} = \bar{\varphi}_k^{(n)}\left\{\hat{x}^{(n,\varphi_k)}\right\}, \tag{3.64}$$

where I omitted the time indices for sake of notational simplicity, the *true* SINR is given by evaluating

$$\mathrm{SINR}_{n,\varphi_k}^{\mathrm{true}} \triangleq \frac{\mathbb{E}\left\{\left\|s^{(n,\varphi_k)}g^{(n)}\right\|^2\right\}}{\mathbb{E}\left\{\left\|s^{(n,\varphi_k)}g^{(n)} - \hat{s}^{(n,\varphi_k)}\right\|^2\right\}}, \tag{3.65}$$

---

[11]Note that these terms will be explained in more detail in the context of the system-level simulator in Section 4.1.

Table 3.1.: Simulation parameters for SINR link-quality model validation simulations.

Parameter	Value
fading model	improved Zheng model [8, 91]
transmitter frequency	2.0 GHz
channel type	PedA, PedB, VehA
power of signaling channels	zero
CSI at receiver	perfect
nr. of spreading codes per stream	15
spreading factor	SF = 16
pre-coding	3GPP [6], algorithm from Appendix A.2
pre-coding delay	11 slots
equalizer span L_f	$\{20, 30, 40\}$ chips
UE speed	$\{3, 120\}$ km/h
nr. of simulated slots	1500, each 2/3 ms

with the expectation operation being conducted by temporal averaging over all symbols in a TTI. The *physical-layer gain* $g^{(n)}$ on stream n represents the attenuation of the overall impulse response at delay τ and is defined as

$$g^{(n)} \triangleq \left\| \left(\mathbf{f}^{(n)}\right)^\text{T} \mathbf{h}_{\tau N_\text{S}+n}^{(u_0,b_0)} \right\|, \quad n = 0, \dots, N_\text{S} - 1. \tag{3.66}$$

The simulation parameters for the physical-layer validation simulations are listed in Table 3.1. Since a full investigation of all possible physical layer operation modes would exceed the scope of this thesis, I restricted myself to the following operation modes:

(i) SISO 1×1 mode,

(ii) Multiple-Input Single-Output (MISO) 2×1 Closed Loop (CL) Single-Stream (SS) TxAA mode,

(iii) MIMO 2×2 CL SS TxAA mode, and

(iv) MIMO 2×2 CL Double-Stream (DS) D-TxAA mode,

which I simulated for different equalizer lengths L_f as well as channel profiles. Note that the UE speed was set according to the ITU recommendations for the respective channel profile.

The results are illustrated in Figure 3.7. All figures depict the HS-PDSCH[12] SINR versus the E_c/N_0, in this simulation given by

$$\frac{E_\text{c}}{N_0} = \underbrace{\overbrace{\frac{P^\text{HS-DSCH}}{|\Phi|}}^{=P^\text{HS-PDSCH}} \frac{1}{\text{SF}}}_{=E_\text{c}} \frac{1}{N_0}, \tag{3.67}$$

---

[12]Remember that this channel corresponds to one particular spreading-code on the physical-layer, as explained in Chapter 2.

(a) SISO 1×1 and MISO 2×1 CL SS TxAA mode in a PedA channel.

(b) MIMO 2×2 CL SS TxAA and DS D-TxAA mode in a PedA channel.

(c) SISO 1×1 and MISO 2×1 CL SS TxAA mode in a PedB channel.

(d) MIMO 2×2 CL SS TxAA and DS D-TxAA mode in a PedB channel.
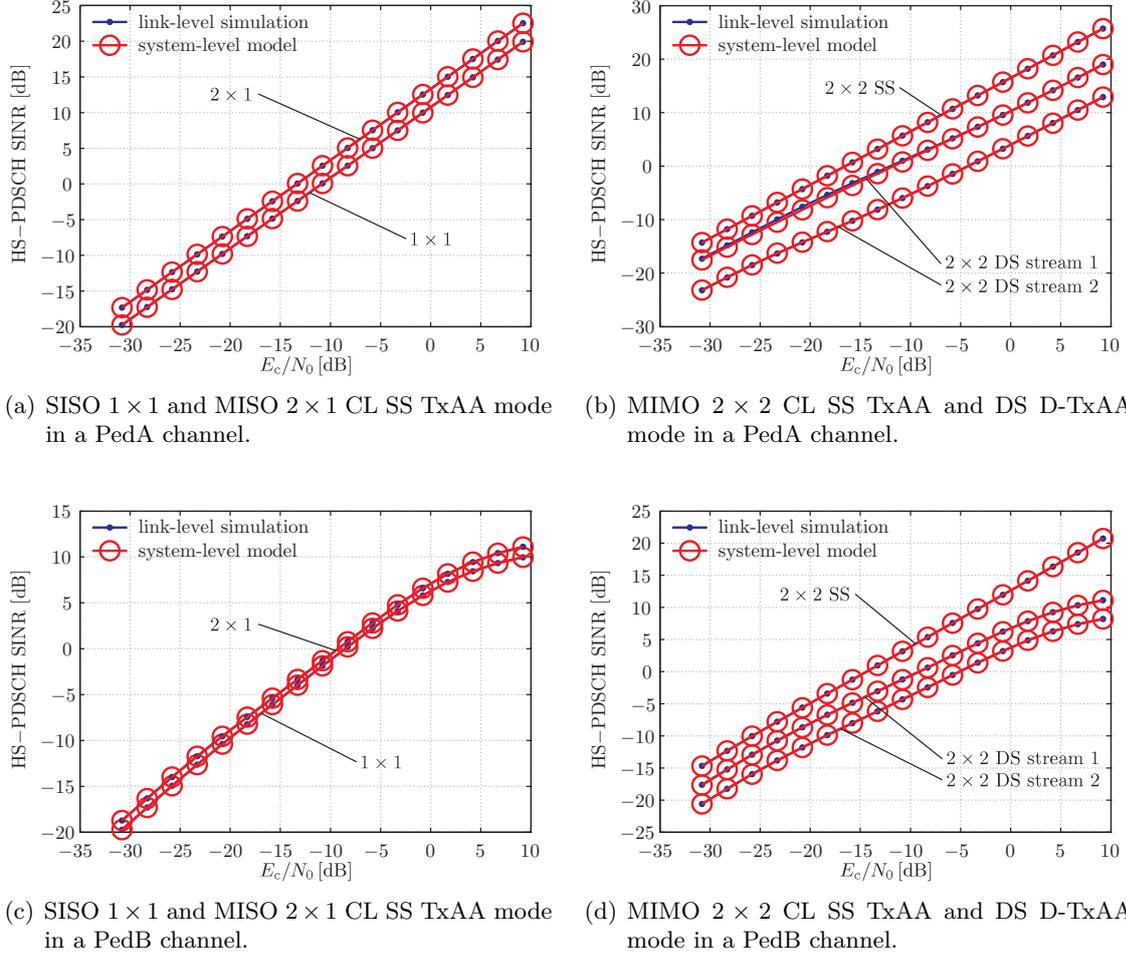
Figure 3.7.: Link-quality model validation results for an equalizer length of $L_\mathrm{f} = 20$ chips in PedA and PedB channels.

with $P^{\text{HS-DSCH}}$ and $P^{\text{HS-PDSCH}}$ denoting the power of the HS-DSCH and the HS-PDSCH, respectively. The E_c/N_0 can be interpreted as a *geometry-factor* here, with higher values corresponding to a UE position closer to the NodeB, see Appendix A.11. Note that for the simulations conducted in this section, I assumed the sets of utilized spreading codes is equal for all streams, $\Phi \equiv \Phi_0 = \Phi_1$, which is also forced by the 3GPP standard in a practical network implementation. Furthermore, since I utilized 15 spreading-codes per stream, no multi-user scheduling was implemented.

Figure 3.7 shows the results for an equalizer span of $L_\mathrm{f} = 20$ chips. In the PedA channel, the model fitting is very accurate for the whole range of simulated E_c/N_0 values. The gain of the second transmit antenna—including the pre-coding gain—as well as the already identified offset between the first and second stream in the DS mode can be easily observed in these plots as well. When looking at the results in case of the PedB channel, it can be observed that in the SISO 1×1, the MISO 2×1 and the MIMO 2×2 DS mode, the HS-PDSCH SINR is saturating for higher E_c/N_0 values. Furthermore, the gain of the second transmit antenna is diminishing. Only
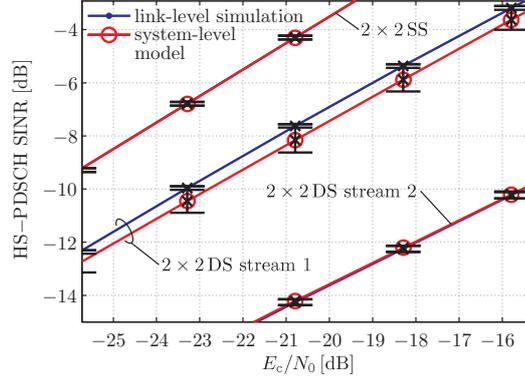
Figure 3.8.: Confidence interval results with 99% confidence level for the simulations of Figure 3.7(b). The Bootstrapping was performed with 1000 bootstrap samples.

in case of the MIMO 2×2 SS mode, the performance is less harmed, which is a result of the higher receive diversity offered by the second receive antenna. Note that in the MIMO 2×2 DS mode, this receive diversity cannot be exploited, because all DoF are utilized for the transmission of spatial multiplexed data streams. Further validation results can be found in Appendix A.5.

In order to assess the quality of the simulated SINR statistics, I also computed the 99% confidence intervals of the estimated mean of the SINR by means of bootstrapping. The results for the simulation of Figure 3.7(b) are presented in Figure 3.8, showing a detail view. It can be observed that the confidence intervals are very small, showing a nearly perfect estimation accuracy due to the large simulated sample sizes. Figure 3.8 also shows a slight deviation between the link-level simulation and the system-level model results for the first stream of the 2×2 DS mode. This is due to the averaging in the intra-cell interference expression. Accordingly, also the confidence intervals for this stream are larger than for all other cases.

Since the results presented so far only illustrate the *mean* SINR fit of the proposed model, I also investigated the statistics of the model as well as the *true* SINR for one specific example. Figure 3.9 depicts the ecdfs of the four transmission modes when an equalizer with span $L_\mathrm{f} = 30$ chips is utilized in an channel with PedB profile. The ecdfs represent the HS-PDSCH SINR when operated at $E_\mathrm{c}/N_0 = -15.8\,\mathrm{dB}$.

It can be observed that the fit of the model even in terms of the SINR statistics is nearly perfect. Thus it can be concluded that the simplifications introduced in Sections 3.3.3 and 3.3.4 do not impose any significant restrictions to the accuracy of the modeling. Further validations have also been conducted by means of an HSDPA measurement campaign [16], utilizing a MIMO testbed [95]. The results also showed similar modeling accuracy under real-world channel conditions.

3.3.8. Complexity

The biggest benefit of utilizing a system-level model instead of a full physical-layer simulation is the savings in terms of computational complexity. To assess the gain of the proposed link-quality model in this context, I investigate the computational complexity both analytically and by means of simulations. As already mentioned in Section 3.3.3, the resulting description of the SINR in Equation (3.62) only requires the loading of the pre-computed equivalent fading parameters and

(a) SISO 1×1 and MISO 2×1 CL SS TxAA mode in a PedB channel.

(b) MIMO 2×2 CL SS TxAA and DS D-TxAA mode in a PedB channel.
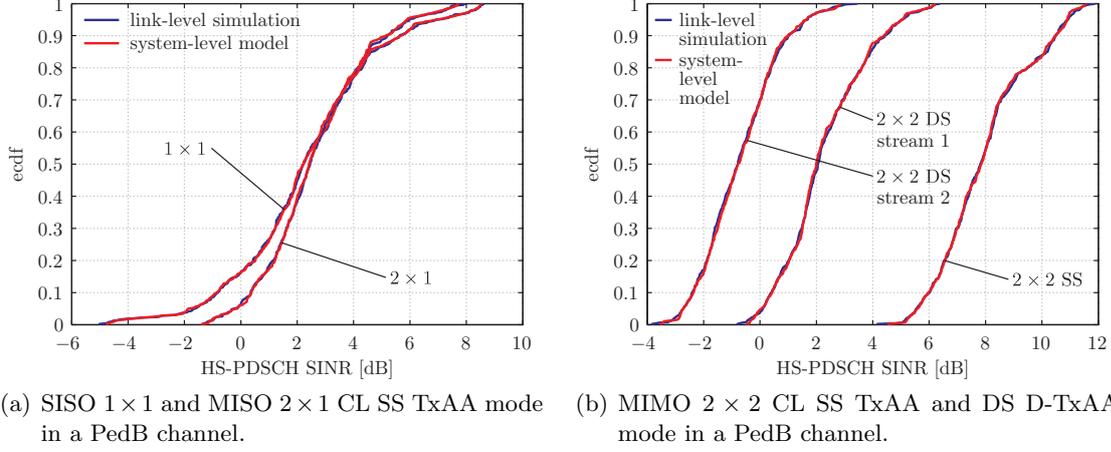
Figure 3.9.: Detailed validation simulation in case of a PedB channel profile, utilizing an equalizer span of $L_\mathrm{f} = 30$ chips, at $E_\mathrm{c}/N_0 = -15.8\,\mathrm{dB}$.

a couple of real-valued scalar multiplications.

In contrast to that, a full evaluation of the physical-layer without introducing the equivalent fading parameter structure would lead to a large effort in calculating not only the interference terms, but also to evaluate the pre-coding choices and the equalizer coefficients. The channel encoding and de-coding procedures, which will be covered by the link-performance model, are contributing to the complexity as well, but in this section, only the savings from the link-quality point of view are investigated. The computational complexity of the physical-layer parts covered by the link-quality model can thus be estimated by evaluating three terms.

(i) The evaluation of the computational complexity of the pre-coding is based on Equation (A.13),

$$\arg \max_{w_2} \mathbf{w}_1^\mathrm{H} \mathbf{R} \mathbf{w}_1 \sim 4\mathcal{O}\Big\{ L_\mathrm{h} N_\mathrm{T}^2 + N_\mathrm{T}^2 N_\mathrm{S} + N_\mathrm{T} N_\mathrm{S}^2 \Big\}, \tag{3.68}$$

which holds if matrix multiplications are assumed to be of order $\mathcal{O}\{k^3\}$ for $k \times k$ matrices.

(ii) Similarly, the computational complexity of the equalizer calculation in Equation (3.14) can be approximated by

$$\mathbf{R}_{\mathbf{x}_{i-\tau}^\mathrm{S} \tilde{\mathbf{x}}_i} \tilde{\mathbf{H}}_\mathrm{w}^\mathrm{H} \Big(\tilde{\mathbf{H}}_\mathrm{w} \mathbf{R}_{\tilde{\mathbf{x}}_i} \tilde{\mathbf{H}}_\mathrm{w}^\mathrm{H} + \mathbf{R}_{\tilde{\mathbf{n}}_i} \Big)^{-1} \sim$$
$$\mathcal{O}\Big\{ N_\mathrm{S}^3 (L_\mathrm{f} + L_\mathrm{h} + 1) + N_\mathrm{S}^3 (L_\mathrm{f} + L_\mathrm{h} - 1)^2 \Big\} + \mathcal{O}\Big\{ N_\mathrm{S}^2 (L_\mathrm{f} + L_\mathrm{h} - 1) N_\mathrm{R} L_\mathrm{f} + N_\mathrm{S}^3 N_\mathrm{R}^3 L_\mathrm{f}^3 \Big\}. \tag{3.69}$$

(iii) Finally, the complexity of the convolution of the transmit signal with the channel and the de-spreading, in a multi-user, multi-NodeB scenario can be evaluated to be

$$\sim \underbrace{\mathcal{O}\{ N_\mathrm{S} (L_\mathrm{f} + L_\mathrm{h} - 1) \}}_{\text{convolution}} + \underbrace{B\mathcal{O}\Big\{ (N_\mathrm{R} L_\mathrm{f})^3 \Big\}}_{\text{receive filtering}} + \underbrace{\sum_{\substack{b=0 \\ b \neq b_0}}^{B} \mathcal{O}\{ U_b N_\mathrm{S} (L_\mathrm{f} + L_\mathrm{h} - 1) \}}_{\text{inter-cell interference}} + \underbrace{\mathcal{O}\{ \mathrm{SF}\, |\Phi_n| \}}_{\text{de-spreading}}. \tag{3.70}$$

Note that these three terms do not take the generation of the channel coefficients and the noise realizations into account.

On the other hand, assuming the computation of the equivalent fading parameters is performed offline, the complexity on system-level utilizing the proposed structure resulting in Equation (3.62) can be approximated by

$$\sim \mathcal{O}\{N_{\text{S}}\left(4 + 2U_0 + B\right)\}. \tag{3.71}$$

By summation of all terms for the full physical-layer evaluation, the *relative* complexity of the proposed model, c_{r}, can be shown to be proportional to

$$c_{\text{r}} \propto \frac{1}{p_3(L_{\text{f}})}, \tag{3.72}$$

when the number of sectors B and the according number of users U_b, as well as the transmission mode, given by N_{T}, N_{R} and N_{T} are fixed. The term $p_3(L_{\text{f}})$ denotes a polynomial of third order in L_{f}, that is

$$p_3(x) \triangleq \sum_{i=0}^{3} a_i x^i, \tag{3.73}$$

with a_i being the coefficients of the polynomial.

To verify this result in a practical setting, I compared the simulation runtimes of the full physical-layer evaluation with the system-level model approach in a MATLAB environment. Figure 3.10 shows the relative complexity, approximated by the relative difference between the simulation runtimes,

$$c_{\text{r}} \approx \frac{t_{\text{system-level}}}{t_{\text{full physical-layer}}}, \tag{3.74}$$

when evaluating only one TTI, but averaging over many channel realizations for different transmission modes,[13] as well as channel profiles. The number of sectors was chosen to be $B = 2$, each with one active user, $U_b \equiv 1$. It can be observed that the savings in terms of the relative computational complexity are enormous, although in the system-level approach, the equivalent fading parameters have to be loaded in memory before being usable. These savings of course scale linearly with the number of simulated TTIs, thus implying even larger gains for longer simulation traces.

Figure 3.10(a) furthermore shows the fit of the analytical third order rational from Equation (3.72) for the MIMO 2×2 DS transmission mode in a PedA channel. It can be observed that by trend the analytically estimated complexity savings are valid.

3.4. Link-Performance Model

So far, the system-level modeling in this chapter has introduced a way of accurately evaluating the link-quality in terms of the post-equalization and despreading SINR. As mentioned in Section 3.3, the link-quality model depends on numerous factors determined by the network, as well as the transmission scheme currently in use.[14] Hence, the link-quality model is strongly related to the system concept.

---

[13]The transmission mode in this context specifies the number of receive antennas N_{R}, transmit antennas N_{T}, and streams N_{S}.

[14]This is also reflected by the different structure of the signal and interference components of the link-quality model in Appendix B.2.
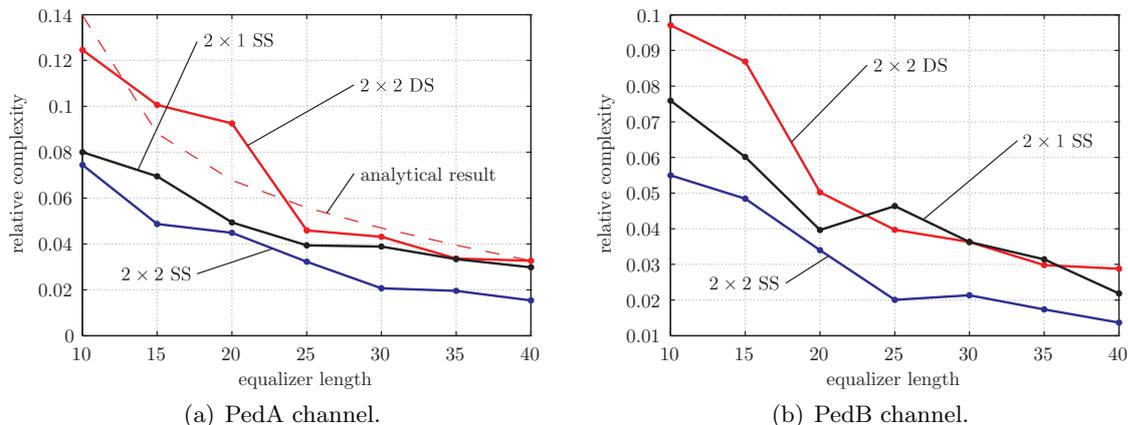
Figure 3.10.: Average computational complexity of the system-level link quality model relative to the full physical-layer evaluation complexity per TTI.

A *link-performance* model, on the other hand, should provide an estimate of the link performance in terms of the BLER or PER when the decisions on the RRM, scheduling, and link-adaptation are already known [80]. Link-performance models generate bit- or block-error probabilities and are used for performance estimation at the system-level simulation run-time. This, in turn, can generate for example retransmissions and affect the slow link-adaptation, as for example the slow outer-loop power-control in Release 4 UMTS systems. In principle, a link-performance model can be viewed as the conditional probability that the transmitted code-word is decoded erroneously given the link-quality during the interleaving period. Since the RRM decisions are already known when the link-performance model is needed in the system-level context, these models are generally less complicated than the link-quality models because for example mismatches due to possibly unknown scheduling decisions are not an issue.

Also note that a suitable link-performance model can be used for a large set of different system-realizations. Since the developed link-quality model represents the complete physical-layer processing in between the channel-coding related code-word processing—as can be observed for example in Figure 3.1—no changes in the link-performance model are needed when details within the link-quality model are changed. Accordingly, for such investigations the equivalent fading parameters can easily be generated for some variations of the physical-layer processing, allowing for flexible investigations of the modeled transmission system.

In times of GSM, system-level link-performance modeling was based on the average PER for all transmissions on one link, thus evaluating an average BLER as a function of the linear average SINR observed during the time a user was served. This may be adequate as long as every packet encounters similar channel statistics, which would imply very large packet or coding-block lengths with respect to the channel coherence time. However, it is known that specific channel realizations, especially for small transport-block lengths, may result in largely different performances from the one predicted by the average link-quality [96].[15] This has a significant impact on network based mechanisms like scheduling. Thus, as already mentioned in Section 3.3, useful modeling of the performance of fast scheduling, fast link-adaptation and

---

[15]This refers also to the discussion about the scheduler influence on the channel statistics at the beginning of Chapter 1.
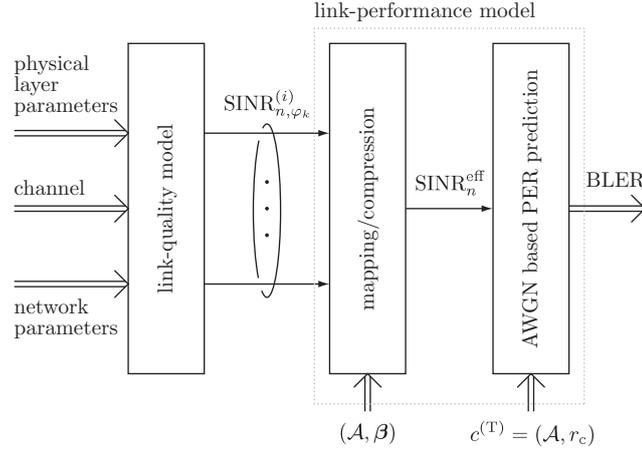
Figure 3.11.: Basic concept of the proposed link-performance model, including the input parameter generation by the link-quality model. The mapping/compression depends on the symbol alphabet $\mathcal{A}$, as well as a vector of tuning parameters $\boldsymbol{\beta}$. Similarly, the AWGN based PER prediction depends on the symbol alphabet and the coding rate r_c of the current transmission, constituting the transmit CQI $c^{(\mathrm{T})}$.

HARQ is impossible with average or large-scale parameters and accordingly small-scale effects have to be included.

3.4.1. Link-Performance Model Concept

The basic structure of the proposed link-performance model and its connection to the proposed link-quality model is depicted in Figure 3.11. The principal idea follows the framework of [80, 84] which I adapted to the needs of MIMO HSDPA.

As illustrated, the link quality model provides small-scale fading dependent link-quality estimates, $\mathrm{SINR}_{n,\varphi_k}$, given by Equation (3.62). Note that, as explained in Chapter 2, the packet unit in HSDPA is given by a sub-frame or transport block with the length of one TTI. A straightforward approach would thus be to evaluate the link-quality once every TTI and utilize the resulting measurements as input parameters to the link-performance model. If, however, the link-quality changes significantly during one sub-frame, a link-performance model utilizing TTI based SINR sampling—corresponding to an *average* SINR evaluation for every sub-frame—would not reflect these variations and thus probably lead to too optimistic performance predictions. Such a situation would occur in a scenario where the users are moving or the channel varies due to changes in the environment.

To overcome this problem, I propose to conduct an *oversampling* in terms of the link-quality model estimates, thus evaluating $\mathrm{SINR}_{n,\varphi_k}$ more than once per sub-frame. In particular, I suggest to evaluate the SINR on a slot basis, that is three times per TTI,

$$\mathrm{SINR}_{n,\varphi_k}^{(i)}, \; i = 1, 2, 3, \tag{3.75}$$

with i denoting the relative time index within one TTI. This obviously allows for an increased accuracy in movement scenarios.[16]

---

[16]To estimate the maximum speed that can be covered accurately by this link-quality model sampling rate, let

Given the slot-sampled link-quality model estimations, the link-performance model has to estimate the link performance in terms of the ACK/NACK report for the individual transport block. In principle, the best—in terms of accuracy—link-performance model approach would be to utilize a multi-dimensional mapping that directly converts the SINRs to the anticipated BLER,

$$\text{SINR}_{n,\varphi_k}^{(i)} \mapsto \text{BLER}, \tag{3.76}$$

but this would require analytic models of very high complexity, or unfeasible large look-up tables. A more suitable way of representing the information contained in the sampled link-quality model data is to compress the input parameters to a few *effective* link-quality parameters. Recent work on that subject tries to extract potential gains in accuracy by mapping the input parameters to two-dimensional output data [99], for example given by the average SINR as well as the variance of the estimated SINR values.

For this thesis, I utilized a compression mapping that results in an one-dimensional *effective* SINR per spatial stream, $\text{SINR}_n^{\text{eff}}$. The idea for the representation of the link-performance in terms of an effective SINR was already proposed in [100], but has not been used for system-level modeling at that time. Let me denote the mapping/compression stage of the proposed link-performance model in Figure 3.11 by

$$f_{\text{M}}(\mathcal{A}, \boldsymbol{\beta}) : \text{SINR}_{n,\varphi_k}^{(i)} \mapsto \text{SINR}_n^{\text{eff}}, \tag{3.77}$$

with $\mathcal{A}$ and $\boldsymbol{\beta}$ denoting the utilized symbol alphabet for the transmission of the current transport block and a vector of tuning parameters, respectively. Note that the HSDPA link-adaptation does not allow for a change of the symbol alphabet within a transport block.

The mapping function $f_{\text{M}}(\mathcal{A}, \boldsymbol{\beta})$ that turned out to be the best in terms of accuracy and flexibility was the so-called Mutual Information Effective Signal to Interference and Noise Ratio Mapping (MIESM). This mapping has initially been proposed in the Radio Access Network (RAN) working meetings of 3GPP [101], and builds upon the Bit-Interleaved Coded Modulation (BICM) capacity as identified in [102],[17]

$$I(x) = \log_2 |\mathcal{A}| - \mathbb{E}_y \left\{ \frac{1}{|\mathcal{A}|} \sum_{d=1}^{\log_2 |\mathcal{A}|} \sum_{b=0}^{1} \sum_{z \in \mathcal{A}_b^{(d)}} \log \frac{\sum_{\hat{x} \in \mathcal{A}} \exp\left[-|y - \sqrt{x}\,(\hat{x} - z)|^2 \right]}{\sum_{\hat{x} \in \mathcal{A}_b^{(d)}} \exp\left[-|y - \sqrt{x}\,(\hat{x} - z)|^2 \right]} \right\}, \tag{3.78}$$

with $|\mathcal{A}|$ denoting the cardinality of the symbol alphabet $\mathcal{A}$, y being a zero mean unit variance complex Gaussian variable and $\mathcal{A}_b^{(d)}$ denoting the set of symbols for which bit d equals b. The resulting mutual information curves in comparison to the Shannon capacity are depicted in

---

me apply the Jakes model [97]. It is well known [49] that the channel coherence T_{C} time can be approximated as a function of the Doppler spread, D_{S}, that is $T_{\text{C}} \approx 1/D_{\text{S}}$. Assuming a Doppler power spectral density as derived by Jakes, the Doppler spread can be approximated by $D_{\text{S}} \approx 2f_{\text{s,max}}$, with $f_{\text{s,max}}$ denoting the maximum Doppler frequency shift relative to the carrier frequency f_{c}. This is not always fulfilled in practice, but is a reasonable approximation [98]. The maximum Doppler frequency shift can be calculated according to $f_{\text{s,max}} = f_{\text{c}}v/c_0$, with v denoting the relative speed of the transmitter/receiver and the scatterers, and c_0 being the light speed. Accordingly, the maximum v to result in a channel coherence time, less than one slot duration of $2/3$ ms is approximately 31.25 km/h. Considering that the target scenario of HSDPA is static this seems to be sufficient for most investigation scenarios.

[17]A list of other mapping functions can be found in [80], including for example the well-known Exponential Effective Signal to Interference and Noise Ratio Mapping (EESM). For GSM, some of the proposed mapping functions were based on the so-called *raw* bit-error probability [103], but was shown to be of less accuracy than other methods [80].
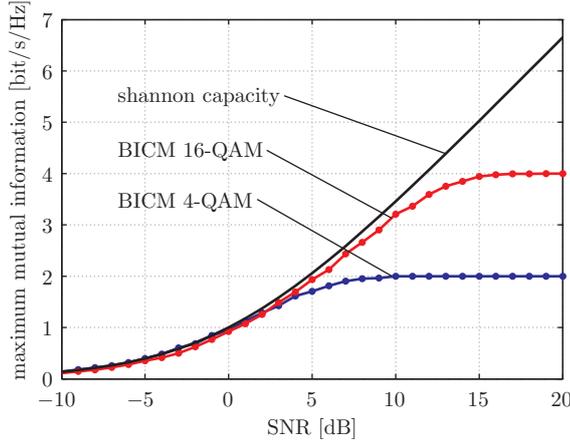
Figure 3.12.: Maximum mutual information of BICM systems according to Equation (3.78) for different symbol alphabets $\mathcal{A}$.

Figure 3.12, where it can be observed that the maximum mutual information curves adapt to the Shannon capacity curve for low SNR values and saturate at $\log_2 |\mathcal{A}|$ bit/s/Hz, which is the effective information rate limitation imposed by the fixed symbol alphabet. I denote the presented curves as *maximum mutual information* because they represent an upper bound on the system performance given the limitations of the symbol alphabet and the interleaver structure but still relying on infinite length channel coding arguments.

Let me point out a few remarks. The expression for the mutual information in Equation (3.78) depends on the demodulator that is utilized. Equation (3.78) holds for the optimum demodulator, other approximate demodulators would need a refinement of the expression. In addition, the interleaver is assumed to be random to obtain the expression for the mutual information, which is valid for large codeblock lengths. Both of these assumptions are not in conflict with the goal of using the BICM mutual information as the compression function for the link-performance modeling of MIMO HSDPA.

With the BICM mutual information being defined in Equation (3.78), the MIESM mapping/compression can be evaluated as

$$f_{\mathrm{M}}(\mathcal{A}, \boldsymbol{\beta}) : \; \mathrm{SINR}_n^{\mathrm{eff}} \triangleq \beta_1 I^{-1} \left\{ \frac{1}{3 \, |\Phi_n|} \sum_{k=1}^{|\Phi_n|} \sum_{i=1}^{3} I \left\{ \mathrm{SINR}_{n, \varphi_k}^{(i)} \frac{1}{\beta_2} \right\} \right\}, \tag{3.79}$$

with $\boldsymbol{\beta} = \begin{bmatrix} \beta_1 & \beta_2 \end{bmatrix}$ defining the tuning parameters. Note that I denoted the set of utilized spreading codes φ_k of stream n by Φ_n again, thus $\varphi_k \in \Phi_n$, $k = 1, \ldots, |\Phi_n|$. This mapping is well suited for linear receivers, but faces its limits when non-linear receiver structures, like ML receivers shall be modeled [104]. In accordance with Section 3.3 however, Equation (3.79) is perfectly applicable for MMSE equalizer receiver structures as recommended for MIMO HSDPA.

After having obtained an effective SINR by $f_{\mathrm{M}}(\mathcal{A}, \boldsymbol{\beta})$, the resulting $\mathrm{SINR}_n^{\mathrm{eff}}$ has to be mapped to an PER,

$$f_{\mathrm{AWGN}}(\mathcal{A}, r_{\mathrm{c}}) : \; \mathrm{SINR}_n^{\mathrm{eff}} \mapsto \mathrm{BLER}_n, \tag{3.80}$$

with r_{c} denoting the code-rate used for the current sub-frame. Note that the combined information $(\mathcal{A}, r_{\mathrm{c}})$ uniquely determines the transmission format for the current transport block. If this

transmission format corresponds to a configuration as defined in the CQI table, I will refer to the combined information as *transmission* CQI, $c^{(\mathrm{T})} \sim (\mathcal{A}, r_{\mathrm{c}})$, as already illustrated in Figure 3.11. Details about the CQI tables can be found in Chapter 2.

In the context of this work, I decided to utilize AWGN performance curves as the mapping from the effective SINR to BLER. This approach is well-known in the literature [80, 84, 104], and has proven to be accurate and robust in terms of applicability for many different transmission scenarios. The fact that the HSDPA link-adaptation works on a sub-frame basis eases the modeling again at this point, because no AWGN performance curves with mixed transmission formats are needed.

The AWGN based mapping $f_{\mathrm{AWGN}}(\mathcal{A}, r_{\mathrm{c}})$ can be acquired by training, meaning a set of AWGN link-level simulations for the corresponding channel-coding and rate-matching, or by analytic approximations. Such analytic approximations usually base upon the cut-off rate of the channel, like in [105], which I also applied in Appendix B.1. For the sake of modeling the link-performance for MIMO enhanced HSDPA, however, I relied on a training based mapping. Thus a set of link-level simulations—for every possible transmission format $c^{(\mathrm{T})}$—forms a look-up table that is utilized as mapping function $f_{\mathrm{AWGN}}(\mathcal{A}, r_{\mathrm{c}})$.

Since the link-quality model, as well as the mapping/compression $f_{\mathrm{M}}(\mathcal{A}, \boldsymbol{\beta})$ evaluate separate performance parameters for every spatial data stream,[18] the defined BLER mapping $f_{\mathrm{AWGN}}(\mathcal{A}, r_{\mathrm{c}})$ can be trained by single-stream scenarios and used independently for the transmitted code-words, $n = 0, \ldots, N_{\mathrm{S}} - 1$.

To finally obtain a sub-frame based ACK/NACK decision that consequently can trigger retransmissions and influences the scheduler, the output BLER of $f_{\mathrm{M}}(\mathcal{A}, \boldsymbol{\beta})$ is mapped to a packet-error event by conducting a binary random experiment with appropriate probability distribution,

$$\xi = \begin{cases} 0 \to \mathrm{ACK} & : \Pr\{\xi = 0\} = 1 - \mathrm{BLER}, \\ 1 \to \mathrm{NACK} & : \Pr\{\xi = 1\} = \mathrm{BLER}. \end{cases} \tag{3.81}$$

This guarantees that the BLER values predicted by the link-performance model are obtained in average.

3.4.2. Training and Validation of the Model

With the mapping function being specified by Equation (3.79), it remains to *train* the model by finding the optimum parameter vector $\boldsymbol{\beta}^{\mathrm{opt}}$, and to *validate* the link-performance model in terms of its BLER prediction error.

For the training, I conducted a set of link-level simulations utilizing the HSDPA physical-layer simulator of [94] for different transmission formats. The simulator is a WCDMA, 3GPP Release 5 standard compliant HSDPA simulator that models the complete physical layer. For the training of the MIESM, the simulator was configured to vary the $I_{\mathrm{or}}/I_{\mathrm{oc}}$ ratio,[19] which can be translated to a variation in the post-equalization and despreading SINR per HS-PDSCH,

$$\mathrm{SINR}^{\mathrm{HS\text{-}PDSCH}} \approx \mathrm{SF} \frac{I_{\mathrm{or}}}{I_{\mathrm{oc}}} \frac{E_{\mathrm{c}}}{I_{\mathrm{or}}} \frac{1}{|\Phi|}. \tag{3.82}$$

This implicitly assumes an average downlink wireless channel gain of one. As explained in the previous subsection, only single-stream SISO simulations are necessary to be able to derive separate link-performance models for every spatial stream—which can be interpreted as individual

---

[18]This is possible due to the independent channel-coding of the streams, as already mentioned.
[19]See Appendix A.11 for the corresponding definitions.

point to point rank one transmission—thus the number of spreading codes used for the current transmission is given by the cardinality $|\Phi|$, where I left the index n for the sake of notational clarity. The instantaneous HS-PDSCH SINR per TTI, needed for the training of the MIESM, however, was extracted from the receive symbols for every received sub-frame, similar to Equation (3.65).

Varying over $I_{\text{or}}/I_{\text{oc}}$, the physical-layer simulator was utilized to generate a large number of channel realizations and assess the decoding performance for all of those. The fraction of erroneous received packets within a set of channel realizations then approximates the BLER for a given channel condition,

$$\text{BLER}_c^{\text{M}} \approx \frac{\text{nr. of NACKs}}{\text{total nr. of channel realizations}}, \tag{3.83}$$

to which I will refer to as *measured* BLER, with c denoting the index of the set of channel realizations within the total set of simulated channel characteristics. The channel condition is defined by the average interference and noise density, approximately given by $I_{\text{or}}/I_{\text{oc}}$. Furthermore, let me denote the BLER estimated by utilizing the MIESM and the AWGN performance curve by $\text{BLER}_c^{\text{E}}(\boldsymbol{\beta})$, which is of course a function of the tuning parameter vector $\boldsymbol{\beta}$. The individual channel condition and approximated BLER performance pairs are used to train the MIESM to compress/map the measured results to the according AWGN performance curve.

Given these definitions, the error of the fitted MIESM in terms of the estimated BLER accuracy can be defined as

$$e_c(\boldsymbol{\beta}) = \text{BLER}_c^{\text{E}}(\boldsymbol{\beta}) - \text{BLER}_c^{\text{M}}, \tag{3.84}$$

or equivalently expressed in the SINR domain,

$$\tilde{e}_c(\boldsymbol{\beta}) = \text{SINR}_c^{\text{eff}}(\boldsymbol{\beta}) - \text{SINR}^{\text{AWGN}}. \tag{3.85}$$

This transformation into the SINR domain is possible because the estimated BLER, denoted by $\text{BLER}_c^{\text{E}}(\boldsymbol{\beta})$, is a one-to-one mapping of the effective SINR, $\text{SINR}_c^{\text{eff}}(\boldsymbol{\beta})$. Thus, given the effective SINR for a specific channel realization c, the model quality depends on the quality of the fit compared to the AWGN reference curve, which determines the estimated BLER, $\text{BLER}_c^{\text{E}}(\boldsymbol{\beta})$. Accordingly, the vector of optimum tuning parameters can for example be found by a Least Squares (LS) fit in the SINR domain,

$$\boldsymbol{\beta}^{\text{opt}} = \arg\min_{\boldsymbol{\beta}} \sum_{c=1}^{N_c} |\tilde{e}_c(\boldsymbol{\beta})|^2, \tag{3.86}$$

with N_c defining the number of channel realization sets within the total set of simulated channel characteristics. This is only one possibility of finding the optimum tuning parameters $\boldsymbol{\beta}$, focusing on a good fit in the overall BLER performance. Other possibilities to find $\boldsymbol{\beta}^{\text{opt}}$ are for example treated in [84]. The main advantage of defining the training metric for $\boldsymbol{\beta}$ in the SINR domain is that the whole relevant range of BLER values is equally weighted. In case Equation (3.84) would be utilized, higher BLER values would clearly dominate the optimization procedure to find $\boldsymbol{\beta}^{\text{opt}}$.

The simulation parameters utilized for the explained MIESM training were chosen as listed in Table 3.2. The channel realizations set size was chosen to be 200 sub-frames, thus limiting the applicability of the MIESM training to a BLER range of $[1, 0.01]$. The LS fit of Equation (3.86) was evaluated utilizing a simplex method as provided by the standard MATLAB command `fminsearch`.[20]

---

[20]Note that `fminsearch` does not guarantee to find a *global* optimum of the optimization problem. Nevertheless,

Table 3.2.: Simulation parameters for the MIESM training.

Parameter	Value
carrier frequency	2 GHz
channel type	SISO 1×1 ITU PedA
UE speed	3 km/h
transmission format definitions	3GPP UE CQI Tables D and I [7]
simulated sub-frames per I_{or}/I_{oc} value	2505
HS-PDSCH E_c/I_{or}	-3 dB
HARQ retransmissions	not active
signaling channels	perfect, non-interfering
channel estimation, synchronization	perfect
receiver	MMSE, $L_f = 40$ chips
equalizer channel update	once per sub-frame

The results of the MIESM training are depicted in Figures 3.13 to 3.15. Figures 3.13(a) and 3.13(b) illustrate the MIESM training results in an ITU PedA channel profile scenario for the UE capability Table D [7], when the transmission CQIs are chosen $c^{(T)} = 7, 14$, respectively. According to the 3GPP CQI table D, these two transmission modes correspond to 4-QAM transmissions, utilizing two and four HS-PDSCH codes, respectively. The resulting effective code-rates can furthermore be evaluated to be 0.34 and 0.67.[21] The two figures show the average BLER performance as a function of the SINR calculated based on the I_{or}/I_{oc} approximation in Equation (3.82), the BLER performance as a function of the linear mean post-equalization and despreading SINR evaluated for every channel realizations set, the resulting trained MIESM BLER performance, and the corresponding AWGN performance curve—utilizing the same transmission format—for sake of showing the MIESM training fit.

In principle, the requirement of the MIESM is to map the cloud of individual BLER performances as a function of the post-equalization and despreading SINR to a corresponding effective SINR that matches the AWGN performance curve as closely as possible. When a close fit is achieved, this denotes that the MIESM modeling is capable of mapping/compressing the post-equalization and despreading SINR as provided by the link-quality model in Equation (3.62) to an effective SINR that can be used for obtaining the predicted BLER from the corresponding AWGN performance curve. Let me furthermore remark that Figures 3.13(a) and 3.13(b) also show that a detailed link-quality model is necessary due to the fact that the I_{or}/I_{oc} based BLER performance curve does not represent the mean of the post-equalization and despreading SINR BLER performance cloud.[22]

Subfigures (a) and (b) in Figures 3.14 and 3.15 illustrate the same information as Figures 3.13(a) and 3.13(b), with the transmission format being specified by $c^{(T)} = 21, 28$ of UE capability Ta-

---

as will be shown in the results, the found optimum is sufficiently well for the purpose of this link-performance modeling, although the solution might be a local optimum.

[21]The evaluation of the effective code-rate is described in Appendix A.12.

[22]By using the term *mean*, I denote the *regression* of the post-equalization and despreading SINR BLER performance cloud. The deviation in the I_{or}/I_{oc} based BLER performance and the measured BLER performance basically implies that inter-stream and intra-cell interference terms have to be considered, as opposed to Equation (3.82).
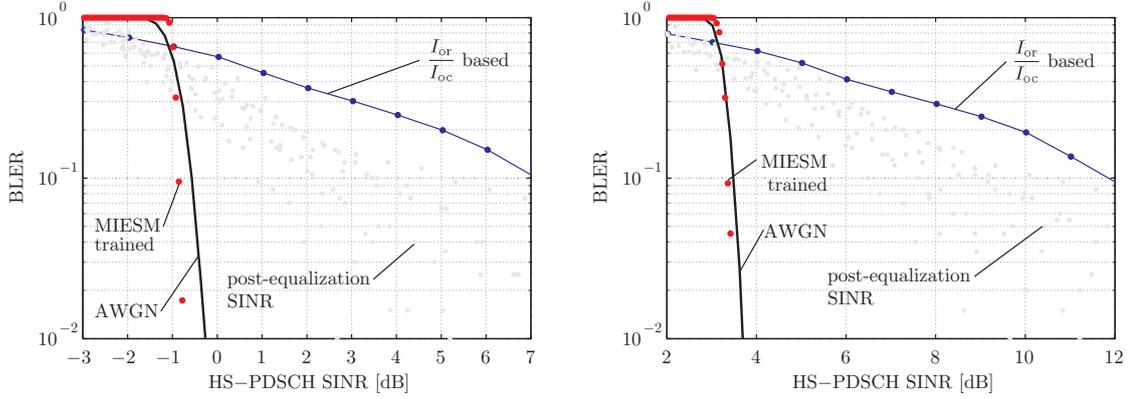
(a) MIESM fitting results for UE capability Table D, $c^{(\mathrm{T})} = 7$, PedA channel.

(b) MIESM fitting results for UE capability Table D, $c^{(\mathrm{T})} = 14$, PedA channel.
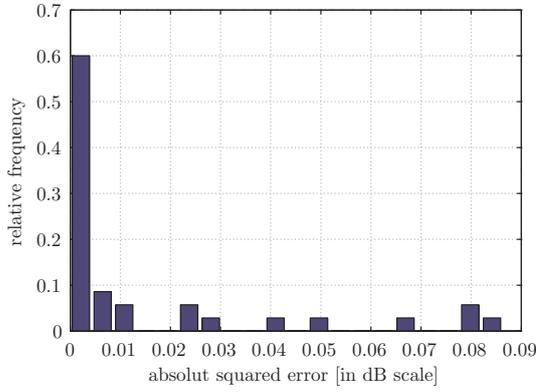
(c) Resulting MIESM modeling error $|\tilde{e}_c(\boldsymbol{\beta}^{\mathrm{opt}})|^2$ distribution for UE capability Table D, $c^{(\mathrm{T})} = 7$, PedA channel.
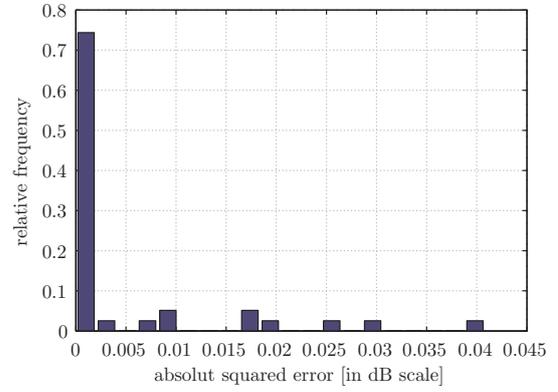
(d) Resulting MIESM modeling error $|\tilde{e}_c(\boldsymbol{\beta}^{\mathrm{opt}})|^2$ distribution for UE capability Table D, $c^{(\mathrm{T})} = 14$, PedA channel.

Figure 3.13.: MIESM training results and resulting modeling error for the UE capability Table D in a PedA channel environment. The transmit CQIs have been chosen to be $c^{(\mathrm{T})} = 7, 14$ which corresponds to a 4-QAM symbol alphabet with an effective code-rate of 0.34 and 0.67, respectively.

ble D for an ITU PedA channel profile scenario in Figure 3.14, and $c^{(\mathrm{T})} = 5, 10$ of UE capability Table I for an ITU PedA channel profile scenario in Figure 3.15.

Compared to Figures 3.13(a) and 3.13(b), the subfigures (a) and (b) in Figures 3.14 and 3.15 show a better fitting of the MIESM effective SINR BLER performance. This is due to the fact that the code-block length is significantly larger for these four transmission formats, and thus the assumption of the random interleaving—utilized in the BICM capacity in Equation (3.78)—is more valid than for smaller code-block lengths.

The resulting optimum tuning parameters $\boldsymbol{\beta}^{\mathrm{opt}}$ for the transmission settings as used for the training in Figures 3.13 to 3.15 together with the transmission format parameters are given in
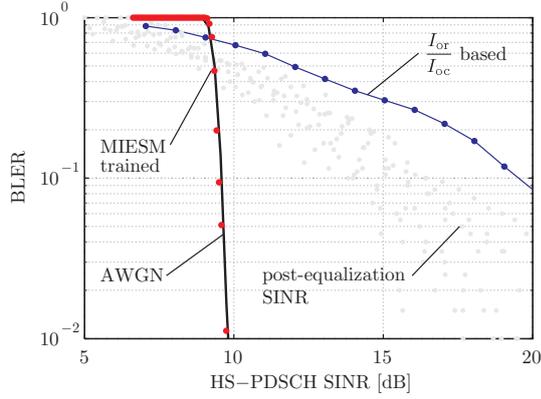
(a) MIESM fitting results for UE capability Table D, $c^{(T)} = 21$, PedA channel.
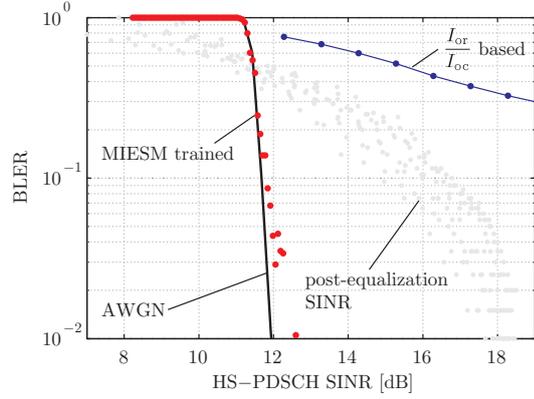
(b) MIESM fitting results for UE capability Table D, $c^{(T)} = 28$, PedA channel.
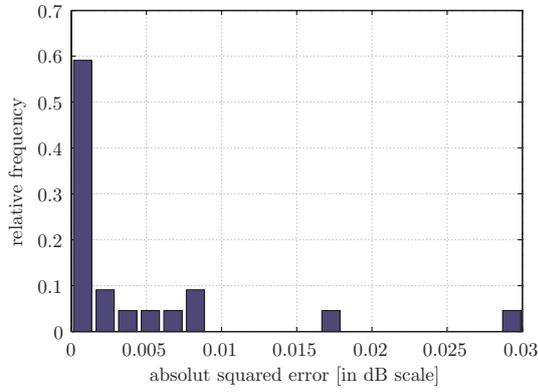
(c) Resulting MIESM modeling error $|\tilde{e}_c(\boldsymbol{\beta}^{\mathrm{opt}})|^2$ distribution for UE capability Table D, $c^{(T)} = 21$, PedA channel.
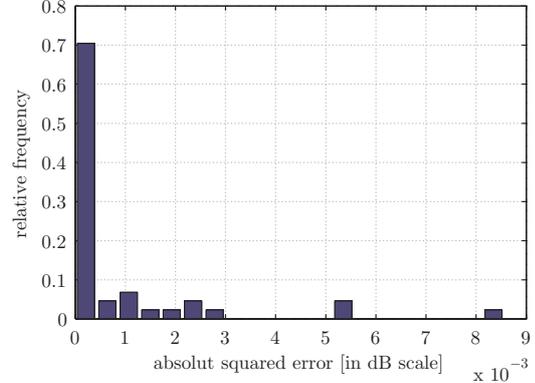
(d) Resulting MIESM modeling error $|\tilde{e}_c(\boldsymbol{\beta}^{\mathrm{opt}})|^2$ distribution for UE capability Table D, $c^{(T)} = 28$, PedA channel.

Figure 3.14.: MIESM training results and resulting modeling error for the UE capability Table D in a PedA channel environment. The transmit CQIs have been chosen to be $c^{(T)} = 21, 28$ which corresponds to a 16-QAM symbol alphabet with an effective code-rate of 0.68 and 0.81, respectively.

Table 3.3. Furthermore, the resulting Goodness Of Fit (GOF)

$$\mathrm{GOF} \triangleq \sqrt{\frac{1}{N_c} \sum_{c=1}^{N_c} |\tilde{e}_c(\boldsymbol{\beta}^{\mathrm{opt}})|^2} \tag{3.87}$$

as the Root Mean Square (RMS) error is numerically listed. Let me note that training has not been performed for every transmission CQI value, but rather the optimum tuning parameters for the transmission formats without MIESM training have been evaluated using linear interpolation in the $\boldsymbol{\beta}^{\mathrm{opt}}$ parameters. This procedure is conjectured not to result in larger modeling errors, due to the fact that the optimum tuning parameters $\boldsymbol{\beta}^{\mathrm{opt}}$ as listed in Table 3.3 appear with only little fluctuations. Furthermore, note that the GOF $|\tilde{e}_c(\boldsymbol{\beta}^{\mathrm{opt}})|^2$ reflects the already stated

(a) MIESM fitting results for UE capability Table I, $c^{(\mathrm{T})} = 5$, PedA channel.

(b) MIESM fitting results for UE capability Table I, $c^{(\mathrm{T})} = 10$, PedA channel.

(c) Resulting MIESM modeling error $|\tilde{e}_c(\boldsymbol{\beta}^{\mathrm{opt}})|^2$ distribution for UE capability Table I, $c^{(\mathrm{T})} = 5$, PedA channel.

(d) Resulting MIESM modeling error $|\tilde{e}_c(\boldsymbol{\beta}^{\mathrm{opt}})|^2$ distribution for UE capability Table I, $c^{(\mathrm{T})} = 10$, PedA channel.
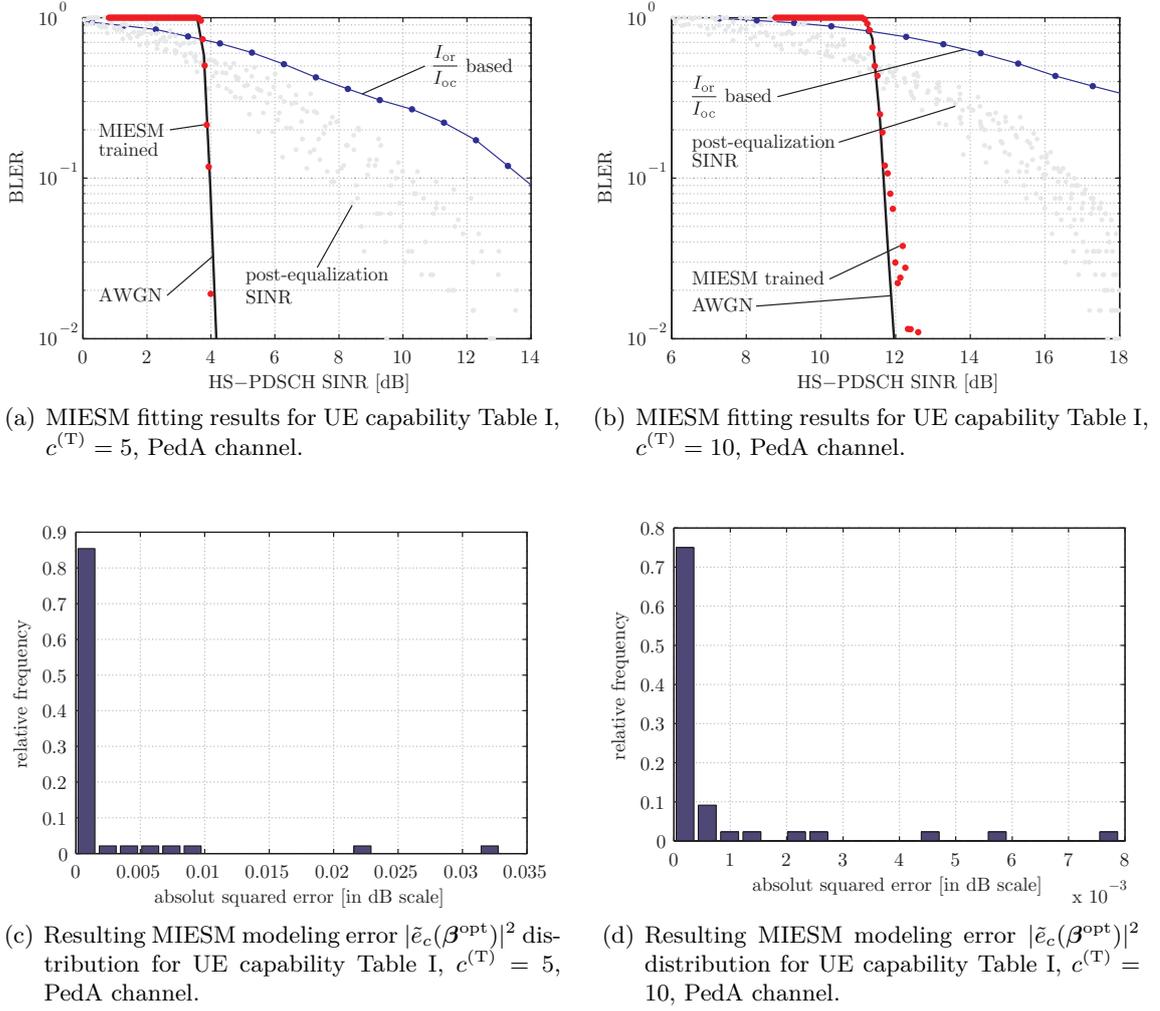
Figure 3.15.: MIESM training results and resulting modeling error for the UE capability Table I in a PedA channel environment. The transmit CQIs have been chosen to be $c^{(\mathrm{T})} = 5, 10$ which corresponds to a 4-QAM transmission with effective code-rate 0.71, as well as a 16-QAM transmission with effective code-rate 0.81.

observation that in case of small TBS, the MIESM mapping/compression is not as well suited for link-performance modeling as it is for larger code-block lengths since for Table D and CQI $c^{(\mathrm{T})} = 7$ the GOF is the numerically the worst.

After having discussed the MIESM training, it remains to specify the validation methodology. In order to assess the modeling error, I evaluated the estimated BLER performance, $\mathrm{BLER}_c^{\mathrm{E}}(\boldsymbol{\beta}^{\mathrm{opt}})$, and compared it to the BLER performance as measured from the link-level simulations, $\mathrm{BLER}_c^{\mathrm{M}}$, utilizing the same channel coefficients. The resulting estimation error distribution, again expressed in the SINR domain, $|\tilde{e}_c(\boldsymbol{\beta}^{\mathrm{opt}})|^2$, is depicted in subfigures (c) and (d) of Figures 3.13 to 3.15, respectively. It can be observed that the error is distributed very close to zero, with a only a few outliers. Furthermore, Figure 3.13(c) shows the largest error magnitude amongst all trained transmission formats, which is in concordance with the MIESM fitting

Table 3.3.: Resulting MIESM tuning parameters for Equation (3.79) and GOF for ITU PedA channel profiles obtained by LS fitting.

CQI table	$c^{(\mathrm{T})}$	TBS [bits]	$\mathcal{A}$	$|\Phi|$	r_{c}	β^{opt}	GOF
D	7	650	4-QAM	2	0.34	[0.98 1.05]	0.72 dB
D	14	2 583	4-QAM	4	0.67	[1.05 0.98]	0.42 dB
D	21	6 554	16-QAM	5	0.68	[1.06 0.96]	0.28 dB
D	28	23 370	16-QAM	15	0.81	[1.07 0.94]	0.21 dB
I	5	10 255	4-QAM	15	0.71	[1.06 1.01]	0.31 dB
I	10	23 370	16-QAM	15	0.81	[1.07 0.94]	0.17 dB

problems due to small code-block lengths as already explained.

Overall, it can be concluded that the MIESM mapping/compression together with AWGN performance curves provides a flexible and accurate way of modeling the link-performance of MIMO HSDPA, which—together with the developed link-quality model—completes the necessary system-level modeling of the physical-layer.

3.5. Summary

At the end of this chapter, let me briefly summarize the main contributions and comment on some points that would be interesting for further research.

In short, I introduced the purpose of system-level modeling and defined a generally applicable concept suited for physical-layer abstractions of wireless networks. Moreover, I applied the concept to derive a link-quality and a link-performance model for MIMO enhanced HSDPA, forming the core of my proposed system-level model. The link-quality model has partly been developed in collaboration with NSN [12, 17] and is currently implemented in their packet-based system-level simulator called *MoRSE*. The proposed model is also the basis for the development of my proposed MIMO HSDPA system-level simulator and the investigations presented in Chapter 4.

Although the scientific work in this chapter investigates the critical assumptions carefully and in great detail, some assumptions and simplifications as well as possible further research thereupon have to be commented.

Regarding the modeling assumptions an even more comprehensive investigation could help to improve the accuracy. In particular, the modeling of the intra-cell interference by its expected value could be tested in greater detail which may lead to a two-dimensional representation, for example by its average and variance. A similar idea was already proposed in [99]. However, it has to be investigated whether a significant gain in accuracy can be achieved. The modeling of the non-data channels, on the other hand, would benefit from a more detailed modeling. In fact, the simplified representation of the interference generated by the non-data channels by means of the established equivalent fading parameters of the data channel neglects the fact that some of the signaling channels are not pre-coded. Future work could establish a similar equivalent fading parameter description for the non-data channels themselves, thus providing a better modeling accuracy and a more detailed understanding of the non-data channel influence on the system performance. Furthermore, the assumption of equal power loading of the transmitted data streams may hold in practice, but it still would be interesting to investigate the implications

of non-homogeneous power loading to optimize the D-TxAA operation of HSDPA. This would correspond to the *water-filling* idea well known from information theory [51].

Also the link-performance model still offers room for further improvement. The influence of the UE speed—and its implications on the channel coherence time—would be worth investigating in greater detail. HSDPA was originally targeted for lower speeds but it may nevertheless be of interest to assess the system-level implications of UEs moving with higher speeds. More related to current practical implications is that the influence of the turbo encoder block length is only explicitly included in the link-performance model at the moment. In fact, if a more detailed modeling of the coding blocklength would be derived, the better understanding of this effect could help to optimize the link-adaptation of HSDPA. Note also that the coding blocklength as an influencing factor is currently not directly reflected in the concept of the presented link-performance model. An improved version of the concept thus would also appear to be more general and could help to develop an analytical representation of the link-performance model. Such a representation would be required for analytical network optimization approaches.

Finally, let me point out that future mobile terminals may rely on non-linear receiver structures to achieve higher data throughput. Due to the structure of the proposed link-quality and link-performance model, however, only linear receive filters can be accurately modeled. This approach is perfectly suited for the MMSE receive filter as recommended for HSDPA by 3GPP [7], but upcoming developments suggest the usage of SIC or even ML like receiver structures. These would require a significant redesign of both models in a number of places. In this context, it might as well be of interest to investigate the modeling of the inter-cell interference in greater detail to allow for the system-level representation of inter-cell interference aware receivers.

Given the characteristics of future generation mobile networks as well as the importance of system-level investigations for network operators and network equipment vendors, accurate system-level modeling will remain an crucial research topic.

Chapter 4.

System-Level-Simulation-Based Optimization of MIMO-Enhanced HSDPA

> Without change there is no innovation, creativity, or incentive for improvement. Those who initiate change will have a better opportunity to manage the change that is inevitable.
>
> *(William Pollard)*

Link-quality and link-performance models serve as the core of any system-level investigation, however for practical performance assessments and optimizations, a system-level simulator covering mostly all procedures, algorithms, and deployment characteristics as illustrated in Figure 3.2 has to be developed. This chapter thus is devoted to develop a suitable *system-level simulator* incorporating the link-quality and the link-performance model of Chapter 3 and its application to conduct HSDPA network performance investigations and optimizations.

Despite the assumptions and limitations of the link-quality and link-performance modeling, also the basic design principles of the system-level simulator confine its applicability for network algorithm testing, equipment development, network planing, or even performance testing. Major manufacturers of mobile communication equipment, like NSN, Motorola or Ericsson operate their own proprietary system-level simulators to derive important results for the standardization process in the 3GPP and to conduct algorithm optimizations. However, these simulators are not publicly available and the commercial ones focus more on network planing, like for example [106]. Some open-source solutions for simulating HSDPA networks are based on the network simulator NS-2 [107], for example [108], however these simulators focus more on the core-network implications—thus the IP domain—than the physical-layer and MAC-hs issues.

For the investigations that were of interest in the context of this thesis, a system-level simulator capable of representing the MAC for HSDPA and some RRC algorithms is more appropriate. A similar simulation approach has been taken in [109], however, the physical-layer was not modeled by a detailed system-level model. Furthermore, the commercial simulator [110] utilizes a comparable concept, however, it does not provide the required flexibility.

Given the simulator requirements for the planned investigations and the lack of suitable open-source MIMO HSDPA system-level simulators meeting those requirements, a new Release 7 HSDPA system-level simulator based on the link-quality and link-performance models of Chapter 3 had to be developed.[1] The design focus is put onto the MAC-hs and RRC routines, thus capturing the wireless access part of the HSDPA network including parts of the RLC layer.

---

[1]Note that the simulator utilized for the investigations in Appendix B.1 being able to represent Release 5 HSDPA is in its basic concept comparable to the simulator structure proposed in this chapter.
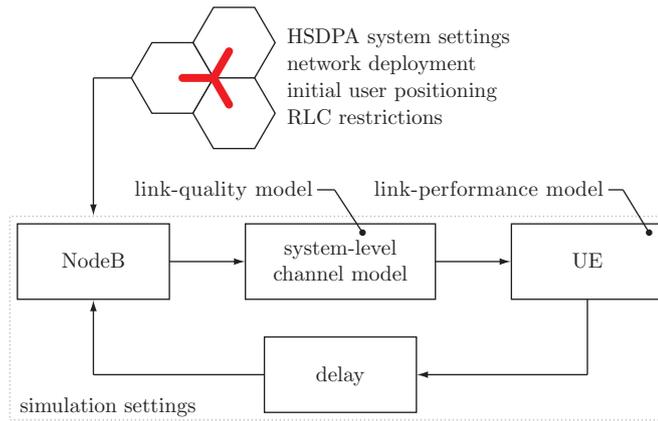
Figure 4.1.: Overview of the proposed basic system-level simulator structure.

The developed simulator then serves as a platform to perform network performance evaluation, algorithm development and testing, as well as cross-layer optimization.

4.1. MIMO HSDPA System-Level Simulator

An overview of the proposed system-level simulator structure is illustrated in Figure 4.1. In principle, the simulator consists of one main simulation loop that spans the *NodeB*, the *system-level channel model*, the *UE*, and a *delay* entity. The simulation is consequently being influenced by the general HSDPA system settings, the chosen network deployment, the initial user positioning, as well as eventual RLC restrictions. In this structure, the link-quality model is incorporated in the system-level channel model to predict the channel quality given decisions on the resource allocation and the user position within the network. The link-performance model on the other hand is a part of the UE entity, where it serves to assess the BLER performance given the output of the system-level channel model and the chosen transmission format.

The simulation loop ranges over time, allowing the NodeB procedures to react to the delayed input and conduct the HSDPA downlink data transmission. The system-level channel model then represents the influence of the physical-layer on the HS-DSCH, producing output data that is used by the UE entity to do the necessary receiver processing and determine potential feedback which is delayed before reaching the NodeB. The simulator is implemented in a MATLAB environment, allowing for flexible and research oriented operation.

The main research interest for the development of the system-level simulator lies in the effects and performance dependencies of the downlink data channel HS-DSCH. Accordingly, the signaling channels are not system-level modeled and are made available without any transmission- or decoding-error. However the feedback delay is necessary to assess the performance of RRC and scheduling algorithms in practical settings.

Of course, a simulator being developed mainly by one person cannot comprise all possible operation modes or network possibilities. Accordingly, many simplifications had to be considered for the programming, the most important ones being:

- Support for three transmission modes, namely D-TxAA, TxAA and plain SISO.

- The supported receiver types are MMSE equalizer and Rake receiver.[2]

- The maximum number of supported streams equals two, $N_S = 2$.[3]

- The supported UE capability classes are 16 and 18 which are the UE capability classes with the highest supported throughput. The according CQI tables in [7] are the Tables C, D, H, and I.

- The supported modulation alphabets are 4-QAM and 16-QAM.

- No handover support between sectors.

- Users are only simulated in the target sector of the center cell, which means that most of the network algorithms are only active in the target sector, where full UE data is available. Given the fact that no handover investigations are supported, the simulation of the neighboring cells as pure interference sources is sufficient.

- No support for inter-cell coordination which prevents the investigation of inter-cell interference management.

- Restriction of the utilizable TFCI set to the set of CQI corresponding TFC, and

- a full buffer assumption.

Most of these simplifications are necessary to make the simulator easier to implement, however they can be relaxed to the expense of additional significant programming work. Although restricting the scope of research questions that can be answered with the simulator, the features of it are more than sufficient for the questions examined in this thesis.

4.1.1. Detailed Simulator Structure

Let me go into more detail on the procedural implementation of the main simulator parts. Figure 4.2 shows the basic procedures of the NodeB-entity implementation in the system-level simulator. The delayed UE output—containing at least the ACK/NACK and CQI feedback information—is first *buffered*. This is necessary, if one of the following algorithms wants to have access to the history of the incoming feedback information to allow for example for the prediction of channel states or achievable data-rates. After this initial stage, the *scheduler* is responsible for determining which user will obtain the physical downlink resources.[4] After the scheduler decision is taken, the NodeB may conduct the so-called *stream decision*, indicating the algorithm potentially deciding upon the number of spatial streams that will be utilized in the downlink transmission. This basically corresponds to the decision between D-TxAA and TxAA transmission modes. Furthermore, let me note that [7] allows the UE to feedback whether one or two streams are requested. Nevertheless it may be sometimes beneficial to overrule the UE request, as will be elaborated in Section 4.3.

Depending on the scheduler and stream decisions, the physical channel utilization in form of the link-adaptation TFC will be determined. The restriction of the set of TFCI to the set of

---

[2]Recall that Interference Cancellation (IC) receiver structures are not modeled by the system-level model developed in Chapter 3.

[3]Note that this is an implementation restriction, the system-level model of Chapter 3 would allow for the simulation of higher order spatial multiplexing schemes.

[4]Or which users will obtain which amount of physical downlink resources in the multi-user scheduling case. Physical downlink resources in this context mainly denotes the number of HS-PDSCHs available for each scheduled user, respectively.
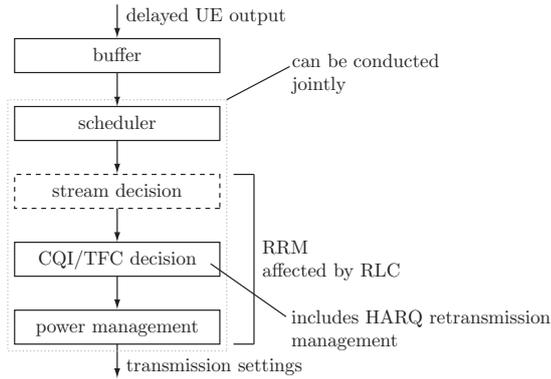
Figure 4.2.: Basic functions flowchart of the NodeB entity in the system-level simulator.

TFC with an entry in the CQI table of the individual UE permits the representation of the TFC in terms of the already defined *transmit* CQI $c^{(\mathrm{T})}$.[5] Note that the *CQI/TFC decision* stage also includes the HARQ retransmission management, because for eventual retransmissions the same transmission settings have to be used [35], not including the rate-matching stage. Finally, the *power management* stage determines how much power is utilized on every stream for every user. In principle, all stages from the scheduler to the RRM stages with the power management at the very end can be conducted jointly, which is for example needed in case of cross-layer optimizations, as in Section 4.4.

The output of the NodeB simulator part—including at least the transmit CQI, the set(s) of utilized HS-PDSCH, the HARQ information,[6] the number of utilized streams, and the network clock index—then forms the set of input parameters to the *system-level channel model.* Figure 4.3(a) illustrates the basic flowchart of it. The first three stages contain the *macro-scale path-loss* model, the evaluation of the *antenna gain* and the *shadow fading* realization. These stages are implicitly affected by the network deployment and the user position. After the large-scale parameters have been determined, the link-quality model from Chapter 3—utilizing stored traces of equivalent fading parameters—produces the SINR measurement data representing the channel quality during the current TTI.

The output of the system-level channel model together with the signaling information of the NodeB output then are used in the *UE* entity of the simulator, illustrated in Figure 4.3(b). The first stage of the UE corresponding simulator part updates the UE position within the target sector. After this necessary stage, the MIESM *mapping/compression* from the link-performance model in Chapter 3 is utilized to derive the effective SINR.

As described in Appendix A.7, the effective SINR is used to derive a suitable CQI feedback $c^{(\mathrm{F})}$ by applying the UE capability corresponding CQI mapping stored in form of a *CQI look-up table.* In case of the current transport block being a retransmission, the next stage evaluates the *HARQ gain* in terms of the effective SINR. From the set of AWGN performance curves, the curve corresponding to the current TFC determines the *ACK/NACK report* of the UE according to the link-performance model of Chapter 3. Finally, the UE entity decides whether the next requested transmission is double- or single-stream and incorporates this information in the CQI

---

[5]Due to the structure of the CQI tables in the D-TxAA case, this representation does not allow the simulation of multi-user scheduling in the double stream transmission mode.

[6]This includes the New Data Indicator (NDI), the Redundancy Version (RV) index, as well as the TSN.

(a) Basic functions flowchart of the system-level channel model entity in the system-level simulator.

(b) Basic functions flowchart of the UE entity in the system-level simulator.
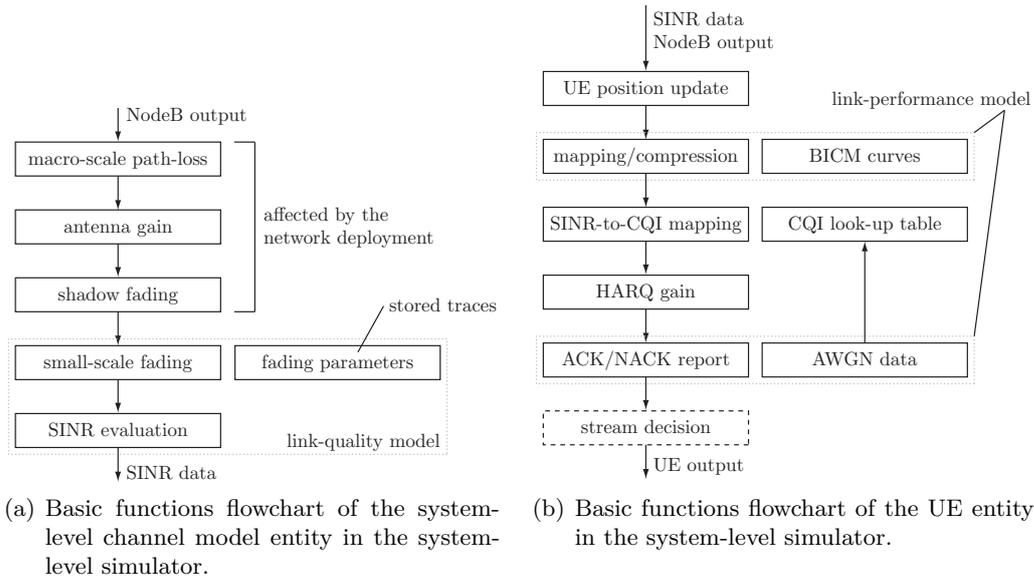
Figure 4.3.: Basic functions of the system-level channel model and the UE entity.

feedback. Recall however that—as explained in the description of the NodeB entity—the UE stream request does not necessarily have to be applied by the NodeB.

The evaluated UE decisions are then fed into the delay buffer which, in the standard configuration, delays the UE feedback by four TTIs. This standard value is determined by the timing relations in HSDPA, see also Chapter 2. Finally, the output of the delay buffer is offered to the NodeB entity, completing the simulation procedure.

For the desired figures of merit to be extracted the input, output, and the internal states of the NodeB and the UE entity can be monitored and traced. Typical performance metrics include the average user- and cell-throughput, BLER traces, and achievable QoS constraints. In the simulator, the throughput of the served user u is defined as the number of successfully transmitted bits per time interval measured in Mbit/s, given by

$$T^{(u)} = \text{TBS} \cdot (1 - \xi) \cdot \frac{1}{t_{\text{TTI}}}, \tag{4.1}$$

with t_{TTI} specifying the duration of one TTI being $2\,\text{ms}$. To obtain average throughput values, these instantaneous throughputs of course have to be averaged over the total simulation duration or by a sliding window average to obtain time traces.

4.1.2. Network Setup

As depicted in Figure 4.1, the network setup of the simulator determines the scenario that is investigated. Part of the network setup is the cell deployment specifying the geographical properties of the network under test. In principle, this deployment data can be obtained from

- *live network data*, possibly including measured path-loss data, antenna characteristics, as well as transmit power constraints, or from

- *standardized network scenarios*, usually following a regular structure, like those provided in [93].

65

(a) Three sector network layout Type I [93].

(b) Antenna gain pattern for a three sector network according to [93].
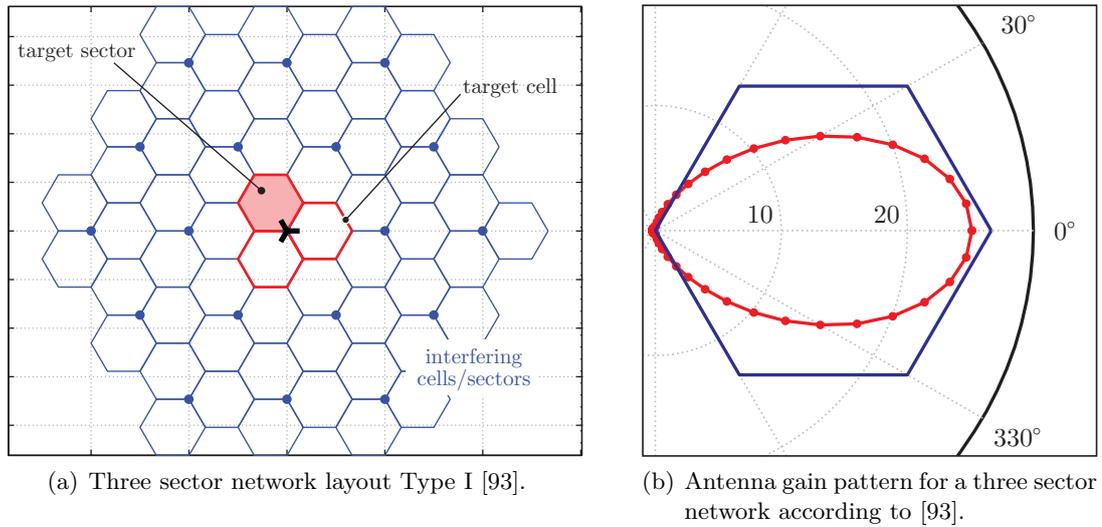
Figure 4.4.: Network deployment details in case of a standardized network scenario. The layout corresponds to the definitions in [93].

For this chapter, I implemented standardized network scenarios in the simulator, however, it has to be noted that the structure of the simulator allows for relying on live network data in the form of *Odyssey*[7] data as utilized by mobilkom austria AG in the network planing process. This data has for example been used in Appendix A.13 to cross-validate the simulator against the mobilkom austria AG simulators.

Cell Deployment

The HSDPA cell deployment for the case of standardized network scenario investigations consists of 19 three-sector sites, as depicted in Figure 4.4. The antenna gain pattern for the sector antennas is modeled according to [112]. This network layout corresponds to the layout Type I [93]. The developed system-level simulator allows for the power of the neighboring base-stations to be controlled independently such that different interference situations can be simulated among which the most important ones are:

- The *single-cell* scenario which can for example serve as an upper bound on the network performance,

- the *full interference* scenario where all neighboring cells transmit continuously with the full available power, which can for example serve as a lower bound in the network performance, and

- the *homogenous* network scenario where all neighboring base-stations behave equal to the target base-station in terms of the power management, which can for example serve as a scenario to assess the predicted average network performance.

As already noted at the beginning of this chapter, the simulator evaluates the necessary network protocols and algorithms only in the target cell. Accordingly, also the power control algorithms

---

[7]Odyssey is a network planing solution developed by Andrew [111].

(a) Macro-scale path-loss for urban micro and urban macro scenarios according to [112].

(b) Pre-equalization SINR $\hat{I}_{\mathrm{or}}/I_{\mathrm{oc}}$ in dB in the target sector according to the urban micro path-loss model.
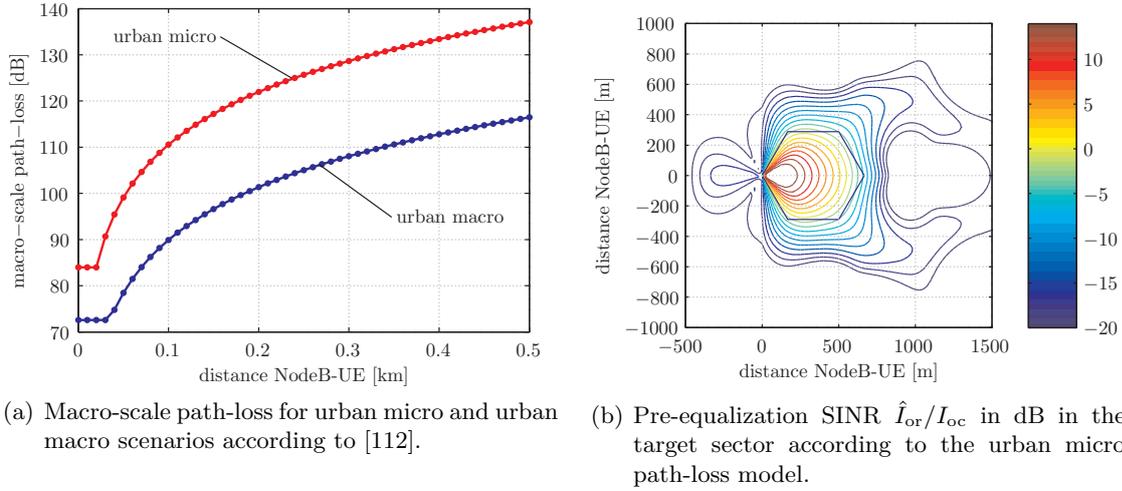
Figure 4.5.: Macro-scale path-loss model results in terms of the path-loss and the resulting average receive power distribution.

are only evaluated in detail for the target cell, which limits the interference scenarios to be assessed. Nevertheless, situations in which the neighboring base-stations have different maximum output powers available can be simulated. Situations of this kind are of interest for mobile network operators to assess for example the implications of new power-amplifiers to support higher output power values onto the interference situation and thus the target base-station performance.

Propagation Modeling

When a standardized network scenario is considered, the propagation modeling is of importance. Propagation models for system-level simulations should be chosen to adequately represent the environment of interest. In [112] different propagation models for urban and suburban environments have been defined. I implemented two of the defined models in the simulator, the European COoperation in the field of Scientific and Technical research (COST) 231 *extended Hata* model and the COST 231 *Walfish-Ikegami* model. The COST 231 extended Hata model is applied in case of suburban macro- and urban macro-cell deployments.[8] The COST 231 Walfish-Ikegami model, on the other hand, is applied in case of urban micro-cell layouts.[9] In the following, let me denote the resulting macro-scale path-loss between user u and base-station b by $\lambda_{\mathrm{m}}^{(u,b)}$. Figure 4.5 depicts the path-loss in dB as predicted by the urban micro and the urban macro model with the settings defined as specified for MIMO HSDPA evaluations [93]. It can be observed that the minimum path-loss is limited to the free-space path-loss in both cases.

To model sectored networks, antennas with a corresponding gain pattern have to be considered, see Figure 4.4. Let me denote the antenna gain as a function of the azimuth between base-station and user by $g_{\mathrm{ant}}(\theta^{(u,b)})$. Figure 4.5 illustrates the resulting pre-equalization SINR $\hat{I}_{\mathrm{or}}/I_{\mathrm{oc}}$ when

---

[8]The extended Hata model is restricted to a carrier frequency between 1.5 GHz and 2.0 GHz, base-station heights between 30 m and 200 m, mobile station heights between 1 m and 10 m, and an inter-NodeB distance between 1 km and 20 km.

[9]The Walfish-Ikegami model is restricted to a carrier frequency between 800 MHz and 2 GHz, a height of the base-station between 4 m and 50 m, and a height of the mobile station between 1 m and 3 m.

the sector antenna of Figure 4.4 [112] is taken into account and a 19 base-station network with homogenous maximum output power of $43\,\text{dBm}$ is assumed.

To account for shadowing effects in the cell area, shadow fading has to be generated for each user-base-station link. As a result of the relief of the terrain in the cell, the shadow fading has to be correlated in the area of the UE motion as well as between links from different base-stations.[10] For these correlation effects, either correlated shadow fading maps for the cell area or correlated time traces can be generated. Time traces are possible due to the fact that the UEs are moving and thus are observing a shadow fading that is changing over time. Note that shadow fading maps with correct statistical properties have been in research for quite some time [113, 114], but they are generally quite difficult to generate and require large amounts of memory.

Accordingly, I decided to employ time-correlated shadow-fading traces in the system-level simulator. The spatial correlation of the shadow-fading is translated into a time-correlation by the model of [115]. This model generates the samples by filtering a log-normal random process $a^{(u,b)}$, following the pdf

$$f_a(a) \triangleq \frac{1}{a\,\sigma\,\sqrt{2\pi}} \exp\left[-\frac{(\ln a - \mu)^2}{2\sigma^2}\right], \quad a > 0, \tag{4.2}$$

where μ and σ are the mean and standard deviation of the natural logarithm of a, which is normally distributed, that is $\ln a \propto \mathcal{N}(\mu, \sigma^2)$. The utilized filter f_shadow is of first order with one pole that guarantees that the resulting autocorrelation $R_{\tilde{a}^{(u,b)}}$ is given by

$$\tilde{a}^{(u,b)} = a^{(u,b)} * f_\text{shadow} \quad \rightarrow \quad R_{\tilde{a}^{(u,b)}}[i] = \sigma^2 \varrho^{vT_s|i|\frac{1}{D}}, \tag{4.3}$$

with ϱ describing the spatial correlation coefficient at correlation distance D, and v being the UE speed. The inter-site correlation is modeled according to [93], such that the resulting shadow fading can be evaluated as

$$\lambda_\text{s}^{(u,b)} = \sqrt{1-\zeta}\tilde{a}^{(u,b)} + \sqrt{\zeta}\varepsilon^{(u)}, \tag{4.4}$$

with ζ denoting the inter-site correlation coefficient and $\varepsilon^{(u)}$ specifying a user-specific random offset value drawn from a zero-mean Gaussian random process.

Finally, the overall path-loss $L^{(u,b)}$ combining all macro- and large-scale effects in the cell—as utilized in Equation (3.62)—is given by

$$L^{(u,b)} = \lambda_\text{m}^{(u,b)} \cdot g_\text{ant}\left(\theta^{(u,b)}\right) \cdot \lambda_\text{s}^{(u,b)}. \tag{4.5}$$

To establish the connection to Equation (3.62) let me note that for sake of notational simplicity the user index u had been omitted, which makes $L^{(b)} = L^{(u,b)}$ in this context.

User Mobility

For a realistic performance evaluation, the simulated UEs in the target cell have to move. Accordingly, I implemented a random movement mobility scheme. At the beginning of a simulation a random position in the target sector according to a uniform probability distribution over the sector area is assigned to each user. Additionally, every user is assigned a random walking direction with uniform distribution over the interval $[0, 2\pi)$. Since the simulator does not allow for the simulation of handover scenarios, when a user leaves the target cell, he becomes de-attached from it and a new user is generated according to the same procedure. This keeps the number of simulated users constant.

---

[10]This means the target sector link and the interfering base-station links.

Simulation Settings

The behavior of the necessary algorithms as well as the simulator itself can be controlled by a number of parameters. A list of the most important simulation settings can be found in Appendix A.15.

4.2. Network Performance Prediction

Network performance prediction is important to test potential gains of new transmission standards with a system-level perspective. This is of particular interest for network operators who have to assess whether to invest in new technologies and in which parts of their network.

The term *network performance* can include many different figures of merit. Usually among the investigated metrics are the average throughput performance, the MIMO utilization and the fairness of the system. Furthermore, throughput density plots, coverage analyses or BLER performance curves can serve to aid the network planing process. The basic functionality of a simulator to evaluate these necessary figures of merit is also crucial to conduct investigations of more advanced algorithms or cross-layer optimizations. Depending on the design of the simulator, also the effects of the operation of different technologies can be investigated, see Appendix B.1. This functionality, however, is not included in the current version of the developed MIMO HSDPA simulator.

4.2.1. Simulation Setup

From the prior description it is apparent that the system-level simulator is very flexible and allows for the investigation of a multitude of network scenarios, channel types, algorithm constraints, and UE specifications. However, a comprehensive treatment of all simulation possibilities and the according figures of merit would exceed the scope of this thesis. Thus, I will focus on a subset of interesting performance figures for this section which I will comment and describe in greater detail. Some of those simulation results will also be of interest for the research in the following sections.

Before listing the simulation results, let me comment on the simulation parameter settings. First, all simulation results are based on a Round Robin (RR) scheduler. Furthermore, no sophisticated traffic modeling is applied but rather a full buffer scenario is simulated. Such investigations result in performance figures that represent the maximum physical-layer capabilities because no buffer limitations are taken into account. However, if traffic statistics are non-uniform, scheduler and resource allocation algorithms experience more degrees of freedom which can be beneficial for the handling of fixed QoS services, for example in terms of delay or throughput jitter.

That being said, the relevant simulation settings can be found in Table 4.1. As illustrated in Figure 4.4, the simulations utilize a 19 site type I hexagonal network layout in an urban micro environment. The NodeB distance was chosen to be $1000\,\mathrm{m}$ and the interfering NodeBs transmission powers are chosen to represent a homogeneous network scenario. The antenna deployment was chosen to represent a $N_\mathrm{T} \times N_\mathrm{T} = 2 \times 2$ MIMO scenario. Accordingly, I also configured the network to allow for D-TxAA transmission and set the UE capability class to be DS compatible. All UEs utilize an MMSE equalizer. The frequency selective channel was modeled according to a PedA channel.

Table 4.1.: Simulation settings for the system-level investigations results.

Parameter	Value
interference scenario	homogeneous network
number of cells	19, layout type I
NodeB distance	1000 m
carrier frequency	1.9 GHz
total transmit power available at NodeB	20 W
total CPICH power	0.8 W
power of other channels	1.2 W
available HS-PDSCHs	15
macro-scale path-loss model	urban micro
antenna utilization	$N_T \times N_R = 2 \times 2$
channel type	ITU PedA
scheduler	RR
active users in target sector	25
user mobility	3 km/h, random direction
UE capability class	20
UE receiver type	MMSE, $L_f = 30$ chips, $\tau = 15$ chips
feedback delay	4 TTI
simulation time	50 000 slots, each 2/3 ms

The feedback delay for reporting the ACK/NACK and the CQI report was set according to the timing constraints [7] to 4 TTIs. Finally, the stream power loading is conducted in a uniform way, thus no power loading of the individual streams is performed. For the HS-DSCH transmission, all 15 possible HS-PDSCH are available which leaves no room for UMTS traffic in the cell thus these results represent a dedicated MIMO HSDPA network.

4.2.2. Single Network Scenario Investigation

The first results that can be obtained from a system-level simulation are based on a single *network realization*. In general, the term *network realization* corresponds to a user positioning and movement realization, given the network layout and algorithm constraints.[11] Although limited in significance for assessing the overall network performance, these results can serve to identify whether and how well the basic adaptation mechanisms of HSDPA work, and to obtain some knowledge about the performance limits of the system.

In Figure 4.6 the resulting ecdfs of the corresponding throughput values and the underlying initial user positioning are depicted. The ecdfs of the worst and the best user throughput represent the performance bounds for the scheduler given the network realization. Depending on the scheduler strategy, in particular its fairness constraints, the sector throughput statistics can be closer to the best user throughput.

---

[11]By the term *algorithmic constraints* I denote the utilization of the power and resource allocation schemes as introduced.

(a) The ecdfs of the worst user, best user and sector throughputs.

(b) UE positioning in the target sector.
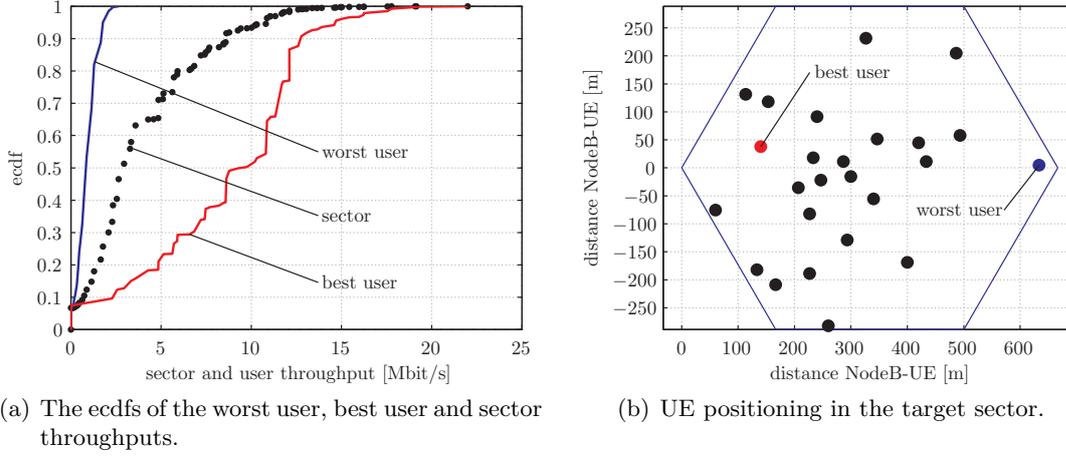
Figure 4.6.: Single network realization SINR and throughput results.
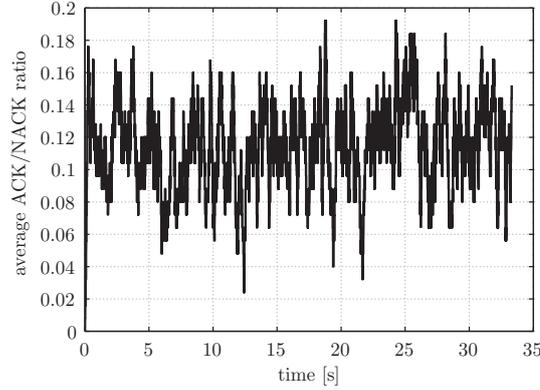
Figure 4.7.: BLER results for a single network realization.

According to the system design [7] and corresponding to the SINR-to-CQI mapping from Appendix A.7, the average ACK/NACK ratio of the cell should be close to its target value of 0.1.[12] To confirm this behavior in the system-level simulator, Figure 4.7 depicts the ACK/NACK ratio when averaged with a sliding window filter of length 125 TTIs. It can be observed that the ACK/NACK ratio fluctuates around its average of 0.11, which is close to its desired target value.

When speaking of the ACK/NACK ratio performance, it has to be noted that the responsible link-adaptation for stream two is much more difficult to calibrate than for stream one. The reason is that due to the pre-coding, stream two experiences a much higher variance of its SINR and thus the link-adaptation has to be configured more conservatively. For optimum operation, the pre-coding and the stream decision should be performed in a joint way.

Figure 4.8 lists the distribution of the stream utilization and the distribution of the CQI reports for the SS and the DS case, respectively. It can be observed that the cell utilizes a SS transmission time approximately two and a half times that of the DS transmission. Furthermore, the CQI distributions show that the dynamic range covered by the link-adaptation fits the observed

---

[12]Note that the term *ACK/NACK ratio* is defined as [nr. of NACK/(nr. of ACK + nr. of NACK)] in this context.

(a) Stream utilization in the given network scenario.

(b) Distribution of the CQI reports from UEs in SS transmission mode.

(c) Distribution of the CQI reports for stream one from UEs in DS transmission mode.

(d) Distribution of the CQI reports for stream two from UEs in DS transmission mode.
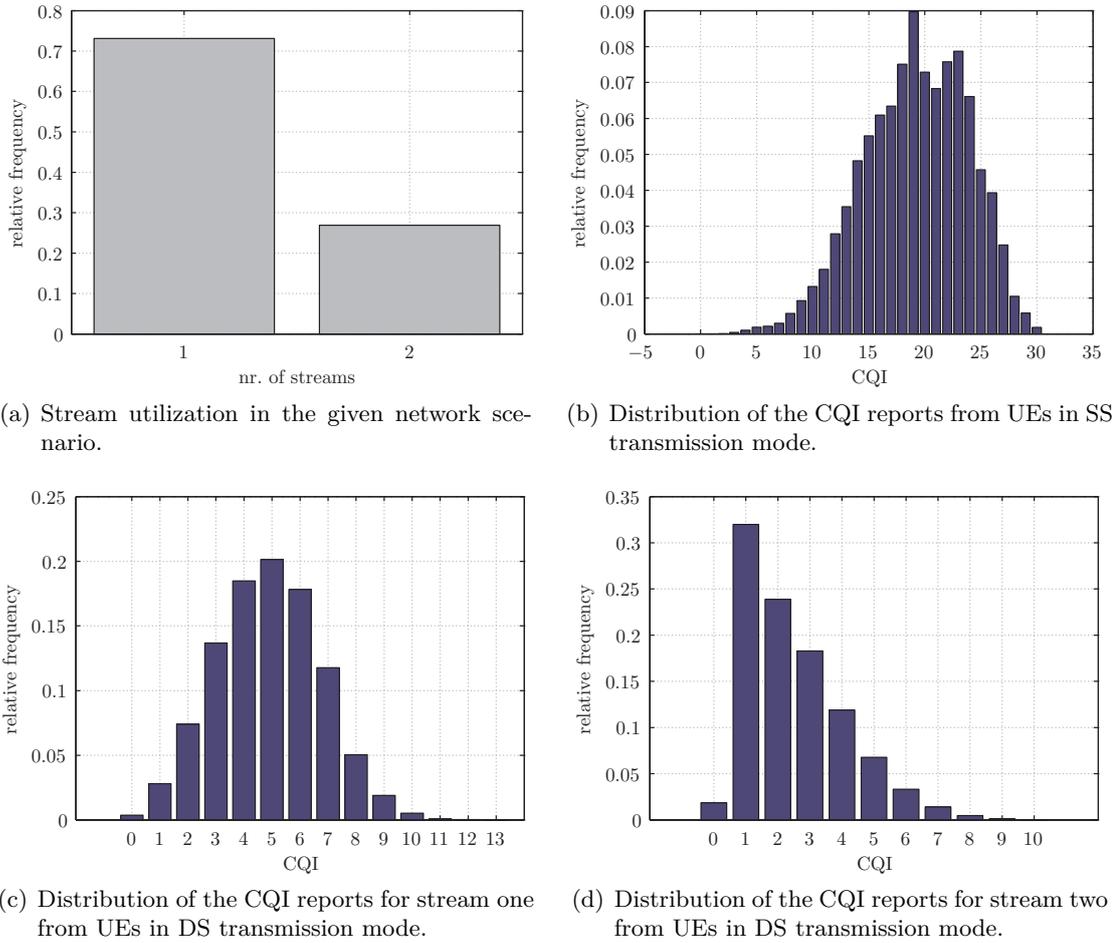
Figure 4.8.: Stream utilization and CQI report distributions.

SINR statistics in the cell well, thus nearly all CQI values are utilized and the distribution is not squeezed to one end. Only the CQI report distribution of stream two is skewed to the lower values which is again a result of the lower average SINR and its higher variance due to the pre-coding.

4.2.3. Average Network Performance

To assess the network performance, a set of network scenarios has to be simulated to average over different user positionings and shadow fading trace realizations. Two exemplary results of such a simulation campaign are shown in Figure 4.9.

Figure 4.9(a) illustrates the obtained throughput performance over distance for all eight simulated network realizations. To clarify the underlying trend I performed a 2nd order polynomial regression utilizing an LS fit. This result can serve as a general guideline for base-station positioning in a wireless network, for example when the cell-edge performance should meet a certain target. If the cell-edge performance should be $2\,\mathrm{Mbit/s}$, the maximum cell-radius is given by $465\,\mathrm{m}$.

Figure 4.9(b) then depicts the overall ecdf of the average user throughput for the whole simulation campaign. Two important observations can be made from this figure:

- The steepness of the curve represents a measurement of the fairness of the system, and

- Figure 4.9(b) shows a distinctive bend of the ecdf around 0.75 in probability.

For a perfectly fair system, the ecdf would be a step function which corresponds to equal average throughputs for all users. To interpret the presented result in context of the simulation settings, let me point out that the utilized RR scheduler is fair in terms of the assigned physical resources. In particular, the number of time slots assigned to every user is—in average—equal for all users. However, resource fairness does not necessarily correspond to data rate fairness.

This is a fundamental difference between wireline and wireless networks, where the physical layer translates assigned resources very unequally to achievable data rates. Based on this observation, the literature also defines fairness coefficients for *data-rate fairness* and for *resource allocation fairness* [45]. The standard definition for the fairness coefficient ϑ is given by [46]

$$\vartheta \triangleq \frac{1}{1 + \sigma_T^2}, \tag{4.6}$$

with the throughput variance σ_T^2 being

$$\sigma_T^2 = \mathbb{E}\left\{ \left(\bar{T}^{(u)} \right)^2 \right\} - \mathbb{E}\left\{ T^{(u)} \right\}^2 \approx \frac{1}{U} \sum_{u=1}^{U} \left(\frac{1}{\kappa} \sum_{k=1}^{\kappa} T_k^{(u)} \right)^2 - \left(\frac{1}{U\kappa} \sum_{u=1}^{U} \sum_{k=1}^{\kappa} T_k^{(u)} \right)^2, \tag{4.7}$$

where U denotes the total number of simulated users in the whole ensemble of individual simulated network scenarios, κ represents the total number of simulated TTIs, and $T_k^{(u)}$ is the throughput of user u in TTI k. This definition thus utilizes second-order moments of the throughput results, whereas the *steepness* of the ecdf of the average user throughput compares the average throughput values directly. The RR scheduler on which these results are based is a resource fair scheduler, explaining the low steepness and the according lower data-rate fairness as illustrated in Figure 4.9(b).

The bend in the ecdf in Figure 4.9(b) is a result of the SS/DS adaptation. Not all users are in such favorable channel conditions to benefit from a DS spatial multiplexing transmission that increases their average throughput values significantly. Accordingly, users that obtain two streams can exploit the assigned resources much more efficiently pushing the throughput to dramatically higher values.

This behavior however also influences the data-rate fairness, especially when a resource-fair RR scheduler is utilized. As a result, the ecdf shows a distinct bend in the upper region. Note also that the position of the bend corresponds to the average DS utilization in the simulation campaign which was 27 %.

Performance comparison for different network configurations

Finally, I want to compare the throughput performance of different network configurations. Figure 4.10 illustrates the network performance in terms of the average and maximum sector throughputs for the following four different network deployments and two different channel characteristics:

(i) $N_\mathrm{T} \times N_\mathrm{R} = 2 \times 2$ Double-Stream (DS) network with ITU PedA channel profile,

(a) Average user throughput over distance from the NodeB.

(b) The ecdf of the average user throughput.
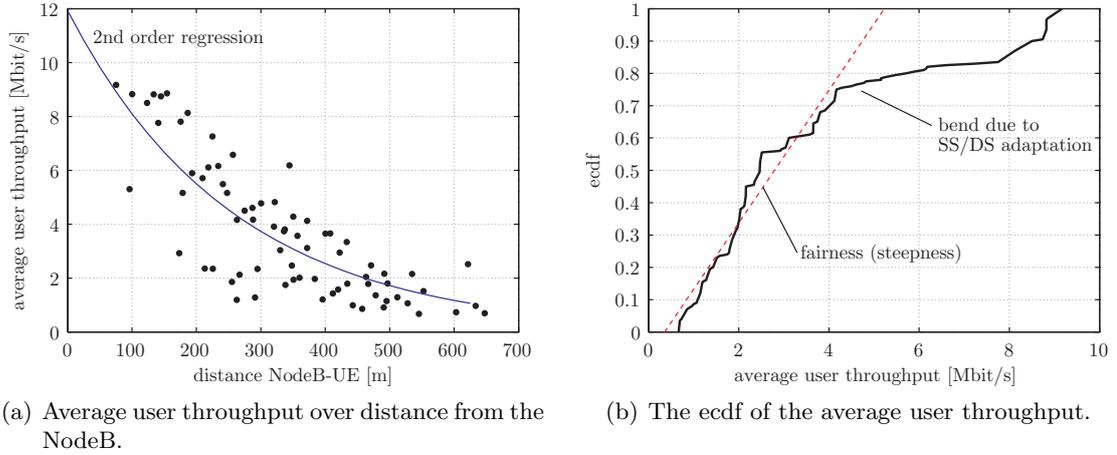
Figure 4.9.: Exemplary throughput results for the system-level simulation campaign.
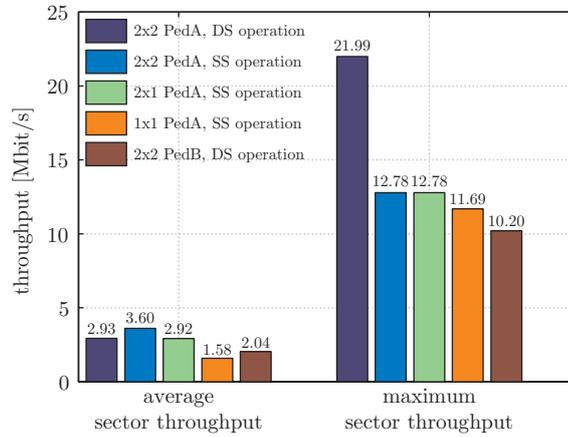
Figure 4.10.: Comparison of average and maximum sector throughputs for five different network deployments.

(ii) 2×2 Single-Stream (SS) network with ITU PedA channel profile,

(iii) 2×1 SS network with ITU PedA channel profile,

(iv) 1×1 SS network with ITU PedA channel profile,

(v) 2×2 DS network with ITU PedB channel profile.

The 2×2 SS network shows the maximum average sector throughput, but with significantly lower maximum sector throughput. If the 2×2 and 2×1 ITU PedA networks in single-stream operation are compared, it can be observed that the average sector throughput benefits from the second receive antenna. In case the channels follow an ITU PedB profile, the network performance both in terms of the average and maximum sector throughput drops significantly. This is because of larger losses due to the less optimal equalization in these large delay channels. Still, the network benefits from the utilization of the second stream (which was 19% in this case). The 1×1 network deployment shows the lowest average sector throughput but a higher maximum sector throughput compared to the 2×2 ITU PedB case, which is again due to deficiencies in terms

of diversity. Finally, let me point out that some initial ideas about a theoretical performance bound comparison of the system-level throughput results can be found in Appendix A.8.

4.3. RLC-Based Stream Number Decision

The results presented so far are based on a stream utilization as requested by the UE. This means that the UE evaluates the number of streams that maximizes the expected throughput in the next upcoming transmission [16]. However, such an estimation depends on a number of factors and can be very challenging. In addition, the interference structure of the cell—which depends on the number of active streams—is then determined by the UE. This is in general undesired by the network operators [116]. Individual enhancements of the user channel quality by means of interference-cancellation or interference-awareness or similar techniques do not impose such problems, see Chapter 5 for further details.

For an efficient and robust network operation, network entities should assign the resources according to overall goals and cost functions, like for example the average cell throughput [26,67, 117], and therefore actively manage the interference situation in the cells, see also Appendix B.1

4.3.1. UE Decision

Before going into detail on the proposed network based algorithm, let me shortly elaborate on a possible stream number decision strategy of the UE. The presented algorithm is also the UE based stream number decision strategy against which the performance of the network will be compared.

The underlying assumption of the algorithm is that the UE assumes that the NodeB will apply the transmission settings corresponding to the fed back CQI values, $c^{(\mathrm{T})} = c^{(\mathrm{F})}$. With this assumption, the data-rate optimum decision from the viewpoint of the UE is to evaluate the individual SINRs for SS and DS operation—for example by estimating it with a slightly modified form of Equation (3.62) like in [16]—and compare the resulting expected throughputs. In particular, if the SS SINR is denoted $\mathrm{SINR}^{\mathrm{SS}}$ and the DS SINRs are denoted $\mathrm{SINR}_1^{\mathrm{DS}}$ and $\mathrm{SINR}_2^{\mathrm{DS}}$, respectively, then the corresponding feedback CQI values are given by

$$\mathrm{SINR}^{\mathrm{SS}} \rightarrow c_{\mathrm{SS}}^{(\mathrm{F})}, \tag{4.8}$$

$$\mathrm{SINR}_1^{\mathrm{DS}} \rightarrow c_{\mathrm{DS},1}^{(\mathrm{F})}, \tag{4.9}$$

$$\mathrm{SINR}_2^{\mathrm{DS}} \rightarrow c_{\mathrm{DS},2}^{(\mathrm{F})}, \tag{4.10}$$

as determined by the utilized SINR-to-CQI mapping designed to achieve a target ACK/NACK ratio of 0.1. Each of these potential feedback CQI values corresponds to a TBS, thus the optimum stream number $N_{\mathrm{S}}^* = 1, 2$ can be formulated as follows

$$N_{\mathrm{S}}^* = \begin{cases} 1 & \text{if } \mathrm{TBS}\left(c_{\mathrm{SS}}^{(\mathrm{F})}\right) > \mathrm{TBS}\left(c_{\mathrm{DS},1}^{(\mathrm{F})}\right) + \mathrm{TBS}\left(c_{\mathrm{DS},2}^{(\mathrm{F})}\right), \\ 2 & \text{else.} \end{cases} \tag{4.11}$$

There is one last implementation detail that should be noted. The CQI tables in case of a double stream transmission specify a minimum TBS of two times 4 581 bits. Thus, in case the channel becomes very poor, the SS corresponding TBS would strictly be lower and thus the proposed algorithm would decide on a DS transmission. However, given the low channel

quality, a successful DS transmission is very unlikely. Accordingly, there is the need for a second constraint,

$$\text{SINR}_1^{\text{DS}} < \text{SINR}^{\text{thres}} \Rightarrow N_{\text{S}}^* = 1, \tag{4.12}$$

to ensure that a SS transmission is requested when the channel quality is low. The threshold SINR, $\text{SINR}^{\text{thres}}$, has been found by means of simulations to obtain the best algorithm performance which resulted in a value of $5\,\text{dB}$ HS-DSCH SINR.

4.3.2. RLC Decision

The information the NodeB has available to base the SS/DS decision on are the CQI feedback values and the ACK/NACK reports of the UEs. This information allows for the design of many different cost functions, of which I want to elaborate the *effective TBS* as introduced in [18]. The effective TBS of a particular user is given by

$$\text{TBS}^{(\text{eff})} \triangleq \text{TBS}\left(c^{(\text{F})}\right) \cdot (1 - \Upsilon), \tag{4.13}$$

with Υ being a sliding window average of the ACK/NACK ratio, as exemplarily shown in Figure 4.7. This parameter thus represents the in the short term average expected TBS that can successfully be transmitted.[13]

With the effective TBS being defined, the optimum number of streams decided by the NodeB is given by

$$N_{\text{S}}^* = \begin{cases} 1 & \text{if } \text{TBS}^{(\text{eff})} < \text{TBS}\left(c^{(\text{D})}\right), \\ 2 & \text{if } \text{TBS}^{(\text{eff})} > \text{TBS}\left(c^{(\text{U})}\right), \\ \text{not changed} & \text{else.} \end{cases} \tag{4.14}$$

The CQI values $c^{(\text{D})}$, $c^{(\text{U})}$ and the corresponding TBS values represent threshold values for the down- and upgrade from DS to SS and vice versa. These two distinct values allow for the realization of a hysteresis which can limit potential oscillation problems of the optimum stream number.

4.3.3. System-Level Simulation Results

To assess the performance of the proposed algorithm in comparison to the UE-based stream decision, system-level simulations were conducted. The same simulation settings as specified in Table 4.1 hold also for these simulation campaign of different network realizations.

Figure 4.11 depicts the average sector throughput for varying up- and downgrade CQI values. Note that the average sector throughput in case of the UE-based algorithm should be a straight line. Due to independent network realizations for all simulated up- and downgrade values, however, the resulting sector throughputs fluctuate slightly. Figure 4.11 shows clearly that given the assumptions on the SINR-to-CQI mapping and the network behavior as a function of the feedback CQI, the effective TBS-based algorithm is outperformed. Even if the best combination of the threshold values $c^{(\text{D})} = 5$ and $c^{(\text{U})} = 30$ is chosen, the UE-based decision achieves by $200\,\text{kbit/s}$ higher average sector throughput.

The main reason is that in case of the network-based decision the NodeB has to decide on the transmission format, or accordingly the transmit CQI value $c^{(\text{T})}$, to be utilized after a change

---

[13]If the TBS would be mapped to a throughput by dividing by the duration of the TTI of $2\,\text{ms}$, this parameter could also be interpreted as the short term average expected throughput.

(a) Performance comparison for varying upgrade threshold when $c^{(D)} = 2$.

(b) Performance comparison for varying downgrade threshold when $c^{(U)} = 28$.
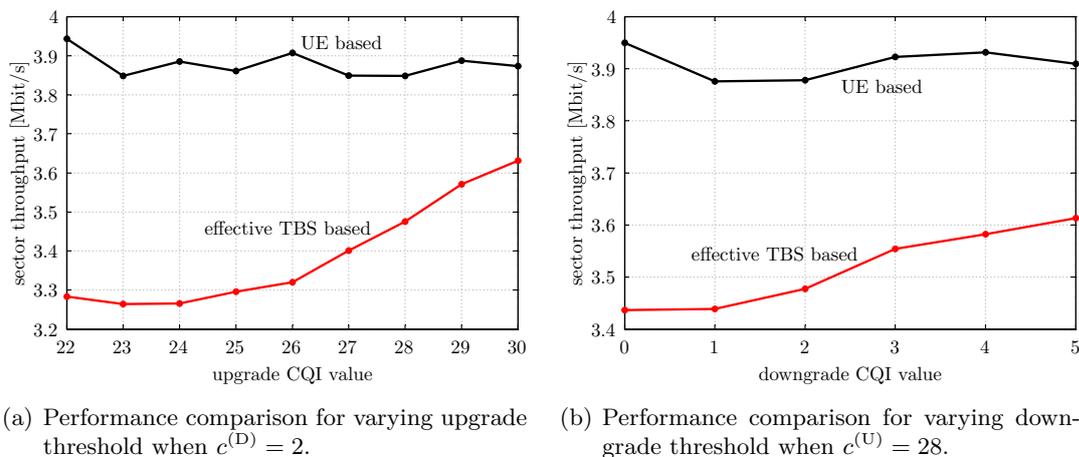
Figure 4.11.: Performance comparison of the UE based and the NodeB based stream number decision.
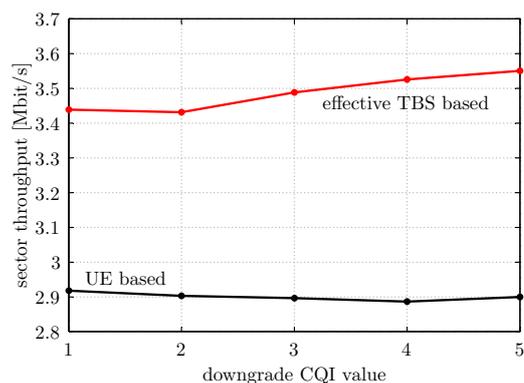
Figure 4.12.: Robustness performance comparison of the UE based and the NodeB based stream number decision when the UE CQI reporting is non-optimal by one.

from SS to DS or vice versa. Since no UE CQI report is available for this initial phase of the changed transmission mode, the network has to estimate the optimum transmission format for the UE until new feedback values for the new transmission mode arrive. This is the reason for the observable performance gap. Further details on this issue can be found in [18].

Figure 4.12 finally shows the performance of the effective TBS-based network stream decision when the UE CQI feedback is assumed to be outdated and the CQI mismatch is equal to one. This means that in case a CQI value of 17 would be optimum for the given channel conditions, the UE had reported a CQI of 16 or 18. Such a scenario occurs for example when the channel coherence time becomes shorter such that—given the fixed delay constraint of the feedback— the CQI feedback does not perfectly represent the channel conditions during the transmission anymore.

It can be observed that the effective TBS-based network stream decision outperforms the UE-based stream decision by approximately 500 kbit/s, where the up- and downgrade CQI values

were set to 30 and 5, respectively. The main reason for this improved performance is that in case of non-perfect UE feedback, no control mechanism is left to ensure an average ACK/NACK ratio of 0.1. The effective TBS-based algorithm however implicitly tries to maximize the sector throughput that can be delivered successfully. With the up- and downgrade thresholds set accordingly, the network is able to stabilize effects that would increase the ACK/NACK ratio.

4.4. Content-Aware Scheduling

As already mentioned in the beginning of this chapter, system-level modeling and simulation can also be utilized to perform cross-layer optimizations. In this section I restate the basic findings of two contributions [19, 20] that are based on investigations with the developed HSDPA system-level simulator to assess the performance of a Content-Aware (CA) cross-layer scheduler.

4.4.1. Introduction

The increase in available downlink data-rate and the developments in the core network architecture make IP traffic in wireless networks more and more important. This traffic consists of a variety of different applications with different degrees of interactivity and technical needs. Thus 3GPP standards define four classes of IP traffic [118], see Appendix A.9.1. These classes have been introduced to ensure certain QoS goals of the customers. However the QoS does not necessarily reflect the QoE [119] of the user. In particular for video applications, stringent constraints in average data-rate, delay, jitter, or data-rate variance do not necessarily map one-to-one to the QoE. Since the QoE finally also determines the users' willingness to pay for certain entertainment services applying it as a metric for network optimization seems intuitive. Accordingly, this section is devoted to introduce a CA scheduler trying to maximize the QoE of the user and to assess its performance.

4.4.2. Video Packet Prioritization in HSDPA

Content awareness of the NodeB scheduler requires the signaling of content information to the MAC-hs layer. In particular, the importance of the encoded slice can then also be signaled exploiting the fields of the Network Abstract Layer (NAL) unit header [120]. At the video streaming server, this priority information can be conveyed to the IP layer. The IP header contains a byte originally designed to specify the Type Of Service (TOS) which is currently used for Differentiate Service (DiffServ) marking [121]. This specifies how a packet has to be handled by each network element.

UTRAN networks provide so called Packet Data Protocol (PDP) contexts to identify and arrange different packet switched connections. Within this method, the user terminal at one side and the GGSN at the other side agree on several parameters, for example the IP address, the PDP type and the QoS profile of the following packets. Each PDP context supports one QoS parameter setting at a time. The QoS information of the corresponding PDP contexts is also available to the MAC-hs layer. To allow for multiple services with different requirements dedicated to one user terminal to run in parallel, multiple PDP contexts are allowed in UMTS.

The basic idea of the cross layer signalization of the video content information is to encapsulate the video packet information in the DiffServ field of the IP header. This information then is passed to the GGSN which, when establishing the PDP contexts to the desired user will establish a set

of PDP contexts,[14] one for each priority class of the video content. According to the Traffic Flow Template (TFT) filter[15] required at the GGSN for the operation of the multiple PDP contexts, the incoming IP packets will be filled in the corresponding flows. The MAC-hs scheduler then can treat these packets arriving through different flows differently, enabling CA scheduling. Further details on the content information delivery from IP to MAC-hs layer can be found in [20].

4.4.3. Content-Aware Scheduler

With the IP packet priority information made available at the MAC-hs scheduler in the NodeB, the question remains how to exploit this information. The basic idea is to protect packets of higher importance for the QoE when decoded and displayed at the user terminal better against transmission errors. Simultaneously the scheduler shall have the flexibility to downgrade the error protection on the physical layer for packets with less priority.

As explained in Chapter 2 and elaborated in Section 4.3, in HSDPA the NodeB has to adapt the transmission settings according to the feedback information of the UEs, $c^{(\mathrm{F})}$. As a matter of fact, if the same quantized set of transmission formats as the table of feedback CQI values is utilized, the NodeB has to perform the mapping

$$\mathcal{T} : c^{(\mathrm{F})} \rightarrow c^{(\mathrm{T})}, \tag{4.15}$$

from feedback CQI $c^{(\mathrm{F})}$ to the transmit CQI $c^{(\mathrm{T})}$ representing the applied code-rate and modulation alphabet utilized for the transmission.

The proposed scheduler introduces an adaptive mapping, depending on the video packet priority. Better protection can be achieved by remapping the transmit CQI to lower values and vice versa. However, if the transmit CQI is lowered to much, the average sector throughput would decrease notifiable which is in general undesired because spectral resources would be wasted.

As elaborated in Appendix A.9, packets belonging to I-frames contribute significantly to the overall video quality, whereas packets belonging to P-frames influence it not that prominent. In particular this holds true for packets of P-frames that are at the end of a Group Of Pictures (GOP). Also note that in average one I-frame corresponds to four P-frames in size. Given these QoE priority information, three scheduling priority classes can be defined

- priority $\nu = 2$: packets belonging to I-frames,
- priority $\nu = 1$: packets belonging to the first ($l_{\mathrm{GOP}} - 4$) P-frames of the GOP,
- priority $\nu = 0$: packets belonging to the last 4 P-frames of the GOP,

where L_{GOP} denotes the length of the GOP in frames. Then the proposed transmission mapping $\mathcal{T}$ of the MAC-hs scheduler is given by

$$\mathcal{T}_\nu : c^{(\mathrm{T})} = c^{(\mathrm{F})} + 1 - \nu. \tag{4.16}$$

To ensure fairness among all active users in the cell, the scheduler selects the served user according to a RR strategy. In addition, the maximum packet delay of the network has been limited by allowing a maximum number of one HARQ retransmission.

---

[14] Let me note that the desired video content signaling requires the setup of one primary and a set of secondary PDP contexts. The full treatment of this interrelation would be beyond the scope of this thesis, however further information can be found in [20].

[15] A TFT filter specifies a set of rules to assign incoming packets to PDP contexts. Details about the design of these filters can be found in [19].

Table 4.2.: System-level simulation settings for the performance assessment of the CA scheduler.

Parameter	Value
interference scenario	homogeneous network
number of cells	19, layout type I
NodeB distance	$750\,\text{m}$
carrier frequency	$1.9\,\text{GHz}$
total transmit power available at NodeB	$20\,\text{W}$
total CPICH power	$0.8\,\text{W}$
power of other channels	$1.2\,\text{W}$
available HS-PDSCHs	15
macro-scale path-loss model	urban micro
antenna utilization	$N_\text{T} \times N_\text{R} = 1 \times 1$
channel type	ITU PedA
active users in target sector	25
user mobility	$3\,\text{km/h}$, random direction
UE capability class	10
UE receiver type	MMSE, $L_\text{f} = 30\,\text{chips}$, $\tau = 15\,\text{chips}$
feedback delay	$4\,\text{TTI}$
HARQ type	Incremental Redundancy (IR)

4.4.4. Simulation Results

To assess the performance gain of the proposed scheduler, system-level simulations of a SISO HSDPA network when transmitting the standard test sequence *Foreman* in Quarter Common Intermediate Format (QCIF) resolution have been conducted. The obtained results are then compared against the typical RR scheduler QoE. The simulation parameters are summarized in Table 4.2.

Figure 4.13 depicts the results in terms of the ACK/NACK ratio and the luminance Peak Signal to Noise Ratio (PSNR), *Y-PSNR*. For the classical RR scheduler no distinction has been made between transport blocks containing I or P encoded frames. As expected, the average ACK/NACK ratio lies around 10 %. For the proposed CA scheduling mechanism, the error probabilities associated to packets containing I and P frames have been presented separately. The proposed CQI mapping allows for the error probability of the transport blocks containing I-frames to decrease by a factor of four, resulting in an average ACK/NACK ratio of around 2.7 %.

The Y-PSNR is an indicator for the QoE performance. Following the discussion in Appendix A.9, three different GOP sizes have been investigated: 30, 45, and 60 frames. As a consequence of the smaller ACK/NACK ratio, Figure 4.13 shows that the quality of the I frames has increased by more than 0.5 dB when using the CA scheduler. Such an increase, however, is not only beneficial in terms of contribution to the average frame quality, but rather also has to be considered advantageous for the quality of the following P-frames. On the one hand, a valid source of prediction is offered to the following P-frames, and on the other hand, in case the previous GOP was damaged, the temporal error propagation of the error is terminated. The
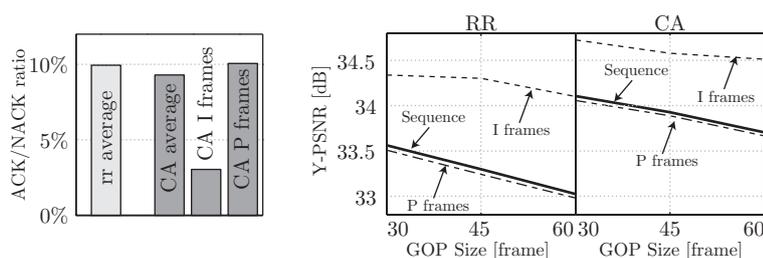
Figure 4.13.: System-level simulation results for the CA scheduler.

overall sequence quality measured using the proposed CA scheduling mechanism is 0.6 dB higher than the one obtained with a classical RR scheduler.

4.5. CPICH Power Optimization

The downlink performance of wireless networks does not only depend on its data-channels, like the HS-DSCH in case of HSDPA, but also on the configuration and performance of the signaling and feedback channels. As a matter of fact, many design goals like the target ACK/NACK ratio or the maximum load of the cell depend on the construction of the signaling and synchronization channels. In particular the CPICH is important for the network planing and its overall performance, see also Chapter 2. The two main duties of it are

- provide reference symbols for the channel estimation at the receiver side, and
- provide a way for the UE to assess the best service base-station thus determining the coverage of the cells.

The cell coverage is an important network planing parameter, because depending on the coverage area, the load of the individual cells can be managed. In addition, UMTS based networks have to deal with *cell breathing* [122],[16] which complicates matters here.

The task to provide means for channel estimation heavily influences the downlink throughput performance as well. Obviously, the channel estimation directly determines the performance of the receiver, for example the quality of the equalization in case of an MMSE equalizer. A higher transmission power of the CPICH would lead, in average, to a better SNR and thus could be conjectured to lead to better channel estimation and correspondingly to better equalization. This would deliver better throughput and error performances. On the other hand, however, an increase in the CPICH power increases the interference imposed on the HS-DSCH, which counterbalances the previous effect. This raises the question how to find the optimum CPICH power value.

The optimization problem of the CPICH power configuration has attracted a lot of attention in the scientific community. Most recent works however focus on the task of network load optimization when specific traffic density maps are available [123–127] and utilizing CPICH SNR targets as a side constraint. Earlier works focus on UMTS systems with active power-control [128, 129]—which is not active in the HSDPA downlink—and also do not take the interference effect of the CPICH into account.

---

[16]Cell breathing is the expansion or contraction of the effective coverage of a cell in response to the number of active mobiles in a network by redirecting UEs to surrounding cells.

In this section I restate the basic findings of my efforts to solve the CPICH power optimization problem for HSDPA networks. This work is based on an enhancement of the link-quality model of Chapter 3 to reflect the influence of the CPICH and utilizes the HSDPA system-level simulator to evaluate the optimum CPICH power values [21].

4.5.1. System-Level Modeling of the CPICH Influence

To numerically assess the influence of the CPICH on the performance of the HS-DSCH, the link-quality model of Chapter 3 has to be refined. So far, always perfect CSI at the UE had been assumed.

Before going into the details on the link-quality model enhancement, let me spent a few words on the CPICH. UMTS based networks offer two different CPICHs, the *primary* and the *secondary* CPICH, where the secondary one is designed to serve dedicated hot spot areas and thus will be neglected in the following. The primary CPICH has the following features:

- the spreading sequence for the primary CPICH is always the same with length 256,
- there is only one primary CPICH in the cell that is broadcasted over the whole cell area, and
- 4-QAM modulation is utilized, which results in a bit-rate of 30 kbit/s.

A detailed description of the primary and secondary CPICH including the channel coding and scrambling sequence details can be found in [34]. In the following, let me denote the primary CPICH only by the name CPICH for sake of notational simplicity.

Link-Quality Model Enhancement

To integrate the CPICH influence in the link-quality model, the employed receive filter—in this work the MMSE equalizer from Equation (3.14)—has to be based on the estimated channel. In particular, if the estimated channel is denoted by $\hat{\tilde{\mathbf{H}}}_{\mathrm{w}}$, the MMSE equalizer is given by

$$\hat{\mathbf{F}} = \mathbf{R}_{\mathbf{x}^{\mathrm{S}}_{i-\tau}\tilde{\mathbf{x}}_i}\hat{\tilde{\mathbf{H}}}^{\mathrm{H}}_{\mathrm{w}}\left(\hat{\tilde{\mathbf{H}}}_{\mathrm{w}}\mathbf{R}_{\tilde{\mathbf{x}}_i}\hat{\tilde{\mathbf{H}}}^{\mathrm{H}}_{\mathrm{w}} + \mathbf{R}_{\tilde{\mathbf{n}}_i}\right)^{-1}. \tag{4.17}$$

As investigated in [21], the estimated channel $\hat{\tilde{\mathbf{H}}}_{\mathrm{w}}$ can statistically be represented by the matrix

$$\hat{\tilde{\mathbf{H}}}_{\mathrm{w}} = \tilde{\mathbf{H}}_{\mathrm{w}} + \mathbf{H}_{\Delta}, \tag{4.18}$$

with the *error* matrix $\mathbf{H}_{\Delta}$ being of the same structure like $\tilde{\mathbf{H}}_{\mathrm{w}}$. This means that $\mathbf{H}_{\Delta}$ has to be generated according to $\mathbf{H}_{\Delta} \triangleq \sigma^2_{\mathrm{MSE}}\mathbf{G}$, with $\mathbf{G}$ being a random Gaussian matrix of the same frequency selectivity structure like $\tilde{\mathbf{H}}_{\mathrm{w}}$ with variance one. The variance σ^2_{MSE} specifies the weighting of the error matrix and is a function of the CPICH transmission power. Accordingly, the equivalent fading parameters can easily be generated utilizing $\hat{\mathbf{F}}$ instead of $\mathbf{F}$ for various CPICH transmission power values.

Modeling Validation

To validate the new equivalent fading parameters, a set of link level simulations has been performed for different antenna configurations, comparing the true SINR as evaluated in Equation (3.65) with the SINR as predicted by the modeling. Figure 4.14 shows the resulting model

(a) SISO $N_T \times N_R = 1 \times 1$ system utilizing one stream in a PedA channel environment.

(b) MISO 2×1 system utilizing one stream in a PedA channel environment.

(c) MIMO 2×2 system utilizing one stream in a PedA channel environment.

(d) MIMO 2×2 system utilizing two streams in a PedA channel environment.
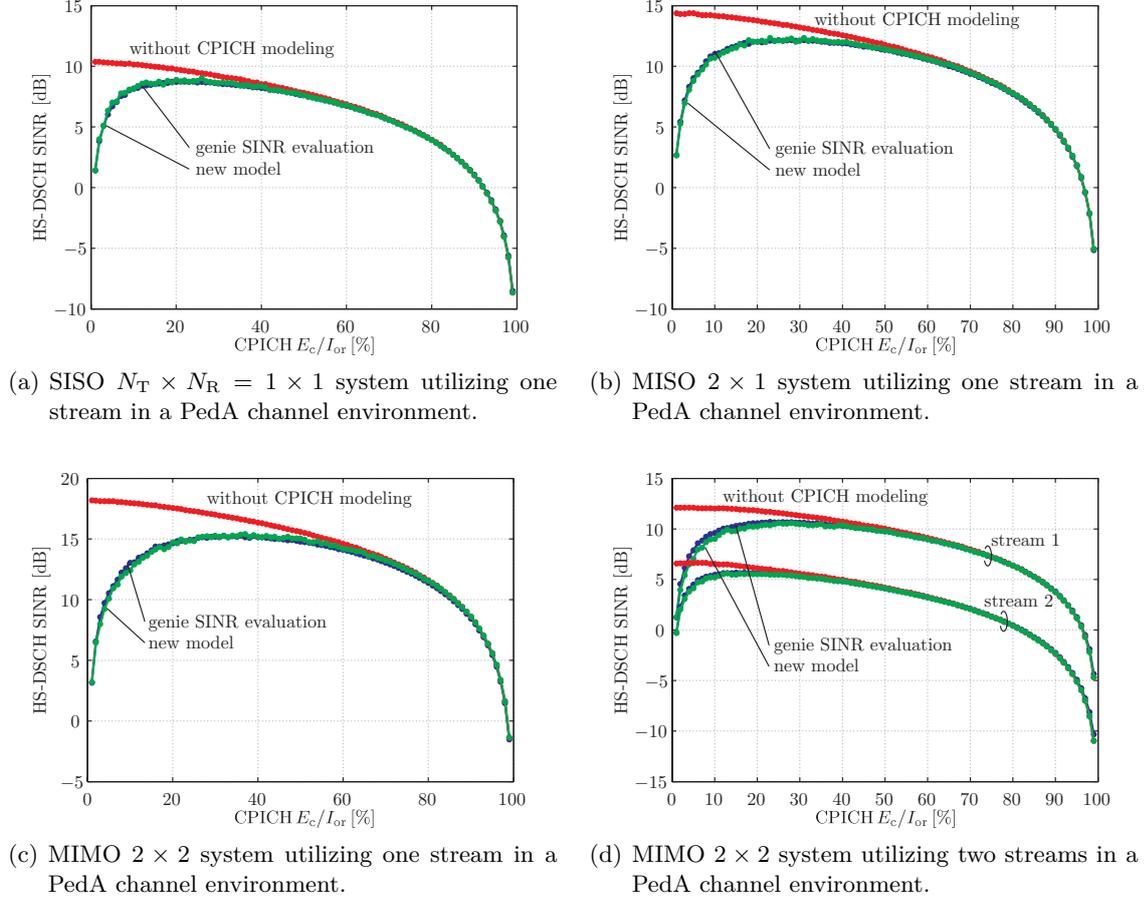
Figure 4.14.: Enhanced link-quality model validation for different antenna configurations and stream utilization.

fittings for varying CPICH E_c/I_{or} when an interference situation of $I_{oc}/\hat{I}_{or} = -6\,\mathrm{dB}$ is assumed at the UE[17] and a standard LS channel estimator is utilized [130].

It can be observed that the simplified equivalent fading parameter modeling based on the statistical error matrix modeling of Equation (4.18) is able to describe the CPICH influence nearly perfect. The dependency on the interference power situation $I_{oc}/\hat{I}_{or}$ which effectively shifts the CPICH SINR as function of the E_c/I_{or} is not further elaborated here, but further details can be found in [21].

4.5.2. CPICH Optimization in the Cellular Context

As observable in Figure 4.14, for a given interference scenario defined by $I_{oc}/\hat{I}_{or}$ an optimum CPICH E_c/I_{or} that maximizes the HS-DSCH SINR can be found. The interference situation for the CPICH, however, depends in the position of the UE in the cell.

---

[17]The parameter E_c/I_{or} specifies the fraction of the total available transmit power utilized for the transmission of the CPICH and $I_{oc}/\hat{I}_{or}$ defines the interference power scenario, see also Appendix A.11. Note that in this section, the average channel power is assumed to be one.

Table 4.3.: System-level simulation settings for the CPICH power optimization.

Parameter	Value
interference scenario	homogeneous network
number of cells	19, layout type I
available transmission power at the NodeB	20 W
NodeB distance	1000 m
carrier frequency	1.9 GHz
available HS-PDSCHs	15
macro-scale path-loss model	urban micro
UE receiver type	MMSE, $L_f = 30$ chips, $\tau = 15$ chips
feedback delay	4 TTI
channel estimation type	LS

Thus, by evaluating the pre-equalization SINR as depicted in Figure 4.5, $I_{oc}/\hat{I}_{or}$ can be calculated for every position in the cell. The optimization procedure then is the following:

(i) calculate the pre-equalization SINR map of the desired network,

(ii) generate a regular grid of positions within the target sector to be evaluated and evaluate the interference situation $I_{oc}/\hat{I}_{or}$ for all grid points,

(iii) calculate the HS-DSCH SINR curves as function of the CPICH E_c/I_{or} given all stored $I_{oc}/\hat{I}_{or}$ values, and

(iv) find the optimum CPICH E_c/I_{or} value of every calculated HS-DSCH SINR curve according to

$$\left(\frac{E_c}{I_{or}}\right)^*_{\text{CPICH}} = \frac{1}{N_S} \sum_{n=1}^{N_S} \arg \max_{\left(\frac{E_c}{I_{or}}\right)_{\text{CPICH}}} \text{SINR}_n^{\text{HS-DSCH}}. \tag{4.19}$$

Table 4.3 lists the system-level simulation settings for the optimization procedure. The resulting optimum CPICH E_c/I_{or} values for all evaluated positions in the target sector when utilizing two streams in a $N_T \times N_R = 2 \times 2$ channel are depicted in Figure 4.15. It can be observed that the optimum CPICH E_c/I_{or} value increases towards the sector edge, which is due to the higher interference power. Furthermore, the PedB channel environment requires significantly higher E_c/I_{or} values to achieve the optimum performance. This is due to the greatly increased delay spread of the PedB channel when compared to the PedA channel, which makes the channel estimation and the equalization much more complicated.

Setting the CPICH E_c/I_{or} to different values depending on the UE position in the sector unfortunately is impossible. Thus, for the network operator the CPICH power has to be set to an average value. A simple option is to perform a linear averaging of all evaluated grid points within the target sector,

$$\overline{E_c/I_{or}} = \frac{1}{|\mathcal{G}|} \sum_{\mathcal{G}} \left(\frac{E_c}{I_{or}}\right)^*_{\text{CPICH}}, \tag{4.20}$$

with $\mathcal{G}$ denoting the grid of target sector positions at which the optimum CPICH $\frac{E_c}{I_{or}}$ has been evaluated. In case of a known traffic density map, the CPICH power averaging could also consider
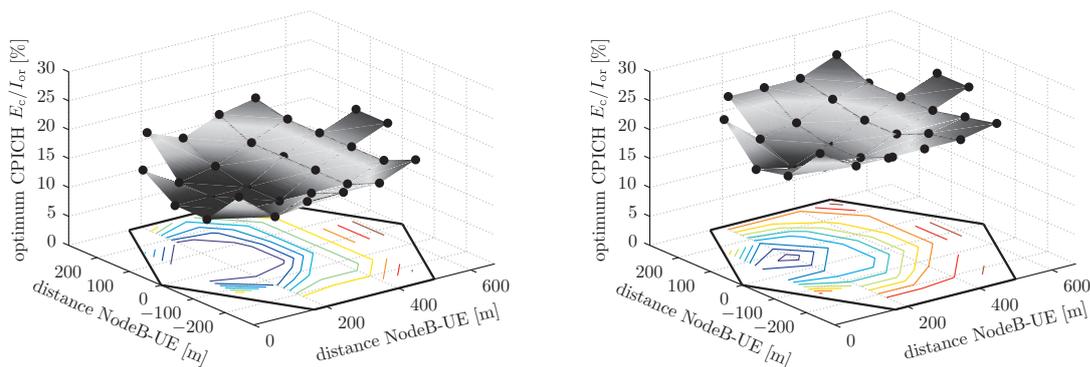
(a) MIMO $N_\mathrm{T} \times N_\mathrm{R} = 2 \times 2$ network utilizing two streams in a PedA channel environment.

(b) MIMO 2×2 network utilizing two streams in a PedB channel environment.

Figure 4.15.: DS utilization CPICH power optimization results for different antenna configurations experiencing PedA and PedB channel environments, respectively.

Table 4.4.: Resulting optimum average CPICH $E_\mathrm{c}/I_\mathrm{or}$ values for different network configurations and channel profiles.

Network configuration	$\overline{E_\mathrm{c}/I_\mathrm{or}}$ [%]
MISO 2×1, TxAA, PedA	11.00
MISO 2×1, TxAA, PedB	19.92
MIMO 2×2, TxAA, PedA	13.08
MIMO 2×2, TxAA, PedB	21.08
MIMO 2×2, D-TxAA, PedA	14.67
MIMO 2×2, D-TxAA, PedB	21.75

this density distribution. The resulting optimum average CPICH $E_\mathrm{c}/I_\mathrm{or}$ values for all evaluated network scenarios are listed in Table 4.4.

Finally, let me note that the presented optimization procedure neglects CPICH *pollution* effects [131] which can cause problems for the UMTS soft handover. To reflect these optimization constraints target CPICH SINR values at the cell edge would have to be defined. Nevertheless, the resulting optimum CPICH power values can serve as a design guideline for HSDPA networks given different antenna configurations and may be particularly helpful for when MIMO networks are put in trial.

4.6. Summary

System-level simulations can serve as a flexible design and test tool for network performance evaluation, algorithm development, and deployment optimization. In this chapter, I presented a possible concept for a MIMO HSDPA network simulator, building upon the system-level model proposed in Chapter 3. Furthermore, four exemplary applications of the simulator were elaborated.

By means of a system-level simulation campaign, network performance predictions for various

deployment scenarios were obtained. I also shortly discussed the consequences of the D-TxAA double-stream operation onto the fairness in the network. On top of that I also proposed a robust RLC stream allocation algorithm and a content-aware scheduler improving the QoE. Both algorithms have been tested by extensive system-level simulations. Finally, optimum CPICH power allocations maximizing the HSDPA link quality for many different network setups have been evaluated.

Although fairly general in its concept, the system-level simulator could benefit significantly from a more structured implementation. In fact, developing a software of this extend in MATLAB is in general quite demanding because the Integrated Development Environment (IDE) is not well suited for such a task. Recently, however, MATLAB introduced object-orientated language extensions providing more flexibility for larger projects. If the simulator were structured according to these new possibilities, extensions to the core functionality would be much easier to implement.

Regarding the channel modeling in the network context, two assumptions worth researching shall be commented. At the moment, the utilized channel model is based on a constant PDP, for example according to the ITU channel profile. However, measurements show that the delay spread becomes smaller with shorter distance to the NodeB. This behavior is currently not represented and would require more sophisticated channel models as well as a refined representation of the equivalent fading parameters. In this context, also a better understanding of the outdoor-to-indoor MIMO channel would help to predict the network performance more realistically. Also refined possibilities in antenna deployment optimization, 3-D antenna gain patterns would have to be implemented. Moreover, it would be of great scientific interest to more rigorously define and assess the connection of classical performance metrics like throughput with fairness. In particular, modern MU optimized transmission systems have to put more focus on fairness criteria. To give better planing guidelines to the network operators, the system-level optimizations should incorporate cell-edge target constraints because usually certain QoS requirements have to be met. In terms of the physical layer investigations in the network context, it would also be very interesting to assess potential performance gains due to MU stream allocation, that is, serving two users simultaneously by means of SDMA [132]. For the content-aware scheduler, future research would have to put focus on how to incorporate the PF user utility function. It would also be of interest to investigate how to extend the applicability of the proposed scheduler to the multi-stream D-TxAA transmission mode. Finally, a full analytical modeling of the CPICH power influence on the system performance would be of great interest. This would allow to utilize convex optimization theory to develop dynamic allocation algorithms.

From a theoretical point of view, the definition and the evaluation of the *cell-capacity* would be of great importance. So far, no theoretical results can be used as a capacity metric to compare against the obtained system-level results. Appendix A.8 lists some initial ideas in this context, but detailed knowledge about this topic is needed to understand the fundamental performance limits of any scheduler and to define and compare against the *optimum network*.

At last, let me point out that a validation of a system-level simulator is in general very demanding. Usually, link-level simulators are not designed to include inter-cell and possibly inter-technology interference necessary. For future mobile networks, it thus would be beneficial if the underlying link-level simulator used to derive parts of the physical-layer abstraction can be utilized to simulate certain network test-scenarios against which the system-level simulator can be validated. In the scope of this work, at least a validation against the mobilkom austria AG trial data was performed in Appendix A.13, showing a good match. However, with a set of test-simulation setups a much more comprehensive validation would be possible.

Chapter 5.

Multi-User MMSE Equalization for MIMO-Enhanced HSDPA

The structure will automatically provide the pattern for the action which follows.

(Donald Curtis)

INTERFERENCE is said to be the most important performance limiting factor of modern cellular communication systems. This especially holds true for WCDMA networks, where frequency selectivity in the downlink channel causes a loss in orthogonality between the utilized spreading codes and imposes restrictive throughput constraints. This issue has already been identified in Chapter 3 for the development of the link-quality model, as well as in the simulation results in Chapter 4. However, besides the unavoidable interference caused by spreading code crosstalk, the question arises whether there exist possibilities to exploit structural properties in the interference for MIMO HSDPA.

The information theoretic principles for this kind of interference problem are represented by the MIMO broadcast channel [133, 134], which is related to the MIMO multiple-access channel in the uplink [135]. Although the capacity regions in case of fading channels are not known yet, all of the results so far indicate the need for interference mitigation to come close to the upper bound on the sum-capacity [136, 137].

Interference can be combated at the transmitter and/or the receiver side. In particular, in the downlink each receiver needs to detect a *single* desired signal, while experiencing two main types of interference. These are caused by the serving NodeB, called *intra-cell* interference, and by a few dominant neighboring NodeBs, called *inter-cell* interference. In the uplink, on the other hand, the base station receiver has to detect *all* desired users in the cell while having to suppress neighboring interference from many different sources.

When interference mitigation is performed at the transmitter, accurate channel state information from all users is needed [138]. The optimum solution known so far for the multi-user case is the utilization of Dirty Paper Coding (DPC) [139], which requires full channel and transmit signal knowledge at a central coordinating entity. A generalization of the classical DPC idea to the case of multiple base-stations has been made in [140]. This requires lots of signaling and feedback information exchange, which is typically not available in cellular context. Beamforming may serve as an approximation to the optimum interference mitigation at the transmitter, but faces some theoretical difficulties [141].

Handling the interference on the receiver side is a difficult job as well, especially in the multi-user case where classical approaches result in complex receiver structures [142–144]. Moreover, also theoretically it is not known to which extend receiver cooperation is needed to achieve a close to capacity performance, apart from the fact that it is not known what the optimum receiver

cooperation really looks like [145, 146]. More practical investigations on this subject are also conducted by 3GPP [147], but so far none of these recommendations have been implemented. In LTE, the X2-interface allows for more flexibility regarding the interference management, which will be exploited in practical implementations [148]. Given the limited battery capabilities of today's handsets, complexity is also an important issue [149]. A good overview over different practical interference situations together with some well known solutions for them can be found in [150].

Coming back to MIMO HSDPA systems, the classical MMSE equalizers recommended by 3GPP do not take any special knowledge of the interference structure into account [151–153]. The only possibility to include some knowledge about the interference structure into these approaches would be to estimate the noise covariance matrix in a way that reflects the interference structure. However, noise covariance estimation is usually performed very coarsly, if not at all treated as white to obtain simpler algorithms due to complexity arguments. Also the equalizer utilized for the simulations in Chapter 4 does not consider these effects. In [153], MU interference terms are considered but the authors investigated a non-standard conform pre-coding scheme and the proposed equalizer works on symbol-level as opposed to the chip-level based receiver presented here. Moreover, no pilot interference structure is taken into account. The D-TxAA MIMO HSDPA operation however implies a spatial structure of the intra-cell interference due to its pre-coding. If the channel quality is low, thus only one stream is supported, the according transmission mode is TxAA,[1] which is also the supported mode when the UE has only one receive antenna available. In case multi-user scheduling for TxAA users takes place, the spatial structure can be exploited to achieve a higher throughput. The same argument also holds for the D-TxAA operation, however, the spatial structure does not allow directly for an exploitation because all DoFs have already been utilized, as described in Theorem 3.1.[2] Nevertheless, since multi-user scheduling when D-TxAA is currently active for the transmission is not very promising to deliver higher spectral efficiencies in the cell [33, 42], the optimization of the receiver structure to take advantage of the knowledge about the spatial interference structure is very important.

5.1. System Model

Figure 5.1 shows the TxAA transmission scheme for one receive antenna, when U users are simultaneously served. In TxAA HSDPA there is only one stream active for every user. Let me thus define the spread and scrambled chip stream of user u at time instant i as

$$\tilde{\mathbf{x}}_i^{(u)} \triangleq \begin{bmatrix} x_i^{(u)} & \cdots & x_{i-L_\mathrm{h}-L_\mathrm{f}+2}^{(u)} \end{bmatrix}^\mathrm{T}, \tag{5.1}$$

which corresponds to the *stacked* transmit chip vector in Chapter 3. For sake of notational simplicity, I omitted the base-station or sector index b in this chapter. The statements and derivations

---

[1]TxAA has been introduced already with UMTS in 1999. In contrast to the double stream operation of MIMO HSDPA, TxAA allows for the same multi-user scheduling techniques as in the classical SISO HSDPA case. For the single-antenna operation, multi-user scheduling—also called *multi-code* scheduling—is well suited to work optimally in terms of the sum-rate throughput and the short-term fairness tradeoff [154]. Future generation mobile networks implicitly build on similar concepts, for example LTE allows scheduling in the time-frequency domain to achieve higher average spectral efficiencies in the cell [155]. Also note that the TxAA scheme allows for an arbitrary number of receive antennas at the UE.

[2]Note that this holds because of the quantized pre-coding codebook of 3GPP [6], but would not necessarily be the case if a different codebook would be used.
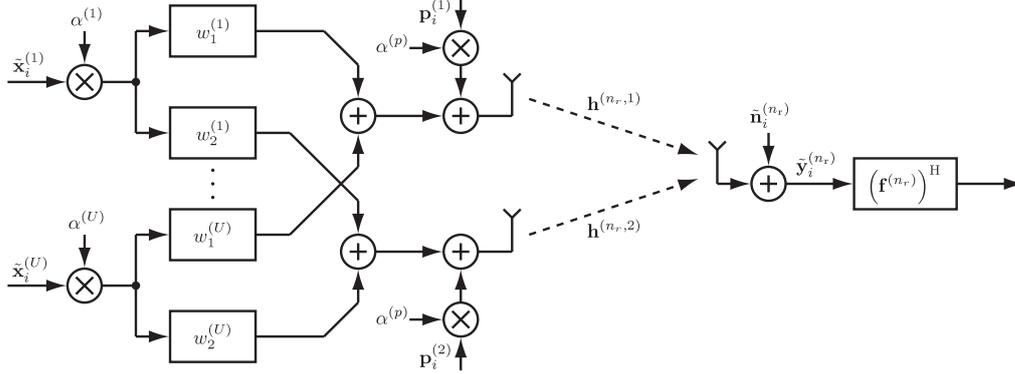
Figure 5.1.: Multi-user transmission in TxAA, for a total number U of simultaneously served users. The pre-coding is conducted individually for every user. At the receiver, only one receive antenna is depicted, although the scheme allows for an arbitrary number of receive antennas.

presented also only take the intra-cell interference components explicitly into account—in contrast to Chapter 3—as there is no need to complicate the mathematical notation unnecessarily. The vector $\tilde{\mathbf{x}}_i^{(u)}$ contains the $L_{\mathrm{h}} + L_{\mathrm{f}} - 1$ most recent transmitted chips. This notation serves to represent the convolution of the transmit signal and the frequency selective MIMO channel in vector matrix notation. Furthermore, note that this chip stream contains the sum of all utilized spreading sequences for user u, thus the potential multi-code utilization of HSDPA is also modeled. Without loss of generality, I assume that the energy of the chip stream $\tilde{\mathbf{x}}_i^{(u)}$ of each user u is normalized to one

$$\left(\sigma_x^{(u)}\right)^2 \equiv \sigma_x^2 = 1, \quad u = 1, \ldots, U. \tag{5.2}$$

Thus, by multiplying $\tilde{\mathbf{x}}_i^{(u)}$ with a factor $\alpha^{(u)}$, the base-station can allocate a certain amount of transmit power to each served user. After the power allocation, the chip streams are weighted by the user-dependent complex pre-coding coefficients $w_1^{(u)}$ and $w_2^{(u)}$ at the first and second transmit antenna, respectively. This has already been explained in Chapter 2, as well as in Appendix A.2. However, the slightly changed notation will be useful for the derivation of the *pre-coding state estimator*, as will be explained later in this chapter. The modeling in this chapter holds for arbitrary pre-coding weights, although the 3GPP recommendation is strongly quantized, see Appendix A.2. The weighted chip streams of all users are then added to the sequences $\alpha^{(\mathrm{p})}\mathbf{p}_i^{(1)}$ and $\alpha^{(\mathrm{p})}\mathbf{p}_i^{(2)}$, representing the sum of all channels that are transmitted without pre-coding, that is, the CPICH, the HS-SCCHs, and other signaling channels—to which I will refer to as non-data channels. Note that this system model represents the signaling channels correctly, in contrast to the description in Section 3.3.5.

The frequency selective channel between the n_{t}-th transmit and the n_{r}-th receive antenna in Figure 5.1 is represented by the vector $\mathbf{h}^{(n_{\mathrm{r}}, n_{\mathrm{t}})}$, $n_{\mathrm{t}} = 1, 2$, composed of the taps of the channel. If the non-data channels $\alpha^{(\mathrm{p})}\mathbf{p}_i^{(1)}$ and $\alpha^{(\mathrm{p})}\mathbf{p}_i^{(2)}$ are neglected for the moment—they will be included for the main derivation again—the multi-user transmission of Figure 5.1 can be represented by U virtual antennas, one for each active user, as illustrated in Figure 5.2.

The resulting equivalent—also called *virtual*—channels between user $u = 1, \ldots, U$ and receive
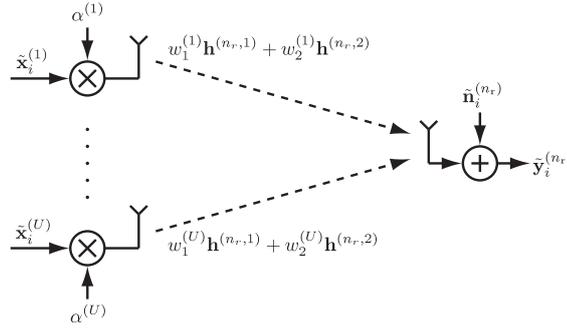
Figure 5.2.: Equivalent representation of the multi-user TxAA transmission, showing U virtual antennas and U virtual channels.

antenna $n_{\mathrm{r}} = 1, \dots, N_{\mathrm{R}}$ are then given by

$$w_1^{(u)} \mathbf{h}^{(n_{\mathrm{r}},1)} + w_2^{(u)} \mathbf{h}^{(n_{\mathrm{r}},2)}. \tag{5.3}$$

From this description it can be seen that the intra-cell interference caused by other users and observed by the desired user u can be treated like being transmitted over up to $U - 1$ different channels. This somehow represents a Single-Input Multiple-Output (SIMO) multiple access channel, instead of a MIMO broadcast channel. Of course, if two users utilize the same pre-coding, their channels cannot be distinguished anymore. The classical MMSE approach however would be determined only by the pre-coding weights $w_1^{(u)}$ and $w_2^{(u)}$ and does not consider the structure of the interference. Thus, the degraded transmission scheme of TxAA imposes an interference situation which cannot be handled well by the classical MMSE equalizer that is only matched to the channel of the desired user. This is in contrast to the SISO HSDPA case, where due to the lack of pre-coding the interference of simultaneously served users is transmitted over the same channel as the one of the desired user. Thus, equalization of the desired user's signal also equalizes the signal of the simultaneously served users.

For the following evaluations, let me define the $L_{\mathrm{f}} \times (L_{\mathrm{h}} + L_{\mathrm{f}} - 1)$ dimensional band matrix, modeling the channel between the n_{t}-th transmit and the n_{r}-th receive antenna as

$$\mathbf{H}^{(n_{\mathrm{r}},n_{\mathrm{t}})} = \begin{bmatrix} h_0^{(n_{\mathrm{r}},n_{\mathrm{t}})} & \cdots & h_{L_{\mathrm{h}}-1}^{(n_{\mathrm{r}},n_{\mathrm{t}})} & 0 \\ \ddots & & \ddots & \\ 0 & h_0^{(n_{\mathrm{r}},n_{\mathrm{t}})} & \cdots & h_{L_{\mathrm{h}}-1}^{(n_{\mathrm{r}},n_{\mathrm{t}})} \end{bmatrix}. \tag{5.4}$$

The full frequency selective MIMO channel can then be modeled by a block matrix $\mathbf{H}$ consisting of $N_{\mathrm{R}} \times N_{\mathrm{T}}$ band matrices,

$$\mathbf{H} = \begin{bmatrix} \mathbf{H}^{(1,1)} & \mathbf{H}^{(1,2)} \\ \vdots & \vdots \\ \mathbf{H}^{(N_{\mathrm{R}},1)} & \mathbf{H}^{(N_{\mathrm{R}},2)} \end{bmatrix}, \tag{5.5}$$

which explicitly shows the restriction of TxAA to utilize only $N_{\mathrm{T}} = 2$ transmit antennas [6]. By stacking the received signal vectors of all N_{R} receive antennas,

$$\tilde{\mathbf{y}}_i = \left[\left(\tilde{\mathbf{y}}_i^{(1)} \right)^{\mathrm{T}} \quad \cdots \quad \left(\tilde{\mathbf{y}}_i^{(N_{\mathrm{R}})} \right)^{\mathrm{T}} \right]^{\mathrm{T}}, \tag{5.6}$$

and by stacking the transmitted signal vectors of all U users and the auxiliary channel signal vectors $\mathbf{p}_i^{(1)}$ and $\mathbf{p}_i^{(2)}$,

$$\tilde{\mathbf{x}}_i = \left[\left(\tilde{\mathbf{x}}_i^{(1)} \right)^{\mathrm{T}} \quad \cdots \quad \left(\tilde{\mathbf{x}}_i^{(U)} \right)^{\mathrm{T}} \quad \left(\mathbf{p}_i^{(1)} \right)^{\mathrm{T}} \quad \left(\mathbf{p}_i^{(2)} \right)^{\mathrm{T}} \right]^{\mathrm{T}}, \tag{5.7}$$

the compact system description follows as

$$\tilde{\mathbf{y}}_i = \mathbf{H} \left(\mathbf{W}^{(\mathrm{MU})} \otimes \mathbf{I}_{L_{\mathrm{h}} + L_{\mathrm{f}} - 1} \right) \tilde{\mathbf{x}}_i + \tilde{\mathbf{n}}_i = \mathbf{H}_{\mathrm{w}} \tilde{\mathbf{x}}_i + \tilde{\mathbf{n}}_i. \tag{5.8}$$

In this formulation, $\tilde{\mathbf{n}}_i$ can be used to incorporate both the thermal noise and the inter-cell interference from other base-stations, which would allow the resulting receive filter some possibilities to combat the inter-cell interference as well.

The $2 \times (U + 2)$ dimensional matrix $\mathbf{W}^{(\mathrm{MU})}$ contains the pre-coding coefficients $w_1^{(u)}$ and $w_2^{(u)}$ of all users, as well as the power coefficients $\alpha^{(u)}$,

$$\mathbf{W}^{(\mathrm{MU})} \triangleq \begin{bmatrix} \alpha^{(1)} w_1^{(1)} & \cdots & \alpha^{(U)} w_1^{(U)} & \alpha^{(\mathrm{p})} & 0 \\ \alpha^{(1)} w_2^{(1)} & \cdots & \alpha^{(U)} w_2^{(U)} & 0 & \alpha^{(\mathrm{p})} \end{bmatrix}. \tag{5.9}$$

This matrix reflects the premise that non-data channels are not pre-coded, thus the two columns on the right side are specified solely by the single parameter $\alpha^{(\mathrm{p})}$ which controls the total power spent on these channels. In general, I also assume that the power available at the base-station is fully spent, thus the coefficients α are prone to a sum-power constraint,

$$\left\| \mathbf{W}^{(\mathrm{MU})} \right\|_{\mathrm{fro}}^2 = \sum_{u=1}^{U} \left(\alpha^{(u)} \right)^2 + 2 \left(\alpha^{(\mathrm{p})} \right)^2 = P, \tag{5.10}$$

with $\| \cdot \|_{\mathrm{fro}}$ denoting the Frobenius norm. Furthermore, I assume the power control to be completely included in the power coefficients $\alpha^{(u)}$ and $\alpha^{(\mathrm{p})}$ which imposes an additional power constraint on the pre-coding coefficients, $\| \mathbf{w}^{(u)} \|^2 = 1$ with $\mathbf{w}^{(u)} \triangleq [w_1^{(u)}, w_2^{(u)}]^{\mathrm{T}}$.

5.2. Intra-Cell Interference-Aware MMSE Equalization

Having the system model being specified, the resulting MMSE equalizer can be derived. Without loss of generality, I will assume that the transmit data sequence of user one has to be reconstructed. Accordingly, the MMSE equalizer coefficients can be calculated by minimizing the quadratic cost function [89]

$$J(\mathbf{f}) = \mathbb{E} \left\{ \left| \mathbf{f}^{\mathrm{H}} \tilde{\mathbf{y}}_i - x_{i-\tau}^{(1)} \right|^2 \right\}, \tag{5.11}$$

with τ again specifying the delay of the equalized signal, and fulfilling $\tau \geq L_{\mathrm{h}}$.[3] Similar to Chapter 3, I will assume perfect channel knowledge at the receiver side here.

The cost function minimizes the distance between the equalized chip stream and the transmitted chip stream in the Euclidean distance sense. In Equation (5.11), the vector $\mathbf{f}$ defines N_{R} equalization filters,

$$\mathbf{f} = \left[\left(\mathbf{f}^{(1)} \right)^{\mathrm{T}} \quad \cdots \quad \left(\mathbf{f}^{(N_{\mathrm{R}})} \right)^{\mathrm{T}} \right]^{\mathrm{T}}. \tag{5.12}$$

---

[3]See Chapter 3 for details on this constraint.

Each filter $\mathbf{f}^{(n_\mathrm{r})} = \left[f_0^{(n_\mathrm{r})} \quad \cdots \quad f_{L_\mathrm{f}-1}^{(n_\mathrm{r})} \right]$ has a length of L_f chips, similar to the equalizer derived in Chapter 3. Note that because of the definition of $\mathbf{f}$ and $\tilde{\mathbf{y}}_i$, the inner product $\mathbf{f}^\mathrm{H}\tilde{\mathbf{y}}_i$ can be implemented by summation of the outputs of the N_R equalization filters $\mathbf{f}^{(n_\mathrm{r})}$. This sum then yields the MMSE estimate of the transmitted chip sequence.

To obtain the optimum receive filter, the cost function $J(\mathbf{f})$ has to be minimized,

$$\mathbf{f}^{(\mathrm{opt})} \triangleq \arg \min_{\mathbf{f}} J(\mathbf{f}), \tag{5.13}$$

which, due to the design of the cost-function, is a convex non-constraint optimization problem [92, 156]. Accordingly, it can be solved by finding the point at which the gradient of the cost function is equal to zero,

$$\nabla J\left(\mathbf{f}^{(\mathrm{opt})}\right) \overset{!}{=} \mathbf{0}_{N_\mathrm{R} L_\mathrm{f}}, \tag{5.14}$$

with $\mathbf{0}_{N_\mathrm{R} L_\mathrm{f}}$ denoting a zero vector of length $N_\mathrm{R} L_\mathrm{f}$. Let me use the same definition of the complex derivative as in [157],[4]

$$z = x + jy \rightarrow \frac{\partial}{\partial z} = \frac{1}{2}\left(\frac{\partial}{\partial x} - j\frac{\partial}{\partial y} \right), \frac{\partial}{\partial z^*} = \frac{1}{2}\left(\frac{\partial}{\partial x} + j\frac{\partial}{\partial y} \right). \tag{5.15}$$

Then it can be shown that the gradient problem can be reformulated to

$$\nabla J(\mathbf{f}) = 2\frac{\partial}{\partial \mathbf{f}^*} J(\mathbf{f}). \tag{5.16}$$

By applying linearity of the expectation and the partial derivative operator, the gradient of the cost function can be shown to be

$$\frac{\partial}{\partial \mathbf{f}^*} J(\mathbf{f}) = \mathbb{E}\left\{ \frac{\partial}{\partial \mathbf{f}^*} \mathbf{f}^\mathrm{H}\tilde{\mathbf{y}}_i\tilde{\mathbf{y}}_i^\mathrm{H}\mathbf{f} - x_{i-\tau}^{(1)}\tilde{\mathbf{y}}_i^\mathrm{H}\mathbf{f} - \mathbf{f}^\mathrm{H}\tilde{\mathbf{y}}_i\left(x_{i-\tau}^{(1)} \right)^* + \left| x_{i-\tau}^{(1)} \right|^2 \right\}, \tag{5.17}$$

which becomes

$$\frac{\partial}{\partial \mathbf{f}^*} J(\mathbf{f}) = \mathbb{E}\left\{ \tilde{\mathbf{y}}_i\tilde{\mathbf{y}}_i^\mathrm{H}\mathbf{f} - \tilde{\mathbf{y}}_i\left(x_{i-\tau}^{(1)} \right)^* \right\}. \tag{5.18}$$

Inserting the input-output relation from Equation (5.8) and assuming uncorrelated data and noise samples, the derivative of the cost function can be further simplified to

$$\frac{\partial}{\partial \mathbf{f}^*} J(\mathbf{f}) = \left[\mathbf{H}_\mathrm{w}\mathbb{E}\left\{ \tilde{\mathbf{x}}_i\tilde{\mathbf{x}}_i^\mathrm{H} \right\}\mathbf{H}_\mathrm{w}^\mathrm{H} + \mathbb{E}\left\{ \tilde{\mathbf{n}}_i\tilde{\mathbf{n}}_i^\mathrm{H} \right\} \right]\mathbf{f} - \mathbf{H}_\mathrm{w}\mathbb{E}\left\{ \tilde{\mathbf{x}}_i\left(x_{i-\tau}^{(1)} \right)^* \right\}, \tag{5.19}$$

---

[4]Note that this definition also implies that

$$\frac{\partial z}{\partial z} = 1, \frac{\partial z}{\partial z^*} = \frac{\partial z^*}{\partial z} = 0,$$

for complex valued numbers z, as well as

$$\frac{\partial \mathbf{z}}{\partial \mathbf{z}} = \mathbf{I}, \frac{\partial \mathbf{z}}{\partial \mathbf{z}^*} = \frac{\partial \mathbf{z}^*}{\partial \mathbf{z}} = \mathbf{0}$$

for complex valued vectors $\mathbf{z}$. This definition extends the differentials to non-homomorphic functions in the complex numbers plane, where the Cauchy-Riemann equations do not hold anymore. A definition like this is necessary because most functions encountered in physical sciences and engineering are not analytic. In the mathematical literature, these relationships are often called *Wirtinger calculus* [158].

which by defining $\mathbf{R}_{xx} \triangleq \mathbb{E}\left\{\tilde{\mathbf{x}}_i \tilde{\mathbf{x}}_i^{\mathrm{H}}\right\}$ and $\mathbf{R}_{nn} \triangleq \mathbb{E}\left\{\tilde{\mathbf{n}}_i \tilde{\mathbf{n}}_i^{\mathrm{H}}\right\}$, as well as assuming the individual transmit chips to be uncorrelated,

$$\mathbb{E}\left\{\tilde{\mathbf{x}}_i \left(x_{i-\tau}^{(1)}\right)^*\right\} = \mathbb{E}\left\{\left|x_{i-\tau}^{(1)}\right|^2\right\} \mathbf{e}_\tau = \sigma_x^2 \mathbf{e}_\tau, \tag{5.20}$$

leads to

$$\frac{\partial J}{\partial \mathbf{f}^*} = \left(\mathbf{H}_{\mathrm{w}} \mathbf{R}_{xx} \mathbf{H}_{\mathrm{w}}^{\mathrm{H}} + \mathbf{R}_{nn}\right) \mathbf{f} - \sigma_x^2 \mathbf{H}_{\mathrm{w}} \mathbf{e}_\tau \overset{!}{=} \mathbf{0}. \tag{5.21}$$

The matrices $\mathbf{R}_{xx}$ and $\mathbf{R}_{nn}$ are the signal and noise covariance matrices, respectively, and the vector $\mathbf{e}_\tau$ is a zero vector of length $(U+2)(L_{\mathrm{h}} + L_{\mathrm{f}} - 1)$ with a single *one* at position τ. The equalizer coefficients for the data stream of the first user are therefore given by

$$\mathbf{f} = \sigma_x^2 \left(\mathbf{H}_{\mathrm{w}} \mathbf{R}_{xx} \mathbf{H}_{\mathrm{w}}^{\mathrm{H}} + \mathbf{R}_{nn}\right)^{-1} \mathbf{H}_{\mathrm{w}} \mathbf{e}_\tau. \tag{5.22}$$

If the transmitted data signals of the users are uncorrelated with equal powers σ_x^2, the covariance matrix $\mathbf{R}_{xx}$ becomes $\sigma_x^2 \mathbf{I}$, and if the noise vector $\tilde{\mathbf{n}}_i$ is assumed white with variance σ_n^2, the noise covariance matrix becomes $\sigma_n^2 \mathbf{I}$. As already mentioned, I will assume the transmit signal variance to be equal to one, because the individual transmit powers of the users are anyways determined by the power coefficients $\alpha^{(u)}$. The variance σ_n^2 on the other hand is specified by the thermal noise power and the sum interference power from the neighboring base-stations. Note that if the receiver shall ideally take the structure of the inter-cell interference into account, effort would have to be put into obtaining an accurate estimation of the covariance matrix $\mathbf{R}_{nn}$, which would not be a scaled identity matrix anymore.

Since this equalizer considers the interference of all users in the cell due to the full knowledge of the matrix $\mathbf{W}^{(\mathrm{MU})}$, it can be called *intra-cell interference aware MMSE equalizer*. The standard equalizer is a special case of this solution and neglects the interference structure imposed by the other users, which I will call Single-User (SU) equalizer in the following. It can be calculated from Equation (5.22) by utilizing the SU pre-coding weight matrix of rank one,

$$\mathbf{W}^{(\mathrm{SU})} = \begin{bmatrix} \alpha^{(1)} w_1^{(1)} \\ \alpha^{(1)} w_2^{(1)} \end{bmatrix} \mathbf{e}_1^{\mathrm{T}}, \tag{5.23}$$

instead of the multi-user matrix $\mathbf{W}^{(\mathrm{MU})}$. Here, $\mathbf{e}_1$ is a zero column-vector of length $U+2$ with a *one* at the first position. Note that if only a single user is receiving data in the cell both equalizers are very similar. The only difference is that the intra-cell interference aware equalizer also considers the interference generated by the non-data channels.

The structure of the derived linear equalizer would in principle also allow for an extension to decision-feedback receivers. However, if the interference caused by the other users is sought to be cancelled, their data has to be estimated and thus the computational complexity of the resulting receiver would be increased significantly. Furthermore, decision-feedback receivers suffer from impractical delay constraints due to the length of the spreading sequences in WCDMA systems as well as error propagation.

5.2.1. Interference Suppression Capability

Having derived the solution of the interference-aware MMSE equalizer, it is of interest to analytically assess its interference-suppression capabilities as well as its performance bounds. To

do so, I adapted the system-level link quality model introduced in Chapter 3 which is capable of describing the post-equalization and despreading SINR for arbitrary linear receivers in a potentially multi-stream closed loop MIMO Code-Division Multiple Access (CDMA) system. The remaining intra-cell interference after equalization—for a specific channel realization and pre-coding state—generated by the desired user and all other active users is explicitly given by

$$P^{\mathrm{intra}} = \sum_{\substack{m=0 \\ m \neq \tau}}^{L_{\mathrm{h}}+L_{\mathrm{f}}-2} \left| \mathbf{f}^{\mathrm{H}} \mathbf{h}_m^{(1)} \right|^2 + \sum_{u=2}^{U} \sum_{m=0}^{L_{\mathrm{h}}+L_{\mathrm{f}}-2} \left| \mathbf{f}^{\mathrm{H}} \mathbf{h}_m^{(u)} \right|^2, \tag{5.24}$$

where in reference to Equation (3.37) I set $N_{\mathrm{S}} = 1$ due to the restriction to the TxAA transmission mode, and the total transmission power per stream, $P^{(u,b_0)}/N_{\mathrm{S}}$ is now incorporated in the power coefficients $\alpha^{(u)}$. These furthermore are contained in the equivalent MIMO channel matrix columns $\mathbf{h}_m^{(u)}$ of the user dedicated channel matrix

$$\mathbf{H}^{(u)} = \mathbf{H} \left(\begin{bmatrix} \alpha^{(u)} w_1^{(u)} & \alpha^{(u)} w_2^{(u)} \end{bmatrix} \otimes \mathbf{I}_{L_{\mathrm{h}}+L_{\mathrm{f}}-1} \right), \tag{5.25}$$

where I assumed perfect channel and noise power knowledge at the receiver.

Equation (5.24) depends on the current realization of the pre-coding state, in particular the pre-coding choices of the interfering users. Thus to assess the average interference suppression capability of the proposed equalizer, I utilize the expected intra-cell interference[5] which for a certain number of active users in the cell becomes

$$\mathbb{E}_w \left\{ P^{\mathrm{intra}} \right\} = \underbrace{\sum_{\substack{m=0 \\ m \neq \tau}}^{L_{\mathrm{h}}+L_{\mathrm{f}}-2} \left| \mathbf{f}^{\mathrm{H}} \mathbf{h}_m^{(1)} \right|^2}_{f_{\mathrm{self}}} + \sum_{u=2}^{U} \underbrace{\mathbb{E}_w \left\{ \sum_{m=0}^{L_{\mathrm{h}}+L_{\mathrm{f}}-2} \left| \mathbf{f}^{\mathrm{H}} \mathbf{h}_m^{(u)} \right|^2 \right\}}_{f_{\mathrm{other}}}, \tag{5.26}$$

with f_{self} and f_{other} denoting the determinative factors for the self- and other-user intra-cell interference remaining after equalization, and $\mathbb{E}_w\{\cdot\}$ being the expectation with respect to the pre-coding coefficients w_1 and w_2 of the other users.

Utilizing the analytical description of the post-equalization intra-cell interference the interference suppression capabilities and the theoretical performance bounds of the proposed equalizer can be evaluated. Table 5.1 lists the simulation parameters I applied to assess the capability of the proposed equalizer to suppress the intra-cell interference caused due to the other active users in the cell. Figure 5.3(a) shows the performance in terms of the interference suppression capabilities, both for the self interference f_{self}, and the other-user interference f_{other}, assuming perfect knowledge of the cell's pre-coding state. Note that I normalized the two coefficients by the total received interference power, which since the channel—by assumption—is normalized to one, corresponds to dividing by the norm of the equalizer $\|\mathbf{f}\|$ and the total transmitted intra-cell power P.

It can be observed that the proposed equalizer is able to outperform the classical SU by significantly reducing the interference term f_{other} of the other users. The self interference term f_{self} on the other hand becomes larger around $5\,\mathrm{dB}$ E_{c}/N_0. As specified by the cost function in Equation (5.11) the interference aware equalizer minimizes the overall interference. Figure 5.3(a) thus illustrates that at higher E_{c}/N_0 the equalizer sacrifices self interference cancellation performance for the sake of a lower overall intra-cell interference.

---

[5]Note that this is a similar to the arguments used in Chapter 3 for the evaluation of the link-quality model.

Table 5.1.: Simulation parameters for the link-quality model examination of the interference suppression capabilities of the multi-user intra-cell interference aware MMSE equalizer.

Parameter	Value
fading model	improved Zheng model [8, 91]
receive antennas	$N_{\mathrm{R}} = 2$
pre-coding codebook	3GPP TxAA [6]
equalizer span	$L_{\mathrm{f}} = 40\,\mathrm{chips}$
equalizer delay	$\tau = 20\,\mathrm{chips}$
pre-codding delay	11 slots
UE speed	$3\,\mathrm{km/h}$
channel profile	ITU PedB [159]
active users	$U = 4$
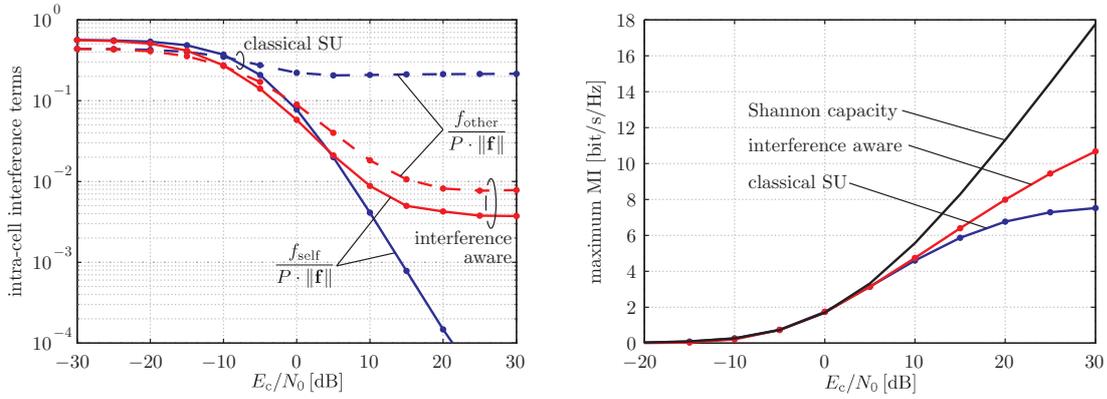
(a) Intra-cell interference terms f_{self} and f_{other} for the classical SU equalizer (blue) and the proposed interference-aware equalizer (red), assuming perfect knowledge of the cell's pre-coding state.

(b) Comparison of the maximum MI performance of the classical SU equalizer and the proposed interference-aware equalizer, assuming Gaussian post-equalization interference.

Figure 5.3.: Theoretical performance investigation in terms of the interference suppression capabilities and the maximum MI.

Based on these results, it is also possible to evaluate bounds for the spectral efficiency. With the expected intra-cell interference being given by Equation (5.24), and considering the desired signal power being proportional to $|\mathbf{f}^{\mathrm{H}}\mathbf{h}_{\tau}^{(u_0)}|^2$ [14], the equivalent downlink data transmission channel including the equalization can be represented as an SISO AWGN channel. The corresponding SINR thus is given by

$$\mathrm{SINR} = \frac{\mathrm{SF}\left|\mathbf{f}^{\mathrm{H}}\mathbf{h}_{\tau}^{(1)}\right|^2}{f_{\mathrm{self}} + f_{\mathrm{other}} + \|\mathbf{f}\|^2 N_0}, \tag{5.27}$$

when considering only intra-cell interference and with SF denoting the spreading factor of the HS-PDSCH. This corresponds to a single-cell scenario. Based on this SINR, the maximum MI can be evaluated as $\mathrm{MI} = \log_2\left(1 + \mathrm{SINR}\right)$, which denotes an upper bound if perfect channel

coding would by utilized. Note however, that this bound assumes a Gaussian distribution of the post-equalization interference, which in practice is not necessarily the case. Nevertheless, the so derived maximum MI can serve as a figure of merit to assess the performance gain achievable by the interference-aware equalizer. Figure 5.3(b) shows the maximum MI for the classical SU equalizer and the interference-aware equalizer together with the Shannon channel capacity of a $N_\mathrm{T} \times N_\mathrm{R} = 2 \times 2$ channel. It can be observed that the proposed equalizer offers significant potential performance gains in the higher E_c/N_0 region.

Moreover, in Appendix A.14 it is shown that under some coarse assumptions, the proposed interference-aware equalizer maximizes the SINR in Equation (5.27). Thus, the equalizer is the best linear filter for the intra-cell interference structure of the TxAA multi-user transmission.

5.2.2. Complexity

Given the solution of the intra-cell interference aware MMSE equalization in Equation (5.22), it is interesting to assess the additional complexity that is needed to compute the proposed filter when compared to the complexity of evaluating the classical SU equalizer.Assuming uncorrelated transmit sequences with constant power, thus implying $\mathbf{R}_{xx} = \sigma_x^2 \mathbf{I}$, the additional complexity can be evaluated by looking at the product $\mathbf{H}_\mathrm{w} \mathbf{R}_{xx} \mathbf{H}_\mathrm{w}^\mathrm{H} \propto \mathbf{H}_\mathrm{w} \mathbf{H}_\mathrm{w}^\mathrm{H}$ that is needed in the inverse part of $\mathbf{f}$ in Equation (5.22). By writing

$$\mathbf{H}_\mathrm{w} \mathbf{H}_\mathrm{w}^\mathrm{H} = \mathbf{H} \left[\mathbf{W}^{(\mathrm{MU})} \left(\mathbf{W}^{(\mathrm{MU})} \right)^\mathrm{H} \otimes \mathbf{I}_{L_\mathrm{h}+L_\mathrm{f}-1} \right] \mathbf{H}^\mathrm{H}, \qquad (5.28)$$

it can easily be seen that the additional cost of the proposed equalizer is only determined by the larger matrix multiplication of $\mathbf{W}^{(\mathrm{MU})} \left(\mathbf{W}^{(\mathrm{MU})} \right)^\mathrm{H}$ instead of $\mathbf{W}^{(\mathrm{SU})} \left(\mathbf{W}^{(\mathrm{SU})} \right)^\mathrm{H}$. In particular, the complexities of these two operation can be approximated by

$$\mathbf{W}^{(\mathrm{MU})} \left(\mathbf{W}^{(\mathrm{MU})} \right)^\mathrm{H} \sim \mathcal{O}\left\{ (U+2)^3 \right\}, \qquad (5.29)$$

$$\mathbf{W}^{(\mathrm{SU})} \left(\mathbf{W}^{(\mathrm{SU})} \right)^\mathrm{H} \sim \mathcal{O}\{ 2 \cdot 2 \}, \qquad (5.30)$$

if matrix multiplications are assumed to be of order $\mathcal{O}\{k^3\}$, with k being the matrix dimension for a square matrix. All the other matrix multiplications and the necessary inversion in Equation (5.22) keep the same complexity, thus the additional complexity imposed by the intra-cell interference aware MMSE equalizer can be evaluated to be proportional to $\mathcal{O}\left\{ (U+2)^3 - 4 \right\}$. The complexity of the matrix inverse, however, can be approximated to be of order $\mathcal{O}\left\{ (N_\mathrm{R} L_\mathrm{f})^3 \right\}$, and since U is typically much smaller than L_f in practical systems, the multiplication of the muti-user pre-coding matrix is negligible. Accordingly, the additional complexity needed for the consideration of the pre-coding state of the cell is very moderate.

5.3. The Cell Pre-Coding State

In TxAA HSDPA, the MIMO channel is estimated by utilizing the CPICH, similar to UMTS. To be able to calculate the receive filter for the HS-DSCH data channel, however, the UE needs to know at least (i) the power offset of the individual HS-PDSCHs compared to the power level of the CPICH, and (ii) the pre-coding coefficients that the base-station applied for the

transmission.[6] The power offset is signaled by higher layers [43], and the pre-coding coefficients of all simultaneous transmissions are signaled on the according HS-SCCHs [35, 41], where every active user has his own channel. This unfortunately makes things difficult for the proposed equalizer, because the HS-SCCHs are scrambled with user-specific scrambling sequences,[7] see also Chapter 2, thus making it impossible to monitor the pre-coding state of the other users active in the cell.

In order to overcome this problem, one can think of three different strategies that are possible:

 (i) change the signaling scheme in the HS-SCCH such that all active users know about the complete pre-coding state in the cell,

 (ii) include some training data in the HS-PDSCHs of the users to be able to estimate the pre-coding state, or

 (iii) blindly estimate the pre-coding state,

whereas (i) is an obvious solution that needs no further explanation. Thus, in the following I will shortly discuss a possible solution for (ii), but the main focus will be dedicated to the blind estimation (iii) because it can be implemented without changes in the current transmission standard.[8]

The principal estimation problem is the following. According to Figure 5.1, every active user can have his own pre-coding coefficient pair $\{w_1^{(u)}, w_2^{(u)}\}$ and his own power factor $\alpha^{(u)}$, where only the coefficients dedicated to the user himself are known. In addition, it is also not known how many users U are currently active. Estimation problems of this kind can be investigated within the framework of random set theory [143], leading to optimum Bayesian ML estimators. However, these solutions require a joint estimation of the data-sequences of all users and the pre-coding state, which is typically very complex and thus disadvantageous for battery powered mobile devices. Accordingly, I will restrict the efforts in this work onto classical approaches with moderate complexity.

As explained in Appendix A.2, according to [6], the pre-coding codebook that is utilized in practice is strongly quantized. In addition, several users may share the same pre-coding vector. Let me define the codebook of pre-coding vectors as

$$\mathcal{W} \triangleq \left\{ \mathbf{v}_1, \ldots, \mathbf{v}_{|\mathcal{W}|} \right\}, \mathbf{w}^{(u)} \in \mathcal{W}, \tag{5.31}$$

with $|\mathcal{W}|$ specifies the cardinality of the codebook. Furthermore, let me denote the set of users being served with the same pre-coding vector as $\mathcal{U}_k = \left\{ u : \mathbf{w}^{(u)} = \mathbf{v}_k \right\}$, with $k = 1, \ldots, |\mathcal{W}|$ denoting the codebook index of the corresponding pre-coding vector. Note that $\bigcup_{k=1}^{|\mathcal{W}|} \mathcal{U}_k$ does not necessarily have to equal $\mathcal{W}$, and that in case no user utilizes the pre-coding vector $\mathbf{v}_k$, the corresponding set is empty $\mathcal{U}_k = \emptyset$.

---

[6]This is due to the fact, that the channel estimation in UMTS and in HSDPA is based on the non pre-coded CPICH, see Chapter 4. Accordingly, at least the pre-coding coefficients for the desired user transmission are needed to evaluate the MMSE equalizer weights for the classical SU equalizer.

[7]The scrambling sequence in HSDPA is a function of the user identification number, known only to the base-station and the particular user.

[8]This is an important argument for nearly all algorithmic improvements for current mobile communication networks. A change in the standard would require huge efforts from both base-station and mobile-equipment vendors, as well as from the 3GPP standardization body, which makes non standard-compliant improvements nearly impossible to be implemented.

Definition 5.1. *The pre-coding state of an HSDPA cell is defined as*

$$\mathcal{P} \triangleq \left\{ \tilde{\alpha}^{(1)}, \dots, \tilde{\alpha}^{(k)}, \dots, \tilde{\alpha}^{(|\mathcal{W}|)}, \alpha^{(p)} \right\}, \tag{5.32}$$

where each $\tilde{\alpha}^{(k)}$ denotes the power coefficient utilized to transmit on a particular pre-coding vector $\mathbf{w}^{(k)}$,

$$\tilde{\alpha}^{(k)} = \sqrt{\sum_{u \in \mathcal{U}_k} \left(\alpha^{(u)} \right)^2}. \tag{5.33}$$

The coefficients $\alpha^{(u)}$ denote the power coefficient of every user $u = 1, \dots, U$, as utilized in Equation (5.9).

With this definition, the two options for the pre-coding state estimation, (ii) training sequences based estimation, and (iii) blind estimation can be defined and their performance assessed.

5.3.1. Training-Sequence-based Pre-Coding State Estimation

Before going into the details on the training sequence based estimator, let me note that the input-output relation in Equation (5.8) can be rewritten as

$$\tilde{\mathbf{y}}_i = \mathbf{H} \begin{bmatrix} \mathbf{X}_i \mathbf{D}_1 \\ \mathbf{X}_i \mathbf{D}_2 \end{bmatrix} \boldsymbol{\alpha} + \tilde{\mathbf{n}}_i, \tag{5.34}$$

with the matrices $\mathbf{D}_1$ and $\mathbf{D}_2$ containing the pre-coding coefficients of the active users,

$$\mathbf{D}_1 = \operatorname{diag} \left\{ w_1^{(1)}, \dots, w_1^{(U)}, 1, 0 \right\}, \tag{5.35}$$

$$\mathbf{D}_2 = \operatorname{diag} \left\{ w_2^{(1)}, \dots, w_2^{(U)}, 0, 1 \right\}, \tag{5.36}$$

and the matrix $\mathbf{X}_i$ is the re-arranged transmit vector $\tilde{\mathbf{x}}_i$,

$$\mathbf{X}_i = \begin{bmatrix} \tilde{\mathbf{x}}_i^{(1)} & \cdots & \tilde{\mathbf{x}}_i^{(U)} & \mathbf{p}_i^{(1)} & \mathbf{p}_i^{(2)} \end{bmatrix}. \tag{5.37}$$

Finally, the vector $\boldsymbol{\alpha}$ lists the utilized power coefficients in the cell,

$$\boldsymbol{\alpha} = \begin{bmatrix} \alpha^{(1)} & \cdots & \alpha^{(U)} & \alpha^{(\mathrm{p})} & \alpha^{(\mathrm{p})} \end{bmatrix}. \tag{5.38}$$

Considering the special structure of the problem in Equations (5.34) and (5.8), some redundancy can be observed. In particular, if two users u_1 and u_2 utilize the same pre-coding vector $\mathbf{w}^{(k)}$, the input-output relation for these two users can also be represented by one *combined* user u', utilizing $\mathbf{w}^{(k)}$ with

$$\alpha^{(u')} = \sqrt{\left(\alpha^{(u_1)} \right)^2 + \left(\alpha^{(u_2)} \right)^2} \tag{5.39}$$

as his effective power coefficient. This is in concordance with the pre-coding state of the cell, as given in Definition 5.1. Furthermore, note that I assumed the non-data channels at the two transmit antennas to deploy the same power coefficient $\alpha^{(\mathrm{p})}$.

Given these arguments, it is sufficient to estimate only the pre-coding state $\mathcal{P}$ in order to describe the whole pre-coding situation in the cell. For the interference-aware MMSE equalizer accordingly the knowledge of $\mathcal{P}$ is sufficient to be able to suppress the intra-cell interference caused by the multi-user data transmission.

Considering the definition of the pre-coding state $\mathcal{P}$ in Equation (5.32), the vector $\tilde{\boldsymbol{\alpha}} = \begin{bmatrix} \tilde{\alpha}^{(1)} & \cdots & \tilde{\alpha}^{(|\mathcal{W}|)} & \alpha^{(\mathrm{p})} \end{bmatrix}^{\mathrm{T}}$ has to be estimated. Let me define the estimation error accordingly as

$$C = \left\| \tilde{\boldsymbol{\alpha}} - \hat{\tilde{\boldsymbol{\alpha}}} \right\|_2^2, \tag{5.40}$$

with $\hat{\tilde{\boldsymbol{\alpha}}}$ denoting the estimate of $\tilde{\boldsymbol{\alpha}}$. In case that training data is available, for example at the beginning of each transmission frame in HSDPA, a possible estimator is given by the LS solution. The pre-coding codebook representing matrices can be set to

$$\tilde{\mathbf{D}}_1 \triangleq \mathrm{diag}\left\{ w_1^{(1)}, \ldots, w_1^{(|\mathcal{W}|)} \right\}, \tag{5.41}$$

$$\tilde{\mathbf{D}}_1 \triangleq \mathrm{diag}\left\{ w_2^{(1)}, \ldots, w_2^{(|\mathcal{W}|)} \right\}. \tag{5.42}$$

In addition, let me assume that the base-station provides orthogonal training sequences $\mathbf{t}^{(k)}$ for every pre-coding vector $\mathbf{w}^{(k)}$, which can be formed into the training matrix

$$\mathbf{S}_{\mathrm{T}} \triangleq \begin{bmatrix} \mathbf{t}^{(1)} & \cdots & \mathbf{t}^{(|\mathcal{W}|)} \end{bmatrix}. \tag{5.43}$$

Then the LS estimator of $\boldsymbol{\theta} = \begin{bmatrix} \tilde{\alpha}^{(1)} & \cdots & \tilde{\alpha}^{(|\mathcal{W}|)} \end{bmatrix}^{\mathrm{T}}$, not including $\alpha^{(\mathrm{p})}$, is given by [92]

$$\hat{\boldsymbol{\theta}}_{\mathrm{LS}} = \Re\left\{ \left(\mathbf{H} \begin{bmatrix} \mathbf{S}_{\mathrm{T}} \tilde{\mathbf{D}}_1 \\ \mathbf{S}_{\mathrm{T}} \tilde{\mathbf{D}}_2 \end{bmatrix} \right)^{\#} \tilde{\mathbf{y}}_i \right\}^{+}, \tag{5.44}$$

where the real-valued operator $\Re\{\cdot\}^{+}$ ensures that the coefficients are real valued and positive, even in the low SNR regime where the noise potentially causes non real-valued estimates. The coefficient $\alpha^{(\mathrm{p})}$ can be calculated by utilizing the sum power constraint in Equation (5.10). Accordingly, the augmented LS estimate of $\tilde{\boldsymbol{\alpha}}$ is given by

$$\hat{\tilde{\boldsymbol{\alpha}}}_{\mathrm{LS}} = \begin{bmatrix} \hat{\boldsymbol{\theta}}_{\mathrm{LS}}^{\mathrm{T}} & 1 - \hat{\boldsymbol{\theta}}_{\mathrm{LS}}^{\mathrm{T}} \hat{\boldsymbol{\theta}}_{\mathrm{LS}} \end{bmatrix}^{\mathrm{T}}. \tag{5.45}$$

5.3.2. Blind Pre-Coding State Estimation

Blind estimation is in general a quite challenging task, in particular in the multi-user context. Typical approaches treat the unknown inputs—in this case the unknown transmit data $\tilde{\mathbf{y}}_i$—as *nuisance parameters* that the estimator has to cope with in order to supply blind estimates of the parameters of interest.

The ML principle provides a systematic way for deducing the Minimum Variance Unbiased (MVU) estimator, maximizing the joint likelihood function $f_{\tilde{\mathbf{y}}}(\tilde{\mathbf{y}}; \boldsymbol{\alpha}, \tilde{\mathbf{x}})$ [160]. As discussed in [161, 162], there exist a number of possibilities to avoid the joint estimation of all parameters, in this case $\boldsymbol{\alpha}$ and $\tilde{\mathbf{x}}_i$. The *unconditional* or *stochastic* ML criterion models the vector of nuisance parameters as a random vector and maximizes the marginal of the likelihood function conditioned to $\tilde{\mathbf{x}}$,

$$f_{\tilde{\mathbf{y}}}(\tilde{\mathbf{y}}; \boldsymbol{\alpha}) = \mathbb{E}_{\tilde{\mathbf{x}}}\left\{ f_{\tilde{\mathbf{y}}|\tilde{\mathbf{x}}}(\tilde{\mathbf{y}}|\tilde{\mathbf{x}}; \boldsymbol{\alpha}) \right\}, \tag{5.46}$$

where $\mathbb{E}_{\tilde{\mathbf{x}}}\{\cdot\}$ stands for the expectation operator with respect to the transmit signal $\tilde{\mathbf{x}}$.

Unfortunately, the unconditional ML estimator is generally unknown, because the expectation with respect to $\tilde{\mathbf{x}}$ typically cannot be solved in closed form. This is also the case for this

particular problem. However, in the low SNR regime, the unconditional likelihood function $f_{\tilde{\mathbf{y}}}(\tilde{\mathbf{y}}; \boldsymbol{\alpha})$ becomes quadratic in the observation with independence of the statistical distribution of the nuisance parameters. This estimator class, however, is also generally difficult to solve and works only reasonably well in the low SNR regime [160].

This fact motivated research in the area of *second-order* estimators, for example the *conditional* ML criterion that models the nuisance parameters as deterministic unknowns and maximizes the compressed likelihood function $f_{\tilde{\mathbf{y}}}\left(\tilde{\mathbf{y}}; \boldsymbol{\alpha}, \hat{\tilde{\mathbf{x}}}\right)$ in which $\hat{\tilde{\mathbf{x}}}$ denotes the ML estimate of $\tilde{\mathbf{x}}$. Unfortunately, for the particular problem of estimating the pre-coding state of the cell, this estimator class cannot be utilized because it would require the matrix $\mathbf{H}_{\mathrm{w}}$ to be tall [162], which in the used signal model is not the case.

Another approach is the Gaussian ML estimator class which models the nuisance parameters as Gaussian random variables in order to obtain an analytical solution for the expectation in $\mathbb{E}_{\tilde{\mathbf{x}}}\left\{f_{\tilde{\mathbf{y}}|\tilde{\mathbf{x}}}(\tilde{\mathbf{y}}|\tilde{\mathbf{x}}; \boldsymbol{\alpha})\right\}$ [163]. This assumptions seems to fit naturally into the system-model because due to multi-code operation many different transmit chips are added up, likely resulting in a near Gaussian distribution of the receive signal.[9] Although there are also other approaches that could be utilized to blindly estimate $\boldsymbol{\alpha}$, for example [164], I decided in favor of this estimator class.

The Gaussian ML estimator for the pre-coding state of an HSDPA cell, is the one minimizing the nonlinear cost function

$$\Lambda_{\mathrm{GML}}(\boldsymbol{\alpha}) = \mathrm{tr}\left[\ln \mathbf{R}(\boldsymbol{\alpha}) + \mathbf{R}^{-1}(\boldsymbol{\alpha})\hat{\mathbf{R}}\right] = \ln \det\left[\mathbf{R}(\boldsymbol{\alpha})\right] + \mathrm{tr}\left[\mathbf{R}^{-1}(\boldsymbol{\alpha})\hat{\mathbf{R}}\right], \qquad (5.47)$$

with $\hat{\mathbf{R}} = \tilde{\mathbf{y}}_i\tilde{\mathbf{y}}_i^{\mathrm{H}}$ denoting the sample covariance matrix, and

$$\mathbf{R}(\boldsymbol{\alpha}) = \mathbf{H}_{\mathrm{w}}\mathbf{H}_{\mathrm{w}}^{\mathrm{H}} + \sigma_n^2\mathbf{I} \qquad (5.48)$$

being its expected value as a function of $\boldsymbol{\alpha}$. Note that I assumed Gaussian white noise with variance σ_n^2 here.

The direct application of this estimator would require the number of users U to be known for the estimation, which is not the case in this problem setting. To overcome this problem, let me point out that $\mathbf{W}^{(\mathrm{MU})}$ from Equation (5.9) can be rewritten as

$$\mathbf{W}^{(\mathrm{MU})} = \mathbf{W}\operatorname{diag}\boldsymbol{\alpha}, \qquad (5.49)$$

with $\mathbf{W}$ containing the same pre-coding coefficients as $\mathbf{W}^{(\mathrm{MU})}$, but without the $\alpha^{(u)}$ coefficients. Recalling that the goal is to estimate the pre-coding state $\mathcal{P}$, the matrix $\mathbf{W}$ can be replaced in the context of Equation (5.48) by

$$\tilde{\mathbf{W}} = \begin{bmatrix} \mathbf{w}^{(1)} & \cdots & \mathbf{w}^{(|\mathcal{W}|)} \end{bmatrix} \operatorname{diag}\left\{ \underbrace{\begin{bmatrix} \tilde{\alpha}^{(1)} & \cdots & \tilde{\alpha}^{(|\mathcal{W}|)} \end{bmatrix}^{\mathrm{T}}}_{\boldsymbol{\theta}} \right\}, \qquad (5.50)$$

thus leading to

$$\mathbf{R}(\boldsymbol{\theta}) = \mathbf{H}\left(\tilde{\mathbf{W}}\tilde{\mathbf{W}}^{\mathrm{H}} \otimes \mathbf{I}\right)\mathbf{H}^{\mathrm{H}} + \sigma_n^2\mathbf{I}, \qquad (5.51)$$

---

[9]For the interference power terms after equalization this assumption does not hold anymore, as shown in Chapter 3.

and the new associated cost-function $\tilde{\Lambda}_{\mathrm{GML}}(\boldsymbol{\theta}) = \mathrm{tr}\left[\ln \mathbf{R}(\boldsymbol{\theta}) + \mathbf{R}^{-1}(\boldsymbol{\theta})\,\hat{\mathbf{R}}\right]$. Please note that as in the training based estimation, $\alpha^{(\mathrm{p})}$ can be calculated from the sum power constraint in Equation (5.10).

The minimum of $\tilde{\Lambda}_{\mathrm{GML}}$ can for example be found by means of iterative or time-recursive scoring methods [157, 163], based on

$$\hat{\boldsymbol{\theta}}_{l+1} = \hat{\boldsymbol{\theta}}_l + \mathbf{J}_{\mathrm{GML}}^{-1}\left(\hat{\boldsymbol{\theta}}\right) \boldsymbol{\nabla}_{\mathrm{GML}}\left(\tilde{\mathbf{y}}; \hat{\boldsymbol{\theta}}\right), \tag{5.52}$$

with $\mathbf{J}_{\mathrm{GML}}^{-1}\left(\hat{\boldsymbol{\theta}}\right)$ and $\boldsymbol{\nabla}_{\mathrm{GML}}\left(\tilde{\mathbf{y}}; \hat{\boldsymbol{\theta}}\right)$ being the Fisher information matrix and the gradient respectively. Alternatively, any other known efficient optimization technique like for example Sequential Quadratic Programming (SQP) methods [165] can be used. Such convex optimization based techniques potentially offer large complexity gains if the underlying problem shows some form of sparsity which allows for a suitable factorization [156].

When utilizing the blind pre-coding state estimator, the overall complexity of the interference aware equalizer is of course increased. The computational complexity order of one step in the optimization process can be approximated by the complexity of evaluating the cost function, which turns out to be proportional to

$$2\left[\mathcal{O}\left\{N_{\mathrm{R}}L_{\mathrm{f}}\left(L_{\mathrm{h}} + L_{\mathrm{f}} - 1\right)^2 \left(U + 2\right) N_{\mathrm{T}}\right\} + \mathcal{O}\left\{(N_{\mathrm{R}}L_{\mathrm{f}})^2\right\} + \mathcal{O}\left\{(N_{\mathrm{R}}L_{\mathrm{f}})^3\right\}\right], \tag{5.53}$$

where I again assumed a matrix multiplication complexity order of $\mathcal{O}\{K^3\}$. If an optimization algorithm based on Newton iterations is utilized, the number of required iterations can also coarsely be bounded by $\log_2 \log_2 1/\varepsilon$ with ε specifying the desired accuracy [156]. In practice I observed a convergence of the utilized algorithm in around eight iterations. The blind pre-coding estimation thus increases the computational complexity much more significantly than the changes in the MMSE equalizer structure.

5.3.3. Estimator Performance

Figure 5.4 shows the Mean Squared Error (MSE) C of the two estimators for different E_{c}/N_0 values. The simulation parameters are the same as in Table 5.1, except that I simulated the performance for one and two receive antennas, respectively. For the LS estimation, I used Hadamard sequences of length 64 for the training. To refine the estimation, I furthermore took advantage of the knowledge that the coefficients $\tilde{\alpha}^{(k)}$ have to be real valued and strictly positive, as well as that the sum power constraint in Equation (5.10) cannot be exceeded. It can be observed in Figure 5.4 that the training based estimator works reasonably well from -20 dB E_{c}/N_0 on, and that the performance saturates at around 10 dB. The blind estimator on the other hand is not able to deliver similar results, and shows an operating range starting approximately at -10 dB E_{c}/N_0. For both estimator classes, the availability of a second receive antenna is beneficial for the pre-coding state estimation. However, for the blind pre-coding state estimator the gain is even more dramatic. Let me note that the (poor) performance of the blind estimator is still sufficient for the proposed equalizer, as will be shown in the next section.

5.4. Performance Evaluation

In order to assess the performance of the proposed equalizer in comparison to the classical SU equalizer, as well as to evaluate the influence of the pre-coding state estimation, I split the
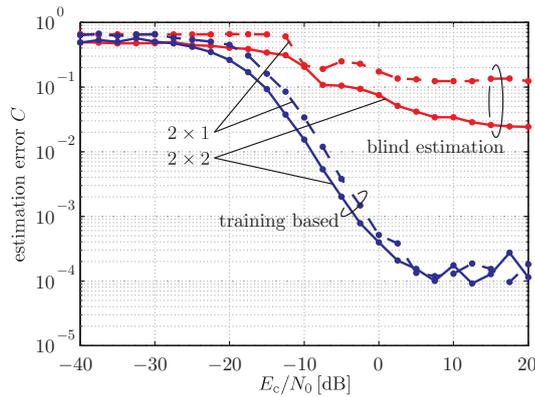
Figure 5.4.: Mean quadratic estimation error C—defined in Equation (5.40)—of the LS and the second-order blind pre-coding state estimators versus E_c/N_0.

simulations into two different parts: (i) physical-layer simulations for a fixed transmission setup of TxAA HSDPA, and (ii) system-level simulations with adaptive feedback and scheduling. Each simulation approach has a different focus, with the physical-layer simulations covering channel encoding and decoding, WCDMA processing, as well as channel estimation in detail. On the other hand, system-level simulations represent a whole HSDPA network, with adaptive feedback, scheduling and RRC algorithms. For the following results I also assumed that the channel and the noise power are perfectly known at the receiver.

5.4.1. Physical-Layer Simulation Results

I conducted physical-layer simulations utilizing a standard compliant WCDMA simulator [94]. The simulation assumptions in Table 5.2 correspond to a cell in which four users are receiving data simultaneously. User one is moving through the cell and obtains pre-coding coefficients as adaptively requested, according to the definition in Appendix A.2 [6]. The three interfering users are assumed to be stationary, thus their pre-coding coefficients and transmit power do not change. In the physical-layer simulations I furthermore assume that all users are always scheduled with the same CQI value, thus no link adaptation besides the pre-coding takes place.

The achieved data throughput of user one in a PedA and PedB environment is plotted in Figures 5.5(a) and 5.5(b), respectively. In both scenarios, the interference-aware MMSE equalizer with perfect knowledge of the pre-coding state significantly outperforms the SU MMSE equalizer. If the pre-coding state of the cell is blindly estimated, the performance of the MMSE equalizer nearly approaches the performance when $\mathcal{P}$ is perfectly known.

The gain in the PedB channel in Figure 5.5(b) is much larger than the gain in the PedA channel which has a much shorter maximum delay spread. This is caused by the larger loss of orthogonality in the PedB environment and the subsequently larger post-equalization interference. In the 2×1 case, the equalizer applying the blind pre-coding state estimation looses significantly compared to the equalizer with perfect knowledge of $\mathcal{P}$, which is a result of the considerably worse estimator performance when only one receive antenna is available, see Figure 5.4. The fact that the performance loss is greater in the PedB channel is due to its larger delay spread, which represents a more challenging environment for the equalizer making it more sensitive to estimation errors in the pre-coding state.

Table 5.2.: Simulation parameters for the physical-layer simulation performance assessment of the interference-aware MMSE equalizer.

Parameter	Value
active users U	4, capability class 6
desired user CQI	13
interfering HS-PDSCH $E_\mathrm{c}/I_\mathrm{or}$	$[-6, -8, -10]\,\mathrm{dB}$
interfering user CQIs	$[16, 11, 8]$
interfering user pre-coding	$[1, \frac{1}{\sqrt{2}}(1-j)], [1, \frac{1}{\sqrt{2}}(-1+j)], [1, \frac{1}{\sqrt{2}}(-1-j)]$
pre-coding codebook	3GPP TxAA [6]
CPICH $E_\mathrm{c}/I_\mathrm{or}$	$-10\,\mathrm{dB}$
other non-data channel $E_\mathrm{c}/I_\mathrm{or}$	$-12\,\mathrm{dB}$
UE speed	$3\,\mathrm{km/h}$
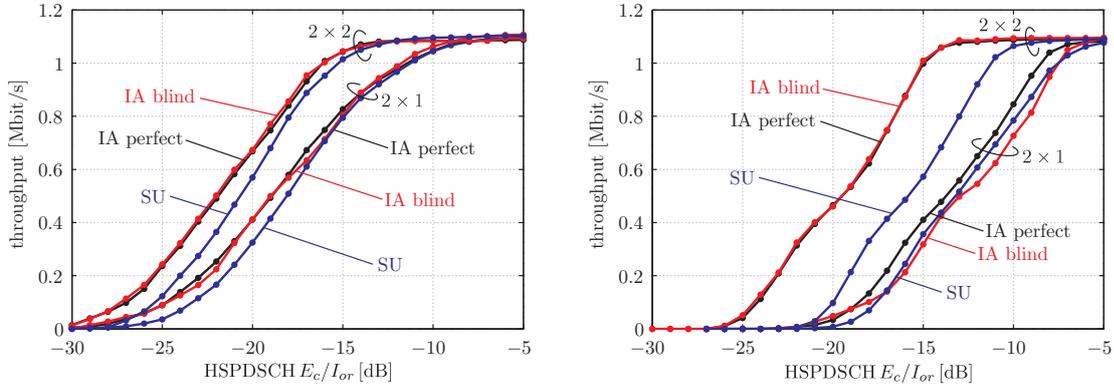
(a) Physical-layer throughput of the desired user in a spatially uncorrelated ITU PedA channel at CQI 13, corresponding to a maximum throughput of 1.14 Mbit/s.

(b) Physical-layer throughput of the desired user in a spatially uncorrelated ITU PedB channel at CQI 13, corresponding to a maximum throughput of 1.14 Mbit/s.

Figure 5.5.: Physical-layer simulation results. The interference-aware equalizer is denoted *IA*.

For larger number of receive antennas, the simulation results show larger performance gains. Especially in Figure 5.5(b), the pre-coding state estimation becomes significantly better in the 2×2 case, thus closing the gap to the throughput performance of the equalizer utilizing perfect knowledge of $\mathcal{P}$. The interference-aware MMSE equalizer can thus effectively utilize the spatial information to suppress the interfering signals. The largest performance increase of the proposed MMSE equalizer was found for the 2×2 PedB environment with $4\,\mathrm{dB}$.

5.4.2. System-Level Simulation Results

To assess the performance on network level, I also conducted a set of system-level simulations with the simulator as described in Chapter 4 [13, 14]. The simulation assumptions in Table 5.3 correspond to a 19 site scenario with a homogeneous network load in which the multi-code scheduler serves four active users simultaneously. All 25 simulated users are moving through the

Table 5.3.: Simulation parameters for the system-level simulation performance assessment of the interference-aware MMSE equalizer.

Parameter	Value
simultaneously active users U	4, capability class 10
transmitter frequency	1.9 GHz
base-station distance	1000 m
total power available at Node-B	20 W
power of non-data channels	2 W
macro-scale pathloss model	urban micro [112]
scheduler	Round Robin
cell deployment	19 cells, layout type I [93]
pre-coding codebook	3GPP TxAA [6]
equalizer span	40 chips
feedback delay	11 slots
UE speed	3 km/h, random direction
simulation time	25 000 slots, each 2/3 ms

(a) The ecdfs of the post equalization and despreading SINR of the HS-DSCH for ITU PedA and PedB channels, as observed on network level.

(b) Average system-level sector throughput results for ITU PedA and PedB environments.
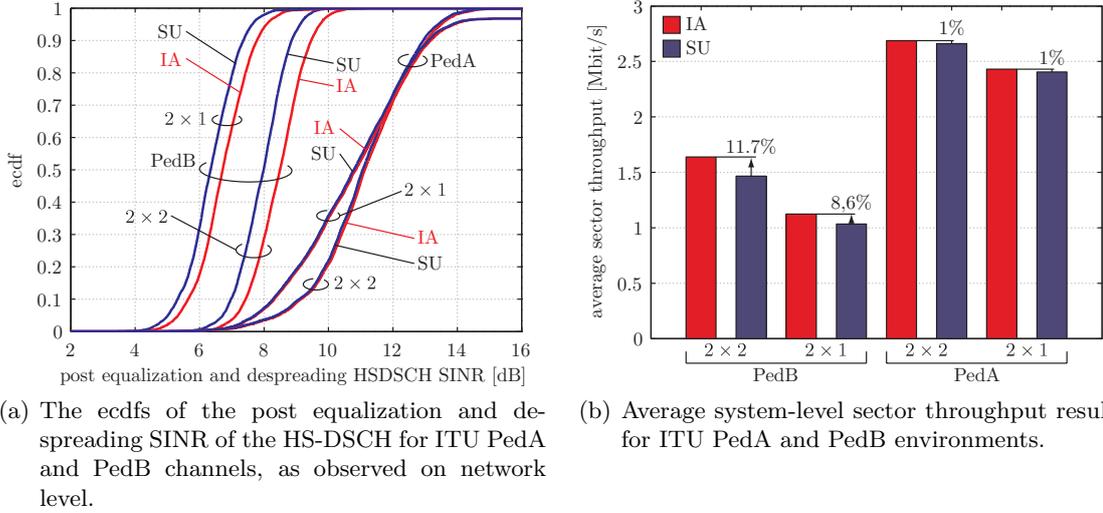
Figure 5.6.: System-level simulation results. The interference-aware equalizer is denoted *IA*.

cell with random directions, adaptively reporting their CQI and pre-coding feedback according to their capability class [7]. The feedback delay was set to eleven slots.

The distributions of the SINR for the PedA and PedB channel, averaged over all active users in the cell are plotted in Figure 5.6(a). It can be observed that the interference aware MU MMSE equalizer is able to deliver significantly higher SINRs for PedB channels. In the PedA environment, the gain is negligible.

Figure 5.6(b) shows the average sector throughput comparison. The interference-aware MU MMSE equalizer outperforms the classical SU MMSE equalizer significantly, with remarkable

gains in the PedB environment of up to 11.7 %. Similar to the physical-layer simulation results, for both channels the equalizer is able to utilize the advantage of multiple receive antennas, in this case the 2×2 MIMO channel, to advance the pre-coding state estimation. Thus, the throughput performance is also higher than the one of the 2×1 single antenna receiver case.

5.5. Summary

In this chapter I proposed and investigated a MU interference-aware MMSE receiver with a blind cell pre-coding state estimator. The developed structure is an extension of the classical SU MMSE equalizer that takes the pre-coded intra-cell interference into account. This allows for achieving significant gains in the throughput performance.

Future research on this receiver would have to include a cancellation of the synchronization channel which has been shown to have a great impact on the performance [16]. Furthermore, the proposed interference-aware receiver only takes the intra-cell interference into account. However, for a close-to-optimum performance also the inter-cell interference should be mitigated. This would require an even more detailed model representing the pre-coding of the neighboring cells in a suitable way. Let me point out that also the proposed cell-pre-coding-state estimator offers room for further research. By a closer investigation of the underlying blind estimation principle—maybe by a low-complexity approximation of a random set theory based approach—and careful design of the utilized optimization algorithm, higher estimation accuracy as well as probably a lower complexity might be achieved.

In the current state, the proposed receiver structure, however, offers a possibility to achieve significant throughput gains in channels with larger delay spread by only moderately increasing the computational complexity.

Chapter 6.

Conclusions

C OMMUNICATION networks represent one of the driving forces behind the development of our modern information society. In particular, wireless networks have proven to enable many data-driven services which we take for granted today.

The wireless link, however, is affected by constraints on the available bandwidth, the maximum allowed transmission power, and deployment confinements of the necessary equipment. Accordingly, modern cellular networks have to exploit the given resources as efficient as possible, utilizing physical-layer processing techniques with high spectral efficiencies, but also optimizing network-based multi-user algorithms.

Unfortunately, research in the field focuses strongly on the individual link, but often neglects the implications when the proposed techniques are employed in a multi-user, multi-base-station context. Network-based algorithms can for example have a significant impact on the channel statistics, but also other procedures like HARQ retransmissions, admission control, and resource allocation protocols heavily affect the individual link. The upcoming network generations include a MAC controlled physical-layer with potential cross-layer optimizations that have to be investigated taking the whole system into account.

System-level modeling and simulation provide such a possibility to investigate and assess many of the requirements and performance implications of communication networks. The main contribution of this thesis thus is the development of a suitable system-model description of MIMO HSDPA networks and the subsequent application of this model to a set of optimizations, both on the network as well as on the individual links.

Contributions of this Thesis

This thesis provides many insights and novel developments, both in the field of system-level modeling and in the optimization of the investigated MIMO HSDPA network.

The proposed *link-quality model* provides a very flexible and accurate analytical description of the MIMO HSDPA link-quality in the network context that was not available before. Utilizing an *equivalent fading parameter structure* the computational complexity of the model is vastly reduced compared to a full physical-layer simulation and thus allows the simulation of large networks. Together with the proposed *link-performance model* which exploits *slot-based sampling* of the link-quality parameters, a comprehensive system-level description of MIMO HSDPA networks was created. The novel *training method* of the link-performance model furthermore allows for an

increased accuracy in the BLER prediction. The flexibility and the accuracy of the model also led to its implementation in the Nokia Siemens Networks (NSN) system-level simulator MoRSE.

Based on the developed model, a *flexible system-level simulator* was programmed, suitable for performance analysis and algorithm testing including the physical- and the MAC-layer. The derived *network performance prediction* results are very valuable for network planning and investment decisions. For the overall network performance, RLC algorithms play an crucial role. The developed *RLC stream number decision algorithm* is shown to be robust against UE CQI reporting inaccuracies, for example due to a small channel coherence time. It allows the network operator to allocate the MIMO resources and thus take control of the interference situation in the cell. Similarly, the proposed *content-aware MAC-hs scheduler* is able to increase the QoE for video-streaming services in HSDPA networks. The concept can also be applied to other services worth prioritizing. Moreover, this cross-layer scheduling approach strongly improves the flexibility compared to available algorithms operating in the physical-layer or in the MAC-layer only.

This thesis also presents advances for the network operation. An HSDPA link-quality optimizing *CPICH power allocation* is presented. It is shown that careful adjustment of the pilot power improves the operation of wireless cellular networks. Accordingly, the presented results are very helpful for MIMO HSDPA field trials or for the optimization of currently deployed HSDPA cell clusters.

As already mentioned, the individual link is also affected by the network behavior. In particular, the interference structure has to be considered in order to derive optimum receiver structures. The proposed *multi-user interference-aware MMSE equalizer* offers large performance gain in channels with larger delay spread. Such channels impose a low spreading code orthogonality which can be regained with the proposed equalizer at only a moderately increased computational complexity. The required *blind pre-coding state estimator* also opens ways for even more sophisticated exploitations of the knowledge about the interference structure in the cell.

Limits of the Work; Future Research

Despite the efforts and care taken during the work on the presented research topics, some remarks regarding the limitations have to be made. One of the most constricting assumptions in the proposed system-level model is that only linear receivers can be accurately represented. This excludes for example SIC and ML based structures that have got more attention recently. In order to incorporate such receiver structures in the system-level model, significant changes in the link-quality and in the link-performance model are necessary. Recent research has started to investigate the implications of ML receivers on the link-performance model, but so far no complete system-level model is available.

Furthermore, another critical point is the behavior of the signaling channels and their modeling in the system-level simulator. Data transmission on the signaling channels is crucial for the operation of any network, however, they are only roughly modeled at the moment. Additionally, in system-level simulations a separate model of the signaling channels would lead to a more realistic representation of the influence on the overall network performance and the implications on RLC algorithms. An accurate representation of the signaling is also advantageous for the development of network equipment.

The proposed model would also benefit from a more detailed investigation of the Doppler effect and its influence on the equivalent fading parameters and the requirements for the slot-based sampling in the link-performance model. It has to be noted, though, that HSDPA is mainly used

in static scenarios which is already well covered by the presented model. Nevertheless, future generation networks may very likely provide service in high-speed transportation like trains.

Finally, I would like to point out that validation is a crucial point in the design of a system-level model. Exhaustive validation of this very complex system-level simulator is impossible, however, standardized test-scenarios that can be simulated in a link-level and a system-level simulator would simplify matters. For MIMO HSDPA this unfortunately was not possible due to the restrictions of the utilized link-level simulator. However, these ideas will be included in the system-level research on LTE in which I am currently involved [166, 167].

Lessons Learned

The research and work conducted in this thesis were very interesting and challenging and led me to a number of insights:

- A structured approach for the research and the necessary programming work is crucial for timely progress. Nowadays, no researcher works on his own but rather is part of a team of colleagues all over the world. Only when the research activities are well structured and documented right from the start, the full potential of collaborations can be exploited.

- The success of a model is not only determined by its scientific appeal and accuracy, but also by its simplicity. Models are not only used by their designer but also by many others. Thus simpler models are much easier to explain and understand, and consequently their acceptance in the scientific community is usually larger. However—as Albert Einstein already pointed out—one should not forget the following:

  "*Make everything as simple as possible, but not simpler.*"

- Validation is the foundation of scientific research. Without meaningful ways of validation, even the best model cannot prove its value. How can one otherwise be sure that one is modeling what one wants to model? Accordingly, means for validation should be kept in mind already during the design of the model to allow for efficient testing.

- Modern wireless communication systems do not allow for an individual treatment of the involved layers anymore. The merging of the lower layers allows cross-layer optimization, but on the other hand makes a separate design of every layer impossible. This, however, requires a much broader understanding of the whole network, which is particularly important to be able to conduct system-level research.

Will we need System-Level Research in the Future?

With growing intelligence of the physical-layer nodes, LTE shifts the RNC algorithms into the *eNodeBs* and enables inter-NodeB communication. This opens a number of possibilities for network optimization and requires detailed investigation of algorithms on large cellular network scale. Without ways to test and predict the functionality of those new algorithms, no meaningful performance comparison can be made. Accordingly, system-level research will even become more important for the next generations of wireless networks.

Appendix A.

Additional Material

MY intention when writing this thesis was to keep the main chapters as precise and structured as possible, thus some of the related information that would have disturbed and/or complicated the reading have been left out on purpose. Some of the details given here however are needed for arranging and conducting the simulations, respectively the understanding of some implementation specific conclusions. Thus I include short discussions about the relevant points in this appendix.

A.1. Standardization, Current Deployment of HSDPA

The 3GPP is the forum where standardization has been handled from the first WCDMA UMTS specification on. It unites many telecommunication standard bodies to coordinate their regional activities in order to establish global standards aligned down to bit level details. The 3GPP was created in December 1998, with the original scope of producing technical specifications and technical reports for 3G mobile systems, both for FDD and TDD modes, respectively. The scope was subsequently amended to include the maintenance and development of GSM, General Packet Radio Service (GPRS) and Enhanced Data Rates for Global system for mobile communications Evolution (EDGE) specifications. The specifications themselves are published regularly, with major milestones being denoted as *Releases* [168].

Figure A.1 shows the chronological development of the 3GPP standardization releases. During the work on Release 4, it became obvious that some improvements for packet access would be needed [33]. Release 5, which was finished in June 2002 thus introduced a high-speed enhancement for the downlink packet data services, HSDPA. The innovation that happened for HSDPA was quite tremendous, including changes in the physical layer, the MAC layer and slight changes in the core network. After some years, to be specific in March 2005, 3GPP finished its work on Release 6, specifying the uplink pendant of HSDPA, called HSUPA.

MIMO has been of interest already during the work on Release 5 and Release 6, however the feasibility studies up to that point concluded that the benefits of it were limited to the extend that the additional complexity could not be justified. Finally, after a long and detailed study-work discussing many proposals [6], MIMO has been included in Release 7 in December 2007. Besides this revolutionary step, the 3GPP added also many other improvements, among which
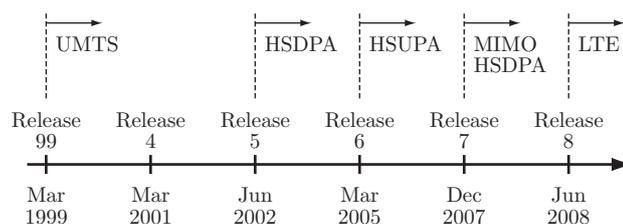
Figure A.1.: Chronological development of the 3GPP standardization releases including important evolutionary steps.

some of the most important were

- the specifications for new frequency bands,

- the utilization of linear MMSE receivers to meet the performance requirements on the wireless link,

- an optimization of the delay in the network, for example by introducing *continuous connectivity* to avoid set-up delays after idle time,

- the definition of 64 QAM as a higher order modulation scheme for SISO HSDPA,

- the specification of a flexible RLC PDU assignment, and

- an investigation of the benefits of a direct tunnel for the user-plane data in HSPA networks.

Recently, in June 2008, Release 8 was published. It contains the next logical step in the evolution of wireless networks, called LTE. The most notably innovations in the RAN in this release are

- the redevelopment of the system architecture, called System Architecture Evolution (SAE),

- a definition of network self-organization in the context of LTE,

- the introduction of *home* base-stations,[1]

- a study of interference cancellation techniques,

- first steps towards circuit switched services for HSDPA, and

- 64 QAM modulation for MIMO HSDPA.

Today, approximately 300 HSDPA networks are operated in 130 countries [169]. In Austria, the first mobile network operator that launched an HSDPA network was mobilkom austria AG. The network went online on January 23, 2006. Currently, downlink speeds up to 7.2 Mbit/s[2] are widely possible in Austria [169, 170], wheras in some specific test areas mobilkom austria AG already offers D-TxAA HSDPA with an data-rate of up to 21.1 Mbit/s. The traffic density in urban areas nowadays demands the allocation of large portions of the channelization code resources to HSDPA, if not the operation on a separate carrier. However, the revenues generated from HSDPA services are becoming rapidly more important for the financial success of mobile network operators in Austria [30], thus legitimating this resource allocation.

---

[1] In the 3GPP terminology, base-stations are also often called *NodeBs*.
[2] This corresponds to user equipment capability class 7 and 8, as will be explained in Section 2.1.

A.2. Pre-Coding Codebook; Pre-Coding Evaluation

The 3GPP technical recommendation [6] specifies a pre-coding codebook for D-TxAA MIMO HSDPA. The pre-coding coefficients for the double-stream operation, are defined as

$$w_1 = w_3 \triangleq \frac{1}{\sqrt{2}}, \tag{A.1}$$

$$w_2 \in \left\{ \frac{1+j}{2}, \frac{1-j}{2}, \frac{-1+j}{2}, \frac{-1-j}{2} \right\}, \tag{A.2}$$

$$w_4 \triangleq -w_2, \tag{A.3}$$

where w_1 and w_2 are utilized by stream one, and w_3 and w_4 are utilized by stream two. Accordingly the pre-coding matrix $\mathbf{W}_{\mathrm{CB}}$ would be given by

$$\mathbf{W}_{\mathrm{CB}} = \begin{bmatrix} w_1 & w_3 \\ w_2 & w_4 \end{bmatrix} = \begin{bmatrix} \mathbf{w}_1 & \mathbf{w}_2 \end{bmatrix} = \mathbf{W}_{\mathrm{CB}}(w_2), \tag{A.4}$$

which is fully determined by the choice of the pre-coding weight w_2 in this case. It also has to be noted that, given the pre-coding weights of Equations (A.1) to (A.3), the pre-coding matrix is *unitary*, thus fulfilling the assumption in Theorem 3.1, in case of a double-stream transmission. For the single-stream transmission, only the pre-coding vector $\mathbf{w}_1$ is utilized.

With this definition of the pre-coding codebook, it remains to elaborate how the *best* pre-coding choice can be determined by the UE. First, it is necessary to define a metric in order to be able to introduce a measure for the term *best*. For this purpose, many different figures of merit could be used, like for example the capacity, achievable maximum rate, or the BLER performance.

The question of the metric to be optimized for the pre-coding in MIMO systems as well as the algorithm solving for the metric has been investigated by researches in great detail. Many approaches have been proposed, for example based on interference alignment ideas [171], utilizing game-theoretic concepts [172], introducing the energy efficiency into the problem [173], taking into account that the channel is only imperfectly known [174], applying DPC[3] techniques [176], aiming for robust solutions [177], or trying to exploit the benefits of joint pre-coding and scheduling [178]. A lot of research has also tried to include coordination among the transmitters, that is the NodeBs, in the problem. In HSDPA, such approaches are currently not supported by the network, however, in LTE the X2-interface will provide means to allow for such algorithms. Despite all these research efforts, the 3GPP recommends the utilization of the SINR as the underlying metric to decide upon the pre-coding vector choice [6, 7]. Only a coordination with the scheduler regarding the pre-coding utilization would be possible.

Defining the SINR as the cost function to be maximized, it is still unclear, *which* SINR should be considered. Given the structure of MIMO HSDPA, see also Figure 2.8, the SINR metric can be evaluated

- before the equalization, thus directly at the receive antennas, or
- after the equalization, which is much more complex to be evaluated.[4]

---

[3]DPC is a technique for pre-destorting the transmit signal to cancel the interference at the receiver end [175].

[4]Note that the post-equalization SINR builds the basis for the system-level model in Chapter 3 with the despreading gain included.

For the UE to utilize the post-equalization SINR as a decision metric for the pre-coding, the receive filter would have to be evaluated for all—or at least a set of—pre-coding possibilities. Given the limited computational power and battery constraints in wireless mobile devices, such calculations are intractable. For sake of completeness, I want to point out that there may be possibilities to assess the post-equalization SINR as a metric by a suitable low-complex representation. If done so, this also allows for the possibility of joint pre-coding and link-adaptation feedback reporting [16]. Moreover, I will not consider this possibility in this work.

Due to its anticipated lower computational complexity, I consider the case of the pre-equalization SINR metric for this work. Considering Equation (3.6), the samples at receive antenna n_r are given by

$$y_i^{(n_\mathrm{r})} = \mathbf{h}_\mathrm{w}^{(n_\mathrm{r})}\mathbf{x}_i + n_i, \tag{A.5}$$

where $\mathbf{h}_\mathrm{w}^{(n_\mathrm{r})} \triangleq (\mathbf{H}_\mathrm{w})_{(n_\mathrm{r},:)}$ is defined to be the n_r-th row of the equivalent MIMO channel matrix $\mathbf{H}_\mathrm{w}$, defined in Equation (3.2). Considering that there are multiple streams transmitted to the receiver, the above equation can be rewritten as

$$y_i^{(n_\mathrm{r})} = \sum_{n=1}^{N_\mathrm{S}} \mathbf{h}_\mathrm{w}^{(n_\mathrm{r},n)}\mathbf{x}_i^{(n)} + n_i, \tag{A.6}$$

where $\mathbf{h}_\mathrm{w}^{(n_\mathrm{r},n)}$ is composed of the columns with indices[5] $n + N_\mathrm{S}[1, L_\mathrm{h}]$ from the vector $\mathbf{h}_\mathrm{w}^{(n_\mathrm{r})}$. The channel vector entries of $\mathbf{h}_\mathrm{w}^{(n_\mathrm{r},n)}$ correspond to the transmit chips of stream n, and correspondingly, $\mathbf{x}_i^{(n)}$ is defined to contain only the transmit chips of that respective stream. With these definitions, the pre-equalization SINR of stream n on receive antenna n_r is given by

$$\rho^{(n,n_\mathrm{r})} = \frac{\mathbb{E}\left\{\left|\mathbf{h}_\mathrm{w}^{(n_\mathrm{r},n)}\mathbf{x}_i^{(n)}\right|^2\right\}}{\mathbb{E}\left\{\sum_{\substack{m=1\\m\neq n}}^{N_\mathrm{S}} \left|\mathbf{h}_\mathrm{w}^{(n_\mathrm{r},m)}\mathbf{x}_i^{(m)}\right|^2\right\} + \mathbb{E}\left\{|n_i|^2\right\}}. \tag{A.7}$$

For simplifying this equation, consider

$$\mathbb{E}\left\{\left|\mathbf{h}_\mathrm{w}^{(n_\mathrm{r},n)}\mathbf{x}_i^{(n)}\right|^2\right\} = \mathbf{h}_\mathrm{w}^{(n_\mathrm{r},n)}\mathbb{E}\left\{\mathbf{x}_i^{(n)}\left(\mathbf{x}_i^{(n)}\right)^\mathrm{H}\right\}\left(\mathbf{h}_\mathrm{w}^{(n_\mathrm{r},n)}\right)^\mathrm{H} = \mathbf{h}_\mathrm{w}^{(n_\mathrm{r},n)}\left(\mathbf{h}_\mathrm{w}^{(n_\mathrm{r},n)}\right)^\mathrm{H}, \tag{A.8}$$

where I assumed the data chips to be i.i.d. uncorrelated with unit variance, $E_\mathrm{c} = 1$. Note also that the stream-specific equivalent MIMO channel row $\mathbf{h}_\mathrm{w}^{(n_\mathrm{r},n)}$ is equal to

$$\mathbf{h}_\mathrm{w}^{(n_\mathrm{r},n)} = \mathbf{H}_{(n_\mathrm{r},:)}\left(\mathbf{I} \otimes \mathbf{w}_n\right) = \mathbf{w}_n^\mathrm{H}\left(\mathbf{H}^{(n_\mathrm{r})}\right)^\mathrm{H}\mathbf{H}^{(n_\mathrm{r})}\mathbf{w}_n, \tag{A.9}$$

according to Equation (3.2), and with $\mathbf{H}^{(n_\mathrm{r})}$ defining the $\mathbb{C}^{L_\mathrm{h} \times N_\mathrm{T}}$ frequency selective MIMO channel matrix that contains the channel coefficients from all transmit antennas to receive antenna n_r. Accordingly, Equation (A.7) becomes

$$\rho^{(n,n_\mathrm{r})} = \frac{\mathbf{w}_n^\mathrm{H}\left(\mathbf{H}^{(n_\mathrm{r})}\right)^\mathrm{H}\mathbf{H}^{(n_\mathrm{r})}\mathbf{w}_n}{\sum_{\substack{m=1\\m\neq n}}^{N_\mathrm{S}} \mathbf{w}_m^\mathrm{H}\left(\mathbf{H}^{(n_\mathrm{r})}\right)^\mathrm{H}\mathbf{H}^{(n_\mathrm{r})}\mathbf{w}_m + \sigma_\mathrm{n}^2}, \tag{A.10}$$

---

[5]I utilize the notation $[a, b]$ do denote all integers between a and b, for example $[3, 9] = 3, 4, \ldots, 9$.

with σ_n^2 defining the variance of the i.i.d. white Gaussian noise.

The UE thus has to find the optimum pre-coding vector for each stream by solving the SINR related problem

$$\mathbf{W}_{\mathrm{CB}}^{\mathrm{opt}} = \arg \max_{\mathbf{W}_{\mathrm{CB}}} \sum_{n=1}^{N_{\mathrm{S}}} \sum_{n_{\mathrm{r}}=1}^{N_{\mathrm{R}}} \rho^{(n,n_{\mathrm{r}})}, \tag{A.11}$$

which optimizes the sum SINR over all receive antennas and streams. This is a particularly difficult problem to solve, in particular because—like in the 3GPP pre-coding codebook—the pre-coding vectors can have dependencies, thus the problem in Equation (A.11) cannot be decoupled for the individual streams.

Accordingly, a low complexity approach would be to optimize

$$\mathbf{w}_n^{\mathrm{opt}} = \arg \max_{\mathbf{w}_n} \sum_{n_{\mathrm{r}}=1}^{N_{\mathrm{R}}} \mathbf{w}_n^{\mathrm{H}} \left(\mathbf{H}^{(n_{\mathrm{r}})}\right)^{\mathrm{H}} \mathbf{H}^{(n_{\mathrm{r}})} \mathbf{w}_n = \arg \max_{\mathbf{w}_n} \mathbf{w}_n^{\mathrm{H}} \underbrace{\left[\sum_{n_{\mathrm{r}}=1}^{N_{\mathrm{R}}} \left(\mathbf{H}^{(n_{\mathrm{r}})}\right)^{\mathrm{H}} \mathbf{H}^{(n_{\mathrm{r}})}\right]}_{\triangleq \mathbf{R}} \mathbf{w}_n \tag{A.12}$$

instead of Equation (A.11), for each stream individually. In the D-TxAA MIMO HSDPA case, only one stream has to be evaluated, because the second stream is directly specified by the codebook, given in Equations (A.1) to (A.3). Thus, in this work, the pre-coding was chosen according to the optimization over the pre-coding weight w_2,

$$w_2^{\mathrm{opt}} = \arg \max_{w_2} \mathbf{w}_1^{\mathrm{H}} \mathbf{R} \mathbf{w}_1, \tag{A.13}$$

which of course favors stream one, thus explaining for example the gap between the ecdfs of the equivalent fading parameters in Figure 3.5.

To overcome the problem of favoring stream one, the optimization problem could be altered to

$$w_2^{\mathrm{opt}} = \arg \max_{w_2} \mathbf{w}_1^{\mathrm{H}} \mathbf{R} \mathbf{w}_1 + \mathbf{w}_2^{\mathrm{H}} \mathbf{R} \mathbf{w}_2, \tag{A.14}$$

thus searching for the best combination of the two pre-coding vectors.

In order to assess the performance of the optimization in Equations (A.13) and (A.14), I conducted a simulation comparing them with the *optimum* pre-coding vector choices, given by the eigenvectors corresponding to the largest eigenvalues of $\mathbf{R}$,[6]

$$\mathbf{w}_n^{\mathrm{opt}} = \mathbf{u}_n, \quad \mathbf{u}_n \triangleq \mathbf{U}_{(:,n)} : \mathbf{R} = \mathbf{U}\boldsymbol{\Lambda}\mathbf{U}^{-1}, \tag{A.15}$$

with $\mathbf{U}$ and $\boldsymbol{\Lambda}$ denoting the unitary matrix of eigenvectors and the matrix of eigenvalues, both sorted according to the magnitude of the eigenvalue. The simulation parameters for the simulation are given in Table A.1. The chip level SINR was chosen to be $E_{\mathrm{c}}/N_0 = 0\,\mathrm{dB}$, which implies that $\sigma_n^2 = 1$.

The simulation results are given in Figure A.2, showing the sum SINR over all streams and receive antennas, $\sum_{n=1}^{N_{\mathrm{S}}} \sum_{n_{\mathrm{r}}=1}^{N_{\mathrm{R}}} \rho^{(n,n_{\mathrm{r}})}$. It can be observed that both algorithms loose compared to the non-quantized pre-coding choice from Equation (A.15). Interestingly, the algorithm greedily aiming for the optimization of stream one from Equation (A.13) outperforms the algorithm considering both streams in Equation (A.14). This is due to the fact that both algorithms are only an approximation to the problem in Equation (A.11). These results also proof the applicability of the algorithm utilized for the simulations in this thesis.

---

[6]Note that $\mathbf{R}$ is a Hermitian positive semi-definite square matrix, thus Singular Value Decomposition (SVD) and eigenvalue decomposition deliver equal results.

Table A.1.: Simulation parameters for the performance comparison of different pre-coding choice algorithms in a 2×2 PedA MIMO channel, with $N_\mathrm{S} = 2$ streams active.

Parameter	Value
fading model	improved Zheng model [8, 91]
antennas	$N_\mathrm{T} \times N_\mathrm{R} = 2 \times 2$
pre-coding codebook	3GPP [6]
pre-coding delay	11 slots
transmitter frequency	$2\,\mathrm{GHz}$
mean equalizer E_c/N_0	$0\,\mathrm{dB}$
UE speed	$3\,\mathrm{km/h}$
channel profile	PedA
simulated slots	10000, each $2/3\,\mathrm{ms}$
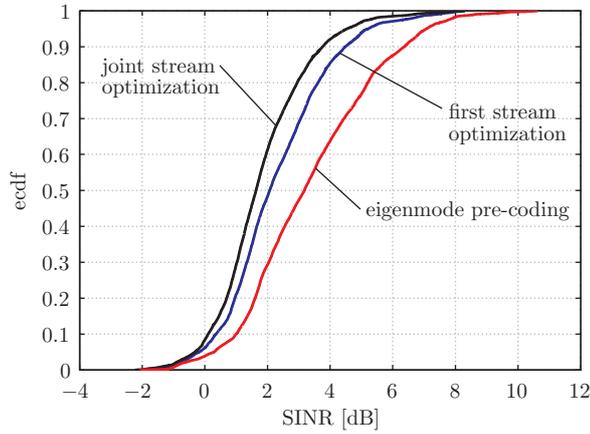
Figure A.2.: Performance of the pre-coding choice algorithms Equations (A.13) and (A.14) compared to the *best* non-quantized pre-coding.

A.3. Additional Equivalent Fading Parameter Statics

Figure A.3 shows the ecdfs of the equivalent fading parameters for the 2×2 single stream transmission. Compared to the results in Figure 3.4, the second receive antenna will be beneficial for the receive filter. This effect can be observed in Figures A.3(a) and A.3(b) where the intra-cell orthogonality o_1^{intra} is significantly lowered and the desired signal gain G_1^s is slightly increased when compared to Figures 3.4(a) and 3.4(b).

Similar effects are also reflected in the results of Figures A.3(c) and A.3(d). Again o_1^{intra} is lowered compared to Figures 3.4(c) and 3.4(d), whereas now the beamforming orthogonality o_1^{BF} is increased, denoting that the other user interference has a higher impact on the physical-layer performance. It also has to be mentioned that due to the second receive antenna, the desired signal gain G_1^s is less affected by the channel delay spread, which can be seen when comparing Figure A.3(c) with Figure A.3(d). In addition the inter-cell interference gain $G_{1,b}^{\mathrm{inter}}$ can be lowered compared to the single receive antenna case in Figure 3.4.

(a) PedA open-loop 2×2 single-stream.

(b) PedB open-loop 2×2 single-stream.

(c) PedA closed-loop 2×2 single-stream.

(d) PedB closed-loop 2×2 single-stream.
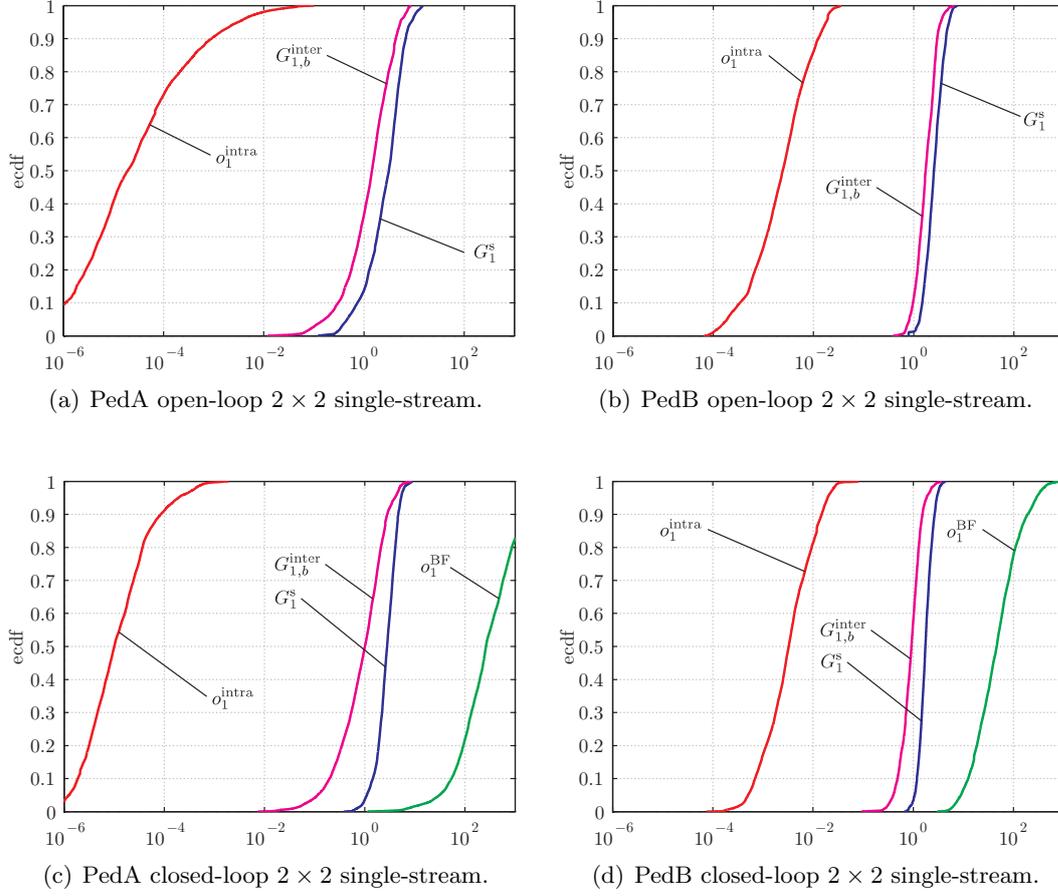
Figure A.3.: The ecdfs of th equivalent fading parameters in case of a single-stream transmission over a $N_\mathrm{T} \times N_\mathrm{R} = 2 \times 2$ MIMO channel.

To illustrate the effect of the pre-coding delay, I furthermore generated the equivalent fading parameters for an ITU Vehicular A (VehA) channel, as shown in Figure A.4. The UE speed for these simulations was set to $120 \, \mathrm{km/h}$. Now the performance of the two streams in terms of their equivalent fading parameters is equal again. This is due to the fact that the delay in the pre-coding leads to a larger mismatch[7] between the actual channel state when the pre-coding is applied and the channel state when the pre-coding choice was evaluated. Accordingly, the pre-coding does not deliver a gain anymore, and simultaneously closing the gap between the equivalent fading parameters of both streams.

A.4. Proof of Theorem 3.1

If the pre-coding matrix $\mathbf{W}_\mathrm{CB}$ is unitary, this means that the individual streams are pre-coded orthogonal to each other, and the pre-coding vectors are normalized to one. In case of the 3GPP codebook [6], this is indeed the case.

---

[7]One could also speak of a smaller *correlation* instead of a larger *mismatch* here.

(a) VehA open-loop 2×2 double-stream. (b) VehA closed-loop 2×2 double-stream.
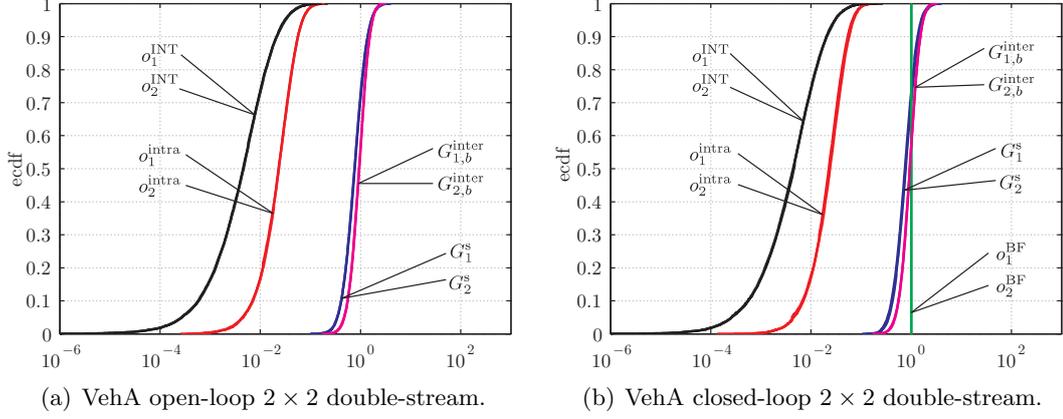
Figure A.4.: The ecdfs of the equivalent fading parameters in case of a double-stream transmission over a $N_{\mathrm{T}} \times N_{\mathrm{R}} = 2 \times 2$ MIMO channel for the ITU VehA channel.

For the proof it obviously suffices to show the assertion before taking the average over the pre-coding vectors, $\mathbb{E}_w\{\cdot\}$. From Equation (3.40), let me first consider the simpler sum

$$\sum_{m=0}^{N_{\mathrm{S}}(L_{\mathrm{f}}+L_{\mathrm{h}}-1)-1} \left| \left(\mathbf{f}^{(n)}\right)^{\mathrm{T}} \mathbf{h}_m^{(u,b_0)} \right|^2 = \left\| \left(\mathbf{f}^{(n)}\right)^{\mathrm{T}} \tilde{\mathbf{H}}_{\mathrm{w}}^{(u,b_0)} \right\|^2, \tag{A.16}$$

where the equality follows from Equation (3.25) and the discussions before that. Here, $\| \cdot \|^2$ denotes the Euclidean norm of a vector. Note that the stacked equivalent MIMO channel matrix, $\tilde{\mathbf{H}}_{\mathrm{w}}^{(u,b_0)}$ can be expressed as

$$\tilde{\mathbf{H}}_{\mathrm{w}}^{(u,b_0)} = \tilde{\mathbf{H}}^{(u_0,b_0)} \left(\mathbf{I}_{L_{\mathrm{f}}+L_{\mathrm{h}}-1} \otimes \mathbf{W}_{\mathrm{CB}}^{(u,b_0)} \right), \tag{A.17}$$

by rearranging the *stacking* and pre-coding in Equations (3.10) and (3.2), thus obtaining the stacked version of the MIMO channel matrix $\tilde{\mathbf{H}}^{(u,b_0)}$ with $\mathbf{W}_{\mathrm{CB}}^{(u,b_0)}$ denoting the pre-coding matrix of user u. By expressing the norm as scalar product, one can obtain

$$\left\| \left(\mathbf{f}^{(n)}\right)^{\mathrm{T}} \tilde{\mathbf{H}}_{\mathrm{w}}^{(u,b_0)} \right\|^2$$
$$= \left(\mathbf{f}^{(n)}\right)^{\mathrm{T}} \tilde{\mathbf{H}}^{(u_0,b_0)} \left(\mathbf{I}_{L_{\mathrm{f}}+L_{\mathrm{h}}-1} \otimes \mathbf{W}_{\mathrm{CB}}^{(u,b_0)} \right) \left(\mathbf{I}_{L_{\mathrm{f}}+L_{\mathrm{h}}-1} \otimes \left(\mathbf{W}_{\mathrm{CB}}^{(u,b_0)}\right)^{\mathrm{H}} \right) \left(\tilde{\mathbf{H}}^{(u_0,b_0)}\right)^{\mathrm{H}} \left(\mathbf{f}^{(n)}\right)^* \tag{A.18}$$
$$= \left(\mathbf{f}^{(n)}\right)^{\mathrm{T}} \tilde{\mathbf{H}}^{(u_0,b_0)} \left(\mathbf{I}_{L_{\mathrm{f}}+L_{\mathrm{h}}-1} \otimes \mathbf{W}_{\mathrm{CB}}^{(u,b_0)} \left(\mathbf{W}_{\mathrm{CB}}^{(u,b_0)}\right)^{\mathrm{H}} \right) \left(\tilde{\mathbf{H}}^{(u_0,b_0)}\right)^{\mathrm{H}} \left(\mathbf{f}^{(n)}\right)^* .$$

However, by assumption, the pre-coding matrix is unitary, hence

$$\sum_{m=0}^{N_{\mathrm{S}}(L_{\mathrm{f}}+L_{\mathrm{h}}-1)-1} \left| \left(\mathbf{f}^{(n)}\right)^{\mathrm{T}} \mathbf{h}_m^{(u,b_0)} \right|^2 = \left\| \left(\mathbf{f}^{(n)}\right)^{\mathrm{T}} \tilde{\mathbf{H}}^{(u_0,b_0)} \right\|^2, \tag{A.19}$$

which is independent of the pre-coding matrix $\mathbf{W}_{\mathrm{CB}}$. Now consider that for an arbitrary matrix $\mathbf{A}$ and some set $\mathcal{I} \subset \mathbb{N}_+$ of indices, $\Pi_{\mathcal{I}}(\mathbf{A})$ denotes the matrix where the columns with indices in

$\mathcal{I}$ are deleted. For the particular index set $[\tau N_\mathrm{S}, \tau N_\mathrm{S} + N_\mathrm{S} - 1]$ it can be shown rather quickly that

$$\Pi_{[\tau N_\mathrm{S}, \tau N_\mathrm{S} + N_\mathrm{S} - 1]}\Big(\tilde{\mathbf{H}}_\mathrm{w}^{(u,b_0)}\Big) = \Pi_{[\tau N_\mathrm{T}, \tau N_\mathrm{T} + N_\mathrm{T} - 1]}\Big(\tilde{\mathbf{H}}^{(u_0,b_0)}\Big) \cdot \Big(\mathbf{I}_{L_\mathrm{f}+L_\mathrm{h}-2} \otimes \mathbf{W}_\mathrm{CB}^{(u,b_0)}\Big), \qquad (A.20)$$

which implies that the operator $\Pi_\mathcal{I}$ preserves the structure of the matrix $\tilde{\mathbf{H}}_\mathrm{w}^{(u,b_0)}$. Hence, using the arguments from above,

$$\sum_{\substack{m=0 \\ m \neq [\tau N_\mathrm{S}, \tau N_\mathrm{S} + N_\mathrm{S} - 1]}}^{N_\mathrm{S}(L_\mathrm{f}+L_\mathrm{h}-1)-1} \left|\Big(\mathbf{f}^{(n)}\Big)^\mathrm{T} \mathbf{h}_m^{(u,b_0)}\right|^2 = \left\|\Big(\mathbf{f}^{(n)}\Big)^\mathrm{T} \Pi_{[\tau N_\mathrm{S}, \tau N_\mathrm{S} + N_\mathrm{S} - 1]}\Big(\tilde{\mathbf{H}}_\mathrm{w}^{(u,b_0)}\Big)\right\|^2$$

$$= \left\|\Big(\mathbf{f}^{(n)}\Big)^\mathrm{T} \Pi_{[\tau N_\mathrm{T}, \tau N_\mathrm{T} + N_\mathrm{T} - 1]}\Big(\tilde{\mathbf{H}}^{(u_0,b_0)}\Big)\right\|^2. \qquad (A.21)$$

This is again independent of the user index u, and exactly equal to γ_s^{-1} in Equation (3.40), thus concluding the proof.

A.5. Further Link-Quality Model Validation Results

Figure A.5 shows the validation results for an equalizer span of $L_\mathrm{f} = 30$ chips. The principal conclusions stay the same, however, compared to Figure 3.7, the saturation of the HS-PDSCH SINR in case of the PedB channel profile is less prominent. The reason for this is that with a larger equalizer span, the receive filter has more DoF to restore the orthogonality, thus leading to a performance more close to the PedA channel with much smaller delay spread than the PedB channel.

Figure A.6 depicts the results for the VehA channel, when the UE speed is set to $120\,\mathrm{km/h}$. It can be observed that the performance of the SISO 1×1 mode and the MISO 2×1 mode become equal, thus the second transmit antenna cannot be exploited to the extend as in low speed scenarios. This is due to the fact that the applied pre-coding is based on outdated channel information, because of the feedback delay, which was already mentioned in Section 3.3.4. The same argument holds for the diminishing performance gap between stream one and stream two in case of the MIMO 2×2 DS mode. However, note that in context of these high UE speeds and according Doppler frequencies as well as small channel coherence time, the applicability of the block-fading assumption is more than questionable. Since the utilized fading simulator is built on this assumption, no inter-symbol interference is taken into account, which limits the significance of the validation in Figure A.6.

A.6. Discussion of Assumption 3.9

To generate the equivalent fading parameter of the inter-cell interference, there are basically two possibilities to guarantee that the pre-coding choices of the neighboring cells are independent of the user channel. It can (i) either be assumed that the neighboring cell utilizes a random pre-coding, or (ii) that the pre-coding is static, that means constant over time. Alternative (i) guarantees a good averaging over different interference situations, however, the pre-coding choices are not correlated over time. On the other hand, alternative (ii) represents a worst case scenario.

In order to decide which one of the two alternatives to use, I performed two sets of simulations:

(a) SISO 1×1 and MISO 2×1 CL SS TxAA mode in a PedA channel.

(b) MIMO 2×2 CL SS TxAA and DS D-TxAA mode in a PedA channel.

(c) SISO 1×1 and MISO 2×1 CL SS TxAA mode in a PedB channel.

(d) MIMO 2×2 CL SS TxAA and DS D-TxAA mode in a PedB channel.
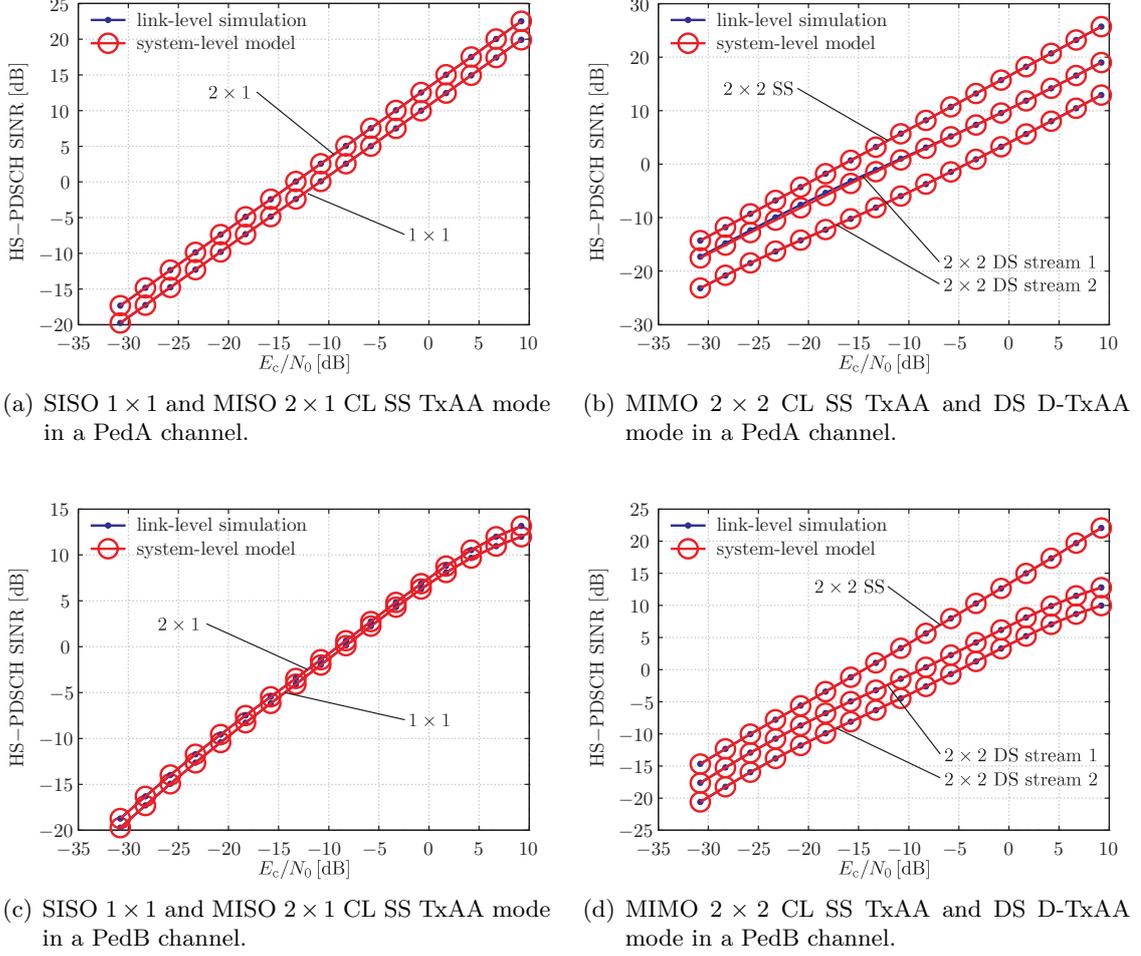
Figure A.5.: Link-quality model validation results for an equalizer length of $L_{\mathrm{f}} = 30$ chips in PedA and PedB channels.

- two simulations to assess the distribution of the utilized pre-coding vector indices for arbitrarily placed users in the cell with independent channel realizations, and

- four simulations to evaluate the statistical deviation in terms of the predicted inter-cell interference for random and for static pre-coding in the neighboring cells.

The pre-coding vector distribution simulations are needed to choose the correct statistical properties for the random pre-coding when utilized in the equivalent fading parameter generation. Afterwards, the inter-cell interference simulations serve to evaluate which pre-coding alternative to utilize in the equivalent fading parameter generation.

The simulation settings for both simulation sets are listed in Table A.2. Figure A.7 shows the resulting distributions for the 3GPP pre-coding vector codebook [6]. The channels of the ten simulated users are drawn independently—however obeying the same channel profile—with their pre-coding choice being evaluated to maximize receive SNR on stream one, see Appendix A.2. It can be observed that the distributions of the pre-coding vectors can be very well approximated by a uniform distribution, both for the ITU PedA, as well as the ITU PedB channel profile.

(a) SISO 1×1 and MISO 2×1 CL SS TxAA mode in a VehA channel.

(b) MIMO 2×2 CL SS TxAA and DS D-TxAA mode in a VehA channel.
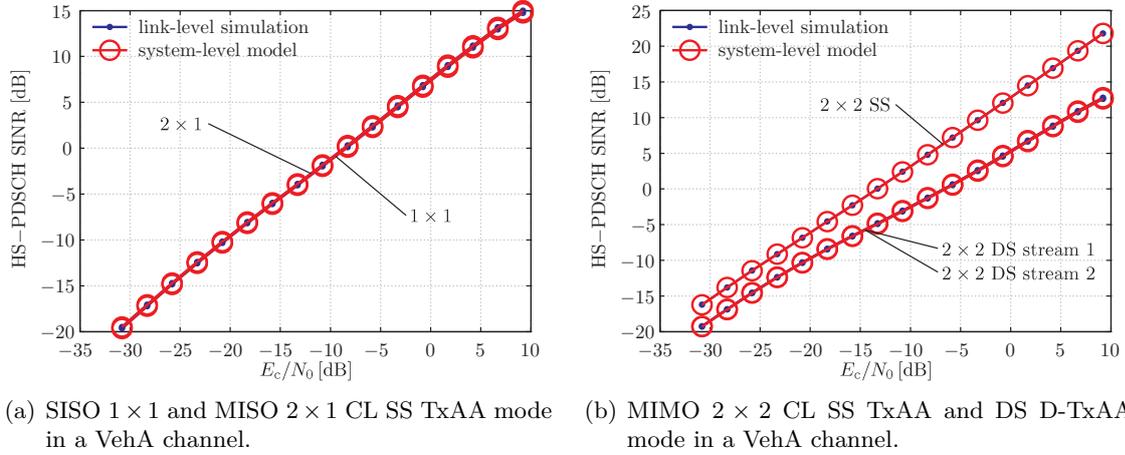
Figure A.6.: Link-quality model validation results for an equalizer length of $L_\mathrm{f} = 30$ chips in a VehA channel.

Table A.2.: Simulation parameters and settings for the verification simulations of the simplified inter-cell interference power, $P_{n,\varphi_k}^{\mathrm{inter}}$, modeling.

Parameter	Value
fading model	improved Zheng model [8, 91]
antennas	$N_\mathrm{T} \times N_\mathrm{R} = 2 \times 2$
pre-coding codebook	3GPP [6]
pre-coding delay	11 slots
transmitter frequency	2 GHz
mean equalizer SNR	10 dB
MMSE equalizer length	$L_\mathrm{f} = 30$ chips
MMSE equalizer delay	$\tau = 15$ chips
UE speed	3 km/h
simulated users	10
simulated slots	10 000, each 2/3 ms

To investigate the statistical properties of the two inter-cell pre-coding generation possibilities, I again sticked to the simulation settings in Table A.2. For these simulations, I assumed equal powers on all streams, and equal powers for all active users in all respective cells, which is likely to be set in a realistic network deployment. Furthermore, I only evaluated the inter-cell interference of one specific neighboring NodeB. The interference arriving from one specific NodeB will be independent of all other neighboring NodeBs due to the fact that the small-scale fading of their corresponding channels—to the desired user—can be assumed independent of each other.

I simulated the inter-cell interference power as given in Equation (3.46) for two cases: (i) all users are served with random pre-coding vectors, and the simplified version (ii) in which all users are served with a static pre-coding vector utilization. Figure A.8 compares the ecdfs of

(a) Pre-coding vector distribution in an ITU PedA channel.

(b) Pre-coding vector distribution in an ITU PedB channel.

Figure A.7.: Pre-coding vector distribution in a $N_\mathrm{T} \times N_\mathrm{R} = 2 \times 2$ MIMO channel for two different channel profiles.

the inter-cell interference in Equation (3.46), normalized to the total power after the receive filter, for different channel types and stream numbers in a Release 7 D-TxAA HSDPA system. The random pre-coding is chosen with a uniform distribution of the pre-coding vectors in the codebook Ω. Note that the MIMO channel matrix for is normalized to an average power of one, that is $\mathbb{E}\left\{ \|\tilde{\mathbf{H}}_\mathrm{w}\|_\mathrm{fro} \right\} = 1$, with $\|\cdot\|_\mathrm{fro}$ denoting the Frobenius norm. Furthermore, since the total available transmit power is one, in case of a single-stream transmission the stream has twice the power of each individual stream in the double stream transmission. This explains why $P_{n,\varphi_k}^\mathrm{inter}$ can be larger than one in the single-stream scenario.
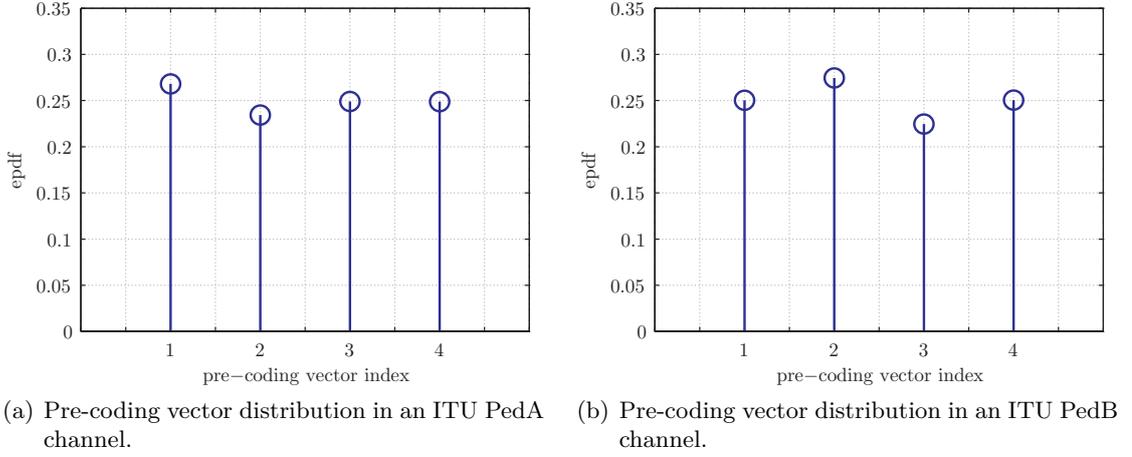
The comparison for the single stream D-TxAA operation in Figures A.8(a) and A.8(b) shows that the static pre-coding and the random pre-coding deliver different results. The random pre-coding leads to an inter-cell interference distribution that is limited to a smaller range, whereas the static pre-coding has outliers exceeding the static pre-coding both at the lower and the upper end of the ecdf. Comparing ITU PedA and PedB channels, it can be observed that the average inter-cell interference in case of the PedB channel is higher, as well as less spread, both for the static and the random pre-coding. It also has to be noted that both pre-coding possibilities lead to approximately the same average inter-cell interference power. Note that this effect of the pre-coding on the distribution of the inter-cell interference has already been mentioned in some of the 3GPP RAN working documents, for example in [179], where it is referred to as *flashlight effect*.

When comparing the ecdfs of the inter-cell interference in case of the double stream operation in Figures A.8(c) and A.8(d), the situation changes dramatically. Still, in case of the PedB channel, the inter-cell interference is higher and more concentrated for both streams, but now the static and the random pre-coding deliver the same distribution of the inter-cell interference. The reason for this behavior is that the pre-coding becomes ineffective in terms of the SDMA gain, which in the intra-cell interference is reflected by the equivalent fading parameter o_n^BF. A rigorous proof of this behavior is provided in Section 3.3.4.

If Assumption 3.9 would not be in force and the pre-coding of the neighboring cells would be evaluated according to the users in these cells, the inter-cell interference would show a behavior
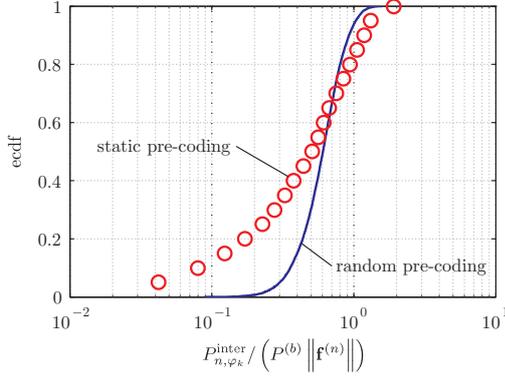
(a) ITU PedA 2×2 MIMO channel, single stream D-TxAA operation.
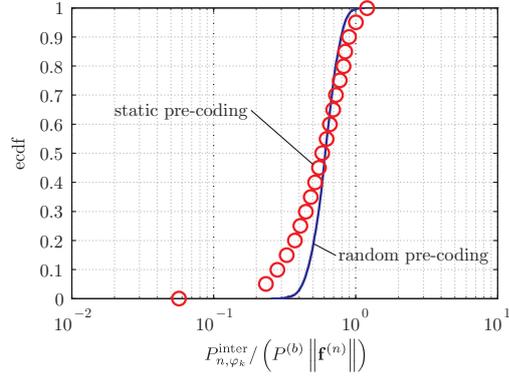
(b) ITU PedB 2×2 MIMO channel, single stream D-TxAA operation.
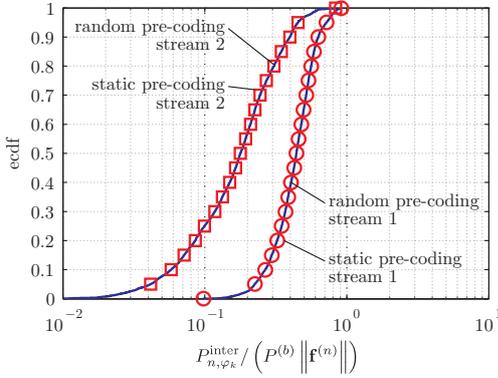
(c) ITU PedA 2×2 MIMO channel, double stream D-TxAA operation.
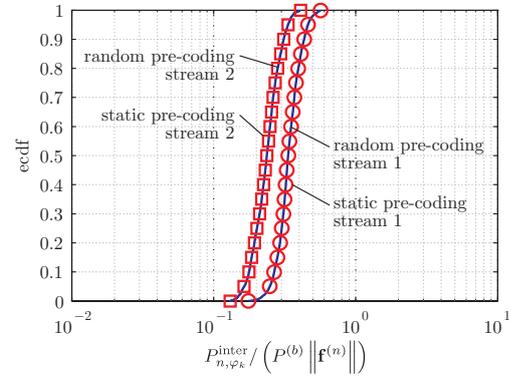
(d) ITU PedB 2×2 MIMO channel, double stream D-TxAA operation.

Figure A.8.: Comparison of the ecdfs of the inter-cell interference power $P_{n,\varphi_k}^{\text{inter}}$ for different channel types and stream numbers, normalized to the total receive power from the cell under investigation, $P^{(b)}$.

somehow between the static and the random inter-cell pre-coding. Network operators, however, are strongly interested in order to assess the limits of the network. Accordingly, for this thesis, I decided in favor of the static pre-coding for the evaluation of the equivalent fading parameter of the inter-cell interference gain, $G_{n,b}^{\text{inter}}$. If a more optimistic evaluation has to be performed, the equivalent fading parameter would have to be evaluated with random pre-coding for the inter-cell interference.

A.7. Auxiliary System-Level Models

In principle, the combination of the link-quality and link-performance model of Chapter 3 is sufficient for the system-level modeling of the MIMO HSDPA physical layer. Nonetheless, for actual system-level simulations, some auxiliary models are needed to enable the simulation of two important link-adaptation strategies, namely the dynamic fast link-adaptation as well as the HARQ gains offered by soft or IR combining of retransmissions at the UE.

A.7.1. SINR-to-CQI Mapping

The SINR-to-CQI mapping is needed to enable the fast TTI-based link-adaptation that has been introduced with Release 5 HSDPA. As explained in Chapter 2, in order for the NodeB to adapt the downlink transmission to the current channel quality, the UE sends a CQI feedback. According to [7], this CQI feedback is defined as follows:

> Based on an unrestricted observation interval, the UE shall report the highest tabulated CQI value for which a single HS-DSCH sub-frame formatted with the TBS, number of HS-PDSCH codes and modulation corresponding to the reported or lower CQI value could be received with a transport block error probability not exceeding 0.1 in a 3-slot reference period ending one slot before the start of the first slot in which the reported CQI value is transmitted.

Accordingly, the UE has to assess for every[8] TTI which transport format associated to a CQI would be the best in terms of largest TBS that does not exceed an average expected BLER of 0.1. Given the identified possibility of modeling the BLER of the downlink by means of the MIESM effective SINR mapping/compression, it is straightforward to use this model also for the assessment of the SINR-to-CQI mapping.

Let me first define the mapping f_{CQI} from the effective SINR, $\mathrm{SINR}_n^{\mathrm{eff}}$, to the feedback CQI $c_n^{(\mathrm{F})}$ of stream n, as

$$f_{\mathrm{CQI}}(\text{UE capability}) : \mathrm{SINR}_n^{\mathrm{eff}} \mapsto c_n^{(\mathrm{F})}, \tag{A.22}$$

which is a function of the UE capability class. Then, the proposed mapping is determined by the 0.1 BLER points of the AWGN reference performance curves, obtained by the extensive link-level simulations for the derivation of the link-performance model. A similar approach has also been proposed by the RAN working groups of 3GPP [39].

Figure A.9 shows the set of AWGN reference performance curves for UE capability Tables D and I, which contain the same curves that were used in the MIESM mapping/compression training in Figures 3.13 to 3.15. Below the set of AWGN curves, the SINR-to-CQI mapping f_{CQI} for each UE capability table is shown, respectively. The mapping is obtained by finding the 0.1 BLER crossing points in the SINR domain, marking the lowest channel-quality in SINR that supports a downlink transmission with the TFC associated to the AWGN curve corresponding CQI $c^{(\mathrm{F})}$. The stair function denotes that a given CQI is reported as long as no higher TFC can achieve an predicted BLER of at most 0.1.[9] It has to be noted that the plots in Figure A.9 are shown as a function of the HS-DSCH SINR instead of the HS-PDSCH SINR like in the MIESM training. The reason for this is that a mapping in the HS-PDSCH SINR domain would lead to an ambiguous (not one-to-one) mapping. The HS-DSCH SINR for this purpose is evaluated as proposed in [39], by summing over all HS-PDSCH despreader outputs,

$$\mathrm{SINR}_n^{\mathrm{HS\text{-}DSCH}} = \sum_{\varphi_k \in \Phi} \mathrm{SINR}_n^{\mathrm{HS\text{-}PDSCH}}, \tag{A.23}$$

which in the effective SINR domain can be interpreted as adding $10 \log_{10} |\Phi_n|$ in the dB scale.

If the set of AWGN target BLER crossing points and corresponding transmit CQI values, $c_n^{(\mathrm{T})}$, is denoted by

$$\mathcal{B}(\text{UE capability}) = \left\{ (c_n^{(\mathrm{T})}, \text{SINR at target BLER}) \right\}, \tag{A.24}$$

---

[8] In a practical network implementation, the CQI reporting period can be defined in multiples of a sub-frame [180].

[9] Note that this suggests the application of a *floor* operation, like in [39] where CQI = $\lfloor$ SNR[dB] $+ 3.5 \rfloor$ as a mapping is proposed.
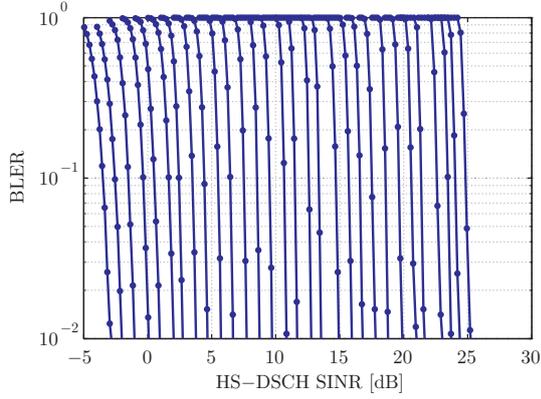
(a) AWGN BLER performance curves for UE capability Table D.
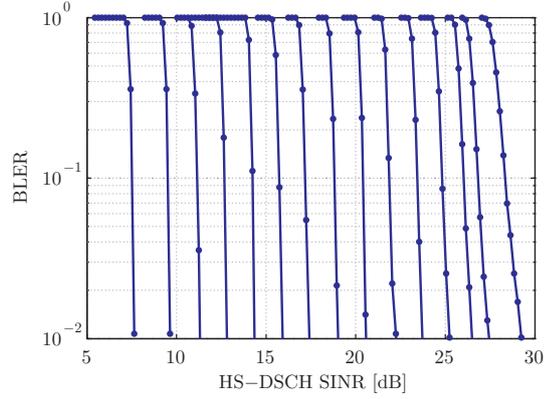
(b) AWGN BLER performance curves for UE capability Table I.
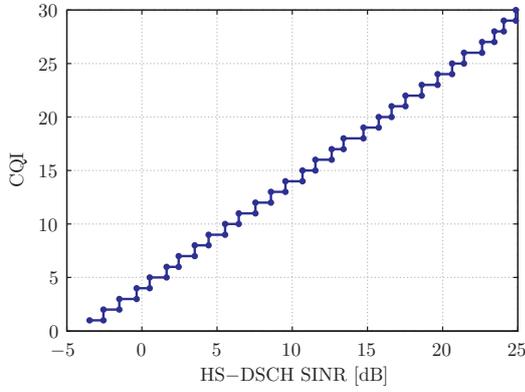
(c) Resulting SINR-toCQI mapping for UE capability table D and a target BLER of 0.1.
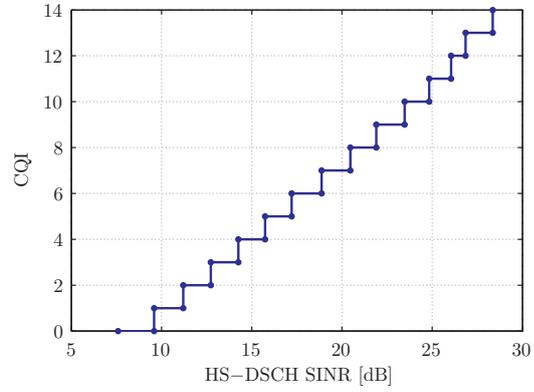
(d) Resulting SINR-toCQI mapping for UE capability table I and a target BLER of 0.1.

Figure A.9.: AWGN BLER performance curves and resulting SINR-to-CQI mappings.

then the resulting SINR-to-CQI mapping can be written as

$$f_{\text{CQI}}(\text{UE capability}) : c_n^{(\text{F})} = \arg \max_{c_n^{(\text{T})} \in \mathcal{B}} \left\{ \text{SINR at target BLER} \left(c_n^{(\text{T})} \right) \leq \text{SINR}_n^{\text{eff, HS-DSCH}} \right\}, \tag{A.25}$$

which achieves the stair-like mapping functions as depicted in Figure A.9.

A.7.2. HARQ Modeling

The second auxiliary model needed has to provide a way to account for the potential gains in soft or IR combining of retransmissions in the UE receive buffer.

For this work, I adopted a model developed in [181], defining the combined SINR after m retransmissions by the equation

$$\left(\text{SINR}_n^{\text{eff}} \right)_m = \epsilon^{m-1} \cdot \eta \left(r_{\text{c}}, \mathcal{A}, m \right) \cdot \sum_{k=1}^{m} \left(\text{SINR}_n^{\text{eff}} \right)_k, \tag{A.26}$$

(a) IR HARQ combining, PedA channel profile, UE capability Table D.

(b) Soft HARQ combining, PedA channel profile, UE capability Table I.
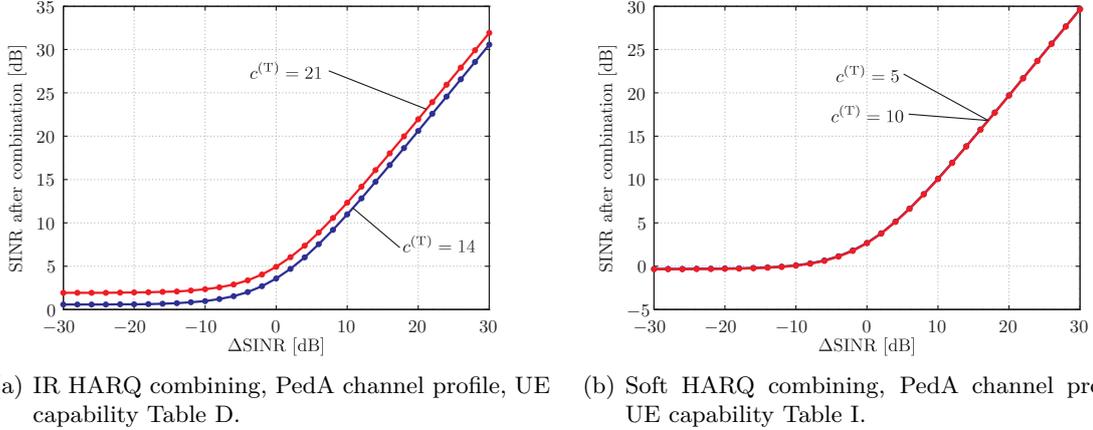
Figure A.10.: HARQ combining gain for different UE capability tables and transmit CQIs as a function of the SINR difference between two transmissions, according to the modeling of [181].

with r_c specifying the code-rate of the first transmission. The individual effective SINRs for each transmission k are denoted as $(\mathrm{SINR}_n^\mathrm{eff})_k$, parameter ϵ describes the soft combining[10] and $\eta(r_\mathrm{c}, \mathcal{A}, m)$ is the IR gain over soft combining for the m-th transmission.

To illustrate the utilized model, Figure A.10 depicts the combined SINR after two transmissions for different UE capability tables, CQIs, and retransmission combining modes as a function of the difference in effective SINR between the two transmissions in dB,

$$\Delta\mathrm{SINR} = (\mathrm{SINR}_n^\mathrm{eff})_1 - (\mathrm{SINR}_n^\mathrm{eff})_2. \tag{A.27}$$

From Figure A.10 it can be observed that the model predicts a higher HARQ combining gain in case of IR combining when the code-rate r_c and thus the transmit CQI value $c_n^{(\mathrm{T})}$ is higher. The reason for this behavior is that in case of higher coding rates, incremental redundancy can extract a higher coding gain than chase combining [37]. In case of soft combining this effect does not exist.

The combined SINR after m retransmissions then can be used again in the BLER mapping of the link-performance model in Equation (3.80) to evaluate whether the HARQ combined sub-frame is estimated to be correctly decodeable or not.

A.8. Semi-Analytical System-Level Performance Bound

Given the obtained system-level results of Section 4.2, it remains to assess how close the MIMO HSDPA throughput performance is to capacity. However, although the MIMO broadcast channels have been investigated quite extensively over the last years [134, 182, 183], general capacity results for the cellular context are still missing.

Given the theoretical lack of a suitable performance bound, I decided to derive a simple approximation of the maximum achievable data-rate when the resources are distributed equally

---

[10]Also often called *chase combining*.
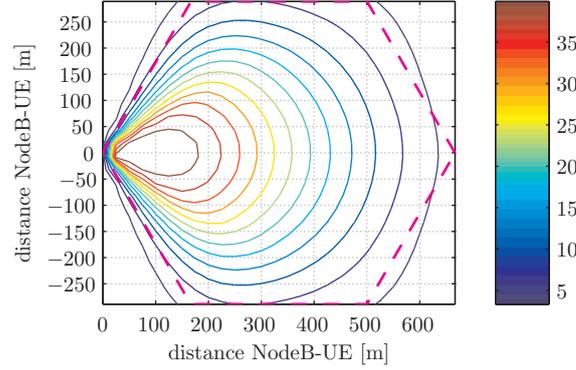
Figure A.11.: Maximum achievable data rate $B_{\mathrm{f}}\, n \log_2 \left[1 + \gamma(x,y) \right]$ as a function of the position in the target sector in Mbit/s.

over the whole cell area. If the area of the sector is denoted $\mathcal{S}$ and the total available bandwidth is B_{f}, then a simple approximation of the maximum achievable data-rate is

$$R_{\mathrm{cell}} = \int_{\mathcal{S}} \frac{B_{\mathrm{f}}}{A} n \log_2 \left[1 + \gamma(x,y) \right] \partial x \partial y, \tag{A.28}$$

where $A = \int_{\mathcal{S}} \partial x \partial y$ being the sector area, n specifies the maximum spatial multiplexing gain, and $\gamma(x,y)$ represents the SINR at position (x,y) in the sector,

$$\gamma(x,y) = \frac{P^{(b_0)}/L^{(b_0)}(x,y)}{\sum_{\substack{b=1 \\ b \neq b_0}}^{B} P^{(b)}/L^{(b)}(x,y) + P^{\mathrm{noise}}}. \tag{A.29}$$

The term $B_{\mathrm{f}}/A \log_2 \left[1 + \gamma(x,y) \right]$ represents a capacity density in bit/s/m^2, with a constant bandwidth density of B_{f}/A in the whole sector. The spatial multiplexing gain n corresponds to the MIMO gain achievable when channel conditions are favorable, as described in Chapter 2. Although this formulation would allow for manyfold optimizations to achieve maximum throughput values, it can serve as a bound in case of fair resource allocation when the users are distributed with uniform density in the target sector.

Figure A.11 depicts the maximum achievable data rate $B_{\mathrm{f}}\, n \log_2 \left[1 + \gamma(x,y) \right]$ as a function of the position in the target sector. When converted to rate density and integrated over the sector area, the resulting maximum achievable data-rate for a 3.84 Mchip/s CDMA system with $n = 2$ DoF can be evaluated to be 16.82 Mbit/s. Comparing this result with the average sector throughput values in Figure 4.10 it becomes apparent how much room for optimization the standard network configuration offers. For sake of completeness, however, it has to be noted that the utilized RR resource fair scheduler can be easily outperformed by a PF scheduler, which would make the gap to the predicted performance bound less dramatic. Nevertheless, even in case of PF scheduling enough room for optimization remains.

A.9. Video Coding and Video Quality Indicators

Streaming applications in third generation networks have been specified by the 3GPP specifications belonging to the class of *Transparent end-to-end Packet-switched Streaming Service*

(PSS). Since the seventh release of [184], defining the mandatory and suggested codecs, the H.264/AVC [185] is mentioned as *suggested* video codec. The H.264/AVC, jointly standardized by the International Standard Organization (ISO) Moving Picture Expert Group (MPEG) and ITU Video Coding Expert Group (VCEG), is currently the state-of-the art video codec for commercial applications. Thus, the coded utilized for the investigations in Section 4.4 was also chosen to be H.264/AVC [19, 20].

The H.264/AVC belongs to the family of the hybrid block based video codecs. These kinds of video codecs exploit the correlation of small regions of the sequence pictures in space and in time. Each sample of the raw video sequence, a video frame, is subdivided into square blocks, called MacroBlocks (MBs). Depending on the frame type, two encoding strategies are allowed. The macroblocks belonging to Intra (I) predicted frames are encoded using the neighboring blocks of the same picture as a source of prediction. For Inter (P) predicted frames, the prediction is searched in the previously encoded pictures. In both cases, the prediction is then refined by means of frequency transformed *residuals*, representing the difference between the original block and the best prediction.

The video encoder has been conceptually subdivided into two functional blocks. The Video Coding Layer (VCL) deals with the proper encoding functionalities whereas the NAL provides network friendliness to the produced data stream, managing the segmentation of the code into NAL Units and reducing the dependency of the data stored in different packets. The maximum size of a NAL unit is specified depending on the network Maximum Transfer Unit (MTU). Therefore, a NAL unit contains a variable number of MBs, representing a picture *slice*, depending on the effectiveness of the considered prediction. For video streaming over third generation networks, the NAL units are further encapsulated into Real-time Transport Protocol (RTP), User Datagram Protocol (UDP) and, finally, IP.

Because of bad channel conditions and/or network congestion, some packet might not be correctly received. At the decoder side *error concealment* techniques reduce the impact of missing packets. Because of the temporal prediction, a missing packet does not only affect the reconstruction of the picture slice it contains but rather all the frames that use that slice as a source of prediction. This effect is referred to as *temporal error propagation*. The temporal error propagation ceases with the following I frame. Packets containing intra encoded information are self contained, i.e. the slice they contain can be reconstructed without the need of information stored in other packets.

The distance, in number of frames, between two consecutive I frames is defined as GOP. The size of the GOP has a strong impact on the quality of the receiver side: small GOPs reduce the temporal propagation of the error. On the other hand, the spatial prediction used in the I frames is much less effective than the temporal one, particularly for high frequency patterns.

Since the error propagation is terminated by a correctly received I frame, preserving the payload of the packets containing encoded I slices is of major importance with respect to the one containing P slices. However, within the P frames of a GOP, one can differentiate between P packets of different importance. Different works in the literature, deal with the unequal error protection of video packets, depending on the impact on the quality the slice they contain have. These methods often call for refined rate distortion analysis and limit the observation on the punctual frame the slice belongs to.

Finally, let me recall that the PSNR has been chosen as video quality performance metric due to its connection to the QoE. Further details on this relation can be found in [186] and references therein.

A.9.1. Quality of Service Management

The UMTS network offers every associated service—thus also HSDPA—a possibility to define certain transmission quality parameters, as observed from a core-network or application-layer based perspective. Accordingly, within the UTRAN, a *bearer service* defining a logical channel, with clearly defined characteristics and functionality can be set up from the source to the destination of an application service [187].

The UMTS bearer service contains a list of attributes to describe the definition of the service quality in terms of measurable performance figures. To simplify the handling of the QoS parameters for the network equipment, as well as reduce the complexity of the processing of these parameters, only four different QoS classes have been defined by 3GPP [118]. The four classes are

- the *conversational class*, working in a real-time fashion, thus preserving the time relation between information entities of the stream, which corresponds to a conversational pattern with stringent and low delay, for example voice traffic,

- the *streaming class*, also working in a real-time fashion but having less stringent delay constraints, for example video streaming traffic,

- the *interactive class*, working on a best-effort basis and thus representing a request-response pattern with the goal to preserve the payload content, for example web-browsing traffic, and

- the *background class*, also working on a best-effort basis, where the destination is not expecting the data within a certain time but the payload still has to be preserved, for example telemetry or email traffic.

These classes then define the attributes associated to the UMTS bearer service [118], in particular

- the traffic class and the source statistics descriptor,

- the maximum bit rate and the guaranteed bit rate,

- the maximum SDU size, the SDU format information, the SDU error ratio, and the delivery of erroneous SDUs,

- the residual bit error ratio as well as the transfer delay, and

- the delivery order, the traffic handling priority and the allocation/retention priority.

By specifying these attributes, the traffic classes can be accurately specified by means of their logical channel requirements for successful operation of the application service. Especially in HSDPA, the MAC-hs entities allow for linking the QoS information established in the UTRAN with the physical-layer, which falls into the category of cross-layer optimization techniques.

A.10. Additional CPICH Power Optimization Results

In Figure A.12 it can be seen that the deployment of more antennas demands higher CPICH E_c/I_{or} values as well due to the increased complexity in the channel estimation for a larger number of channel coefficients. Moreover, when comparing Figure A.12 and Figure 4.15, the utilization of a second stream—thus the operation of the HSDPA network in D-TxAA mode— does not seem to significantly influence the optimum distribution of the CPICH E_c/I_{or} values.

(a) MISO $N_T \times N_R = 2 \times 1$ network utilizing one stream in a PedA channel environment.

(b) MISO 2×1 network utilizing one stream in a PedB channel environment.

(c) MIMO 2×2 network utilizing one stream in a PedA channel environment.

(d) MIMO 2×2 network utilizing one stream in a PedB channel environment.
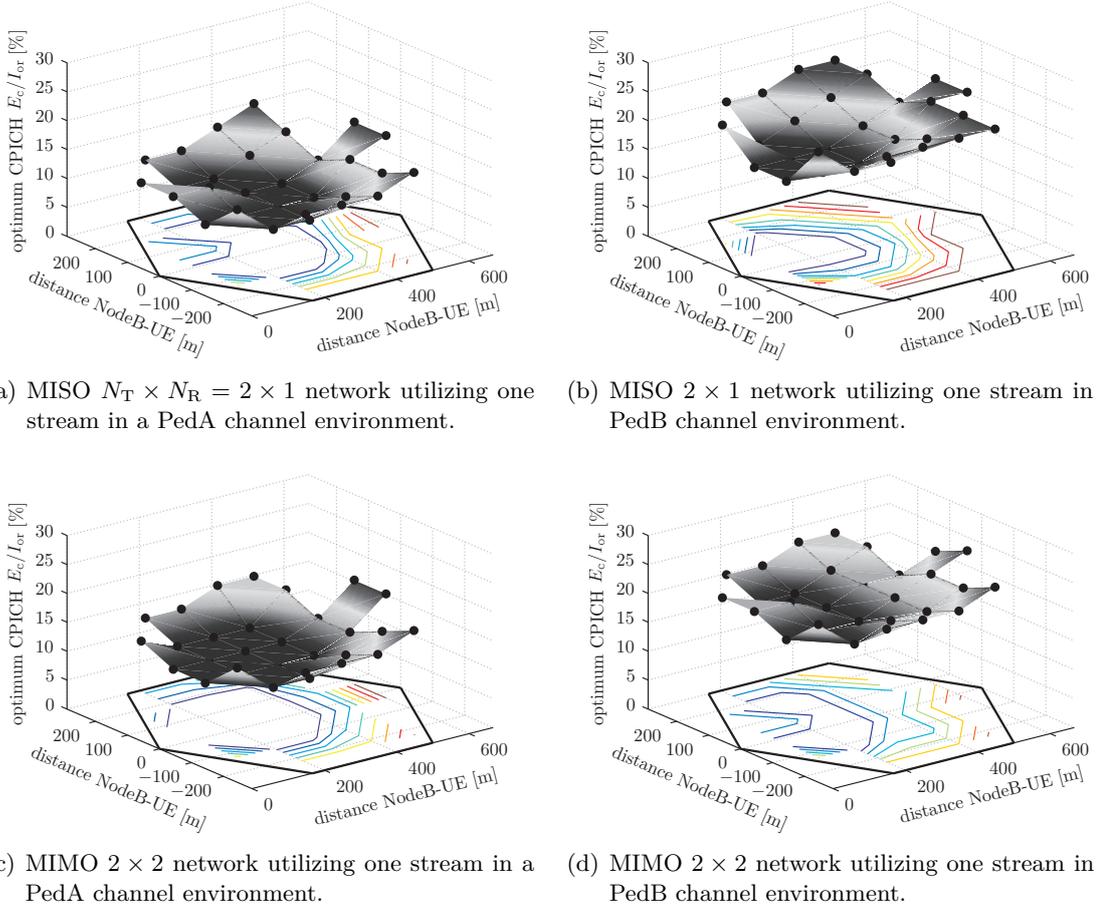
Figure A.12.: SS utilization CPICH power optimization results for different antenna configurations experiencing PedA and PedB channel environments, respectively.

The key drivers of the optimum E_c/I_{or} remain the channel delay spread and the number of employed antennas or equivalently the number of channel coefficients to be estimated.

A.11. WCDMA Chip Energy and PSD Parameters

For sake of completeness, let me cite four important definitions from [40]. The chip energy and Power Spectral Density (PSD) parameters introduced in the WCDMA context are defined as

- E_c defines the average energy per Pseudo Noise (PN) chip,

- I_{or} is evaluated as the total transmit PSD (integrated in a bandwidth of $(1 + \alpha)$ times the chip rate and normalized to the chip rate, with α specifying the roll-off factor of the RRC transmit pulse shaping filter) of the downlink at the NodeB antenna connector,

- $\hat{I}_{or}$ is evaluated as the received PSD (again integrated in a bandwidth of $(1 + \alpha)$ times the chip rate and normalized to the chip rate) of the downlink signal as measured at the UE antenna connector, and

- I_{oc} is evaluated as the PSD (integrated in a noise bandwidth equal to the chip rate and normalized to the chip rate) of a band-limited white noise source (simulating interference from other cells, which are not defined in a test procedure) as measured at the UE antenna connector.

A.12. Calculating the Effective Code-Rate

Let me address here how the effective code-rate in the context of HSDPA is calculated. As mentioned in Chapter 2, the number of bits transmitted utilizing one sub-frame is specified by the UE capability table and the TFCI. In the context of the MIESM training of Chapter 3, the transmission format is chosen from the set of CQI values, thus being fully specified by the according 3GPP CQI tables, in particular Table D and Table I. Furthermore, the timing conventions for HSDPA are that one HS-PDSCH sub-frame consists of 3×2560 chips, since it consists of three slots with 2560 chips each. The number of symbols that can be transmitted using one HS-PDSCH thus is given by $3 \cdot 2560/16$ since the spreading factor is fixed to $\mathrm{SF} = 16$ for HSDPA. Accordingly, the total available number of bits per sub-frame can be evaluated by considering the number of bits per symbol, $\log_2 |\mathcal{A}|$, and the number of HS-PDSCHs, $|\Phi|$, thus leading to $3 \cdot 2560/16 \cdot \log_2 |\mathcal{A}| \cdot |\Phi|$. Denoting the TBS of the transmit CQI $c^{(\mathrm{T})}$ to be $\mathrm{TBS}(c^{(\mathrm{T})})$, the effective code-rate is given by

$$r_{\mathrm{c}} = \frac{\mathrm{TBS}\big(c^{(\mathrm{T})}\big)}{\frac{3 \cdot 2560}{16} \log_2 |\mathcal{A}| \cdot |\Phi|}.$$

A.13. Validation of the System-Level Simulator with Odyssey Data

The work presented in Chapter 4 is based on a generic regular network structure that is designed to represent realistic cellular environments. However, in reality, network operators have to plan and deploy their networks according to many restrictions and constraints so that the resulting network layouts diverge often significantly from regular and symmetric structures.

For planing purposes network operators utilize special tools [10, 111] to predict the influences of electrical and mechanical tilts and azimuth of the deployed antennas. These tools usually rely on path-loss maps of the network region generated from ray-tracing models that are calibrated by field measurements. These maps also sometimes also serve to assess the expected traffic throughput per day/week which is needed in order to do suitable backhaul capacity planing.

In order to evaluate the validity of the developed system-level simulator, mobilkom austria AG provided path-loss and network setup data for a specific region in Vienna where HSDPA trial runs were conducted. The provided data included

- the positions of the NodeBs included in the trial run,

- the sector antenna azimuths,

- path-loss data files with $10\,\mathrm{m}$ resolution for all NodeBs,

- maximum transmit power values for all NodeBs, and

- the resulting ecdf of the CPICH $E_{\mathrm{c}}/I_{\mathrm{oc}}$ for every sector.
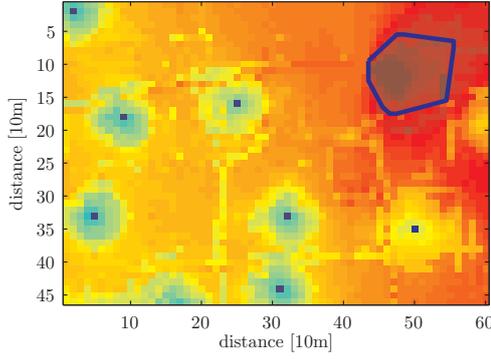
(a) Visual representation of the CPICH power distribution in the investigated region of interest.
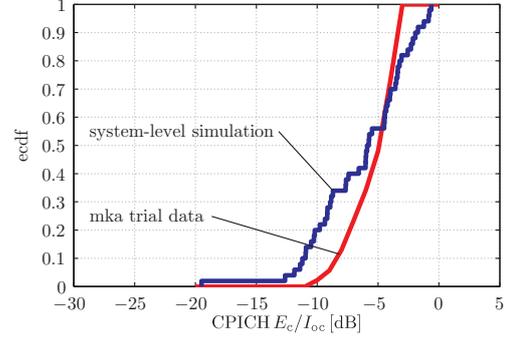
(b) The ecdf of the CPICH $E_{\mathrm{c}}/I_{\mathrm{oc}}$ in the sector as marked in the figure to the left in comparison to the mobilkom austria AG trial data results.
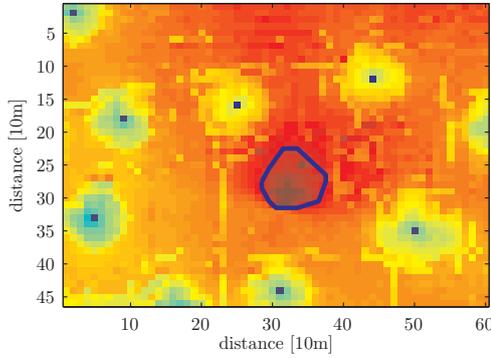
(c) Visual representation of the CPICH power distribution in the investigated region of interest.
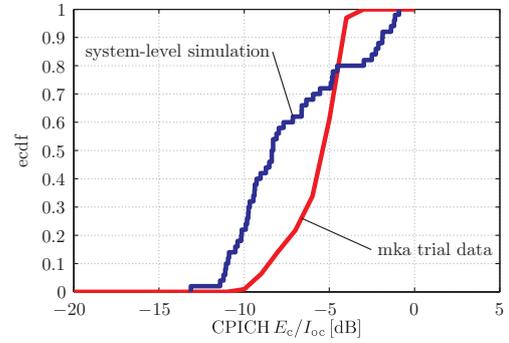
(d) The ecdf of the CPICH $E_{\mathrm{c}}/I_{\mathrm{oc}}$ in the sector as marked in the figure to the left in comparison to the mobilkom austria AG trial data results.

Figure A.13.: Comparison of the CPICH $E_{\mathrm{c}}/I_{\mathrm{oc}}$ obtained from the developed system-level simulator with the mobilkom austria AG trial data.

Given the format of the provided data, the system-level simulator of Chapter 4 could be modified to utilize the available data for the NodeB positions, the maximum transmission power and the path-loss information.

Based on this network deployment information, I conducted a set of system-level simulations with 50 users begin active in the chosen target cell, respectively. Figure A.13 illustrates the distribution of the CPICH $E_{\mathrm{c}}/I_{\mathrm{oc}}$ in the investigated region of interest and the ecdf for two chosen target cells. It can be observed that the average CPICH $E_{\mathrm{c}}/I_{\mathrm{oc}}$ is very similar for the first evaluated target sector, and differs by approximately 3 dB for the second evaluated target sector. The shapes of the ecdfs also show some deviations but are in general representing the same shape. Since the trial data is also the result of a system-level like simulation campaign it is difficult to tell why these differences arise. However, one of the main reasons is likely that the developed system-level simulator of Chapter 4 does not take any traffic modeling into account. The mobilkom austria AG data includes a traffic weighting as a function of the position that directly influences the resulting CPICH $E_{\mathrm{c}}/I_{\mathrm{oc}}$ distribution.

Nevertheless, the ecdf comparison shows that the system-level simulator is able to produce comparable CPICH results thus indicating that the propagation and network deployment modeling is suitable for mobilkom austria AG needs.

A.14. SINR Optimality of Interfernce-Aware MMSE Equalizer

To show that the developed interference-aware MMSE receiver is maximizing the SINR, given some side-constraints, let me note that Equation (5.8) can be written as

$$
\tilde{\mathbf{y}}_i = \mathbf{H}_{\mathrm{w}} \tilde{\mathbf{x}}_i + \tilde{\mathbf{n}}_i = \underbrace{\sum_{u=1}^{U} \mathbf{H}_{\mathrm{w}}^{(u)} \tilde{\mathbf{x}}_i^{(u)}}_{\text{user data}} + \underbrace{\sum_{p=1}^{2} \mathbf{H}_{\mathrm{w}}^{(U+p)} \mathbf{p}_i^{(p)}}_{\text{pilot data}} + \tilde{\mathbf{n}}_i, \tag{A.30}
$$

with

$$
\mathbf{H}_{\mathrm{w}} = \left[\ \underbrace{\mathbf{H}_{\mathrm{w}}^{(1)}, \dots, \mathbf{H}_{\mathrm{w}}^{(U)}}_{\text{user channels}}, \underbrace{\mathbf{H}_{\mathrm{w}}^{(U+1)}, \mathbf{H}_{\mathrm{w}}^{(U+2)}}_{\text{pilot channels}} \ \right]. \tag{A.31}
$$

For simplicity, let me assume that the transmit signal covariance matrix is given by the identity matrix and that the noise covariance matrix is given by the scaled identity matrix $N_0 \mathbf{I}$. This does not impose too restrictive constraints, since the power allocation can always be represented by a suitable choice of the power coefficients $\alpha^{(u)}$ and $\alpha^{(\mathrm{p})}$.

If the inter-cell interference is neglected, the SINR of the desired user $u = 1$ as given in Equation (5.27) can then also be expressed as

$$
\mathrm{SINR} = \frac{\overbrace{\mathrm{SF} \left| \mathbf{f}^{\mathrm{H}} \mathbf{H}_{\mathrm{w}}^{(1)} \mathbf{e}_\tau \right|^2}^{\triangleq S}}{\underbrace{\left\| \mathbf{f}^{\mathrm{H}} \mathbf{H}_{\mathrm{w}}^{(1)} \right\|^2 - \left| \mathbf{f}^{\mathrm{H}} \mathbf{H}_{\mathrm{w}}^{(1)} \mathbf{e}_\tau \right|^2}_{\triangleq I_1, = f_{\text{self}}} + \underbrace{\sum_{u=2}^{U} \left\| \mathbf{f}^{\mathrm{H}} \mathbf{H}_{\mathrm{w}}^{(u)} \right\|^2}_{\triangleq I_2, = f_{\text{other}}} + \underbrace{\sum_{p=1}^{2} \left\| \mathbf{f}^{\mathrm{H}} \mathbf{H}_{\mathrm{w}}^{(U+p)} \right\|^2}_{\triangleq I_3} + \underbrace{\left\| \mathbf{f} \right\|^2 N_0}_{I_{\mathrm{N}}}}, \tag{A.32}
$$

where I additionally included the interference caused by the pilot channels. By considering

$$
X \triangleq \frac{S}{S + I_1 + I_2 + I_3 + I_{\mathrm{N}}} = \frac{\frac{S}{I_1 + I_2 + I_3 + I_{\mathrm{N}}}}{\frac{S}{I_1 + I_2 + I_3 + I_{\mathrm{N}}} + 1} = \frac{\mathrm{SINR}}{\mathrm{SINR} + 1} \le 1, \tag{A.33}
$$

the SINR can be written as $\mathrm{SINR} = X/(1 - X)$, and accordingly maximizing X will maximize the SINR. Consequently, the SINR maximizing optimum receiver is given by the optimization problem

$$
\mathbf{f}^{\mathrm{opt}} = \max_{\mathbf{f}} \frac{\left| \mathbf{f}^{\mathrm{H}} \mathbf{H}_{\mathrm{w}}^{(1)} \mathbf{e}_\tau \right|^2}{\left\| \mathbf{f}^{\mathrm{H}} \mathbf{H}_{\mathrm{w}}^{(1)} \right\|^2 + \sum_{u=2}^{U} \left\| \mathbf{f}^{\mathrm{H}} \mathbf{H}_{\mathrm{w}}^{(u)} \right\|^2 + \sum_{p=1}^{2} \left\| \mathbf{f}^{\mathrm{H}} \mathbf{H}_{\mathrm{w}}^{(U+p)} \right\|^2 + \left\| \mathbf{f} \right\|^2 N_0}, \tag{A.34}
$$

since the multiplicative factor SF can be neglected. By rewriting, one can obtain

$$
\mathbf{f}^{\mathrm{opt}} = \max_{\mathbf{f}} \frac{\overbrace{\mathbf{f}^{\mathrm{H}} \mathbf{H}_{\mathrm{w}}^{(1)} \mathbf{e}_{\tau} \mathbf{e}_{\tau}^{\mathrm{H}} \left(\mathbf{H}_{\mathrm{w}}^{(1)}\right)^{\mathrm{H}} \mathbf{f}}^{\triangleq \mathbf{A}}}{\mathbf{f}^{\mathrm{H}} \underbrace{\left[\sum_{u=1}^{U} \mathbf{H}_{\mathrm{w}}^{(u)} \left(\mathbf{H}_{\mathrm{w}}^{(u)}\right)^{\mathrm{H}} + \sum_{p=1}^{2} \mathbf{H}_{\mathrm{w}}^{(U+p)} \left(\mathbf{H}_{\mathrm{w}}^{(U+p)}\right)^{\mathrm{H}} + N_0 \mathbf{I}\right]}_{\triangleq \mathbf{B} = [\mathbf{H}_{\mathrm{w}} \mathbf{H}_{\mathrm{w}}^{\mathrm{H}} + N_0 \mathbf{I}]} \mathbf{f}}. \tag{A.35}
$$

This is a problem of the form $\max_{\mathbf{x}} \mathbf{x}^{\mathrm{H}} \mathbf{A} \mathbf{x} / \left(\mathbf{x}^{\mathrm{H}} \mathbf{B} \mathbf{x}\right)$, which if $\mathbf{B}$ is Hermitian[11] can be formulated as

$$
\max_{\mathbf{f}} \frac{\mathbf{f}^{\mathrm{H}} \mathbf{A} \mathbf{f}}{\mathbf{f}^{\mathrm{H}} \mathbf{B} \mathbf{f}} = \max_{\mathbf{f}} \frac{\mathbf{f}^{\mathrm{H}} \mathbf{A} \mathbf{f}}{(\mathbf{C} \mathbf{f})^{\mathrm{H}} \mathbf{C} \mathbf{f}} \xrightarrow{\tilde{\mathbf{f}} \triangleq \mathbf{C} \mathbf{f}} \max_{\tilde{\mathbf{f}}} \frac{\tilde{\mathbf{f}}^{\mathrm{H}} \left(\mathbf{C}^{\mathrm{H}}\right)^{-1} \mathbf{A} \mathbf{C}^{-1} \tilde{\mathbf{f}}}{\tilde{\mathbf{f}}^{\mathrm{H}} \tilde{\mathbf{f}}}. \tag{A.36}
$$

Now note that $\mathbf{A}$ is of rank one, and since rank $\mathbf{A} \mathbf{C} = \min(\text{rank } \mathbf{A}, \text{rank } \mathbf{C})$, thus $(\mathbf{C}^{\mathrm{H}})^{-1} \mathbf{A} \mathbf{C}^{-1}$ is of rank one as well. Accordingly, the Rayleigh coefficient in Equation (A.36) has a distinct solution, given by

$$
\tilde{\mathbf{f}}^{\mathrm{opt}} = \left(\mathbf{C}^{\mathrm{H}}\right)^{-1} \mathbf{H}_{\mathrm{w}}^{(1)} \mathbf{e}_{\tau} \Rightarrow \mathbf{f}^{\mathrm{opt}} = \mathbf{C}^{-1} \tilde{\mathbf{f}} = \mathbf{B}^{-1} \mathbf{H}_{\mathrm{w}}^{(1)} \mathbf{e}_{\tau} = \left[\mathbf{H}_{\mathrm{w}} \mathbf{H}_{\mathrm{w}}^{\mathrm{H}} + N_0 \mathbf{I}\right]^{-1} \mathbf{H}_{\mathrm{w}}^{(1)} \mathbf{e}_{\tau}, \tag{A.37}
$$

which is—given the assumptions of this section—equal to the solution in Equation (5.22), thus proving the intra-cell SINR optimality of the proposed interference-aware equalizer.

A.15. List of Most Important System-Level Simulator Settings

The following table lists some of the most important parameters of the MIMO HSDPA system-level simulator described in Chapter 4. All relevant settings of the current implementation status can be found in the file `load_dtxaa_parameters.m`.

Parameter	Description
NodeB distance	Configures the NodeB distance in case of a standard network scenario
Theta 3 dB	Specifies the 3 dB beamwidth of the sector antennas
Antenna gain	Specifies the gain in dBi of the sector antennas
Environment	Determines the simulated environment when a standardized network scenario is generated, options: urban micro and urban macro
UMTS chiprate	CDMA chiprate, 3.84 Mchips/s in general
Carrier frequency	Frequency of the HSDPA carrier
Nr. of simulated users	Total number of simulated users in the target sector
D-TxAA operation active	Determines wether double-stream D-TxAA can be utilized by the network

---

[11] Note that when $\mathbf{B}$ is Hermitian it can be represented by $\mathbf{B} = \mathbf{C}^{\mathrm{H}} \mathbf{C}$, and if $\mathbf{B}$ is of full rank, so is $\mathbf{C}$. Both statements follow directly from a SVD contemplation of $\mathbf{B}$.

Parameter	Description
Nr. of available HS-PDSCHs	Specifies the number of spreading sequences available for HSDPA operation
Max. NodeB output power	Determines the maximum NodeB output power
CPICH power	Specifies the transmission power of the CPICH, in the MIMO case the power spent for both CPICH
Other channels power	Determines the transmission power of all other signaling and feedback channels
Nr. of samples	Specifies the number of simulated samples in slots and thus the simulation length
Feedback delay	Determines the delay of the the UE feedback to arrive at the NodeB entity in the simulator
Max. nr. of retransmissions	Limits the maximum number of retransmissions available for the NodeB before marking a packet as non-deliverable
Scheduler type	Sets the utilized scheduler, depending on the scheduler class some further parameters then define its behavior
Nr. of transmit antennas	—
Nr. of receive antennas	—
UE capability class	Specifies the UE capabilities in terms of maximum throughput, retransmission combining and MIMO capabilities. See also Chapter 2 for further details.
UE speed	Determines the speed of the UEs for the movement through the sector
Receiver type	Specifies the receiver type of the UE, options: MMSE and Rake
Equalizer span	Specifies the length of the receive filter for all simulated UEs
Equalizer delay	Specifies the delay of the receive filter for all simulated UEs

Appendix B.

Further System-Level Modeling, Simulations, Optimizations, and Validation

> You have to lay the groundwork ahead of time. If you haven't done that, do it now.
>
> *(Lee Miller)*

HIGH speed data transmissions in wireless networks have effectively been enabled already with the introduction of Release 5 HSDPA. Mobile wireless network operators have SISO HSDPA networks deployed in many countries with different maximum up- and downlink speeds, see Chapter 2 for more information hereon. Accordingly, although SISO HSDPA has been actively been researched for many years now, some open questions still remain to be of interest, especially in the network context.

This thesis has been funded by one of the major network operators in Austria, the mobilkom austria AG,[1] which currently has the largest HSDPA deployment in Austria. Parts of the work presented in this chapter also were of particular interest for their network deployment in 2006 and 2007, when I started working as a doctoral candidate.

The consolidated findings of the work recapitulated in this chapter furthermore was very helpful in building the basic groundwork for the development of the more advanced system-level models in Chapter 3, as well as the practical implementation of the system-level simulator in Chapter 4 and the optimizations carried out with it. The presented work was partly published at international conferences [15, 26], but it has to be noted that not always every single aspect has been deeply investigated due to the fact that MIMO techniques became the more important focus.

Finally, let me point out that the following sections contribute to a deeper understanding of the HSDPA performance in today's networks, even for the MIMO enhancements. Accordingly, I intended to include these to round-off the concept of this thesis.

B.1. Mixed Traffic Optimization for SISO HSDPA

As mentioned in Chapter 2, HSDPA is designed so that it can be operated within an existing 5 MHz band that is already utilized by Release 4 DCHs, thus allowing for sharing the power amplifier at the Node-B. Accordingly, one part of the available Node-B power and spreading codes is used for the DCHs and another part can be used for the HSDPA operation. This specific mode of operation is of particular interest for the network operators in the phase of the

---

[1]AG is the German term for a public cooperation.

HSDPA deployment, and even if HSDPA is widely installed, a mixed carrier operation is more cost-efficient for cells that are not fully loaded.

Despite the significance of the study of the network performance behavior in such a scenario, not much work has been performed in order to assess the average user throughput, the total cell throughput, or to derive specific recommendations for the network planning process. The available work discusses only a very limited part of the whole topic, for example [67], where only the ITU VehA channel profile has been considered. This is a fairly unusual since most of the HSDPA traffic occurring in a network will be requested by slowly moving UEs.

A big difference in the work presented in this section compared to Chapters 3 and 4 is that the simulation approach is *snapshot*-based. This means that no correlation in time is considered, but the rather a snapshot of the current network state is evaluated. By averaging over multiple of those snapshots, each with individual and independent channel realizations, the average network performance can be evaluated. However, such a modeling approach has the drawback that no enhanced scheduling mechanisms—which implicitly build upon the correlation of the channel in time—can be assessed. Nevertheless, the average results presented remain valid for RR schedulers that do not take the reported CQI feedback into account.[2]

B.1.1. System Model

Channel Modeling

The radio propagation model throughout Appendix B.1 considers basically three different parts: macro-scale path-loss λ_{m}, shadow fading λ_{s}, and small-scale fading with multiple paths and no correlation in time. This corresponds to the restriction of the simulator to conduct only snapshot simulations. Accordingly, the channel between the base station and the user equipment can be written as

$$h_i = \lambda_{\mathrm{m}} \cdot \lambda_{\mathrm{s}} \cdot \sum_{l=1}^{L_{\mathrm{h}}} \sqrt{p_l} \cdot r_l \cdot \delta_{i-i_l}, \tag{B.1}$$

where the random variables r_l represent L_{h} independent Rayleigh fading processes at fixed time slots, δ denotes the Dirac function and p_l, i_l are the relative power and delay of the multipath components, according to the ITU channel profiles [159]. In contrast to Chapter 3, L_{h} denotes the number of taps of the channel.

The macro-scale path-loss λ_{m} depends only on the distance d between the base station and the user equipment, which I model according to the COST 231 Model [112]. The shadow fading λ_{s} is modelled by a lognormal random variable with zero mean and variance $\sigma_{\lambda_{\mathrm{s}}}^2 = 8\,\mathrm{dB}$, with no correlation in time.

HSDPA Modeling

The necessary system-level modeling here is again split into a link-quality model and a link-performance model, as described in Chapter 3. For deriving the link-quality model, I assumed a

---

[2]The system-level simulator developed with the modeling and assumptions presented in this section formed the first implementation of a system-level simulator for HSDPA networks. However after having the system-level model for MIMO HSDPA as presented in Chapter 3 developed, a new and more flexible simulator architecture was implemented that succeeded this first version. Nevertheless, besides the work presented here, the SISO HSDPA system-level simulator proofed to be valuable for other investigations as well [188, 189].

single antenna Rake receiver at the UE side.[3]

As channel quality metric I considered the SINR after Rake-combining and despreading on symbol-level combined at the despreader outputs for each active user u in the cell, according to

$$\text{SINR}^{(u)} = \sum_{m=1}^{N_{\text{F}}} \frac{\text{SF} \cdot \frac{P^{\text{HS-DSCH}}}{\gamma} \cdot |h_m|^2}{P^{\text{intra, residual}} + P^{\text{inter}} + P^{\text{noise}}}, \tag{B.2}$$

where SF = 16 denotes the spreading factor, $P^{\text{HS-DSCH}}$ is the power used for transmitting the HS-DSCH, $P^{\text{intra, residual}}$ and P^{inter} represent the residual intracell interference in the downlink and the transmitted interfering power from the neighbouring base stations, respectively, and P^{noise} denotes the noise power as seen at the receiver. The residual intracell interference after Rake processing, arriving at the receiver from the serving base station, is given by [78],

$$P^{\text{intra,residual}} = P^{\text{intra}} \cdot \sum_{\substack{l=1 \\ l \neq k}}^{L_{\text{h}}} |h_l|^2, \tag{B.3}$$

where h_l denotes the current channel realisation, and P^{intra} is the total power transmitted in the serving cell.

The structure of the Rake receiver is implicitly reflected in Equation Equation (B.2), because the useful signal power in the numerator is added up whereas in the denominator it is cancelled out from the interference power, which is consecutively done for all N_{F} available fingers. I assume perfect CSI at the receiver so that the receiver weights and the location of the fingers can be chosen perfectly. Accordingly, only the squared absolute values of the channel coefficients for each tap, $|h_i|^2$ occur in the equation. Furthermore, I assume that the transmission power of the HS-DSCH is divided equally between all used HS-PDSCHs,

$$P_k^{\text{HS-PDSCH}} \equiv P^{\text{HS-PDSCH}} = P^{\text{HS-DSCH}}/\gamma, \tag{B.4}$$

with $\gamma = 1, \ldots, 15$ representing the number of assigned spreading codes.[4]

For the link-performance model, I chose an analytical approach based on link-level simulations, as in [190]. In principle, link-level simulations have been used to provide a limited number of points in an SINR versus BLER plot for a specific transport format. In the simulations, I consider the case that the desired user for HSDPA traffic always gets the full available transmission power, and there is enough data to transmit. This is often referred to as full buffer assumption. Accordingly, I assume that the scheduler in the NodeB decides to serve the user with the transport format that is specified by the reported CQI. Thus only a link performance modelling for the transport formats of each mobile category class, given by the possible CQI values is needed. As for example in [191], it turns out that under AWGN conditions, the link-level results, utilizing a standard Rake receiver together with Turbo coding, can analytically be well approximated by

$$\text{BLER} = \left\{ 10^{\left(2^{\frac{\text{SINR} - 1.03\text{CQI} + 5.26}{\sqrt{3} - \log_{10} \text{CQI}}} \right)} + 1 \right\}^{-\frac{1}{0.7}}, \tag{B.5}$$

---

[3]The Rake receiver is still heavily used for SISO HSDPA devices, at least for UE capability classes supporting a speed of up to 3.6 Mbit/s.

[4]Note that γ corresponds to the cardinality of the spreading code set Φ_0 in Chapter 3.
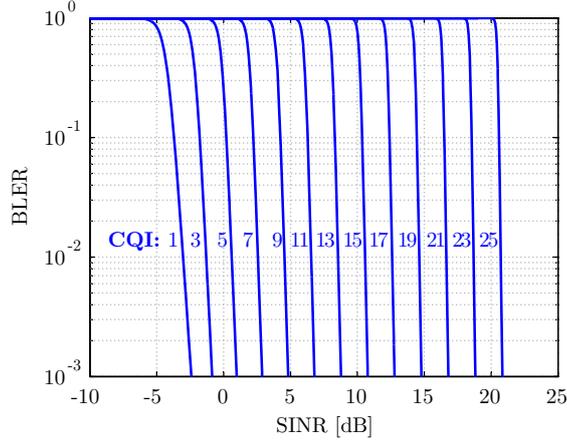
Figure B.1.: Analytical fit of the BLER versus SINR relation under AWGN conditions for different CQI values if a standard Rake receiver and turbo coding is utilized.

where in contrast to [191], I use the post-despreading symbol-level SINR, as defined in Equation (B.2). The coding rate of the turbo-code has been varied from 0.21 to 0.75 in the link-level simulations to reflect typical coding rates for the different CQI values [39].

Figure B.1 depicts the relation between the SINR and the BLER for all uneven CQI values. Furthermore, it has to be noted that due to the snapshot based simulation approach chosen, the HARQ retransmission gains were not modeled, in contrast to the modeling in Chapter 3.

Release 4 modeling

To predict the achievable cell throughput, also a Release 4 model is developed. The whole network traffic generated by the DCHs is described by the current load situation of the cell, given by the transmission power value P^{DCH}. Of course, this prevents an exact modeling of the fast power control of the users since P_{DCH} just describes the average transmission power.

An almost suitable concept for the model is explained in [3], where the estimation of the average needed base station transmission power for a given DCH traffic based on the downlink load factor is investigated. I adapted the idea therein to obtain a suitable description.

According to [192], the link quality equation for Release 4 DCH downlink connections, in a cell b, is given by

$$\varrho^{(u)} = \frac{W p^{(u)} \frac{1}{L_{b,u}}}{R^{(u)} \left[\left(1 - \beta^{(u)}\right) \cdot \frac{P^{\mathrm{intra}}}{L_{b,u}} + P^{\mathrm{intra}} \cdot \sum_{\substack{b'=1 \\ b' \neq b}}^{B} \frac{1}{L_{b',u}} + P^{\mathrm{noise}} \right]}, \tag{B.6}$$

where $\varrho^{(u)}$ denotes the required bit level SINR, E_{b}/N_0, for a specific user u, requesting a service with bit rate $R^{(u)}$. The chip rate of the system is given by W, $L_{b,u}$ represents the path loss of base station b to DCH user u, $\beta^{(u)}$ stands for the orthogonality factor as observed by user u, P^{intra} is the total transmit power of the base-station, and P^{noise} stands for the received thermal noise power. The total number of considered base stations is given by B. The main interest here is $p^{(u)}$, representing the required transmission power of base station b in order to supply user u

with the defined service. The sum of it equals the DCH cell load,

$$\sum_{u=1}^{U} p^{(u)} = P^{\text{DCH}}, \tag{B.7}$$

with U denoting the total number of active DCH users in the cell.

For modeling purpose, let me assume the same service for all DCH users in the cell, given by the required bit level SINR and the requested rate,

$$\varrho^{(u)} \equiv \varrho, \quad R^{(u)} \equiv R. \tag{B.8}$$

In analogy to [3], I furthermore introduce the own cell to other cell interference ratio, given by

$$\mathcal{O} = \sum_{\substack{b'=1 \\ b' \neq b}}^{B} \frac{L_{b,u}}{L_{b',u}}. \tag{B.9}$$

Since the DCH users should not be modeled explicitly, I substituted $\mathcal{O}$ and $L_{b,u}$ by their averages over the cell area

$$\mathcal{O} \to \bar{\mathcal{O}}, \quad L_{b,u} \to \bar{L}_b. \tag{B.10}$$

The orthogonality factor β can be calculated in a simple way as described in [78],

$$\beta^{(u)} = 1 - \left(\sum_{l=1}^{L_{\text{h}}} \frac{\left| \tilde{h}_l^{(u)} \right|^2}{1 - \left| \tilde{h}_l^{(u)} \right|^2} \right)^{-1}, \tag{B.11}$$

with $\tilde{h}_l^{(u)} = \sqrt{p_l} r_l^{(u)}$ describing the complex valued coefficient of the channel tap l, for each user u, respectively.[5] The user dependency in this case is only introduced because of the small-scale fading channel statistics. In analogy to the simplifications already introduced above, I substitute the orthogonality factor $\beta^{(u)}$ by its average $\bar{\beta}$, which is achieved by using the average channel tap values $\mathbb{E}\left\{|h_l|^2\right\} = p_l$, determined by the ITU channel profiles.

With this simplifications, and after some algebra, the number of DCH users that can be served given a specific data rate can be derived to be

$$U = \frac{P^{\text{DCH}}}{P^{\text{intra}} \cdot \frac{\varrho R}{W} \cdot \left[(1 - \bar{\beta}) + \bar{\mathcal{O}} \right] + P^{\text{noise}} \cdot \frac{\varrho R}{W} \cdot \bar{L}_b}. \tag{B.12}$$

Power split

The total available transmit power in each cell is shared between HSDPA and DCH users. Let me express the total intra-cell transmission power as

$$P^{\text{intra}} = P^{\text{DCH}} + P^{\text{HS-DSCH}} + P^{\text{other}}, \tag{B.13}$$

where P^{other} incorporates the power from other needed common channels, for example the CPICH. Accordingly, both, Equation (B.2) and Equation (B.12) depend on the transmission power of the DCH and the HSDPA traffic.

As described in Chapter 2, there are two different possibilities of allocating the power of HSDPA in the base station downlink power budget [44], and both possibilities will be treated in the following.

---

[5] Note that the channel power normalization requires the sum of the taps to equal one, $\sum_{l=1}^{L_{\text{h}}} |\tilde{h}_l^{(u)}|^2 = 1$.
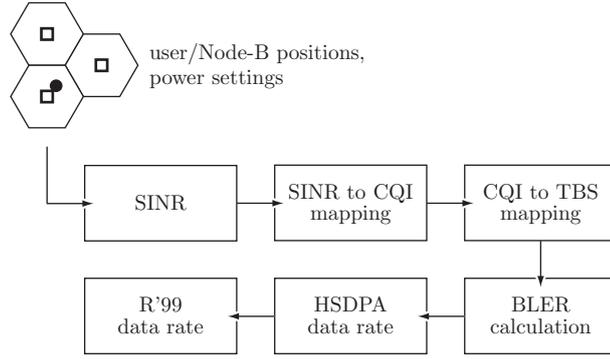
Figure B.2.: Overview of the snapshot based SISO HSDPA system-level simulator.

B.1.2. Simulation Details

Figure B.2 shows a coarse overview of the snapshot system level simulator, as implemented in MATLAB. With a fixed network situation, the SINR can be calculated according to Equation (B.2), which then is mapped to the CQI value that will be reported by the UE that is currently under investigation. The mapping utilized in this section is given by

$$\text{CQI} = \text{SINR[dB]} + 3.5, \tag{B.14}$$

as defined in [39]. The evaluated CQI can then successively be mapped to a TBS, which denotes the maximum amount of data that can be transmitted via the network in one TTI to the UE, without exceeding an average BLER of 0.1 [180]. The HSDPA user data rate can be calculated according to

$$R^{(u)} = \text{TBS} \cdot \frac{1}{2\text{ms}} \cdot (1 - \text{BLER}), \tag{B.15}$$

which is consecutively averaged over fading realizations.

Since I assume that the desired user is served with the transport format according to the reported CQI value, I implicitly also assume that the user gets the full available HSDPA transmission power. This means that no other user is served in parallel. Thus, by averaging over the cell the average user performance within the cell can be evaluated, which I will denote *HSDPA user data rate* in the following. In the simulator, the intercell interference is modelled by assuming a homogeneous network operation, which means that the actual transmission power of the neighbouring NodeBs is chosen exactly equal to the power of the serving NodeB.

The Release 4 data rate is evaluated based on the modeling in Equation (B.12), where the service that is requested by all users is adjusted by the required data rate of it. This means that the average cell data rate can be calculated corresponding to the actual power settings of the network by consecutively multiplying the calculated number of served users by the specified data rate.

Network Model

Due to its general applicability, for SISO HSDPA investigations, I decided in favor of a hexagonal network layout, organized in a serving cell and two rings of neighbouring base stations. This results in a total of 19 cells. This layout is described as *cellular layout 2* in [6]. The antennas
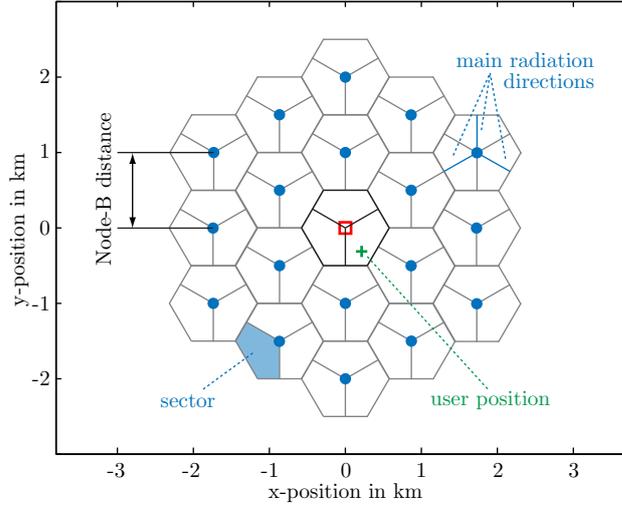
Figure B.3.: Network structure and user positioning within the serving NodeB, defined by an NodeB distance of 1 km.

used at the NodeBs that split the cell area into three sectors are modelled by

$$L^i_{\mathrm{ant}}(\theta^i) = \bar{L}^i_{\mathrm{ant}} \cdot 10^{\left(-\frac{1}{10}\min\left\{12\left(\frac{\theta^i}{70°}\right),20\right\}\right)}, \tag{B.16}$$

where I denoted the mean antenna gain by $\bar{L}^i_{\mathrm{ant}} = 14\mathrm{dBi}$, and the index i represents the sector.

To assess the average cell data rates to the power settings chosen, for each snapshot a large number of users that are distributed with uniform probability within the serving cell are simulated. The users are furthermore only simulated explicitly within the serving cell, all other cells are modelled only by their total transmission power. Figure B.3 illustrates the network structure and the user positioning within one sector.

B.1.3. Results

Let me present the simulation results of the modelled system, which can serve for identifying possible improvements of the performance by adjusting the power and code settings in the network.

RNC controlled HS-DSCH power

First, I performed some simulations with the HS-DSCH power controlled by the RNC and with a fixed Release 4 load. The simulation parameters are given in Table B.1.

The results of a simulation carried out for a Release 4 load[6] of 20 % are depicted in Figure B.4. It can be seen that the average total cell data rates show a maximum around 3.5 W, and the average HSDPA user data rate shows its maximum around 6.5 W of HS-DSCH power.

---

[6]The Release 4 load is defined as fraction of the maximum Node-B power,

$$P^{\mathrm{DCH}} = P^{\mathrm{NodeB,max}} \cdot (\mathrm{R4\ load})/100.$$

Table B.1.: Simulation parameters for the simulations with RNC controlled HS-DSCH power.

Parameter	Value
NodeB distance	$0.75\,\mathrm{km}$
maximum NodeB power	$43\,\mathrm{dBm}$
P^{other}	$33\,\mathrm{dBm}$
shadow fading variance	$8\,\mathrm{dB}$
channel type	ITU PedA
available HS-PDSCH codes	5
HS-DSCH power	variable
UE capability class	6
receiver noise figure	$7\,\mathrm{dB}$
Rake fingers	4
Release 4 load	fixed, $20\,\%$
DCH required service SINR	$\varrho = 5.2\,\mathrm{dB}$
DCH service data rate	$R = 384\,\mathrm{kbit/s}$
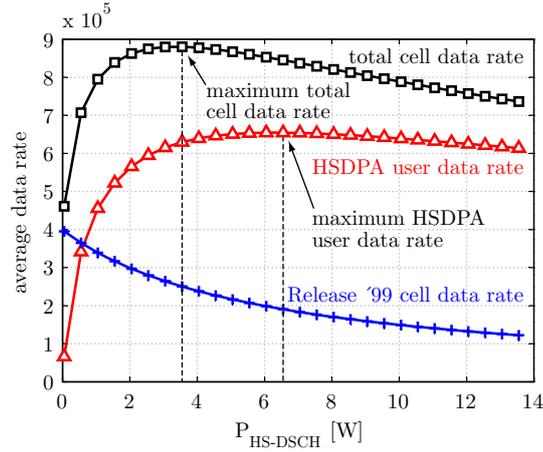
Figure B.4.: Average data rates evaluated according to the simulation settings in Table B.1 with RNC power control of the HS-DSCH.

Therefore, in case that the HS-DSCH power is RNC controlled, the optimum power setting depending on the optimization criteria, which can be either the average HSDPA data rate or the average cell data rate, can be found. Furthermore, it can be seen that in case of an ITU PedA channel profile, HSDPA offers a broad power operating range in which the throughput is nearly optimum.

By running a set of these simulations, I was able to analyse the relation between the HS-DSCH power level, at which the maximum of the average total cell data rate is achieved, and the Release 4 load of the cell. The results are illustrated in Figure B.5, for different NodeB distances. It can be seen that the optimum HS-DSCH power scales with the Release 4 load, but then starts to drop down, which is caused by the limited maximum NodeB transmission power.
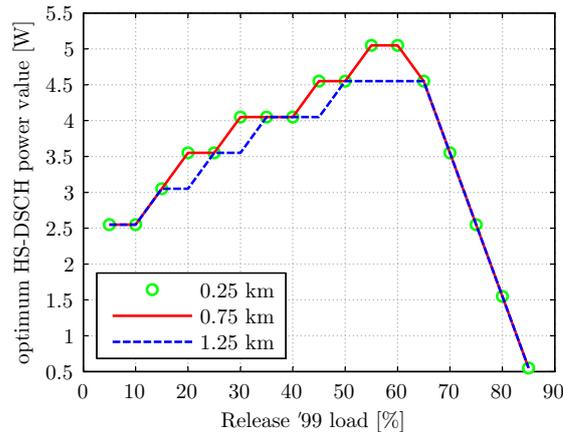
Figure B.5.: Relation between the Release 4 load of the cell, and the according HS-DSCH power that maximizes the average total cell throughput. The simulation parameters are set to those in Table B.1, except for the NodeB distance.

It furthermore can be observed that the resulting curves do not differ a lot for different cell sizes. This is because the transmission powers of the neighbouring cells are equally scaled with the transmission power of the serving NodeB according to the simulation assumptions and thus the shape of the total cell data rate is approximately only shifted up and down, but not further distorted.

NodeB controlled HS-DSCH power

After the investigation of the network performance in case of RNC controlled HS-DSCH power management, I also evaluated the behavior in case of fast NodeB HS-DSCH power control. The simulation parameters are nearly equal to the ones in Table B.1, the only difference being that the Release 4 load is now variable.

The results of the simulations are shown in Figure B.6. In contrast to the situation before, it can be seen that the optimum power distribution—in terms of the total cell data rate—is located at a higher amount of Release 4 traffic. Accordingly, it seems reasonable to *downgrade* users continuously observing a bad channel condition to a 384 kbit/s bearer, which is an optimizing criteria for the RRC algorithms used within the network.

A suitable admission control to the HSDPA would thus always try to balance the Release 4 load such that the total cell throughput for both, Release 4 and HSDPA users would be maximized.

B.2. Link-Quality Model for STTD

As mentioned in Chapter 3, system-level simulations have to rely on simplified physical-layer abstractions that have to be as accurate as possible without loosing their flexibility in terms of scenarios represented.

For this section, I adopted the same system-level modeling principle as described in Chapter 3, however I will only present the link-quality model for the STTD transmission mode. Since Alamouti STTD coding [55], was decided against by the standardization body in Release 7 of HSDPA [6], my research interest in this transmission technique dropped, because the main goal of
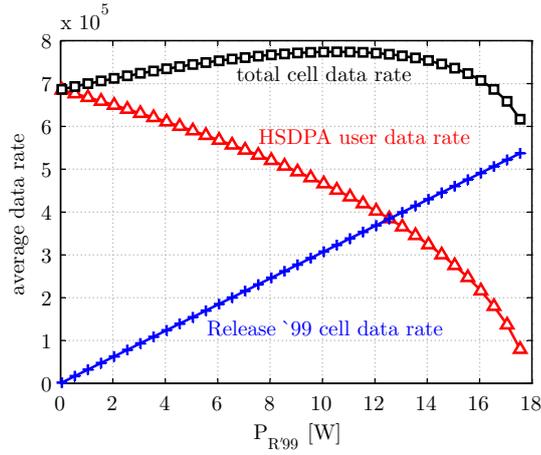
Figure B.6.: Average data rates for fast NodeB power control of the HS-DSCH.

this thesis was to represent the downlink data channel of HSDPA. Nevertheless, the standard [7] allows for the utilization of STTD for the signaling and control channels in HSDPA, like for example the HS-SCCH [34], to gain in transmission reliability.

The link-quality model offers a first step for an accurate system-level modeling of the control channels, which would allow for interesting research of the influence of these channels onto the network performance in the network context. However, since in this work the link-performance modeling part is missing, it has to be noted that in order to apply the findings in a system-level simulator, a link-performance model considering the specific channel coding of the control channels would have to be developed. That being said, some of the findings of the link-quality model nevertheless are important and can serve as a design guideline for the appliance of STTD in networks.

B.2.1. System Model for STTD

The basic system model of a $2 \times N_\mathrm{R}$ STTD system is depicted in Figure B.7. Note that by this system-model I assume the Alamouti encoding to be performed on the symbol level. Another approach would be to perform the Alamouti STBC on chip level, thus after spreading and/or scrambling. The encoded symbols—after channel encoding and symbol mapping—are space-time encoded according to the Alamouti scheme and are then spread and scrambled, with equal sequences for both antennas. Note that this is a similar to Assumption 3.10 in Chapter 3. Furthermore, I also implicitly assumed that Assumption 3.5 of Chapter 3 is fulfilled. The essential assumption behind the Alamouti encoding is that the MIMO channel $\mathbf{H}$ stays constant for the two consecutive channel uses of the Alamouti STBC. At the receiver side, a space-time MMSE equalizer first restores the orthogonality and estimates the sent chip vectors, which are then despread and -scrambled so that the resulting symbols can be space-time decoded by means of Maximum Ratio Combining (MRC).

Let me describe the frequency selective channel matrix by

$$\mathbf{H} = \begin{bmatrix} \mathbf{h}_0^{(1)} & \cdots & \mathbf{h}_{L_\mathrm{h}-1}^{(1)} \\ \vdots & \vdots & \vdots \\ \mathbf{h}_0^{(N_\mathrm{R})} & \cdots & \mathbf{h}_{L_\mathrm{h}-1}^{(N_\mathrm{R})} \end{bmatrix}, \tag{B.17}$$
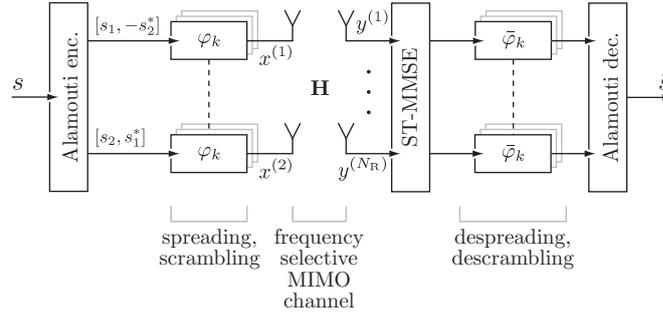
Figure B.7.: Basic system model of a $2 \times N_\mathrm{R}$ Alamouti encoded MIMO HSDPA transmission.

where each vector $\mathbf{h}_l^{(n_\mathrm{r})} = \begin{bmatrix} h_l^{(1,n_\mathrm{r})} & h_l^{(2,n_\mathrm{r})} \end{bmatrix}$ comprises the channel coefficients from transmit antenna 1 and 2 to receive antenna $n_\mathrm{r} = 1, \ldots, N_\mathrm{R}$ as observed on multipath component $l = 0, \ldots, L_\mathrm{h} - 1$.[7] Accordingly, the transmitted chips can be described by the vector

$$\mathbf{x}_i = \begin{bmatrix} x_i^{(1)} & x_i^{(2)} & \cdots & x_{i-L_\mathrm{h}+1}^{(1)} & x_{i-L_\mathrm{h}+1}^{(2)} \end{bmatrix}^\mathrm{T}, \tag{B.18}$$

so that the input-output relation can be written in the form

$$\mathbf{y}_i = \begin{bmatrix} y_i^{(1)} & \cdots & y_i^{(N_\mathrm{R})} \end{bmatrix}^\mathrm{T} = \mathbf{H}\mathbf{x}_i + \mathbf{n}_i. \tag{B.19}$$

Here, the vector $\mathbf{n}_i = \begin{bmatrix} n_i^{(1)} & \cdots & n_i^{(N_\mathrm{R})} \end{bmatrix}^\mathrm{T}$ describes additive white Gaussian noise.

For the evaluation of the MMSE equalizer, the input-output relation can be stacked, similar to the procedure in Section 3.3.1. The resulting input-output relation then is similar to the one in Equation (3.11),

$$\tilde{\mathbf{y}}_i = \tilde{\mathbf{H}}\tilde{\mathbf{x}}_i + \tilde{\mathbf{n}}_i, \tag{B.20}$$

with the *stacked* MIMO channel matrix being defined as

$$\tilde{\mathbf{H}} = \begin{bmatrix} \mathbf{H} & \mathbf{0}_{N_\mathrm{R} \times 2} & \cdots & \mathbf{0}_{N_\mathrm{R} \times 2} \\ \mathbf{0}_{N_\mathrm{R} \times 2} & \mathbf{H} & \ddots & \vdots \\ \vdots & \ddots & \ddots & \mathbf{0}_{N_\mathrm{R} \times 2} \\ \mathbf{0}_{N_\mathrm{R} \times 2} & \cdots & \mathbf{0}_{N_\mathrm{R} \times 2} & \mathbf{H} \end{bmatrix}. \tag{B.21}$$

Note that in contrast to Equation (3.11), this does not include any pre-coding.

Accordingly, the MMSE receive filter is the result of the Wiener-Hopf equation, see Equation (3.14)

$$\mathbf{F} = \mathbf{R}_{\mathbf{x}_{i-\tau}^\mathrm{S} \tilde{\mathbf{x}}_i} \tilde{\mathbf{H}}^\mathrm{H} \left(\tilde{\mathbf{H}} \mathbf{R}_{\tilde{\mathbf{x}}_i} \tilde{\mathbf{H}}^\mathrm{H} + \mathbf{R}_{\tilde{\mathbf{n}}_i} \right)^{-1}. \tag{B.22}$$

B.2.2. Computationally Efficient Link-Quality Model

The basic arguments for forming the receive signal in a multi-cell, multi-user context, as described in Section 3.3.2 also applies in the context of this modeling. However, for the Alamouti STBC

---

[7]Note that this effectively limits the applicability of the model to the two transmit antenna case, $N_\mathrm{T} = 2$. However, since Alamouti STBC is suboptimal for more than two transmit antennas anyways [53, 193], this coding scheme would most probably not used at all thus not imposing a too great restriction.

encoding transmission, the transmit vectors of two consecutive channel uses are

$$1: \quad \mathbf{x}_i = \begin{bmatrix} x_i^{(1)} & x_i^{(2)} & \cdots & x_{i-L_{\mathrm{f}}-L_{\mathrm{h}}+2}^{(2)} \end{bmatrix}^{\mathrm{T}}, \tag{B.23}$$

$$2: \quad \mathbf{x}_{i'} = \begin{bmatrix} -\left(x_{i'}^{(2)}\right)^* & \left(x_{i'}^{(1)}\right)^* & \cdots & \left(x_{i'-L_{\mathrm{f}}-L_{\mathrm{h}}+2}^{(1)}\right)^* \end{bmatrix}^{\mathrm{T}}, \tag{B.24}$$

where $i' = i + \mathrm{SF}$ denotes the chip stream index at which the second channel use—on symbol level—begins, with SF denoting the chosen spreading code length. Accordingly, those two vectors may partly overlap.

At the receiver, the estimated chips are despreaded and -scrambled. Afterwards, the received symbols are coherently combined by means of MRC and then quantized and decoded. Due to the linearity of the despreading and -scrambling, the coherent combining can also be conducted in the chip domain. This means that in Figure B.7 the descrambling and -spreading changes places with the Alamouti decoder. Thus, the output of the Alamouti decoder, neglecting the noise term, is given by

$$
\begin{aligned}
\hat{\hat{x}}_i^{(1)} &= \frac{\hat{x}_i^{(1)} - \left(\hat{x}_{i'}^{(2)}\right)^*}{2} \\
&= \frac{1}{2}\left[\sum_{m=0}^{2(L_{\mathrm{f}}+L_{\mathrm{h}}-1)-1} \left(\mathbf{f}^{(1)}\right)^{\mathrm{T}} \mathbf{h}_m x_{i-\lfloor m/2 \rfloor}^{(\lfloor m/2 \rfloor)} - \sum_{m=0}^{2(L_{\mathrm{f}}+L_{\mathrm{h}}-1)-1} \left(\left(\mathbf{f}^{(2)}\right)^{\mathrm{T}} \mathbf{h}_m\right)^* \left(x_{i'-\lfloor m/2 \rfloor}^{(\lfloor m/2 \rfloor)}\right)^*\right],
\end{aligned}
\tag{B.25}
$$

and

$$
\begin{aligned}
\hat{\hat{x}}_i^{(2)} &= \frac{\hat{x}_i^{(2)} + \left(\hat{x}_{i'}^{(1)}\right)^*}{2} \\
&= \frac{1}{2}\left[\sum_{m=0}^{2(L_{\mathrm{f}}+L_{\mathrm{h}}-1)-1} \left(\mathbf{f}^{(2)}\right)^{\mathrm{T}} \mathbf{h}_m x_{i-\lfloor m/2 \rfloor}^{(\lfloor m/2 \rfloor)} + \sum_{m=0}^{2(L_{\mathrm{f}}+L_{\mathrm{h}}-1)-1} \left(\left(\mathbf{f}^{(1)}\right)^{\mathrm{T}} \mathbf{h}_m\right)^* \left(x_{i'-\lfloor m/2 \rfloor}^{(\lfloor m/2 \rfloor)}\right)^*\right],
\end{aligned}
\tag{B.26}
$$

where I omitted denoting the user base-station index pair (u, b) as well as the utilized spreading and scrambling code pair (φ_k, ψ) as used in Chapter 3 for sake of notational simplicity.

For the link-measurement model, however, only the resulting power of the estimated chip sequences is of interest. By assuming that the channel stays constant over the two consecutive channel uses and that there is no power loading of the individual transmit antennas, it follows that the power of the two estimated chip streams $\hat{\hat{x}}_i^{(1)}$ and $\hat{\hat{x}}_i^{(2)}$ is respectively given by

$$
P_x = \frac{1}{4} \sum_{m=0}^{2(E+L-1)-1} \left[\left|\left(\mathbf{f}^{(1)}\right)^{\mathrm{T}} \mathbf{h}_m\right|^2 + \left|\left(\mathbf{f}^{(2)}\right)^{\mathrm{T}} \mathbf{h}_m\right|^2\right] \sigma_x^2. \tag{B.27}
$$

Similar to the arguments in Chapter 3, the total received power can then be segmented into different interference terms,[8] in particular

---

[8] Note that for these expressions, it is necessary to include the user base-station index pair, (u, b) to denote the channels that are carrying the corresponding transmit signals.

- the desired signal power,

$$P^{\mathrm{s}} = \frac{1}{4}\left[\left|\left(\mathbf{f}^{(1)}\right)^{\mathrm{T}}\mathbf{h}_{2\tau}^{(u_0,b_0)}\right|^2 + \left|\left(\mathbf{f}^{(2)}\right)^{\mathrm{T}}\mathbf{h}_{2\tau+1}^{(u_0,b_0)}\right|^2\right]P_{\varphi_k}^{(u_0,b_0)}, \tag{B.28}$$

- the intersymbol interference,

$$P^{\mathrm{INT}} = \frac{1}{4}\left[\left|\left(\mathbf{f}^{(1)}\right)^{\mathrm{T}}\mathbf{h}_{2\tau+1}^{(u_0,b_0)}\right|^2 + \left|\left(\mathbf{f}^{(2)}\right)^{\mathrm{T}}\mathbf{h}_{2\tau}^{(u_0,b_0)}\right|^2\right]P_{\varphi_k}^{(u_0,b_0)}, \tag{B.29}$$

- the intra-cell interference,

$$P^{\mathrm{intra}} = \frac{1}{4}\sum_{\substack{m=0 \\ m\neq[2\tau,2\tau+1]}}^{2(L_{\mathrm{f}}+L_{\mathrm{h}}-1)-1}\left[\left|\left(\mathbf{f}^{(1)}\right)^{\mathrm{T}}\mathbf{h}_{m}^{(u_0,b_0)}\right|^2 + \left|\left(\mathbf{f}^{(2)}\right)^{\mathrm{T}}\mathbf{h}_{m}^{(u_0,b_0)}\right|^2\right]\cdot\sum_{u=0}^{U(b_0)}P^{(u,b_0)}, \tag{B.30}$$

- and the inter-cell interference,

$$P^{\mathrm{inter}} = \sum_{\substack{b=1 \\ b\neq b_0}}^{B}\frac{1}{4}\sum_{m=0}^{2(L_{\mathrm{f}}+L_{\mathrm{h}}-1)-1}\left[\left|\left(\mathbf{f}^{(1)}\right)^{\mathrm{T}}\mathbf{h}_{m}^{(u_0,b)}\right|^2 + \left|\left(\mathbf{f}^{(2)}\right)^{\mathrm{T}}\mathbf{h}_{m}^{(u_0,b)}\right|^2\right]\cdot\sum_{u=0}^{U(b)}P^{(u,b)} \tag{B.31}$$

In concordance with Chapter 3, $P_{\varphi_k}^{(u,b)}$ denotes the transmit power spent for user u from base-station b on spreading code φ_k.

The four power terms together with the thermal noise power P^{noise}—which can be calculated as described in Chapter 3—then form the desired SINR per spreading code on symbol level after equalization and despreading/descrambling,

$$\mathrm{SINR}_{\varphi_k} =$$

$$\frac{\mathrm{SF}\cdot G^{\mathrm{s}}\cdot P_{\varphi_k}^{(u_0,b_0)}\frac{1}{L^{(b_0)}}}{\mathrm{SF}\cdot o^{\mathrm{INT}}P_{\varphi_k}^{(u_0,b_0)}\frac{1}{L^{(b_0)}} + o^{\mathrm{intra}}\frac{1}{L^{(b_0)}}\cdot\sum_{u=0}^{U(b_0)}P_{\varphi_k}^{(u,b_0)} + \sum_{\substack{b=1 \\ b\neq b_0}}^{B}\frac{1}{L^{(b)}}G_b^{\mathrm{inter}}\cdot\sum_{u=0}^{U(b)}P_{\varphi_k}^{(u,b)} + P^{\mathrm{noise}}}, \tag{B.32}$$

where I defined the following equivalent fading parameters:

- the equivalent fading parameter of the desired signal,

$$G^{\mathrm{s}} \triangleq \frac{1}{4}\left[\left|\left(\mathbf{f}^{(1)}\right)^{\mathrm{T}}\mathbf{h}_{2\tau}^{(u_0,b_0)}\right|^2 + \left|\left(\mathbf{f}^{(2)}\right)^{\mathrm{T}}\mathbf{h}_{2\tau+1}^{(u_0,b_0)}\right|^2\right], \tag{B.33}$$

- the equivalent fading parameter of the intersymbol interference,

$$o^{\mathrm{INT}} \triangleq frac14\left[\left|\left(\mathbf{f}^{(1)}\right)^{\mathrm{T}}\mathbf{h}_{2\tau+1}^{(u_0,b_0)}\right|^2 + \left|\left(\mathbf{f}^{(2)}\right)^{\mathrm{T}}\mathbf{h}_{2\tau}^{(u_0,b_0)}\right|^2\right], \tag{B.34}$$

- the equivalent fading parameter of the intra-cell interference,

$$o^{\mathrm{intra}} \triangleq \frac{1}{4}\sum_{\substack{m=0 \\ m\neq[2\tau,2\tau+1]}}^{2(L_{\mathrm{f}}+L_{\mathrm{h}}-1)-1}\left[\left|\left(\mathbf{f}^{(1)}\right)^{\mathrm{T}}\mathbf{h}_{m}^{(u_0,b_0)}\right|^2 + \left|\left(\mathbf{f}^{(2)}\right)^{\mathrm{T}}\mathbf{h}_{m}^{(u_0,b_0)}\right|^2\right], \tag{B.35}$$

Table B.2.: Simulation parameters for the generation of the equivalent fading parameters of the Alamouti STTD link-quality model representation.

Parameter	Value
receive antennas	$N_{\mathrm{R}} = 2$
mean receive SNR	$10\,\mathrm{dB}$
equalizer length	$L_{\mathrm{f}} = 30\,\mathrm{chips}$
equalizer delay	$\tau = 15\,\mathrm{chips}$
transmitter frequency	$2\,\mathrm{GHz}$
mobile speed	$3\,\mathrm{km/h},\ 120\,\mathrm{km/h}$
channel profile	ITU PedA, VehA
simulated slots	10000, each $2/3\,\mathrm{ms}$

(a) Statistics of STTD equivalent fading parameters, PedA, 2×2.

(b) Statistics of STTD equivalent fading parameters, VehA, 2×2.
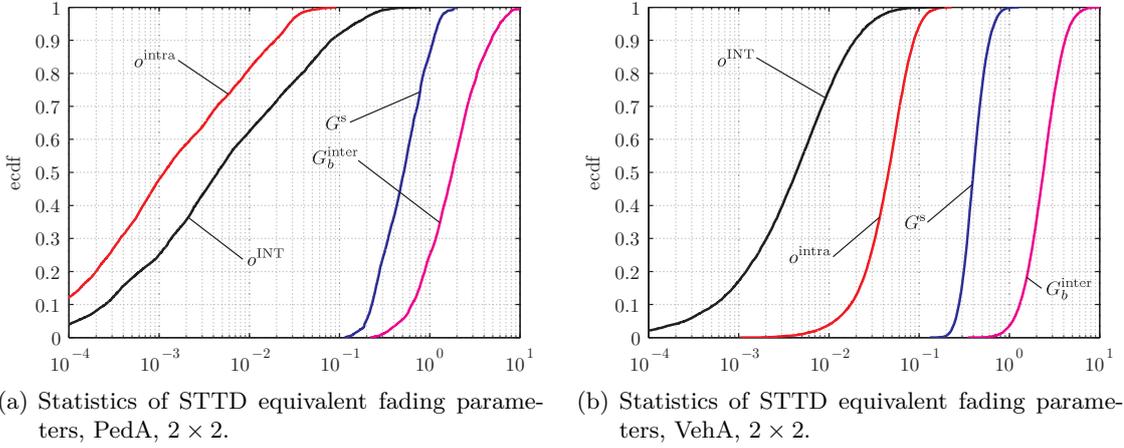
Figure B.8.: Statistics of the Alamouti STTD equivalent fading parameters for a ITU PedA and VehA 2×2 scenarios.

- and the equivalent fading parameter of the inter-cell interference,

$$
G_b^{\mathrm{inter}} \triangleq \frac{1}{4} \sum_{m=0}^{2(L_{\mathrm{f}}+L_{\mathrm{h}}-1)-1} \left[\left| \left(\mathbf{f}^{(1)} \right)^{\mathrm{T}} \mathbf{h}_m^{(u_0,b)} \right|^2 + \left| \left(\mathbf{f}^{(2)} \right)^{\mathrm{T}} \mathbf{h}_m^{(u_0,b)} \right|^2 \right], \tag{B.36}
$$

with all of them allowing to be calculated prior to the system-level simulation, like in Chapter 3.

B.2.3. Generation of the Equivalent Fading Parameters

To assess the characteristics of the developed equivalent fading parameter representation of the link-quality model, I performed various simulations for a number of channels and system setups. The statistical evaluation was carried out by utilizing the improved Zheng model [8, 91] to generate Rayleigh fading with the desired statistical properties.

The simulation results in form of the ecdfs of the equivalent fading parameters for the settings from Table B.2 are shown in Figures B.8 and B.9. In Figure B.8(a) it can be observed that
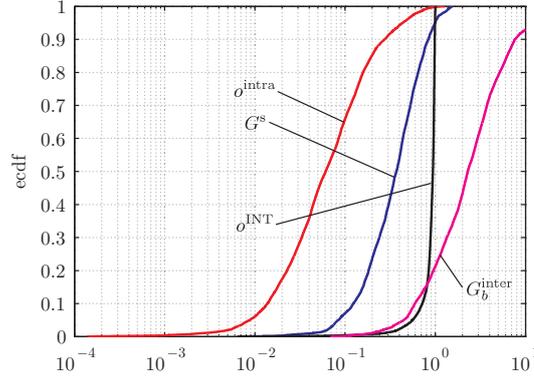
Figure B.9.: Statistics of the Alamouti STTD equivalent fading parameters for an ITU PedA 2×1 scenario.

the fading parameters determining the inter-stream o^{INT} and intra-cell interference o^{intra} are far below the equivalent fading parameter gain influencing the desired signal G^{s}. This implies that the equalizer is very well able to restore the orthogonality of the spreading codes. The parameter representing the inter-cell interference G^{inter} seems to be quite high at the first glance, which is due to the power normalization of the Rayleigh fading.[9]

Figure B.8(b) shows the results for a similar setting, but in an ITU VehA channel scenario and a mobile speed of $120 \, \mathrm{km/h}$. The fading parameters determining the interference o^{INT}, o^{intra}, and G^{inter} are considerably larger, whereas the mean value of G^{s} nearly stays constant. This of course implies that the equalizer is less able to restore the spreading code orthogonality, thus leading to a lower post-equalization SINR.

Finally, Figure B.9 shows the simulation results again for an ITU PedA channel as in Figure B.8(a) but now in a 2×1 MIMO channel. In particular it can be observed that the interstream interference parameter o^{INT} is much larger than in Figure B.8(a). This is due to the inherent problem of a 2×1 Alamouti transmission in a WCDMA system, since the receiver observes— due to the scrambling code that is considerably longer than the spreading code sequence—in consecutive channel uses not a superposition of equal chips. Thus the only possibility to decode is to estimate the two transmitted chips out of one receive value, respectively, which leads to a performance degradation. This is reflected in the exceptional large values of o^{INT}. A possible solution for this problem would be to conduct the MRC on symbol level, after the necessary descrambling.

---

[9]The average receive power of every base-station simulated is assumed to be one. In system-level simulations, this parameter is weighted with the path-loss from the neighbouring Node-B.

List of Abbreviations

3GPP	3rd Generation Partnership Project
ACK	ACKnowledged
AMC	Adaptive Modulation and Coding
AWGN	Additive White Gaussian Noise
BICM	Bit-Interleaved Coded Modulation
BLER	BLock Error Ratio
CA	Content-Aware
CDMA	Code-Division Multiple Access
CL	Closed Loop
COST	European COoperation in the field of Scientific and Technical research
CPICH	Common Pilot CHannel
CQI	Channel Quality Indicator
CRC	Cyclic Redundancy Check
CSI	Channel State Information
DCCH	Dedicated Control CHannel
DCH	Dedicated CHannel
DiffServ	Differentiate Service
DoF	Degrees of Freedom
DPC	Dirty Paper Coding
DPCCH	Dedicated Physical Control CHannel
DPDCH	Dedicated Physical Data CHannel
DS	Double-Stream
DSTTD-SGRC	Double Space-Time Transmit Diversity with Sub-Group Rate Control
DTCH	Dedicated Traffic CHannel
D-TxAA	Double Transmit Antenna Array
ecdf	empirical cumulative distribution function
EDGE	Enhanced Data Rates for Global system for mobile communications Evolution
EESM	Exponential Effective Signal to Interference and Noise Ratio Mapping
epdf	empirical probability density function
FBI	FeedBack Information
FDD	Frequency Division Duplex
GGSN	Gateway-General packet radio service Support Node
GOF	Goodness Of Fit

GOP	Group Of Pictures
GPRS	General Packet Radio Service
GSM	Global System for Mobile communications
HARQ	Hybrid Automatic Repeat reQuest
HSDPA	High-Speed Downlink Packet Access
HS-DPCCH	High-Speed Dedicated Physical Control CHannel
HS-DSCH	High-Speed Downlink Shared CHannel
HSPA	High-Speed Packet Access
HS-PDSCH	High-Speed Physical Downlink Shared CHannel
HS-SCCH	High-Speed Shared Control CHannel
HSUPA	High-Speed Uplink Packet Access
IC	Interference Cancellation
IDE	Integrated Development Environment
IP	Internet Protocol
IR	Incremental Redundancy
ISI	Inter-Symbol Interference
ISO	International Standard Organization
ITU	International Telecommunication Union
LS	Least Squares
LTE	Long Term Evolution
MAC	Medium Access Control
MAC-d	Medium Access Control dedicated
MAC-hs	Medium Access Control for High-Speed Downlink Packet Access
max C/I	Maximum Carrier-to-Interference Ratio
MB	MacroBlock
MI	Mutual Information
MIESM	Mutual Information Effective Signal to Interference and Noise Ratio Mapping
MIMO	Multiple-Input Multiple-Output
MISO	Multiple-Input Single-Output
ML	Maximum Likelihood
MMSE	Minimum Mean Squared Error
MoRSE	Mobile Radio Simulation Environment
MPEG	Moving Picture Expert Group
MRC	Maximum Ratio Combining
MSE	Mean Squared Error
MTU	Maximum Transfer Unit
MU	Multi-User
MVU	Minimum Variance Unbiased

NACK	Non-ACKnowledged
NAL	Network Abstract Layer
NBAP	NodeB Application Part
NDI	New Data Indicator
N-SAW	N Stop And Wait
NSN	Nokia Siemens Networks
OFDMA	Orthogonal Frequency-Division Multiple Access
OSI	Open Systems Interconnection
PARC	Per-Antenna Rate Control
PCI	Precoding Control Information
PDCP	Packet Data Convergence Protocol
pdf	probability density function
PDP	Packet Data Protocol
PDU	Packet Data Unit
PedA	Pedestrian A
PedB	Pedestrian B
PER	Packet Error Ratio
PF	Proportional Fair
PN	Pseudo Noise
PSD	Power Spectral Density
PSNR	Peak Signal to Noise Ratio
QAM	Quadrature Amplitude Modulation
QCIF	Quarter Common Intermediate Format
QoE	Quality of Experience
QoS	Quality of Service
RAN	Radio Access Network
RF	Radio Frequency
RLC	Radio Link Control
RMS	Root Mean Square
RNC	Radio Network Controller
RR	Round Robin
RRC	Radio Resource Control
RRM	Radio Resource Management
RTP	Real-time Transport Protocol
RV	Redundancy Version
SAE	System Architecture Evolution
SCM	Spatial Channel Model
SCME	Spatial Channel Model Extended

SDMA	Spatial Division Multiple Access
SDU	Service Data Unit
SGSN	Serving-General packet radio service Support Node
SIC	Successive Interference Cancellation
SID	Size Index Identifier
SIMO	Single-Input Multiple-Output
SINR	Signal-to-Interference-and-Noise Ratio
SISO	Single-Input Single-Output
SNR	Signal-to-Noise Ratio
SQP	Sequential Quadratic Programming
SS	Single-Stream
STBC	Space-Time Block Code
STTD	Space-Time Transmit Diversity
SU	Single-User
SVD	Singular Value Decomposition
TBS	Transport Block Size
TDD	Time Division Duplex
TFC	Transport Format Combination
TFCI	Transport-Format Combination Indicator
TFT	Traffic Flow Template
TOS	Type Of Service
TPC	Transmit Power-Control
TrCH	Transport CHannel
TSN	Transmission Sequence Number
TTI	Transmission Time Interval
TxAA	Transmit Antenna Array
UDP	User Datagram Protocol
UE	User Equipment
UMTS	Universal Mobile Telecommunications System
UTRAN	Universal mobile telecommunications system Terrestrial Radio Access Network
V-BLAST	Vertical Bell Laboratories Layered Space-Time
VCEG	Video Coding Expert Group
VCL	Video Coding Layer
VehA	Vehicular A
VHSIC	Very High Speed Integrated Circuits
VoIP	Voice over IP
WCDMA	Wideband Code-Division Multiple Access

List of Symbols

This list of symbols generally holds throughout the thesis. However, if clearly stated in the text, it may had been necessary to redefine one or multiple of these, so the meaning should always be checked in concordance with the corresponding section.

α	power coefficient
$\mathcal{A}$	symbol alphabet
b	base-station/sector index
B	total number of base-stations/sectors
B_f	bandwidth
$\boldsymbol{\beta}$	link-performance model tuning parameter vector
$c^{(\mathrm{F})}$	feedback CQI
c_r	relative complexity
$c^{(\mathrm{T})}$	transmit CQI
$\mathbb{C}$	set of complex numbers
d	distance between UE and target NodeB
E_c	average chip energy
$\mathbf{f}$	receive filter
$\mathbf{F}$	space-time MMSE equalizer
f_other	other user interference fraction
f_self	self interference fraction
φ	spreading code
Φ	spreading code set
$G_{n,b}^\mathrm{inter}$	inter-cell interference fading parameter
G_n^s	fading parameter of desired signal
h	scaler complex channel coefficient
$\mathbf{h}$	stacked equivalent MIMO channel column
$\mathbf{H}$	MIMO channel
$\mathbf{H}_\mathrm{w}$	pre-coded equivalent MIMO channel
$\tilde{\mathbf{H}}_\mathrm{w}$	stacked equivalent MIMO channel

$\hat{\tilde{\mathbf{H}}}_{\mathrm{w}}$	estimated equivalent MIMO channel
i	discrete time index
I_{oc}	total white noise interference PSD at UE
I_{or}	total transmit PSD at NodeB
k	spreading code index
L	macro-scale and shadow fading path-loss
L_{f}	equalizer length
L_{h}	maximum channel delay
λ_{m}	macro-scale path-loss
λ_{s}	shadow fading path-loss
m	column index
n	stream index
n	noise
N_0	noise PSD
n_{r}	receive antenna index
N_{R}	total number of receive antennas
N_{S}	number of spatial streams
n_{t}	transmit antenna index
N_{T}	total number of transmit antennas
$\mathbb{N}$	set of integers
o_n^{BF}	fading parameter of pre-coding effect
o_n^{INT}	inter-stream fading parameter
o_n^{intra}	intra-cell interference fading parameter
Ω	set of pre-coding weights
$\mathcal{P}$	pre-coding state
ψ	scrambling code
R	rate
r_{c}	effective coderate
$\mathbb{R}$	set of real numbers
s	modulated symbol
SF	spreading factor
σ_{n}^2	noise covariance

T	evaluated throughput
T_c	chip duration
τ	filter delay
ϑ	fairness coefficient
$\mathcal{T}$	transport format mapping
u	user index
U	total number of users
$u^{(\mathrm{s})}$	scheduled user
ν	content priority indicator
w	pre-coding weight
$\mathbf{W}$	pre-coding matrix
x	transmit signal
y	receive signal

Bibliography

[1] Y. Li and J. I. Agbinya, "Emerging markets and benefits of fixed to wireless substitution in africa," in *Proc. IEEE International Conference on Mobile Business (ICMB)*, Jul. 2005, pp. 605–609.

[2] M. Reardon. (2009, Apr.) CEOs see wireless as answer to economic crisis. [Online]. Available: www.cnn.com/2009/TECH/biztech/04/02/wireless.might.solve.economic.crisis/

[3] H. Holma and A. Toskala, *WCDMA for UMTS – Radio Access For Third Generation Mobile Communications*, 3rd ed. John Wiley & Sons, Ltd, 2005.

[4] G. J. Foschini, "Layered space-time architecture for wireless communication in a fading environment when using multiple antennas," *Bell Labs Technical Journal*, vol. 1, no. 2, pp. 41–59, 1996.

[5] E. Dahlman, S. Parkvall, J. Skold, and P. Beming, *3G Evolution: HSDPA and LTE for Mobile Broadband.* Academic Press, Jul. 2007.

[6] Technical Specification Group Radio Access Network, "Multiple-input multiple-output UTRA," 3rd Generation Partnership Project (3GPP), Tech. Rep. TR 25.876 Version 7.0.0, Mar. 2007.

[7] ——, "Physical layer procedures (FDD)," 3rd Generation Partnership Project (3GPP), Tech. Rep. TS 25.214 Version 7.4.0, Mar. 2007.

[8] Y. Zheng and C. Xiao, "Simulation models with correct statistical properties for rayleigh fading channels," *IEEE Transactions on Communications*, vol. 51, no. 6, pp. 920–928, Jun. 2003.

[9] Technical Specification Group Radio Access Network, "Evolved universal terrestrial radio access (E-UTRA); LTE physical layer – general description," 3rd Generation Partnership Project (3GPP), Tech. Rep. TS 36.201 Version 8.3.0, Mar. 2009.

[10] (2009, May) Symena GmbH. [Online]. Available: www.symena.com

[11] S. Shakkottai, T. S. Rappaport, and P. C. Karlsson, "Cross-layer design for wireless networks," *IEEE Communications Magazine*, vol. 41, no. 10, pp. 74–80, Oct. 2003.

[12] M. Wrulich, C. Mecklenbräuker, J. Wehinger, S. Eder, and I. Kambourov, "Upgrading methodology for MIMO system-level simulations," Telecommunications Research Center Vienna (ftw.), project report C10, 2007.

[13] M. Wrulich, S. Eder, I. Viering, and M. Rupp, "Efficient link-to-system level model for MIMO HSDPA," in *Proc. IEEE 4th Broadband Wireless Access Workshop*, 2008.

[14] M. Wrulich and M. Rupp, "Computationally efficient MIMO HSDPA system-level modeling," *EURASIP Journal on Wireless Communications and Networking*, 2009.

[15] ——, "Efficient link measurement model for system level simulations of Alamouti encoded MIMO HSDPA transmissions," in *Proc. ITG International Workshop on Smart Antennas (WSA)*, Darmstadt, Germany, Feb. 2008.

[16] C. Mehlführer, S. Caban, M. Wrulich, and M. Rupp, "Joint throughput optimized CQI and precoding weight calculation for MIMO HSDPA," in *Proc. 42nd Asilomar Conference on Signals, Systems and Computers*, Oct. 2008.

[17] M. Wrulich and C. Reyes, "Upgrading methodology for MIMO system-level simulations," Telecommunications Research Center Vienna (ftw.), project report C12, 2008.

[18] G. Lilley, M. Wrulich, and M. Rupp, "Network based stream-number decision for MIMO HSDPA," in *Proc. ITG International Workshop on Smart Antennas (WSA)*, Feb. 2009.

[19] L. Superiori, M. Wrulich, P. Svoboda, M. Rupp, J. Fabini, W. Karner, and M. Steinbauer, "Content-aware scheduling for video streaming over HSDPA networks," in *Proc. IEEE Second International Workshop on Cross-Layer Design*, 2009.

[20] L. Superiori, M. Wrulich, P. Svoboda, and M. Rupp, "Cross-layer optimization of video services over HSDPA networks," in *Proc. ICST International Conference on Mobile Lightweight Wireless Systems*, 2009.

[21] A. Mateu-Torelló, "CPICH power optimization for MIMO HSDPA," Master's thesis, Vienna University of Technology, Mar. 2009.

[22] M. Wrulich, C. Mehlführer, and M. Rupp, "Interference aware MMSE equalization for MIMO TxAA," in *Proc. IEEE 3rd International Symposium on Communications, Control and Signal Processing (ISCCSP)*, 2008, pp. 1585–1589.

[23] C. Mehlführer, M. Wrulich, and M. Rupp, "Intra-cell interference aware equalization for TxAA HSDPA," in *Proc. IEEE 3rd International Symposium on Wireless Pervasive Computing*, 2008, pp. 406–409.

[24] M. Wrulich, C. Mehlführer, and M. Rupp, *Handbook of HSDPA/HSUPA Technology.* CRC Press, 2009, ch. Advanced Receivers for MIMO HSDPA, in print preparation.

[25] ——, "Managing the interference structure of MIMO HSDPA: A multi-user interference aware MMSE receiver with moderate complexity," 2009, submitted to IEEE Transactions on Wireless Communications.

[26] M. Wrulich, W. Weiler, and M.Rupp, "HSDPA performance in a mixed traffic network," in *Proc. IEEE Vehicular Technology Conference Spring (VTC)*, May 2008, pp. 2056–2060.

[27] P. Svoboda, W. Karner, and M. Rupp, "Traffic analysis and modeling for world of warcraft," in *Proc. IEEE International Conference on Communications (ICC)*, 2007, pp. 1612–1617.

[28] Commission of the European Communities, "Progress report on the single european electronic communications market (14th report)," Commission of the European Communities, Tech. Rep. SEC (2009) 376, 2008. [Online]. Available: http://eur-lex.europa.eu/LexUriServ/LexUriServ.do?uri=COM:2009:0140:FIN:EN:PDF

[29] ——, "Towards a single european telecoms market – focus on Austria," Commission of the European Communities, Tech. Rep., Mar. 2009. [Online]. Available: http://ex.europa.eu/information_society/doc/factsheets/14thimplementation/14th-progress-report-at-final.pdf

[30] H. Wittig, "The power of mobile broadband – implications for european telcos and equipment vendors," J.P. Morgan Securities Ltd., Tech. Rep., May 2008.

[31] A. Grinschgl and G. Serentschy, "Kommunikationsbericht 2007," Rundfunk und Telekom Regulierungs-GmbH, Tech. Rep., 2007. [Online]. Available: http://www.rtr.at/de/komp/KBericht2007/K-Bericht_2007.pdf

[32] Technical Specification Group Radio Access Network, "UTRA high speed downlink packet access (HSDPA); overall description; stage 2," 3rd Generation Partnership Project (3GPP), Tech. Rep. TS 25.308 Version 5.0.0, Sep. 2001.

[33] H. Holma and A. Toskala, *HSDPA/HSUPA for UMTS: High Speed Radio Access for Mobile Communications.* John Wiley & Sons, Ltd., 2006, ISBN 0-470-01884-4.

[34] Technical Specification Group Radio Access Network, "Physical channels and mapping of transport channels onto physical channels (FDD)," 3rd Generation Partnership Project (3GPP), Tech. Rep. TS 25.211, Version 8.4.0, Mar. 2009.

[35] ——, "Multiplexing and channel coding (FDD)," 3rd Generation Partnership Project (3GPP), Tech. Rep. TS 25.212 Version 8.5.0, Mar. 2009.

[36] E. Malkamaki, D. Mathew, and S. Hamalainen, "Performance of hybrid ARQ techniques for WCDMA high data rates," *Proc. IEEE 53rd Vehicular Technology Conference Spring (VTC)*, vol. 4, pp. 2720–2724, 2001.

[37] P. Frenger, S. Parkvall, and E. Dahlman, "Performance comparison of HARQ with chase combining and incremental redundancy for HSDPA," *Proc. VTS IEEE 54th Vehicular Technology Conference Fall (VTC)*, vol. 3, pp. 1829–1833, 2001.

[38] P. Wu and N. Jindal, "Performance of hybrid-ARQ in block-fading channels: A fixed outage probability analysis," Nov. 2008, submitted to IEEE Transactions on Wireless Communications.

[39] Members of TSG-RAN Working Group 4, "Revised HSDPA CQI proposal," 3GPP, Tech. Rep. R4-020612, 2002.

[40] Technical Specification Group Radio Access Network, "User equipment (UE) radio transmission and reception (FDD)," 3rd Generation Partnership Project (3GPP), Tech. Rep. TS 25.101, Version 8.6.0, Mar. 2009.

[41] ——, "Medium access control (MAC) protocol specification," 3rd Generation Partnership Project (3GPP), Tech. Rep. TS 25.321 Version 7.0.0, Mar. 2006.

[42] S. Blomeier, *HSDPA - Design Details & System Engineering.* INACON, 2006, ISBN 978-3-936273-42-7.

[43] Technical Specification Group Radio Access Network, "Radio link control (RLC) protocol specification," 3rd Generation Partnership Project (3GPP), Tech. Rep. TS 25.322 Version 8.4.0, Mar. 2009.

[44] K. Pedersen and P. Michaelsen, "Algorithms and performance results for dynamic HSDPA resource allocation," in *Proc. IEEE 64th Vehicular Technology Conference (VTC)*, Sep. 2006, pp. 1–5.

[45] I. de Bruin, G. Heijenk, M. El Zarki, and L. Zan, "Fair channel-dependent scheduling in CDMA systems," in *Proc. IST Mobile and Wireless Communications Summit*, Jun. 2003, pp. 737–741.

[46] M. H. Ahmed, H. Yanikomeroglu, and S. Mahmoud, "Fairness enhancement of link adaptation techniques in wireless access networks," in *Proc. IEEE Vehicular Technology Conference Fall (VTC)*, vol. 3, Oct. 2003, pp. 1554–1557.

[47] C. Wengerter, J. Ohlhorst, and A. Golitschek Edler von Elbwart, "Fairness and throughput analysis for generalized proportional fair frequency scheduling in OFDMA," in *Proc. IEEE 61st Vehicular Technology Conference (VTC) Spring*, vol. 3, Jun. 2005, pp. 1903–1907.

[48] I. E. Telatar, "Capacity of multi-antenna gaussian channels," *European Trans. on Telecom.*, vol. 10, pp. 585–595, 1999.

[49] A. Paulraj, R. Nabar, and D. Gore, *Introduction to Space-Time Wireless Communications*. Cambridge University Press, 2003, ISBN 0521826152.

[50] S. A. Jafar and M. J. Fakhereddin, "Degrees of freedom for the MIMO interference channel," *IEEE Transactions on Information Theory*, vol. 53, no. 7, pp. 2637–2642, Jul. 2007.

[51] D. Gesbert, M. Shafi, D. Shiu, P. J. Smith, and A. Naguib, "From theory to practice: An overview of MIMO space-time coded wireless systems," *IEEE Journal on Selected Areas in Communications*, vol. 21, no. 3, pp. 281–302, Apr. 2003.

[52] V. Tarokh, N. Seshadri, and A. R. Calderbank, "Space-time codes for high data rate wireless communication: Performance criterion and code construction," *IEEE Transactions on Information Theory*, vol. 44, no. 2, pp. 744–765, Mar. 1998.

[53] M. Wrulich, "Capacity analysis of MIMO systems," Master's thesis, Vienna University of Technology, Mar. 2006.

[54] L. Zheng and D. N. C. Tse, "Diversity and multiplexing: A fundamental tradeoff in multiple-antenna channels," *IEEE Transactions on Information Theory*, vol. 49, no. 5, pp. 1073–1096, May 2003.

[55] S. Alamouti, "A simple transmit diversity technique for wireless communications," *IEEE Journal on Selected Areas in Communications*, vol. 16, no. 8, pp. 1451–1458, Oct. 1998.

[56] A. Lozano and N. Jindal, "Transmit diversity v. spatial multiplexing in modern MIMO systems," Nov. 2008, submitted to IEEE Transactions on Wireless Communications.

[57] J.-C. Belfiore, G. Rekaya, and E. Viterbo, "The golden code: A 2x2 full-rate space-time code with nonvanishing determinants," *IEEE Transactions on Information Theory*, vol. 51, no. 4, pp. 1432–1426, Apr. 2005.

[58] H. Bölcskei, D. Gesbert, C. B. Papadias, and A.-J. Van der Veen, Eds., *Space-Time Wireless Systems – From Array Processing to MIMO Communications*. Cambridge University Press, 2006, ISBN 978-0-521-85105-3.

[59] Motorola, "MIMO evaluation proposal," 3rd Generation Partnership Project (3GPP), Tech. Rep. TSG R1 #44 060615, Feb. 2006.

[60] Q. Spencer, C. Peel, A. Swindlehurst, and M. Haardt, "An introduction to the multi-user MIMO downlink," *IEEE Communications Magazine*, vol. 42, no. 10, pp. 60–67, Oct. 2004.

[61] D. Gesbert, M. Kountouris, R. Heath, C.-B. Chae, and T. Salzer, "Shifting the MIMO paradigm," *IEEE Signal Processing Magazine*, vol. 24, no. 5, pp. 36–46, Sep. 2007.

[62] H. Holma, A. Toskala, K. Ranta-aho, and J. Pirskanen, "High-speed packet access evolution in 3GPP release 7," *IEEE Communications Magazine*, vol. 45, no. 12, pp. 29–35, Dec. 2007.

[63] L. Haring, B. Chalise, and A. Czylwik, "Dynamic system level simulations of downlink beamforming for UMTS FDD," in *Proc. IEEE Global Telecommunications Conference (GLOBECOM)*, vol. 1, 2003, pp. 492–496.

[64] A. Czylwik and A. Dekorsy, "System-level performance of antenna arrays in CDMA-based cellular mobile radio systems," *EURASIP J. Appl. Signal Proc.*, no. 9, pp. 1308–1320, 2004.

[65] K. Peppas, A. Alexiou, F. Lazarakis, and T. Al-Gizawi, "Performance evaluation at the system level of reconfigurable space-time coding techniques for HSDPA," *EURASIP J. Appl. Signal Proc.*, no. 11, pp. 1656–1667, 2005.

[66] T. Nihtila and V. Haikola, "HSDPA MIMO system performance in macro cell network," in *Proc. IEEE Sarnoff Symposium*, 2008, pp. 1–4.

[67] K. I. Pedersen, T. F. Lootsma, M. Stottrup, F. Frederiksen, T. Kolding, and P. E. Mogensen, "Network performance of mixed traffic on high speed downlink packet access and dedicated channels in WCDMA," in *Proc. IEEE 60th Vehicular Technology Conference (VTC)*, vol. 6, 2004, pp. 4496–4500.

[68] P. Sai A and C. Furse, "System level analysis of noise and interference analysis for MIMO system," in *Proc. IEEE Antennas and Propagation Society International Symposium (AP-S)*, 2008, pp. 1–4.

[69] P. Gkonis, D. Kaklamani, and G. Tsoulos, "Capacity of WCDMA multicellular networks under different radio resource management strategies," in *Proc. 3rd International Symposium on Wireless Pervasive Computing (ISWPC)*, 2008, pp. 60–64.

[70] M. Castañeda, M. Ivrlac, J. Nossek, I. Viering, and A. Klein, "On downlink intercell interference in a cellular system," in *Proc. IEEE 18th International Symposium on Personal, Indoor and Mobile Radio Communications (PIMRC)*, 2007, pp. 1–5.

[71] K. Peppas, T. Al-Gizawi, F. Lazarakis, D. Axiotis, A. Moussa, and A. Alexiou, "System level evaluation of reconfigurable MIMO techniques enhancements for HSDPA," in *Proc. IEEE Global Telecommunications Conference (GLOBECOM)*, vol. 5, 2004, pp. 2869–2873.

[72] A. Pollard and M. Heikkila, "A system level evaluation of multiple antenna schemes for high speed downlink packet access," in *Proc. IEEE 15th International Symposium on Personal, Indoor and Mobile Radio Communications (PIMRC)*, vol. 3, 2004, pp. 1732–1735.

[73] C. Shuping, L. Huibinu, Z. Dong, and K. Asimakis, "Generalized scheduler providing multimedia services over HSDPA," in *Proc. IEEE International Conference on Multimedia and Expo*, 2007, pp. 927–930.

[74] D. Skoutas, D. Komnakos, D. Vouyioukas, and A. Rouskas, "Enhanced dedicated channel scheduling optimization in WCDMA," in *Proc. 14th European Wireless Conference (EW)*, 2008, pp. 1–5.

[75] D. Staehle and A. Mader, "A model for time-efficient HSDPA simulations," in *Proc. IEEE 66th Vehicular Technology Conference Fall (VTC)*, 2007, pp. 819–823.

[76] D. Moltchanov, Y. Koucheryavy, and J. Harju, *Wired/Wireless Internet Communications*, ser. Lecture Notes in Computer Science. Springer Berlin / Heidelberg, 2005, vol. 3510/2005, ch. Simple, Accurate and Computationally Efficient Wireless Channel Modeling Algorithm, pp. 234–245, ISBN 978-3-540-25899-5.

[77] ——, "Cross-layer modeling of wireless channels for data-link and IP layer performance evaluation," *ELSEVIER Computer Communications*, no. 29, pp. 827–841, 2006.

[78] A. Seeger, M. Sikora, and A. Klein, "Variable orthogonality factor: A simple interface between link and system level simulation for high speed downlink packet access," in *Proc. IEEE 58th Vehicular Technology Conference Fall (VTC)*, Sep. 2003, pp. 2531–2534.

[79] S. W. Golomb, "Mathematical models – uses and limitations," *Simulation*, vol. 4, no. 14, pp. 197–198, 1970.

[80] Members of WINNER, "Assessment of advanced beamforming and MIMO technologies," WINNER, Tech. Rep. IST-2003-507581 D2.7 v1.0, 2003.

[81] S. Hämäläinen, H. Holma, and K. Sipilä, "Advanced WCDMA radio network simulator," in *Proc. IEEE International Symposium on Personal, Indoor and Mobile Radio Conference (PIMRC)*, Sep. 1999, pp. 951–955.

[82] B. Sklar, "Rayleigh fading channels in mobile digital communication systems. I. characterization," *IEEE Communications Magazine*, vol. 35, no. 9, pp. 136–146, Sep. 1997.

[83] S. Hämäläinen, P. Slanina, M. Hartman, A. Lappeteläinen, H. Holma, and O. Salonaho, "A novel interface between link and system level simulations," in *Proc. ACTS Summit*, Oct. 1997, pp. 509–604.

[84] K. Brueninghaus, D. Astely, T. Salzer, S. Visuri, A. Alexiou, S. Karger, and G. A. Seraji, "Link performance models for system level simulations of broadband radio access systems," in *Proc. IEEE 16th International Symposium on Personal, Indoor and Mobile Radio Communications (PIMRC 2005)*, vol. 4, Sep. 2005, pp. 2306–2311.

[85] T. Nihtila, J. Kurjenniemi, and E. Virtej, "System level analysis of interference aware LMMSE chip equalization in HSDPA network," in *Proc. IEEE 12th Symposium on Computers and Communications (ISCC)*, 2007, pp. 133–138.

[86] J. Mirkovic, G. Orfanos, and H.-J. Reumerman, "MIMO link modeling for system level simulations," in *Proc. IEEE 17th International Symposium on Personal, Indoor and Mobile Radio Communications (PIMRC)*, 2006, pp. 1–6.

[87] A. Szabo, N. Geng, A. Seegert, and W. Utschick, "Investigations on link system level interface for MIMO systems," in *Proc. IEEE 3rd International Symposium on Image and Signal Processing and Analysis (ISPA)*, vol. 1, Sep. 2003, pp. 365–369.

[88] J. Ramos, M. D. Zoltowski, and H. Liu, "A low-complexity space-time RAKE receiver for DS-CDMA communications," *IEEE Signal Processing Letters*, vol. 4, no. 9, pp. 262–265, Sep. 1997.

[89] J. Proakis, *Digital Communications*, 4th ed. McGraw-Hill Science Engineering, Aug. 2000.

[90] B.-H. Kim, X. Zhang, and M. Flury, "Linear MMSE space-time equalizer for MIMO multi-code CDMA systems," *IEEE Transactions on Communications*, vol. 54, no. 10, pp. 1710–1714, 2006.

[91] T. Zemen and C. Mecklenbräuker, "Time-variant channel estimation using discrete prolate spheroidal sequences," *IEEE Transactions on Signal Processing*, vol. 53, no. 9, pp. 3597–3607, Sep. 2005.

[92] T. K. Moon and W. C. Stirling, *Mathematical Methods and Algorithms for Signal Processing.* Prentice-Hall, 2000, ISBN 0-201-36186-8.

[93] Technical Specification Group Radio Access Network, "Spatial channel model for multiple input multiple output (MIMO) simulations," 3rd Generation Partnership Project (3GPP), Tech. Rep. TS 25.996 Version 7.0.0, Jun. 2007.

[94] F. Kaltenberger, K. Freudenthaler, S. Paul, J. Wehinger, C. F. Mecklenbräuker, A. Springer, and J. Berkmann, "Throughput enhancement by cancellation of synchronization and pilot channel for UMTS high speed downlink packet access," in *Proc. IEEE 6th Workshop on Signal Processing Advances in Wirless Communications (SPAWC)*, 2005, pp. 580–584.

[95] S. Caban, C. Mehlführer, R. Langwieser, A. L. Scholtz, and M. Rupp, "Vienna MIMO testbed," *EURASIP Journal on Applied Signal Processing, Special Issue on Implementation Aspects and Testbeds for MIMO Systems*, 2006.

[96] M. Lampe, H. Rohling, and W. Zirwas, "Misunderstandings about link adaptation for frequency selective fading channels," in *Proc. IEEE 13th International Symposium on Personal, Indoor and Mobile Radio Communications (PIMRC)*, vol. 2, Aug. 2002, pp. 710–714.

[97] W. C. Jakes, Ed., *Microwave Mobile Communications.* IEEE Press, 1974, ISBN 0-7803-1069-1.

[98] D. Baum, D. Gore, R. Nabar, S. Panchanathan, K. Hari, V. Erceg, and A. Paulraj, "Measuerement and characterization of broadband MIMO fixed wireless channels at 2.5 GHz," in *Proc. IEEE International Conference on Personal Wireless Communications*, Nov. 2000, pp. 203–206.

[99] L. T. Berger, "Performance of multi-antenna enhanced HSDPA," Ph.D. dissertation, Aalborg Universitet, Aalborg, Denmark, Jun. 2005.

[100] S. Nanda and K. Rege, "Frame error rates for convolutional codes on fading channels and the concept of effective eb/n0," *IEEE Transactions on Vehicular Technology*, vol. 47, no. 4, pp. 1245–1250, Nov. 1998.

[101] Nortel Networks, "Effective SIR computation for OFDM system-level simulations," 3rd Generation Partnership Project (3GPP), Lisbon, Portugal, TSG-RAN WG1 meeting #35 R1-031370, Nov. 2003.

[102] G. Caire, G. Taricco, and E. Biglieri, "Capacity of bit-interleaved channels," *IEE Electronics Letters*, vol. 32, no. 12, pp. 1060–1061, Jun. 1996.

[103] H. Olofsson, M. Almgren, C. Johansson, M. Hook, and F. Kronstedt, "Improved interface between link level and system level simulations applied to GSM," in *Proc. IEEE 6th International Conference on Universal Personal Communications*, vol. 1, Sep. 1997, pp. 79–83.

[104] J. Zhuang, L. Jalloul, R. Novak, and J. Park, "IEEE 802.16m evaluation methodology document (EMD)," IEEE, Tech. Rep. IEEE 802.16m-08/004r1, Mar. 2008.

[105] B. Zerlin, M. Ivrlac, W. Utschick, J. Nossek, I. Viering, and A. Klein, "Joint optimization of radio parameters in HSDPA," in *Proc. IEEE 61st Vehicular Technology Conference (VTC) Spring*, vol. 1, 2005, pp. 295–299.

[106] AWE Communications. (2009, Jul.) Wave propagation and radio network planning. [Online]. Available: www.awe-communications.com

[107] S. McCanne and S. Floyd. (2009, Jul.) The network simulator ns-2. [Online]. Available: www.isi.edu/nsnam/ns

[108] M. Folke and S. Landström, "An NS module for simulation of HSDPA," Lulea University of Technology, Tech. Rep., Apr. 2006.

[109] X. Yan, J. Khan, and B. Jones, "An adaptive resource management technique for a HSDPA network," in *Proc. IFIP International Conference on Wireless and Optical Communication Networks (WOCN)*, 2007, pp. 1–5.

[110] I. Viering, C. Buchner, E. Seidel, and A. Klein, "Real-time network simulation of 3GPP long term evolution," in *Proc. IEEE International Symposium on a World of Wireless, Mobile and Multimedia Networks (WoWMoM)*, 2007, pp. 1–3.

[111] Andrew. (2009, Jul.) Odyssey cellular radio planning. [Online]. Available: www.commscope.com/andrew/eng/product/network/odyssey/index.html

[112] D. J. Cichon and T. Kürner, *COST 231 – Digital Mobile Radio Towards Future Generation Systems*.   COST, 1998, ch. 4.

[113] K. Kumaran, S. E. Golowich, and S. Borst, "Correlated shadow-fading in wireless networks and its effect on call dropping," *Wireless Networks*, vol. 8, pp. 61–71, 2002.

[114] J. Weitzen and T. J. Lowe, "Measurement of angular and distance correlation properties of log-normal shadowing at 1900 MHz and its application to design of PCS systems," *IEEE Transactions on Vehicular Technology*, vol. 51, no. 2, pp. 265–273, Mar. 2002.

[115] M. Gudmundson, "Correlation model for shadow fading in mobile radio systems," *IEE Elec. Let.*, vol. 27, pp. 2145–2146, Nov. 1991.

[116] A. Mäder, D. Staehle, and M. Spahn, "Impact of HSDPA radio resource allocation schemes on the system performance of UMTS networks," in *Proc. IEEE 66th Vehicular Technology Conference Fall (VTC)*, 2007, pp. 315–319.

[117] H. Chao, Z. Liang, Y. Wang, and L. Gui, "A dynamic resource allocation method for HSDPA in WCDMA system," in *Proc. IEE International Conference on 3G Mobile Communication Technologies*, 2004, pp. 569–573.

[118] Technical Specification Group Services and System Aspects, "Quality of service (QoS) concept and architecture," 3rd Generation Partnership Project (3GPP), Tech. Rep. TS 23.107 Version 8.0.0, Dec. 2008.

[119] G. Gómez and R. Sanchez, *End-to-End Quality of Service over Cellular Networks.* John Wiley & Sons, Ltd., 2006.

[120] Network Working Group, "RTP payload format for H.264 video," Internet Engineering Task Force, Tech. Rep. RFC 3984, 2004.

[121] ——, "An architecture for differentiated services," Internet Engineering Task Force, Tech. Rep. RFC 2475, 1998.

[122] K. L. Thng, B. S. Yeo, and Y. H. Chew, "Performance study on the effects of cell-breathing in WCDMA," in *Proc. IEEE 2nd International Symposium on Wireless Communication Systems*, Aug. 2005, pp. 44–49.

[123] L. Chen and D. Yuan, "Automated planning of CPICH power for enhancing HSDPA performance at cell edges with preserved control of R99 soft handover," in *Proc. IEEE International Conference on Communications (ICC)*, Apr. 2008, pp. 2936–2940.

[124] I. Siomina and D. Yuan, "Enhancing HSDPA performance via automated and large-scale optimization of radio base station antenna configuration," in *Proc. IEEE Vehicular Technology Conference Spring (VTC)*, Apr. 2008, pp. 2061–2065.

[125] L. Chen and D. Yuan, "Achieving higher HSDPA performance and preserving R99 soft handover control by large scale optimization in CPICH coverage planing," in *Proc. IEEE Wireless Telecommunications Symposium (WTS)*, Mar. 2009, pp. 1–6.

[126] I. Siomina and D. Yuan, "Optimization of pilot power for load balancing in WCDMA networks," in *Proc. IEEE Global Telecommunications Conference (GLOBECOM)*, vol. 6, Jan. 2004, pp. 3872–3876.

[127] L. Chen and D. Yuan, "CPICH power planning for optimizing HSDPA and R99 SHO performance: Mathematical modelling and solution approach," in *Proc. IFIP 1st Wireless Days Conference (WD)*, Nov. 2008, pp. 1–5.

[128] M. Garcia-Lozano, S. Ruiz, and J. Olmos, "CPICH power optimisation by means of simulated annealing in an UTRA-FDD environment," *Electronics Letters*, vol. 39, no. 23, pp. 1676–1677, Oct. 2003.

[129] Y. Sun, F. Gunnarsson, and H. Hiltunen, "CPICH power settings in irregular WCDMA macro cellular networks," in *Proc. IEEE 14th International Symposium on Personal, Indoor and Mobile Radio Communications (PIMRC)*, vol. 2, Aug. 2003, pp. 1176–1180.

[130] C. Mehlführer and M. Rupp, "Novel tap-wise LMMSE channel estimation for MIMO W-CDMA," in *Proc. IEEE 51st Global Telecommunications Conference (GLOBECOM)*, Nov., 2008.

[131] J. Niemelä and J. Lempäinen, "Mitigation of pilot pollution through base station antenna configuration in WCDMA," in *Proc. IEEE 60th Vehicular Technology Conference (VTC) Fall*, vol. 6, Aug. 2004, pp. 4270–4274.

[132] V. Jungnickel, M. Schellmann, L. Thiele, T. Wirth, T. Haustein, O. Koch, W. Zirwas, and E. Schulz, "Interference aware scheduling in the multiuser MIMO-OFDM downlink," *IEEE Communications Magazine*, vol. 47, no. 6, pp. 56–66, Jun. 2009.

[133] A. J. Goldsmith, S. A. Jafar, N. Jindal, and S. Vishwanath, "Capacity limits of MIMO channels," *IEEE Journal on Selected Areas in Communications*, vol. 21, no. 5, pp. 684–702, Jun. 2003.

[134] H. Weingarten, Y. Steinberg, and S. Shamai, "The capacity region of the Gaussian multiple-input multiple-output broadcast channel," *IEEE Transactions on Information Theory*, vol. 52, no. 9, pp. 3936–3964, Sep. 2006.

[135] P. Viswanath and D. N. C. Tse, "Sum capacity of the vector gaussian broadcast channel and uplink-downlink duality," *IEEE Transactions on Information Theory*, vol. 49, no. 8, pp. 1912–1921, Aug. 2003.

[136] H. Sato, "An outer bound to the capacity region of broadcast channels," *IEEE Transactions on Information Theory*, vol. 24, no. 3, pp. 374–377, May 1978.

[137] R. Dabora and A. J. Goldsmith, "The capacity region of the degraded finite-state broadcast channel," in *Proc. IEEE Information Theory Workshop (ITW)*, 2008, pp. 11–15.

[138] H. Zhang and H. Dai, "Cochannel interference mitigation and cooperative processing in downlink multicell multiuser MIMO networks," *EURASIP J. Wireless Commun. Netw.*, vol. 2, pp. 222–235, Dec. 2004.

[139] U. Erez and S. ten Brink, "A close-to-capacity dirty paper coding scheme," *IEEE Transactions on Information Theory*, vol. 51, no. 10, pp. 3417–3432, Oct. 2005.

[140] C. T. K. Ng, N. Jindal, A. J. Goldsmith, and U. Mitra, "Power and bandwidth allocation in cooperative dirty paper coding," in *Proc. IEEE International Conference on Communications (ICC)*, 2008, pp. 1018–1023.

[141] M. Sharif and B. Hassibi, "A comparison of time-sharing, DPC, and beamforming for MIMO broadcast channels with many users," *IEEE Transactions on Communications*, vol. 55, no. 1, pp. 11–15, Jan. 2007.

[142] F. Petre, M. Engels, A. Bourdoux, B. Gyselinckx, M. Moonen, and H. D. Man, "Extended MMSE receiver for multiuser interference rejection in multipath DS-CDMA channels," in

Proc. IEEE VTS 50th Vehicular Technology Conference Fall (VTC), vol. 3, Sep. 1999, pp. 1840–1844.

[143] E. Biglieri and M. Lops, "Multiuser detection in a dynamic environment. part I: User identification and data detection," *IEEE Transactions on Information Theory*, vol. 53, no. 9, pp. 3158–3170, Sep. 2007.

[144] E. Virtej, M. Lampinen, and V. Kaasila, "Performance of an intra- and inter-cell interference mitigation algorithm in HSDPA system," in *Proc. IEEE 67th Vehicular Technology Conference Spring (VTC)*, 2008, pp. 2041–2045.

[145] C. T. K. Ng, N. Jindal, A. J. Goldsmith, and U. Mitra, "Capacity gain from two-transmitter and two-receiver cooperation," *IEEE Transactions on Information Theory*, vol. 53, no. 10, pp. 3822–3827, Oct. 2007.

[146] T. Holliday, A. J. Goldsmith, and H. V. Poor, "Joint source and channel coding for MIMO systems: Is it better to be robust or quick?" *IEEE Transactions on Information Theory*, vol. 54, no. 4, pp. 1393–1405, Apr. 2008.

[147] Technical Specification Group Radio Access Network, "Feasibility study on interference cancellation for UTRA FDD user equipment (UE)," 3rd Generation Partnership Project (3GPP), Tech. Rep. TR 25.963 Version 7.0.0, Apr. 2007.

[148] G. Boudreau, J. Panicker, N. Guo, R. Chang, N. Wang, and S. Vrzic, "Interference coordination and cancellation for 4G networks," *IEEE Communications Magazine*, vol. 47, pp. 74–81, Apr. 2008.

[149] L. Mailaender, "Linear MIMO equalization for CDMA downlink signals with code reuse," *IEEE Transactions on Wireless Communications*, vol. 4, no. 5, pp. 2423–2434, Sep. 2005.

[150] J. Andrews, "Interference cancellation for cellular systems: A contemporary overview," *IEEE Wireless Communications Magazine*, vol. 12, no. 2, pp. 19–29, Apr. 2005.

[151] M. Melvasalo, P. Janis, and V. Koivunen, "MMSE equalizer and chip level inter-antenna interference canceler for HSDPA MIMO systems," in *Proc. IEEE 63rd Vehicular Technology Conference Spring (VTC)*, vol. 4, 2006, pp. 2008–2012.

[152] S. Shenoy, M. Ghauri, and D. Slock, "Receiver designs for MIMO HSDPA," in *Proc. IEEE International Conference on Communications (ICC)*, 2008, pp. 941–945.

[153] H. Zhang, M. Ivrlac, J. A. Nossek, and D. Yuan, "Equalization of multiuser MIMO high speed downlink packet access," in *Proc. IEEE 19th International Symposium on Personal, Indoor and Mobile Radio Communications (PIMRC)*, 2008, pp. 1–5.

[154] D. I. Kim and S. Fraser, "Two-best user scheduling for high-speed downlink multicode CDMA with code constraint," in *Proc. IEEE Global Telecommunications Conference (GLOBECOM)*, vol. 4, 2004, pp. 2569–2663.

[155] J. Huang, V. G. Subramanian, R. Agrawal, and R. A. Berry, "Downlink scheduling and resource allocation for OFDM systems," *IEEE Transactions on Wireless Communications*, vol. 8, no. 1, pp. 288–296, Jan. 2009.

[156] S. Boyd and L. Vandenberghe, *Convex Optimization*. Cambridge University Press, 2004.

[157] S. Haykin, *Adaptive Filter Theory*, 4th ed. Prentice-Hall, 2002, ISBN 978-0-13-090126-2.

[158] W. Wirtinger, "Zur formalen theorie der funktionen von mehr complexen veränderlichen," in *Mathematische Annalen*, 1927, pp. 357–375.

[159] Members of ITU, "Recommendation ITU-R M.1225: Guidelines for evaluation of radio transmission technologies for IMT-2000," International Telecommunication Union (ITU), Tech. Rep., 1997.

[160] S. M. Kay, *Fundamentals of Statistical Signal Processing. Estimation Theory.* Prentice-Hall, 1993, vol. 1, ISBN 0-13-345711-7.

[161] B. Ottersten, M. Viberg, and T. Kailath, "Analysis of subspace fitting and ML techniques for parameter estimation from sensor array data," *IEEE Transactions on Signal Processing*, vol. 40, no. 3, pp. 590–600, Mar. 1992.

[162] J. Villares and G. Vázquez, "Second-order parameter estimation," *IEEE Transactions on Signal Processing*, vol. 53, no. 7, pp. 2408–2420, Jul. 2005.

[163] ——, "The gaussian assumption in second-order estimation problems in digital communications," *IEEE Transactions on Signal Processing*, vol. 55, no. 10, pp. 4994–5002, Oct. 2007.

[164] P. Stoica and N. Arye, "MUSIC, maximum likelihood, and Cramer-Rao bound," *IEEE Transactions on Acoustics, Speech, and Signal Processing*, vol. 37, no. 5, pp. 720–741, May 1989.

[165] M. J. D. Powell, *A Fast Algorithm for Nonlinearly Constrained Optimization Calculations.* Springer Berlin / Heidelberg, 1978, vol. 630, pp. 144–157, ISBN 978-3-540-08538-6.

[166] C. Mehlführer, M. Wrulich, J. Colom Ikuno, D. Bosanska, and M. Rupp, "Simulating the long term evolution physical layer," in *Proc. 17th European Signal Processing Conference (EUSIPCO)*, Glasgow, Scotland, 2009.

[167] J. Colom Ikuno, M. Wrulich, and M. Rupp, "Performance and modeling of LTE H-ARQ," in *Proc. ITG International Workshop on Smart Antennas (WSA)*, Feb. 2009.

[168] European Telecommunications Standards Institute (ETSI). The 3rd generation partnership project (3GPP). [Online]. Available: www.3gpp.org

[169] GSM Association. HSPA – high speed packet access – mobile broadband today. [Online]. Available: hspa.gsmworld.com

[170] Rundfunk und Telekom Regulierungs-GmbH, "RTR telekom monitor," Rundfunk und Telekom Regulierungs-GmbH, Tech. Rep. 1, 2009. [Online]. Available: http://www.rtr.at/de/komp/TKMonitor_1_2009/TM1-2009.pdf

[171] G. Caire, S. A. Ramprashad, H. C. Papadopoulos, C. Pepin, and C.-E. W. Sundberg, "Multiuser MIMO downlink with limited inter-cell cooperation: Approximate interference alignment in time, freuquency and space," in *Proc. 46th Annual Allerton Conference on Communication, Control and Computing*, Sep. 2008, pp. 730–737.

[172] J. Gao, S. A. Vorobyov, and H. Jiang, "Same theoretic solutions for precoding strategies over the interference channel," in *Proc. IEEE Global Telecommunications Conference (GLOBECOM)*, Dec. 2008.

[173] S. M. Betz and H. V. Poor, "Energy efficient communications in CDMA networks: A game theoretic analysis considering operating costs," *IEEE Transactions on Signal Processing*, vol. 56, no. 10, pp. 5181–5190, Oct. 2008.

[174] Y. Guo and B. C. Levy, "Worst-case MSE precoder design for imperfectly known MIMO communications channels," *IEEE Transactions on Signal Processing*, vol. 53, no. 8, pp. 2918–2930, Aug. 2005.

[175] M. H. M. Costa, "Writing on dirty paper," *IEEE Transactions on Information Theory*, vol. 29, no. 3, pp. 439–441, May 1983.

[176] A. D. Dabbagh and D. J. Love, "Precoding for multiple antenna Gaussian broadcast channels with successive zero-forcing," *IEEE Transactions on Signal Processing*, vol. 55, no. 7, pp. 3837–3850, Jul. 2007.

[177] V. Sharma, I. Wajid, A. B. Gershman, H. Chen, and S. Lambotharan, "Robust downlink beamforming using positive semi-definite covariance constraints," in *Proc. ITG International Workshop on Smart Antennas (WSA)*, Feb. 2008.

[178] M. Fuchs, G. Del Galdo, and M. Haardt, "Low-complexity space-time frequency scheduling for MIMO systems with SDMA," *IEEE Transactions on Vehicular Technology*, vol. 56, no. 5, pp. 2775–2784, Sep. 2007.

[179] Ericsson, "Closed loop transmit diversity in HSDPA," 3rd Generation Partnership Project (3GPP), Denver, USA, TSG-RAN WG1 meeting #44 R1-060566, Feb. 2006.

[180] Technical Specification Group Radio Access Network, "Radio interface protocol architecture," 3rd Generation Partnership Project (3GPP), Tech. Rep. TS 25.301 Version 8.5.0, Mar. 2009.

[181] F. Frederiksen and T. Kolding, "Performance and modeling of WCDMA/HSDPA transmission/H-ARQ schemes," *Proc. IEEE 56th Vehicular Technology Conference Fall (VTC)*, vol. 1, pp. 472–476, 2002.

[182] T. M. Cover, "Comments on broadcast channels," *IEEE Transactions on Information Theory*, vol. 44, no. 6, pp. 2524–2530, Oct. 1998.

[183] R. S. Blum, "MIMO capacity with interference," *IEEE Journal on Selected Areas in Communications*, vol. 21, no. 5, pp. 793–801, Jun. 2003.

[184] Technical Specification Group Services and System Aspects, "Transparent end-to-end packet-switched streaming service (PSS); protocols and codecs," 3rd Generation Partnership Project (3GPP), Tech. Rep. TS 26.234 version 8.3.0, Jun. 2009.

[185] T. Wiegand, G. J. Sullivan, G. Bjontegaard, and A. Luthra, "Overview of the H.264/AVC video coding standard," *IEEE Transactions on Circuits and Systems for Video Technology*, vol. 13, no. 7, pp. 560–576, Jul. 2003.

[186] Q. Huynh-Thu, "Scope of validity of PSNR in image/video quality assessment," *IET Electronics Letters*, vol. 44, no. 13, 2008.

[187] A.-B. García, M. Alvarez-Campana, E. Vázquez, and J. Berrocal, "Quality of service support in the UMTS terrestrial radio access network," in *Proc. 9th HP Openview University Association Conference*, 2002.

[188] B. Fañanás Mata, "Investigation of HSDPA schedulers," Bachelor thesis, Vienna University of Technology, Oct. 2008.

[189] M. E. Feliz Fernández, "HSDPA CQI mapping optimization based on real network layouts," Bachelor thesis, Vienna University of Technology, Dec. 2008.

[190] F. Brouwer, I. de Bruin, J. Silva, N. Souto, F. Cercas, and A. Correia, "Usage of link-level performance indicators for HSDPA network-level simulations in E-UMTS," in *Proc. IEEE 8th International Symposium on Spread Spectrum Techniques and Applications*, 2004, pp. 844–848.

[191] R. Litjens, "HSDPA flow level performance and the impact of terminal mobility," in *Proc. IEEE Wireless Communications and Networking Conference*, vol. 3, 2005, pp. 1657–1663.

[192] K. Sipilä, K.-C. Honkasalo, J. Laiho-Steffens, and A. Wacker, "Estimation of capacity and required transmission power of WCDMA downlink based on a downlink pole equation," in *Proc. IEEE Vehicular Technology Conference Spring (VTC)*, May 2000, pp. 1002–1005.

[193] S. Sandhu and A. J. Paulraj, "Space-time block codes: A capacity perspective," *IEEE Communications Letters*, vol. 4, no. 12, pp. 384–386, Dec. 2000.